University of Nevada, Reno

Observing Semi-Arid Ecoclimates across Mountain Gradients in the Great Basin, USA

A dissertation submitted in partial fulfillment of the requirements for the degree of Doctor of Philosophy in Geography

by

Scotty Strachan

Dr. Scott Mensing/Dissertation Advisor

August, 2016

THE GRADUATE SCHOOL

We recommend that the dissertation
prepared under our supervision by

SCOTTY STRACHAN

Entitled

Observing Semi-Arid Ecoclimates across Mountain Gradients in the Great Basin, USA

be accepted in partial fulfillment of the
requirements for the degree of

DOCTOR OF PHILOSOPHY

Scott Mensing, Ph. D., Advisor

Constance Millar, Ph. D., Committee Member

David Charlet, Ph. D., Committee Member

Stephanie McAfee, Ph. D., Committee Member

Robin Tausch, Ph. D., Graduate School Representative

David W. Zeh, Ph. D., Dean, Graduate School

August, 2016

Abstract

Observation of climate and ecohydrological variables in mountain systems is a necessary (if challenging) endeavor for modern society. Water resources are often intimately tied to mountains, and high elevation environments are frequently home to unique landscapes and biota with limited geographical distributions. This is especially true in the temperate and semi-arid mountains of the western United States, and specifically the Great Basin. Stark contrasts in annual water balance and ecological populations are visible across steep elevational gradients in the region; and yet the bulk of our historical knowledge of climate and related processes comes from lowland observations. Interpolative models that strive to estimate conditions in mountains using existing datasets are often found to be inaccurate, making future projections of mountain climate and ecosystem response suspect. This study details the results of high-resolution topographically-diverse ecohydrological monitoring, and describes the character and seasonality of basic climatic variables such as temperature and precipitation as well as their impact on soil moisture and vegetation during the 2012-2015 drought sequence. Relationships of topography (elevation/aspect) to daily and seasonal temperatures are shown. Tests of the PRISM temperature model are performed at the large watershed scale, revealing magnitudes, modes, and potential sources of bias that could dramatically affect derivative scientific conclusions. A new method of precipitation phase partitioning to detect and quantify frozen precipitation on a sub-daily basis is described. Character of precipitation from sub-daily to annual scales is quantified across all major Great Basin vegetation/elevation zones, and the relationship of elevation to precipitation phase, intensity, and amount is explored. Water-stress responses of Great Basin conifers including *Pinus flexilis, Pinus longaeva,* and *Pinus ponderosa* are directly observed, showing potential differences in drought adaptation. Overall results highlight the seasonal flexibility of semi-arid conifer water use, as well as the tendency of topoclimate to buffer mountain ecosystems from extreme seasonal events. Methods and

practices used in this study are globally applicable to mountain observatory efforts; especially the themes of topographic diversity, siting design, and leverage of technology and cyberinfrastructure.

Acknowledgments

The data and results presented in this work are representative of not only my own effort, but that of many key people and entities that provided scientific guidance, material assistance, education, and moral support during my journey. This work would not have been possible without them.

First, the patience and support of my wife Anthea Strachan and sons James and Calvin Strachan have kept me focused and interested in pursuing the science in spite of obstacles. Their help and encouragement at home and in the field made the difference during the most challenging of times.

Primary support for the observations, support cyberinfrastructure, data processing, and conference/publication dissemination came from several sources ultimately funded by the hard-working American taxpayer. The National Science Foundation (NSF) Geography and Spatial Sciences grant BCS-1230329, NSF-EPSCoR grants EPS-0814372 and IIA-1301726, the UNR College of Science dean's office, and the UNR office of the Vice-President for Research and Innovation funded the scientific operations in the Walker Basin as well as the construction and continued operation of the NevCAN observational network. Permit agreements with the USDA Forest Service, Bureau of Land Management, the U.S. Fish & Wildlife Service, and the Long Now Foundation enabled specimen collections and the installation of equipment.

The support and encouragement of the Nevada state EPSCoR administrative office, UNR collaborators Sergiu Dascalu, Fred Harris, and the rest of the UNR cyberinfrastructure group was critical in enabling the work of acquiring and compiling the NevCAN data.

Collaborators and science advisors Brad Lyles and Greg McCurdy from the Desert Research Institute were instrumental in setting up and operating the NevCAN sensor systems, and continue to selflessly

supply unique insight and information that only decades of Great Basin field science knowhow can provide.

Collaborator Chris Daly and his research group provided generous access to PRISM model data for the Walker Basin and proactively contributed to the investigative process for the air temperature testing section of this work. Chris' knowledge of mountain climate processes in the western U.S. has been and continues to be a significant influence on my thinking in this area.

NevCAN field installations and operations were aided significantly by colleagues Britt Johnson, Brian Bird, AJ Wolff, Lynn Fenstermaker, Dale Devitt, Jay Arnone, and Richard Jasoni, as well as my incredible brother Charlie Strachan. NevCAN operations would have been seriously hampered without accessibility to Jill Heaton's Big Field Truck.

My fellow students and colleagues Mackenzie Kilpatrick, Jehren Boehm, Ben Trustman, Anna Patterson, Jasmine Kleiber, and Justin White all helped with fieldwork, tech support, and comradely good times. The many other students in the Geography and Hydrology programs that came to the field or kept up classroom spirits are very much appreciated.

Data transport and field networking support was provided by the Nevada Seismological Laboratory and the efforts of Dave Slater, Graham Kent, Ken Smith, John Torrisi, and the rest of the NSL team. The gracious collaboration of Mary Swetich and Bill Kingston at Great Basin College in Ely, Nevada made constant connectivity to the Snake Range field sites possible.

The UNR Geography Department (notably Scott Mensing, Jill Heaton, Victoria Randlett, and Shari Baughman) provided a generally supportive community that helped keep my work on track, relevant, and readable.

My interests in mountain ecohydrology, community-driven science, and best practices have flourished as a result of inspiration from people like climate scientist Kelly Redmond, hydroclimatology professor Daniel Obrist, business school professor Bret Simmons, Great Basin knowledge source Don Grayson, Stu Weiss and his turns of phrase, Andy Bunn and the rest of the CIRMOUNT community, many wonderful international colleagues associated with the Mountain Research Initiative, data and observation working group partners Renée Brown and Eric Kelsey, and the efforts of many other Great Basin field scientists before me.

The encouragement, questions, and general advice from scientist and AAAS Fellow Farrel Lytle was particularly motivational during this process, as were the annual harvests from the Lytle garden in Eagle Valley. You never know who you will meet out in the Great Basin.

Collaborator, mentor, and friend Connie Millar cannot be acknowledged enough for her patience, her willingness to hold my feet to the fire, and her personal investment in the next generation of field scientists. I am only one of many who have been given wider opportunity and better critical thinking skills as a result of her tireless and selfless dedication to the mountain science community.

Outside feedback, research support, and property access all crucially came from the Long Now Foundation, particularly via Zander Rose, Laura Welcher, and Dave Tilford, whom I thank profusely for their part in this work. Interacting with people who always place logistics, effort, and purpose into the long term perspective has been most refreshing.

My long-suffering Ph.D. committee of Robin Tausch, David Charlet, Connie Millar, Steph McAfee, and Scott Mensing are especially to be recognized for their dedication to thorough and comprehensive field science, without which our knowledge of environmental processes remains conjecture.

Finally, because all formal education has a beginning, I remain in debt to my early teachers Sharon Swindler, Charlene Malnack, and Julie Grossman at Desert Son Christian School in Hawthorne, Nevada; also my homeschooling and tireless mother Jean Strachan, and my first higher-education instructors at Western Nevada Community College. These individuals gave me the tools necessary to learn rapidly, communicate clearly, think critically, and treat all people with equal respect. Applied skills of dedication, persistence, and hard work came from countless personal examples (and practice!) while growing up in the rural communities of Hawthorne and Yerington, Nevada. My respect for the scientific process as a valuable tool comes from my father and Great Basin traveler Donald Strachan, who has always told me that “science depends on observation, son.” And so it does.

Table of Contents

List of Tables

List of Figures

Introduction

A need for mountain climate observations

Climate in mountainous terrain at ecohydrologically-important scales (e.g. sub-kilometer) remains challenging to both observe and estimate. Scientific disciplines ranging from snow hydrology to ecology to paleoclimatology struggle to obtain accurate data in complex topography with reasonable estimates of uncertainty on the most basic of climatic parameters (e.g. Lundquist and Cayan 2007; Fridley 2009; Dobrowski 2011; Graae et al. 2012; Stoklosa et al. 2015). This lack of knowledge could have profound effects on interpretation of cause and effect relationships in ecohydrology (Lookingbill and Urban 2005; Minder et al. 2010; Warren et al. 2014; Oyler et al. 2015). Research on mountain processes continues to be recognized as crucial for the resilience of socio-ecological systems on a global scale (Messerli and Ives 1997; Viviroli and Weingartner 2004; Foley et al. 2005; Gurung et al. 2012), and therefore scientific investigators and policymakers will use whichever data are available in an information-poor environment, regardless of whether or not these data have been tested for local accuracy.

Climate model performance in mountainous areas is problematic for a number of reasons, including incorrect spatial-topographic scale, scarce *in-situ* calibration data, and inadequate process knowledge (Knutti et al. 2010; Luce et al. 2013). Error is high in both short and long-term forecasting of snowlines, water balance, and temperatures in complex terrain due to this lack of information (Salzmann et al. 2007; Dobrowski et al. 2009; Daly et al. 2010). Projecting future mountain system processes using synoptic conditions from global or regional models remains a challenge because of these factors. Over recent decades, however, use of remote sensing and gridded model products for ecology, hydrology, and climate science has exploded, while at the same time there has been a worldwide decline in the number of ground-based observation stations (Beniston et al. 1997; Laternser and Schneebeli 2003;

Mitchell and Jones 2005; Lawrimore et al. 2011; Yatagai et al. 2012). The distribution of ground-based stations is highly biased towards lower elevations, providing inadequate representation of mountain geography resulting in the potential for increased model error at mid and high elevations (Hasenauer et al. 2003; Pepin and Seidel 2005; Bales et al. 2006; Stahl et al. 2006). The reasons for the dearth of high-elevation observations are straightforward: maintaining consistent and accurate climatological observations in mountains is difficult, time-consuming, and expensive. Historically, all measurements required manual observation; however, over the last 50 years, automated instruments have replaced manual operation in many locations (Begert et al. 2005; Fiebrich 2009). Mountain environments have proven to be a challenge for maintaining automated stations, and so this aspect of climate monitoring has grown more slowly than the efforts at lower elevations.

Notable exceptions to this general trend in the United States include the SNOTEL (SNOw TELemetry) and the RAWS (Remote Automated Weather Stations) networks. SNOTEL comprises a series of upper-elevation sites maintained for seasonal streamflow prediction that also include basic meteorology sensors (NRCS 2015), and RAWS involves a distributed weather network primarily centered on fire risk and are found mostly at lower or middle elevations (http://www.raws.dri.edu/). Both of these networks, as well as the newer Climate Reference Network (USCRN; Diamond et al. 2013), are not evenly distributed in all areas or across representative topography. This is also true for longer-term records. A 1992 survey of nonfederal automated stations in operation in the U.S. and Canada showed that station density in very mountainous regions was extremely low, especially in the states of Nevada, Montana, and Wyoming (Meyer and Hubbard 1992). Issues related to microclimate and site positioning have been discovered during comparative analysis in these and other networks (e.g. Gallo 2005; Oyler et al. 2015).

Given the need for better ground-truth data for models and remote sensing, as well as the stagnation of ground-based observation, there is a need within the scientific community to increase monitoring

station density, especially in mountain ecosystems. This can be accomplished by: 1) developing cost-effective practices for constructing and maintaining high-elevation observation sites capable of delivering high-quality, gap-free data; and 2) demonstrating the value of the information provided by such stations. This work addresses both of these goals.

Climate in the Great Basin: North America's "Empty Quarter"

The Great Basin hydro-ecologic region of North America is no different from much of the world's mountainous areas in that high-elevation observations are historically scarce. This semi-arid zone of interior drainage extends from the crest of California's Sierra Nevada mountain range in the west to the peaks of the Wasatch and Uinta mountains in Utah, as well as large portions of Oregon, bits of Idaho, and even a corner of Wyoming (Figure 1). The landscape of the Great Basin is dominated by mountains, but in a unique manner; hundreds of long, relatively narrow ranges of steep mountains are separated by broad, open valleys. Dozens of these mountain ranges exceed 3000 m in height, creating a stark contrast between the relatively dry desert below and the subalpine settings above (Wells 1983; Grayson 2011). It is in these mountains where the annual water balance for local watersheds is determined, as distinct gradients of precipitation are present.

Pacific frontal-type storm events deposit the bulk of rain or snow in the mountains through a combination of local orographic effects (Roe 2005) and air mass evolution downstream of the Sierra Nevada rainshadow (Houghton 1979). The presence of the Sierra Nevada range and its influence on moisture blocking is the defining physio-climatic feature of the Great Basin, and is primarily responsible for its semi-arid nature. Proximity of the Sierra to the Pacific Ocean and abrupt elevation changes from sea level to over 3000 m ensure that a substantial portion of the moisture present in westerly flow is extracted orographically or by other mountain-atmosphere interactions such as blocking lateral airflow

from the Sierra barrier jet (Parish 1982; Daly et al. 1994; Dettinger et al. 2004; Lundquist et al. 2010). While this modified westerly flow dominates the transport of moisture into the Great Basin, there are other synoptic mechanisms that contribute to overall precipitation totals in the region. Transiting "cut-off" low pressure systems are disconnected from troughs in the northeast Pacific and move inland, most prominently in the springtime seasonal window (Nieto et al. 2005; Oakley and Redmond 2014). Cyclonic circulation associated with these low-pressure systems over the continent can pull moisture from the eastern Pacific up into the Great Basin, bypassing blocking orography and creating "upslope" precipitation events on the lee side of mountain ranges (Reinking and Boatman 1986) or potentially moving moisture parallel to the axis of mountain-valley orientations without perpendicular orographic effects.

Another source of Great Basin moisture is the North American Monsoon (NAM), a summertime phenomenon of southerly moisture flow. While the NAM is considered a dominant climate feature of the American Southwest, it also can strongly affect the south-central portion of the Great Basin (Douglas et al. 1993; Means 2013). Because the NAM precipitation at the local scale is driven by daytime heating and convective activity, the effect of mountain ranges on precipitation amounts is not as dramatic as frontal/orographic interactions. The impact of these various seasonal and circulatory mechanisms on mountain precipitation in the Great Basin remains uninvestigated because of extremely limited data (Houghton 1979), which contributes to high levels of uncertainty in climate models for the region (Brekke et al. 2013). Studies incorporating precipitation in the Great Basin are usually regional in scale and leverage interpolated models of precipitation (e.g. Dettinger et al. 1998; Wise 2010; Wang et al. 2012), which in turn are mostly based on low-elevation observations and remain largely untested across elevation gradients. These gradients, like all mountain environments of the world, play a crucial role in local ecology and regional hydrology.

Lower-elevation Great Basin environments experience a net water deficit; surplus in mountain ranges provides recharge, making snowpack a critical part of the annual water budget (Welch et al. 2007). It is projected that mountains across the western U.S. will retain less snowpack outside of the winter season in the future (Gleick and Chalecki 1999; McCabe and Wolock 1999; Dettinger et al. 2004), and significant changes to annual water budgets are possible (Knowles and Cayan 2004), although not necessarily driven by temperature alone as annual-to-decadal precipitation amounts are certainly not static (Hamlet et al. 2005; Andrews 2012). The impact of snow as a primary precipitation mode in mountains is dominated by the springtime runoff phenomenon, although mountain-block infiltration and recharge is a secondary effect. It is generally accepted that snowpack creates higher infiltration amounts as compared to rain (Maule et al. 1994; Berghuijs et al. 2014), although this depends strongly on the local soil maximum infiltration rate *versus* typical rainfall or snowmelt rates and duration. Interactions between precipitation and deeper groundwater recharge are also complex, and it is possible that projected changes in the snow/rain ratio favoring liquid precipitation do not necessarily equal greater shallow-aquifer recharge in snow-dominated regions (Huntington and Niswonger 2012). Sparseness of data on precipitation, temperature, snowpack, soil, and groundwater trends in general hinders long-term assessment, modeling, and projections in many mountain regions (Stewart 2009), and the Great Basin is certainly no exception given that it is likely the least-instrumented region in the contiguous United States (Mock 1996), as well as one of the most mountainous.

The ecology of the Great Basin is ultimately tied to long-term precipitation inputs and their mechanisms. The semi-arid region is separated into the colder, higher-elevation Great Basin Desert ecoclimatic zone in the north and the warmer, lower elevation Mojave Desert in the south (Grayson 2011). Both of these sub-regions depend on precipitation (especially snow) in mountain ranges to recharge soil moisture and eventually local aquifers, sustaining diverse ecological communities such as subalpine and montane

forests populated with unique, geographically-isolated species. The long-term (multi-millennial) survivorship of individuals and small populations within these species (e.g. Great Basin bristlecone pine, *Pinus longaeva*) indicates that in spite of notable swings in palaeoclimatic conditions, enough regularity in water input persisted in the past to preserve these individuals and isolated populations in a water-limited context.

Details of these past drought and pluvial periods at seasonal-to-decadal scales are largely unknown, although inferences can be made using palaeoecological and palaeoclimatic evidence (e.g. LaMarche Jr. 1973; Spaulding and Graumlich 1986; Wigand and Nowak 1992; Hughes and Diaz 1994; Nowak et al. 1994; Graham et al. 2007; Mensing et al. 2008). These sorts of palaeo records do not contain the ability to resolve actual precipitation amounts or phase (rain or snow), or even strict temperature regimes, although precipitation seasonality and general temperature ranges are inferred using present-day plant species' spatial-climatic distributions. In fact, the relationship of snow and its seasonal persistence to vegetative communities/zones is unknown, although Great Basin conifers typically associated with high-elevation, snow-dominated environments are occasionally found in locations with very little seasonal snowfall (Charlet 1996), and a cool springtime growing season seems to be the single common feature across the region (Comstock and Ehleringer 1992).

These dichotomies create something of a problem for parameterization of predictive niche models as well as interpretation of plant-derived palaeoecology records. Between the precipitation and its ultimate fate lies the land surface, which in the Great Basin is generally composed of a variety of soils typical of semi-arid environments with complex geology: low to moderately-developed organic horizons with textures that range from sand to clay (Sperry and Hacke 2002; Miller et al. 2013). Shallow Great Basin soils can be subject to frequent hydrologic disturbances due to high interannual variability in the climate (Castelli et al. 2000). Arid and semi-arid ecohydrology is viewed as being driven by precipitation

pulse dynamics, or the sporadic arrival of water on the landscape, which are in turn strongly moderated by soil conditions (e.g. Rodriguez-Iturbe 2000; Austin et al. 2004; Robinson et al. 2008). Reynolds at al. (2004) also point out that the character of the storms which bring precipitation to the landscape are important, as the rainfall rate and total volume ultimately combine with antecedent soil conditions to form "effective" precipitation. Because seasonal snowfall is a standard feature of Great Basin mountains, it stands to reason that the form of the precipitation in this semi-arid region (i.e. frozen, liquid, or mixed) must have some influence on determining seasonal soil moisture and therefore impact the near-surface ecohydrology as well as the amount of mountain-block recharge. In the Great Basin at large, the seasonal nature of frozen precipitation, mountain temperature regimes, individual storm impacts, and ecological responses are not well quantified via observation across mountain gradients, and thus these processes are worthy of increased observation and study.

This work seeks to demonstrate that: 1) additional observations of temperature and precipitation are needed across mid-elevations in order to further develop our scientific picture of Great Basin mountain climate regimes; 2) precipitation measurements in semi-arid zones with high interannual climate variability must be quantified by phase and "effectiveness" in order to be more useful for ecohydrologic applications; 3) rather than being limited by seasonal temperatures, upper-elevation trees in the Great Basin are capable of using available water to maintain vigor across a substantial portion of the year; and 4) acquiring the data to answer these questions requires a methodological approach to designing and operating automated observation systems for extreme environments. These questions and approaches, while certainly relevant to the Great Basin, are also applicable to many other parts of the world where mountain gradients exist.

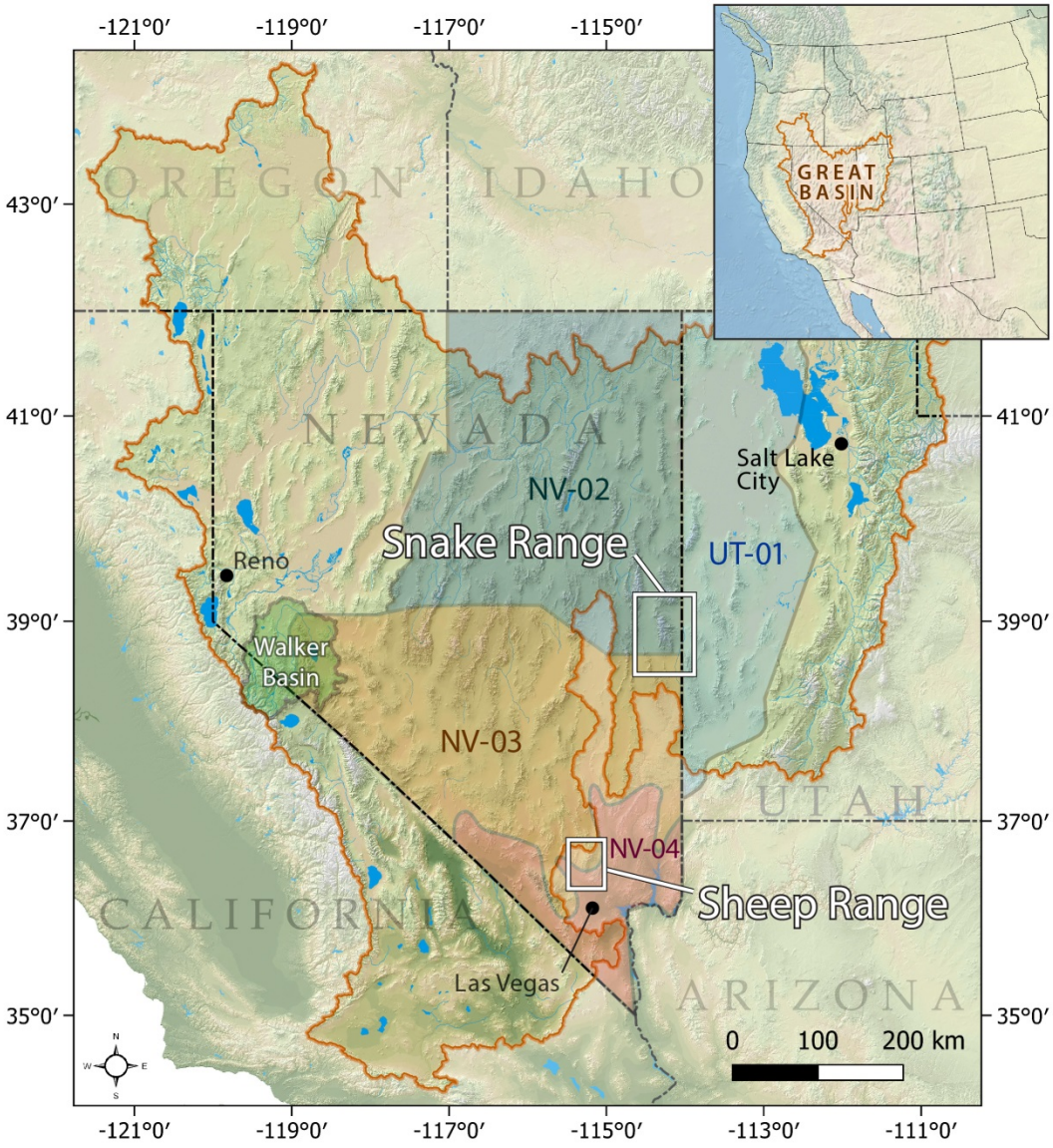

Figure 1. The Great Basin of North America.

This area comprises a substantial portion of the interior western United States. Shown in the figure are the study areas referenced in this work; the Walker Basin, the Snake Range, and the Sheep Range. The State Climate Divisions NV-02, NV-03, NV-04, and UT-01 are also indicated. In this case, the strict hydrographic Great Basin boundary is indicated (orange line); however, there are many definitions of the Great Basin, including ethnographic, floristic, and physiographic, each with slightly different boundaries (Grayson 2011).

Chapter 1 Mid-slope thermal regimes in temperate mountains, and testing a popular gridded model (PRISM)

Motivation

Of particular concern is our understanding of climate on mountain slopes. Long-term observations of daily temperature are common in valley environments, and upper-air data from soundings and sparsely-distributed high-elevation sites provide a fairly accurate picture of high peak and ridgetop conditions. Between the two elevational extremes lies a large part of the atmospheric boundary layer, a dynamic region of air which extends from the lower "free atmosphere" and is directly influenced by energy interactions with the earth's surface (Garratt 1994). The thickness of this boundary layer changes with time of day as well as local and regional meteorological conditions. Mountainous geography within this zone (i.e. slope and lower ridge features), is not only subject to strong local departures from regional conditions but is also the least-represented in terms of *in-situ* observation (Hasenauer et al. 2003; Pepin and Seidel 2005; Bales et al. 2006; Stahl et al. 2006). Topoclimate is a phenomenon that disconnects near-surface temperature from strict dependence on free-air elevational lapse rates, and it is likely the key to ecological resilience during episodes of shifting climates (Kimball and Weihrauch 2000; Dobrowski 2011; Scherrer and Körner 2011; Lenoir et al. 2013). The physical area comprising high-elevation slopes is often quite large compared to summits, ridgetops, and canyon bottoms (Strahler 1952), resulting in large amounts of catchment area where ecohydrologic processes can be subject to topoclimatic disconnects.

Management and scientific questions associated with hydrologic resources, ecological communities, and biological risk in mountains are bound up in this conundrum of uncertainty driven by the non-linearity of true climatic regimes on slopes (Weiss et al. 1993; Wigmosta et al. 1994; Diodato 2005; Lookingbill and

Urban 2005; Van De Ven et al. 2007; Daly et al. 2010; Krause et al. 2015). The dearth of real observations across critical elevation gradients has not slowed the proliferation of ecological niche or hydrologic modeling efforts in mountains, many of which continue to predict linear, elevationally-driven extinction (e.g. upslope movement of distributions) of species and snowpacks as a result of predicted global atmospheric warming (e.g. Knowles and Cayan 2004; Barnett et al. 2005; Thuiller et al. 2005; Hamann and Wang 2006; Randin et al. 2009). Modeling efforts related to these topics generally use gridded climate products as input (themselves models) without sufficient consideration as to their accuracy or applicability. For example, a high-profile review of habitat modeling in ecology virtually side-stepped methodologies and assumptions in the use of gridded climate surfaces and bioclimatic envelopes, instead focusing on the need to incorporate the complexities of community dynamics to improve accuracy (Guisan and Thuiller 2005). Other highly-cited efforts to improve the validity of species distribution models focus on issues such as niche theory and scale (Pearson and Dawson 2003), the concept of "non-analogue climate" (Fitzpatrick and Hargrove 2009), or a combination of "challenges", none of which involve investigation of actual topoclimatic conditions (Araújo and Guisan 2006).

Some ecological studies start with the premise that species distribution and occupied niches are driven largely by physical processes on landscape features (Austin and Van Niel 2011), but this school of thought certainly does not dominate the literature. Species distribution modeling (SDM) and similar tools have very specific management applications that must be played out at fine geographic scales, and dependence on gridded data without fine-scale testing multiplies the already significant uncertainty issues present in ecological modeling.

Hydrological modeling involves processes and interactions that are often quantified at some engineering level and do not depend on organism behavior (Jakeman and Hornberger 1993; Singh and Woolhiser 2002; Renard et al. 2010). Uncertainty in studies of near-surface hydrology at the watershed scale,

therefore, may be primarily limited by quality of data and calibration information as opposed to the challenges of behavioral stochasticity that occur within ecology. It is important to get the relationship between temperature and topography correct, because watershed-scale estimates of components of the hydrologic cycle (including runoff, infiltration, aquifer recharge, and evaporation/ablation) depend strongly on these variables.

Gridded products extrapolating point observations of climate parameters to landscape scales have advanced in recent years (Brohan et al. 2006; Daly et al. 2008; Haylock et al. 2008; Thornton et al. 2012). Accuracy of these modeling efforts varies with density and quality of source data networks (Hamlet and Lettenmaier 2005; Daly 2006; Hofstra et al. 2009; McEvoy et al. 2014; Oyler et al. 2015; Stoklosa et al. 2015), and as mentioned previously it is in mountainous regions that observational data are the most scarce. Source data for models are concentrated in valley-situated ground stations and ridgetops or in the free atmosphere, leaving mountain slopes poorly represented in observational datasets. Temporal and spatial resolutions of models are increasing, but new calibration and verification data are not necessarily following suit. Local verification observations are not a common practice in analyses that leverage gridded climate datasets for process modeling or ecological niche prediction.

In-situ measurements of climate parameters such as air temperature are critical inputs to this process, as remotely sensed estimates of near-surface (e.g. 2 m) air temperature still contain significant sources of error (Kalma et al. 2008; Hengl et al. 2012). Ground-based validation of interpolated climate products within climate regions is therefore an important scientific activity, in order to inform users on model quality/accuracy as well as provide feedback to the modelers themselves on the performance of their products in varying geographical and seasonal settings (Minder et al. 2010; McGuire et al. 2012; Holden et al. 2015). Given all of these considerations, this chapter explores the diversity of temperature regimes across elevation and aspect on typical Great Basin mountain slopes, tests the accuracy of a popular

gridded temperature model product, and finally explores the nature of error in a commonly-used gridded model and implications for different applications.

Study area and observation methods

Geography

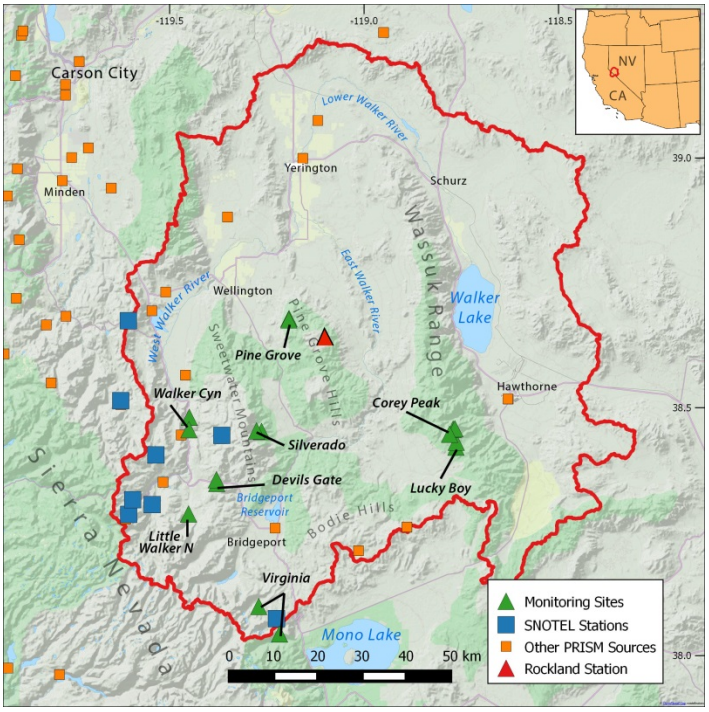

Figure 2: Walker Basin study area map.

Sixteen monitoring sites in mountainous topography were installed within the 10,200 km^2 Walker River Basin. This watershed is considered to be on the climate-ecological transition zone between the Sierra Nevada and Great Basin Desert ecoregions of North America (Figure 2). The monitoring sites are associated with an ongoing palaeoclimate study (Strachan, *in prep*) using upper and lower treeline species that are common to the western Great Basin. *Pinus flexilis* (PIFL), *Pinus monophylla* (PIMO), and *Juniperus occidentalis* (JUOC) are species which typically form open old-growth woodlands rather than closed-canopy forests, and are associated with distinct lower (PIMO and JUOC) and upper (PIFL) elevation vegetative zones (Billings 1951; Tausch et al. 1981; Charlet 1996). Because each of these species has a different biogeographic history and realized niche, their presence in both old and new growth on the various study sites is likely indicative of microclimatic differences in water balance and seasonal thermal regime (Rocher and Tausch 1994; Charlet 2007). Placing the context of this temperature study within the dominant vegetative zones is important for interpretation of the

results, as the vegetative populations and old growth on each study site represent long-term differences in local climate conditions.

Table 1.1: Study site characteristics.

Site	Elev (m)	Slope (°)	Aspect (°N)	Dominant species	Site pair name
Lucky.N	2480	21	325	*Pinus monophylla*	Lucky Boy
Lucky.S	2497	30	136	*Pinus monophylla*	Lucky Boy
DevGate.N	2378	39	352	*Juniperus occidentalis*	Devils Gate
DevGate.S	2360	27	200	*Juniperus occidentalis*	Devils Gate
CoreyLow.N	2977	32	329	*Pinus flexilis*	n/a
Corey.N	3104	34	307	*Pinus flexilis*	Corey Peak
Corey.S	3111	22	101	*Pinus flexilis*	Corey Peak
Silverado.N	2937	31	270	*Pinus flexilis*	Silverado
Silverado.S	2897	26	157	*Pinus flexilis*	Silverado
PineGrove.N	2355	18	347	*Pinus monophylla*	Pine Grove
PineGrove.S	2371	17	226	*Pinus monophylla*	Pine Grove
Kavenaugh.N	3000	37	310	*Pinus flexilis*	Virginia
Lundy.S	2911	33	212	*Pinus flexilis*	Virginia
WalkerCyn.N	2036	45	12	*Pinus monophylla*	Walker Canyon
WalkerCyn.S	1967	38	188	*Pinus monophylla*	Walker Canyon
LWalker.N	2452	16	304	*Juniperus occidentalis*	n/a

The study sites range in elevation from 1967–3111 m, and are generally co-located in opposite-aspect pairs. Sites are distributed across four mountain ranges, ranging from west to east (Figure 2), and represent a spatial gradient from Eastern Sierra to Great Basin ecosystems. Topographic site positioning varies (Table 1.1): the locations were intended to represent opposite aspects of homogenous mid-slope features rather than peaks, ridgetops, gullies, or canyon floors. In this way, the observations are specifically targeted at near-surface air conditions that are free of influence from local cold-air pools, lake effects, elevated wind velocity, or wind eddies. Thus, the primary drivers of air temperature on the study sites are radiative processes, larger-scale airflow, and local lapse rates (Daly et al. 2008).

While it is true that processes such as cold-air pooling, windiness, and snow presence have dramatic and important eco-hydrological effects at the point scale, proper characterization of general air conditions across mid-slope topography is the first step to accurately model air temperature behavior at the watershed scale. The study locations are therefore optimized such that *in-situ* observations focus on

response of temperature to larger-scale topographic characteristics such as elevation, slope, and aspect, which represent the first order of variability in mountainous terrain.

In-situ observation methods

At each site, observations of daily maximum temperature (T_{MAX}) and daily minimum temperature (T_{MIN}) in °C were made using Maxim iButton DS1922L thermochron dataloggers placed between 1.5 and 2 m height above ground level in the vegetation interspace on each site (Figure 3). The common collection timeframe for all sites is 1 October 2013 through 1 September 2015, providing 23 months of data.

Figure 3: Field sensor deployments.

Gill-type shields house the iButton thermochrons between 1.5 and 2 m height on open woodland slopes, in an attempt to reproduce “standard” weather station observations in mountainous topography.

The iButtons were configured using Maxim 1-Wire software to log their case temperature every 60 minutes. Real-Time-Clock (RTC) drift of each iButton was evaluated at collection intervals (~9 months) to ensure that cumulative RTC error did not exceed 50% of the observation interval (30 min). In order to replicate standard weather station temperature measurements as closely as possible, the iButtons were placed inside 6-plate Gill-type radiation shields using non-conductive mounting holders that mimicked typical temperature probe head positioning. In addition, one iButton at each site was placed at ground level inside an opening in the main mounting pole to qualitatively assess snow presence/absence as well as ground-level overnight low temperatures. For long-term testing/evaluation purposes, an additional iButton/shield combination was placed at 1.7 m height on a scientific-grade weather station located at 2600 m elevation in the center of the study watershed (Rockland Station; Figure 2). Reference instruments included a Campbell Scientific CR3000 datalogger, an HMP-60 temperature and relative humidity probe, and a Type-T thermocouple installed in identical shielding and configured to Western Regional Climate Center (WRCC) and World Meteorological Organization (WMO) specifications (WMO 2008). During the 2013–2015 interval, wintertime bias in observed temperatures due to snow presence or interference with sensors at 1.7 m heights was minimized at all sites by record-setting low snowpack levels across the region (Swain 2015), verified qualitatively with the ground-level iButtons.

Testing of the iButton/Gill shield deployment design revealed that this configuration logging at hourly intervals is capable of capturing the same daily T_{MAX} and T_{MIN} as the Campbell Scientific equipment at Rockland Station. Over a continuous 93-week timeframe, bias (calculated as *iButton* - *Campbell*) of the iButton daily T_{MAX} compared to the HMP-60 probe and Type-T thermocouple was 0.20°C and 0.45°C (standard deviation σ = 0.64 and 0.66), respectively (Figure 4; *blue*). Bias (*iButton* - *Campbell*) of the iButton daily T_{MIN} compared to the HMP-60 probe and Type-T thermocouple was 0.15°C and -0.41°C (σ = 0.40 and 0.39), respectively (Figure 4; *purple*). It should be pointed out that the two Campbell sensor

types themselves diverged, with mean *HMP-60* - *Thermocouple* of 0.25°C for T_{MAX} and -0.56°C for T_{MIN} (σ = 0.31 and 0.10, respectively, Figure 4; *green*).

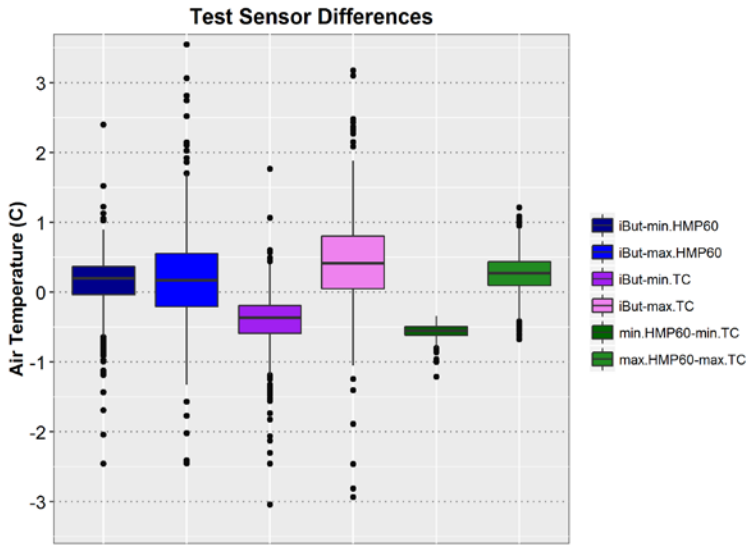

Figure 4: Test sensor differences.

Differences in observations between three different temperature sensors deployed on Rockland Station for 93 continuous weeks. Boxplot edges represent the first and third quartiles, and the centerline represents the median.

Engineering specifications for Maxim DS1922L iButtons require that all data loggers are calibrated/validated against National Institute of Standards and Technology (NIST) traceable reference devices, with a temperature accuracy of ±0.5°C when post-processed with Maxim iButton software (*Maxim Integrated*, 2016). Campbell Scientific specifications state that HMP60 probes within calibration are accurate to ±0.6°C (Campbell Scientific 2016). Bias and standard deviation of the paired measurement differences were less than 1°C in all cases (Figure 4); thus, using the iButtons in this manner for daily T_{MAX} and T_{MIN} is functionally equivalent to using research grade sensors in an environment with significant solar exposure (non-canopied).

Opposite-aspect thermal regimes on woodland slopes

Climate refugia in mountains are often associated with limited-space zones separated by elevation such as mountain tops, canyon bottoms, or footslopes. However, the semi-arid mountains of the Great Basin possess huge disparities in vegetation species mix and density at identical elevations but on northern *versus* southern exposed slopes (Figure 5).

This is generally a reflection of microclimatic conditions (mix of growing season temperatures, snow retention, and warm season drought stress) that are driven by insolation and modulated by disturbance mechanisms, geomorphology, and soil development. Once in place, a denser forest or woodland creates additional shade and wind-buffering protection that provides further positive microclimatic feedback in terms of soil moisture recharge timing by lowering local sublimation/evaporation rates and increasing snow retention (e.g. Reba et al. 2012; Harpold et al. 2015).

Figure 5: Photo of vegetation/aspect partitioning.

On this ridge in the Snake Range, Nevada, vegetation communities are sharply separated by pinyon-juniper-mahogany on the south (left) exposure, whereas the northern (right) exposure contains a montane conifer mix of several species associated with higher elevations.

Temperatures on opposite-aspect slopes in the Walker Basin were investigated to see: 1) whether there were relationships between topographic characteristics and the basic ecohydrologic variables of frost-free days, degree-days, and monthly mean daily T_{MAX}, T_{MIN}, and T_{MEAN}; and 2) whether topographic aspect serves as a quantifiable substitute for elevation on open slopes in Great Basin woodland environments. Topography-temperature relationships were tested using standard linear regression techniques.

Table 1.2: Calculated topographic variables.

Variable	Description	Value range (this study)	Reference
Elev	Elevation of 10 m DEM, meters	3110 – 1967	
Slope	Slope steepness, degrees	44.9 – 16.1	
Asp	Aspect, degrees	351.9 – 12.3	
TPI	Topographic Position Index	1.68 – (-3.81)	Guisan et al. 1999
TRI	Terrain Ruggedness Index	7.6 – 2.1	Riley et al. 1999
DAH	Diurnal Anisotropic Heating Index	0.57 – (-0.67)	
StdH	Standardized Height, meters	3003 – 1493	
SlopH	Slope Height, meters	280 – 21	Böhner and Antonić 2009;
NormH	Normalized Height	0.95 – 0.25	Böhner and Selige 2006
MSP	Mid-Slope Position	0.89 – 0.12	
VllyD	Valley Depth, meters	79 – 8	
TRASP	Topographic Radiation Index	0.99 – 0.02	Roberts and Cooper 1989

Topographic Variables

Several topographic characteristics for each site (Table 1.2; Guisan et al. 1999; Riley et al. 1999; Böhner and Antonić 2009) were computed using 1/3 arc-second (~10 m) digital elevation models (DEMs) with open-source Quantum Geographic Information System (GIS) software (QGIS Development Team 2015) running SAGA (System for Automated Geo-scientific Analysis) processing algorithms (Böhner and Selige 2006). *Elev* is the elevation derived from the DEM for each site point location. *Slope* is the steepness of the land surface from horizontal in degrees of angle. *Asp* is the cardinal aspect of the site point location in degrees from true north. *TPI* is the Topographic Position Index, a measure of local prominence with a default bandwidth setting of 75 m. *TRI* is the Terrain Ruggedness Index, a measure of amount of elevation difference between adjacent grid cells. *DAH*, or Diurnal Anisotropic Heating, is an index which represents incident radiative energy exposure. *StdH* is a measure of relative slope position within the catchment area, taking into account drainage minimums and summit heights. *SlopeH* is a measure of the total homogenous slope height associated with each point. *NormH* is the normalized altitude of the terrain, stretched between the summit and lowest point in the watershed. *MSP*, or mid-slope position, represents the fractional vertical position of each site on its associated slope feature. *VllyD* is the vertical

distance to the nearest channel network base level, i.e. a local-scale valley/drainage depth from each site point location.

In addition, a Topographic Radiative Aspect index (TRASP; *Roberts and Cooper,* 1989) was derived from aspect values using the formula:

$$TRASP = 0.5 - \frac{\cos[\left(\frac{\pi}{180}\right)(Asp - 30)]}{2}$$

Where *TRASP* is a daily radiation loading index between zero and one with zero being the coolest and one being the warmest slopes, and where *Asp* is the cardinal aspect of the slope in degrees east of north. Both TRASP and DAH represent diurnal heat loading exposures, where slopes facing southwest experience greater total radiative loading during daylight hours on clear days.

Topographic characteristics of the study sites as calculated by the GIS applications and dominant tree species abbreviations (*Spp.D*) are shown in Table 1.3. Of particular interest for tests of temperature relationships to topography in this study (where siting was intentionally partitioned by elevation and aspect) are elevation, TPI, DAH, and TRASP. Because siting was also focused on medium- and low-density old-growth woodland environments, there is a certain amount of selection bias towards sites that are ecologically viable in the long term for such organisms. For instance, not all opposite-aspect groups experience tremendous differences in radiative indices (i.e. DAH and TRASP) even if the aspects are nearly 180° apart.

Table 1.3: Calculated topographic characteristics of sites.

Site Names	Elevation	Slope	Aspect	TPI	TRI	DAH	StdH	SlopH	MSP	VllyD	TRASP	Spp.D
Lucky Boy North	2480	21	325	1.57	2.73	-0.20	2294	49	0.71	8	0.29	PIMO
Lucky Boy South	2497	30	136	0.88	3.98	0.18	2240	80	0.61	19	0.64	PIMO
Devils Gate North	2378	39	352	1.45	5.92	-0.52	1855	62	0.12	49	0.11	JUOC
Devils Gate South	2360	27	200	-0.60	3.50	0.43	1546	21	0.39	48	0.99	JUOC
Corey Peak Low North	2977	32	329	0.75	4.46	-0.31	2669	103	0.66	21	0.26	PIFL
Corey Peak North	3104	34	307	1.68	4.79	-0.14	3003	280	0.90	16	0.44	PIFL
Corey Peak South	3111	22	101	-0.01	2.84	-0.07	2789	138	0.67	28	0.34	PIFL
Little Walker North	2452	16	304	-0.10	2.12	-0.04	1577	26	0.39	58	0.46	JUOC
Silverado Divide South	2897	26	157	0.45	3.44	0.30	2506	121	0.54	36	0.80	PIFL
Silverado Divide North	2937	31	270	-0.67	4.29	0.20	2229	74	0.19	50	0.75	PIFL
Pine Grove North	2355	18	347	1.44	2.30	-0.24	2160	39	0.67	8	0.13	PIMO
Pine Grove South	2371	17	226	1.11	2.23	0.27	2132	37	0.60	9	0.98	PIMO
Kavenaugh Ridge North	3000	37	310	-3.81	5.88	-0.17	1635	26	0.51	80	0.41	PIFL
Lundy Canyon South	2911	33	212	-0.50	4.53	0.51	2412	100	0.42	41	1.00	PIFL
Walker Canyon North	2036	45	12	0.49	7.60	-0.67	1493	30	0.28	54	0.02	PIMO
Walker Canyon South	1967	38	188	-0.28	5.65	0.57	1515	23	0.16	32	0.96	PIMO

Frost-Free Days

Frost-free days (FFD) represent the number of days when $T_{MIN} > 0°C$. Total observed frost-free days (FFD_{OBS}) from 1 Oct 2013 – 1 Sept 2015 were calculated for each site and regressed individually against the topographic variables elevation, TPI, DAH, and TRASP in a test of whether prominence, altitude, or heat-loading aspect are associated with FFD_{OBS}. The only variable that has a significant relationship to FFD_{OBS} is elevation (inverse relationship; adjusted $r^2 = 0.79$, $p < 0.0001$), with TPI (adjusted $r^2 = 0.01$, $p = 0.36$), DAH (adjusted $r^2 = 0.07$, $p = 0.93$), and TRASP (adjusted $r^2 = 0.06$, $p = 0.88$) having no relationship at the watershed scale. The slopes of the relationships for sites with positive and negative DAH differed slightly (Figure 6; -5.8 and -5.0, respectively), but this difference did not test as significant in an analysis of covariance using elevation and DAH = positive/negative as test interaction terms [$F(1, 12) = 0.011$, $p = 0.917$]. The unpaired site "Little Walker North" appears to be an outlier (Figure 6); its gross topographic position also indicates that it could be affected by large-scale cold-air convergence, which was not

evaluated in this study, and the fact that it is unpaired does not provide for an independent check on local geographic bias.

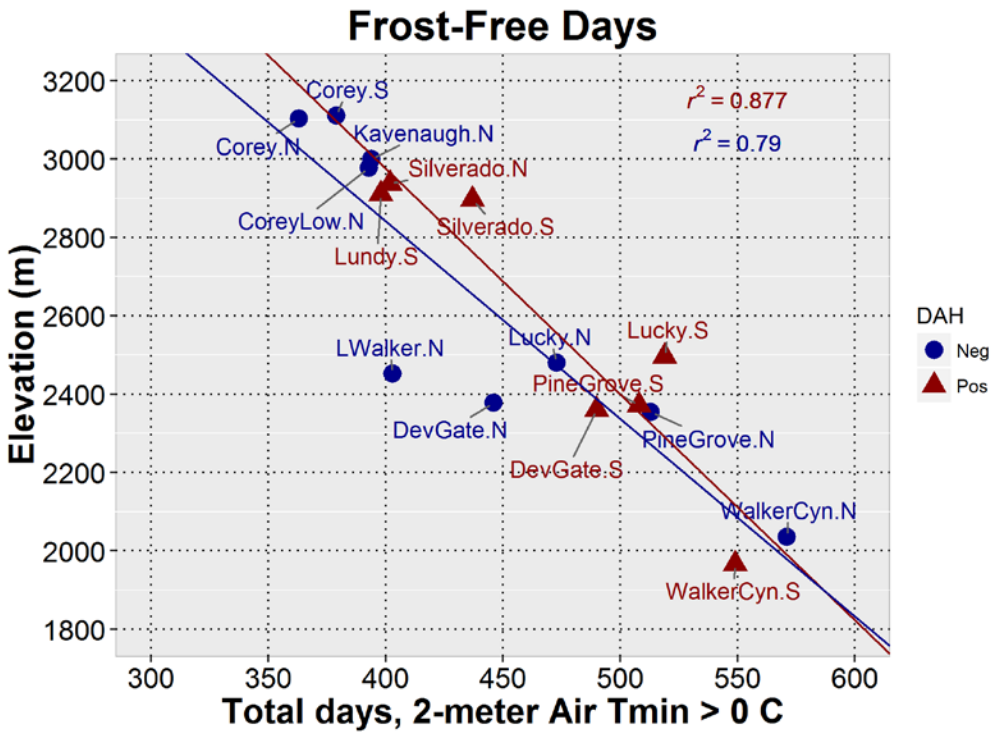

Figure 6: Frost-free days vs. elevation.

FFD_{OBS} from 1 Oct 2013 – 1 Sept 2015 plotted against elevation and separated by positive (high) and negative (low) DAH index values. The unpaired site "Little Walker North" appears to be an outlier, which may be affected by large-scale cold air convergence.

After removing the unpaired "Little Walker North" site from the dataset, a subsequent analysis was run on the opposite-aspect site pairs to control for elevation and therefore evaluate aspect. First, the ordinary least squares (OLS) relationship between elevation and FFD_{OBS} was re-calculated using the remaining 15 sites in order to standardize for elevation:

$$FFD_{\mathrm{STD}} = 887.83 - 0.165Elev,$$

where FFD_{STD} represents modeled total frost-free days for 1 Oct 2014 – 1 Sept 2015, and *Elev* is elevation in meters. The relationship is significant (adjusted $r^2 = 0.891$, $p < 0.0001$). The residuals (FFD_{RES}

= FFD_{OBS} - FFD_{STD}) were then differenced between pairs of sites (Corey Peak, Silverado, Devils Gate, Pine Grove, Lucky Boy, Walker Canyon, and Virginia; Table 1.1) to evaluate the impact of radiative loading on the number of days that a site remained above freezing. Table 1.4 shows the differences in radiative loading (DAH and TRASP) and FFD_{RES}, using the calculations $\Delta FFD = FFD_{RES(SOUTH)} - FFD_{RES(NORTH)}$, $\Delta DAH = DAH_{SOUTH} - DAH_{NORTH}$, and $\Delta TRASP = TRASP_{SOUTH} - TRASP_{NORTH}$ for all seven site pairs.

Table 1.4: Elevation-corrected frost-free day differences between site pairs.

Site Pair	ΔFFD	ΔDAH	ΔTRASP
Walker Canyon	-33.46	1.24	0.94
Pine Grove	-2.23	0.51	0.85
Devils Gate	41.04	0.95	0.89
Lucky Boy	48.83	0.38	0.35
Silverado	28.3	0.10	0.05
Virginia	-10.73	0.68	0.59
Corey Peak	17.14	0.06	-0.10

Some site pairs show strong positive differences (south = more FFD, north = less FFD) where positive differences in DAH and TRASP occur (south = higher heat loading, north = less at Devils Gate, Silverado, and Lucky Boy). Other site pairs show opposite effects (Walker Canyon, Pine Grove, and Virginia). These results suggest that while radiative aspect probably plays a part in moderating FFD, other mechanisms can override this influence at the point scale.

Of equal or perhaps more import for certain species is the actual frost-free season, i.e. the time period between the last frost of spring and the first frost of autumn. This timeframe is considered another metric of general growing season length for plants, and has been increasing over recent decades in the western United States based on observations from long-term weather stations (Easterling 2002; Kunkel et al. 2004). To investigate differences in this variable between sites and across the watershed, the 2014 frost-free season was calculated (Figure 7). It is evident that for the 2014 season at least, the frost-free interval was controlled by larger-scale air masses that affected the entire region. This is inferred from the observation that both last and first frosts of the season were generally synchronous in time across

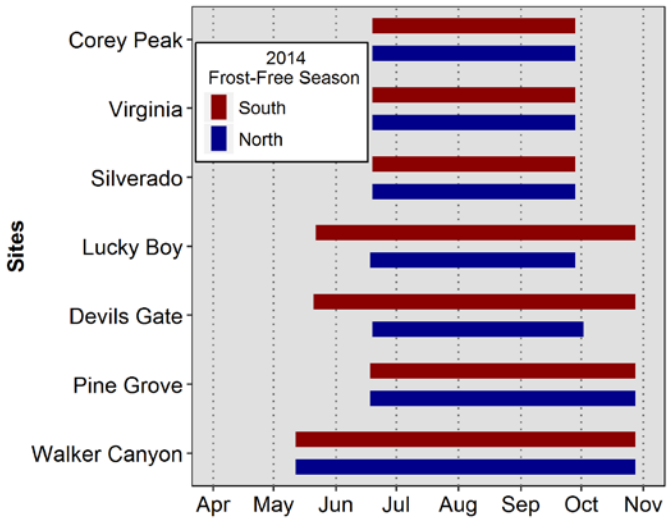

Figure 7: Frost-free 2014 season.

The frost-free 2014 season is shown for all seven site pairs, arranged from high (top) to low (bottom) elevation. Southerly-exposed sites at lower elevations all experienced longer frost-free intervals than northerly exposures. Consistent timing of first and last frosts across all sites in the watershed point to large-scale atmospheric events such as storm fronts or similar encroaching air masses.

geographic space. Site position at the upper elevations did not serve to extend the frost-free season; however, in two cases at lower elevations the south-exposed sites experienced extended frost-free periods and in general, lower-elevation sites experienced longer intervals than high elevations. This indicates that radiative exposure differences (positive Δ*DAH*) can overcome cool weather effects in the transition seasons in some cases but not others.

Degree-Days

Growing degree-days (GDD) represent heat energy accumulation as a function summing daily temperature above some base temperature threshold T_{BASE}. This concept has been used in the fields of ecology and agricultural sciences to predict the onset of the growing season, as well as crop yield and plant phenological stages. Similar thermal sums are also a common feature in mountain hydrologic models as part of snowmelt processes (Rango and Martinec 1995; Bergström et al. 2001; Hock 2003). A commonly-used base temperature is T_{BASE} = 5°C for conifer/shrub ecological studies, as it is related to the impact of 1.5–2 m air temperatures on actual ground-surface temperatures, thawing of near-surface soil water, and warming of the rooting zones of plants (Crookston et al. 2010; Thompson et al. 2012;

Bentz et al. 2013; Thompson et al. 2015). GDD for the intervals Jan 1 – Sept 1 in both 2014 and 2015 were calculated from observations (Figure 8) using the following equation:

$$GDD_{OBS} = \sum \left[\frac{T_{\mathrm{MAX}} + T_{\mathrm{MIN}}}{2} - T_{\mathrm{BASE}} \right]$$

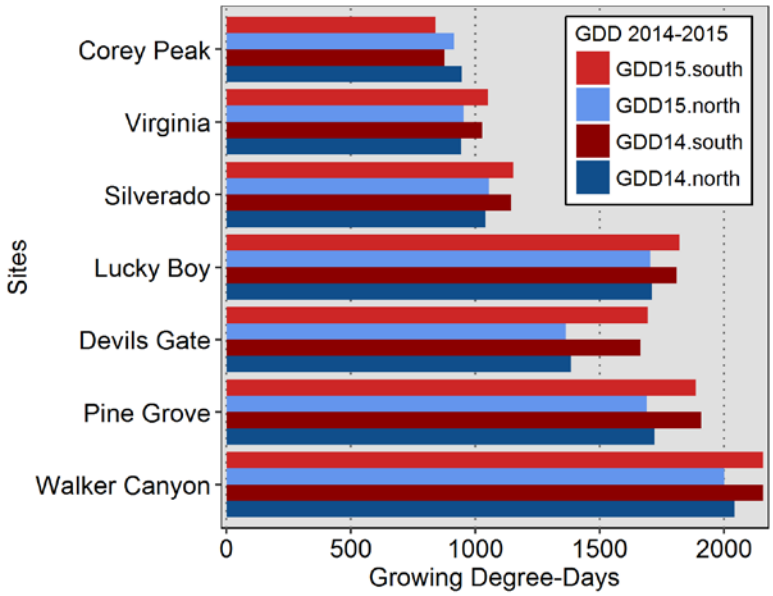

Figure 8: Total growing degree-days.

GDD totaled for the seven site pairs for the interval Jan 1 – Sept 1 in years 2014 and 2015. Site pairs are ordered by elevation, with higher-elevation sites at the top of the chart.

where GDD_{OBS} is observed GDD, T_{MAX} and T_{MIN} are daily maximum and minimum temperature, and T_{BASE} is the base temperature (5°C in this case). If $[(T_{MAX} + T_{MIN})/2] < T_{BASE}$, then $[(T_{MAX} + T_{MIN})/2] = T_{BASE}$. If $[(T_{MAX} + T_{MIN})/2] > T_{BASE}$, then GDD_{OBS} increments positively for the day by the daily mean temperature. Days are cumulatively summed such that any given day in the season is associated with the total "degree-days" above T_{BASE} up to that time.

Although the most accurate measure of daily mean would be to use hourly data or better, the above equation using daily T_{MAX} and T_{MIN} is a commonly applied method when calculating GDD (McMaster and Wilhem 1997). This makes these results comparable to other studies.

It is evident that GDD is closely tied to elevation (Figure 9), but also that there are differences between aspects. First, the relationship between GDD_{OBS} and the same topographic variables that were examined with frost-free days, i.e. elevation (adjusted $r^2 = 0.87$, $p < 0.0001$), TPI (adjusted $r^2 = 0.02$, $p = 0.262$),

DAH (adjusted r^2 = 0.006, p = 0.754), and TRASP (adjusted r^2 = 0.060, p = 0.702) was evaluated across all 16 study sites in the watershed. As might be expected, only elevation proved to have a strong relationship with GDD_{OBS} at the watershed scale (Figure 9).

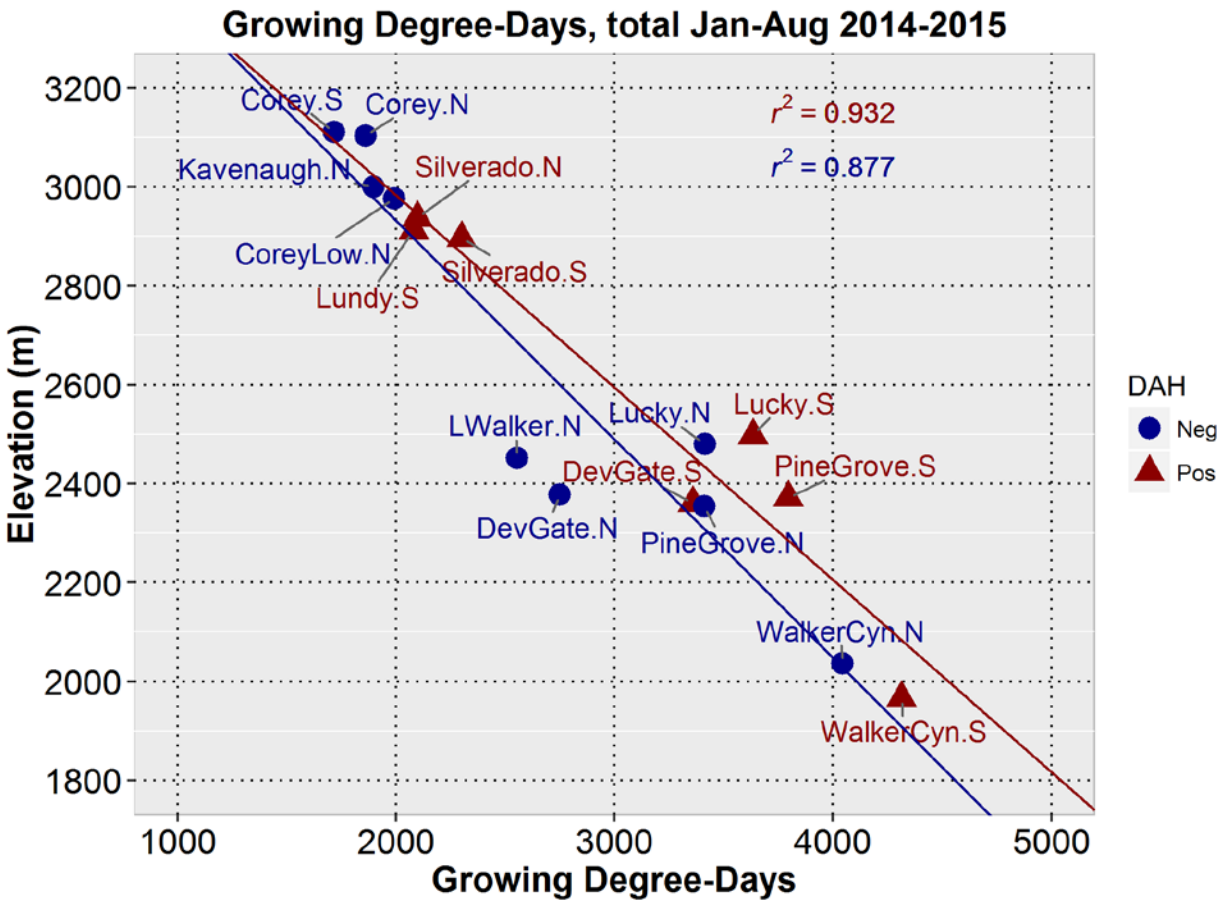

Figure 9: Growing degree-days *versus* elevation.

Total growing degree-days for the years 2014 and 2015 were summed together using the interval January 1 – September 1 in each year, and these overall totals plotted against elevation. The results indicate a tight relationship with elevation across multiple mountain ranges in the Walker Basin, with some horizontal dispersion based on whether the heat loading index DAH is positive (high) or negative (low).

The impact of aspect at the local scale was assessed using the same method as in the FFD analysis. Site pairs were standardized for elevation by using the OLS relationship between elevation and GDD_{OBS} for all sites except the unpaired outlier Little Walker North:

$$GDD_{\mathrm{STD}} = 8733.11 - 2.24Elev$$

where GDD_{STD} is modeled total growing degree-days for Jan–Aug 2014–2015 and *Elev* is elevation in meters. The relationship is significant ($r^2 = 0.917$, $p < 0.0001$). The residuals ($GDD_{RES} = GDD_{OBS} - GDD_{STD}$) were then differenced between the site pairs in a similar fashion to the FFD analysis in order to evaluate the impact of radiative loading on the total GDD for the January–August timeframe from both 2014 and 2015. Figure 9 illustrates the relationship of radiative loading (DAH and TRASP) to GDD, using the calculations $\Delta GDD = GDD_{RES(SOUTH)} - GDD_{RES(NORTH)}$, $\Delta DAH = DAH_{SOUTH} - DAH_{NORTH}$, and $\Delta TRASP = TRASP_{SOUTH} - TRASP_{NORTH}$ for all seven site pairs.

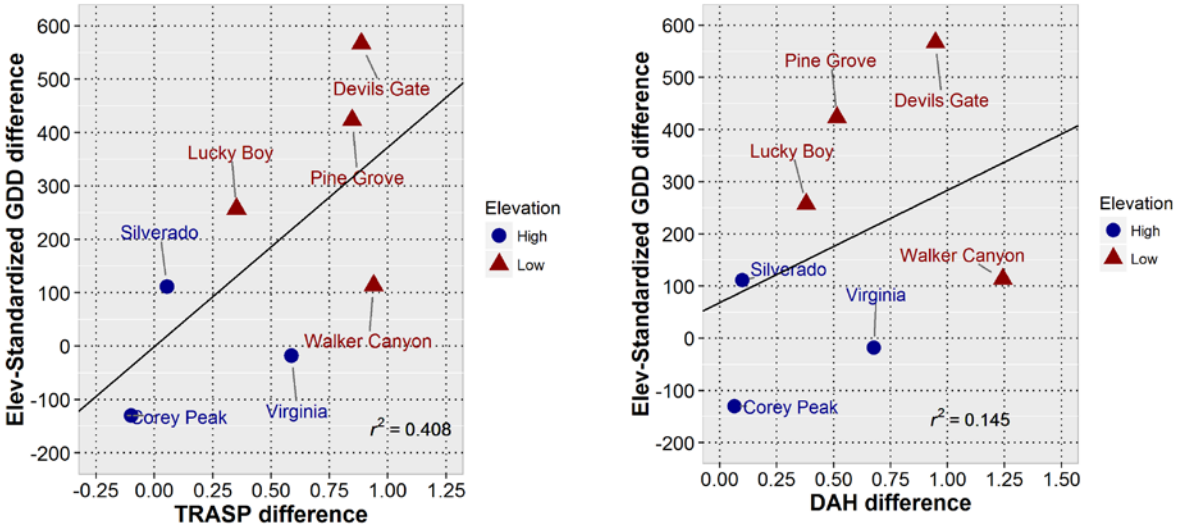

Figure 10: Relationship of degree-days to radiative loading.

The relationship of GDD to aspect-driven radiative loading across the watershed is not statistically significant at high confidence levels using these data, with p-values of p=0.123 (TRASP) and p=0.400 (DAH) when using OLS regression methods to calculate the slopes of the relationships.

All site pairs show departures in the same direction (greater radiation loading = more GDD, lower radiation loading = less GDD), but the relationship is highly variable across geographic space (Figure 10). These results demonstrate that while there is a relationship between radiative loading and thermal sums on open woodland slopes, there are other mechanisms at work that change the nature of the

relationship locally. These mechanisms are most likely related to a combination of site-specific topographic position relative to larger-scale air flow, vegetation canopy shading, and average wind velocity. In addition, the small sample size of seven site pairs, coupled with unequal differences in radiative aspect between sites in each pair, creates significant problems where comparative replication is concerned. While this study was not designed explicitly for this test, a follow-up study could be performed that would probably demonstrate a clearer relationship.

Monthly Means and Lapse Rates

Other measurements of temperature frequently used for climate/landscape/environmental studies are monthly mean maximum and minimum. These assemble daily observations into monthly aggregates, which allow comparisons of data at seasonally-relevant timescales. Accordingly, the daily T_{MAX} and T_{MIN} for each full month of observation from Oct 1 2014 – Sept 1 2015 were aggregated to mean values $TMAX_{MEAN}$ and $TMIN_{MEAN}$ (Figure 11). Some sites show consistent departures in $TMAX_{MEAN}$ between aspects, while others do not. The Pine Grove and Devils Gate pairs, for instance, show excellent differentiation of daily T_{MAX} between north and south aspects across all seasons, despite member sites being in fairly close proximity and at similar elevations.

Overall month-to-month patterns are well-replicated across the watershed. Seasons appear to break down in typical fashion over the two years, i.e. June-July-August (JJA) are the hottest months, September-October-November (SON) and March-April-May (MAM) are transitional months, and December-January-February (DJF) is the coldest season. At most sites, January 2014 stands out as a warm interlude, with both February and March 2014 cooler in comparison. Winter/Spring 2015 appears to be warmer than 2014 between January and April, with a cooler May that transitioned into a hot June and a slightly cooler July. Figure 11 also clearly demonstrates the relationship of temperature to

elevation that was evident in the frost-free days and degree-day analyses, with overall monthly temperatures shifting downwards from lower elevations (e.g. Walker Canyon) to upper elevations (e.g. Corey Peak).

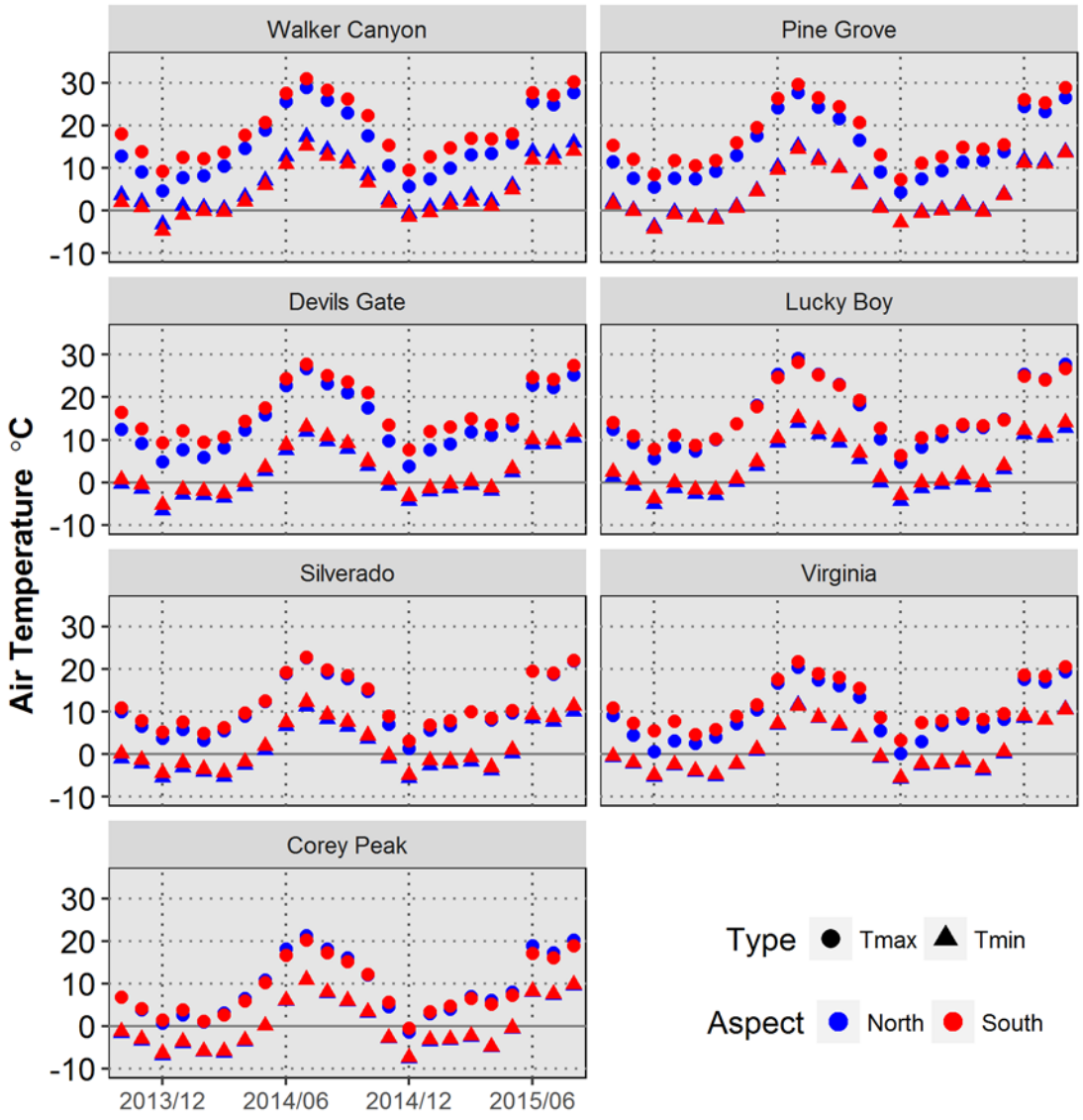

Figure 11: Mean daily T_{MAX} and T_{MIN} by month.

Mean daily T_{MAX} and T_{MIN} are shown for each month during the observation period for each site pair. Some sites show strong departures between aspects, while others do not. Lower elevations (*top four charts*) see similar month-to-month responses as high elevations (*bottom three charts*), but have more spread between mean diurnal extremes.

Table 1.5: Mean daily lapse rates by month and season. Both daytime highs (T_{MAX}) and overnight lows (T_{MIN}) are shown for site groups on north and south aspects. Units are in -°C km^{-1} (all slopes are negative, i.e. temperature decreases with elevation).

	$TMAX_{MEAN}$		$TMIN_{MEAN}$	
Month	**North**	**South**	**North**	**South**
2013/10	6.25	9.95	5.35	3.93
2013/11	6.33	8.87	4.87	3.81
2013/12	6.63	7.90	5.11	4.93
2014/01	6.79	8.65	5.17	3.94
2014/02	7.43	10.05	5.76	4.82
2014/03	7.84	9.90	6.13	5.04
2014/04	8.56	10.72	6.16	5.00
2014/05	9.41	10.79	6.58	5.51
2014/06	9.90	11.48	6.61	4.78
2014/07	9.96	10.99	6.93	5.01
2014/08	9.50	10.95	6.61	5.18
2014/09	8.32	10.35	6.15	5.18
2014/10	6.72	9.67	5.58	4.05
2014/11	6.34	8.86	4.74	4.06
2014/12	6.80	8.75	5.91	5.13
2015/01	6.63	8.87	4.31	3.39
2015/02	6.82	9.22	5.13	3.91
2015/03	6.60	9.50	5.96	4.58
2015/04	8.04	10.60	6.52	5.45
2015/05	8.42	9.80	6.11	5.21
2015/06	8.95	10.58	6.35	4.56
2015/07	8.76	10.66	6.25	4.76
2015/08	9.61	11.28	6.85	5.09
Season				
DJF	6.85	8.91	5.23	4.35
MAM	8.15	10.22	6.24	5.13
JJA	9.45	10.99	6.60	4.90
SON	6.79	9.54	5.34	4.21

The basic inverted relationship between tropospheric air temperature and altitude is a well-established physical fact, but the precise behavior of this lapse rate near the surface in mountainous terrain has been demonstrated to be complex and geographically-dependent (Bolstad et al. 1998; Pepin and Seidel 2005; Minder et al. 2010). Seasonal and diurnal variabilities are known features of lapse rates (e.g. Blandford et al. 2008), and the contribution of topographic aspect to variation in the elevation/temperature relationship has also been partially explored (e.g. Tang and Fang 2006; Dobrowski et al. 2009).

In order to investigate the nature of the monthly-to-seasonal relationship of altitude and diurnal temperature on elevated slopes across the Walker Basin watershed, lapse rates of the monthly values $TMAX_{MEAN}$ and $TMIN_{MEAN}$ were calculated for both northerly and southerly aspects for the seven site pairs. A simple linear regression was used to fit a straight line through the observations ordered by elevation (Figure 12). Table 1.5 shows the resulting lapse rates in units of -°C km^{-1}, as well as the seasonal averages; all slopes are negative, i.e. temperature decreases with elevation. Steeper overall slopes (higher rates of temperature change per unit of elevation) are observed for mean daily T_{MAX} on north and south aspects (7.9°C km^{-1} and 9.9°C km^{-1}, respectively) compared to mean daily T_{MIN} (5.9°C km^{-1} and 4.7°C km^{-1}). Note that most T_{MAX} rates exceed

the standard environmental lapse rate (6.5°C km^{-1}), while the T_{MIN} rates are below or just equal to it. Southerly slopes experience the largest daytime lapse rates but also the smallest nighttime lapse rates across all seasons (Table 1.5). The steeper daytime rates are possibly due to increases in average wind velocity at higher elevation sites relative to lower sites, which would increase near-surface cooling during times of high solar radiation. Seasonal variation is also clearly present. JJA lapse rates for T_{MAX} remain the steepest, averaging 11.0°C km^{-1} on south exposures and 9.5°C km^{-1} on north exposures. Monthly mean T_{MAX} lapse rate changes between the seasons DJF and JJA were 2.6°C km^{-1} and 2.1°C km^{-1} for north and south aspects, respectively. Monthly mean T_{MIN} lapse rate changes between DJF and JJA were 1.4°C km^{-1} and 0.6°C km^{-1} for north and south aspects, respectively (Table 1.5).

The tendency of south slopes to show (slightly) smaller differences in elevational temperature change overnight is possibly a function of low sample size rather than a real phenomenon. The lowest elevation site on a south aspect (Walker Canyon South) has exhibited “cooler” conditions for its elevation when compared to the other lower-elevation woodland sites (i.e. Devils Gate, Pine Grove, and Lucky Boy) in both the frost-free and degree-day analyses, as discussed above. The very low position of this site on lapse rate regression lines could skew the slopes given the sample size (n=7; *bottom point*, *red lines*; Figure 12).

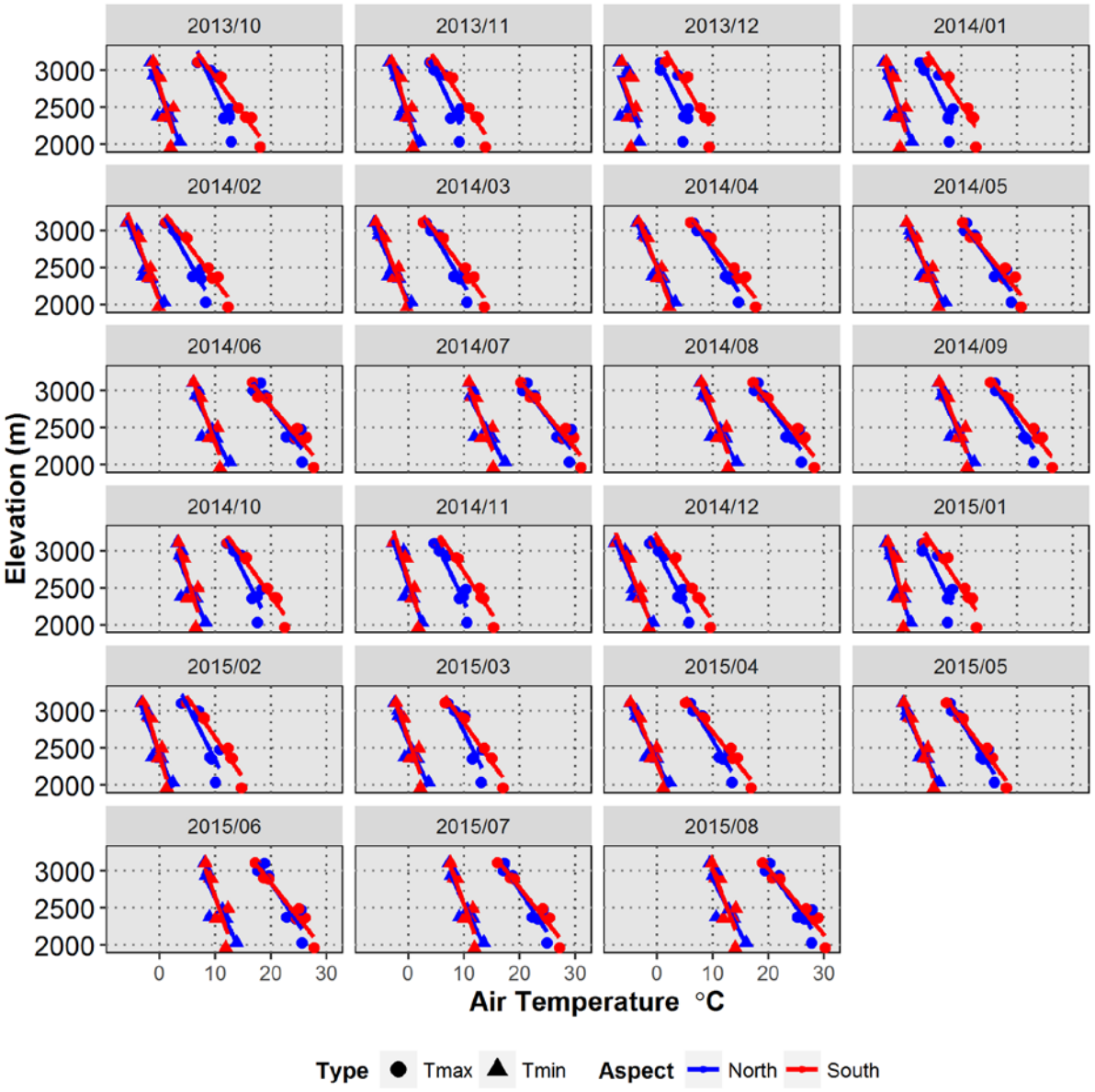

Figure 12: Monthly lapse rates of the mean daily T_{MAX} and T_{MIN} for southerly and northerly exposures.

Discussion on the influence of elevation and aspect on temperatures

Evaluation of the various analyses presented indicates that both elevation and aspect are important topographic controls on the variability of temperature at multiple spatial and temporal scales across a large semi-arid watershed, even when controlling for exposed ridgetops and cold air pools. Study sites

represented opposing aspects in typical open-canopy upper- and lower-elevation Great Basin woodland environments in four adjacent mountain ranges within the watershed, on elevated slopes free from regular cold-air pooling. Study sites were not perfectly controlled for radiative aspect; however, the mean DAH index was 0.01 and TRASP was 0.54, indicating a lack of bias in radiative exposure. Of 16 total sites, 14 were situated in the opposing-aspect configuration at similar elevations and typically within close spatial proximity. Observation methods used (sensor type, shading/shielding, mounting height) replicated "standard" passively-aspirated weather-station measurements over full seasonal cycles.

Frost-free days (FFD), were shown to have a statistically significant relationship with elevation (9.2 days/100 m for the Jan 1 – Sept 1 interval), and a possible secondary relationship with aspect. For example, of the three upper-elevation site pairs, two exhibited increased FFD on nominally south-oriented slopes, while one did not. Ironically, the local radiative aspects of the first two pairs were approximately neutral, whereas the third site pair had a strong difference in GIS-calculated radiative aspects TRASP and DAH (Table 1.4) and thus a counter-intuitive relationship with FFD. Two of the lower-elevation site pairs experienced significant increases in FFD on south slopes, one pair had no differences, and the last pair had greater FFD on the north slope, despite strong differences in radiative aspect (Table 1.4). It is evident therefore that mechanisms are at work other than aspect-controlled insolation. Although all of these sites are located high above cold air dam features and on relatively steep slopes, making them immune to all but the deepest regional inversions (which would affect both sides of a site pair), some sites may be cooled by additional nighttime katabatic airflow or cold-air convection from higher slopes. Qualitative examination of larger-scale siting characteristics indicates this is a possibility, and it is evident that lack of local topographic convergence on elevated slope features may sometimes be negated by large-scale (i.e. > 25 km^2) multi-drainage convergence

Figure 13: Example of large-scale topographic influence.

Despite its location 100 m above the canyon floor (and beyond presumed cold-air pooling), the south-exposed (188°N, Table 1.1; DAH = 0.57, TRASP = 0.96, Table 1.3) site in the Walker Canyon pair (*left*) experiences more elevation-corrected FFD and only moderately more GDD than its north-exposed counterpart (*right*). The most notable difference in large-scale topography surrounding the sites is that the south site is above a drainage which has many times more upstream accumulation area than the north site, increasing the possibility that nighttime katabatic flow affects it, even though it is above the cold "pool".

effects (Figure 13), warranting future investigation of "macrosite" cold air flow patterns in the Walker Basin, similar to the mapping examples of Lundquist et al. (2008).

The frost-free season of 2014 was 1–2 months longer on north and south exposures of the two lowest-elevation site pairs, as well as the south exposures of the higher of the lower-elevation site pairs (Figure 7), which are at similar elevations and close spatial proximity. This indicates that while elevation serves as the ultimate control of transitional-season freezing events on elevated Great Basin slopes (i.e. above cold-air pools), aspect can serve to moderate these events by months even within close spatial

proximity. Last and first frosts of the season were strongly synchronized across all sites, indicating that these were controlled by rapid synoptic-scale events across the watershed.

The second variable of interest, growing degree-days (GDD), was shown to also have a strong relationship with elevation (123 degree-days/100 m for the Jan 1 – Sept 1 interval, T_{BASE} = 5°C). GDD for the Jan 1 – Sept 1 period in both years was very similar (Figure 8). When corrected for elevation and compared at the local scale, GDD also had a weak relationship to aspect-driven radiative loading (Figure 10). In these results as well as the FFD analysis, the site pair at Walker Canyon stands out as having less difference between north and south exposures than expected given the difference in radiative loading. Once again, this points to the mechanisms postulated above (Figure 13).

Finally, monthly means and lapse rates were calculated for both daytime highs and overnight lows. Seasonal behavior of site pairs was described, including replication of month-to-month patterns. The varying dependence of temperature on elevation was evaluated by comparing relative lapse rates of T_{MAX} and T_{MIN} for all site pairs and months, and in each month and season (Table 1.5). No evidence of persistent cold air pools at any of the seven site pairs was found; all sites were located on mid-slopes in similar dominant vegetation types at comparable elevations, and these were remarkably low snow years (Swain 2015), suggesting that these lapse rates are not confounded by cold-air pool locations, exposed ridgetops, canopy cover, or snow influence. Consequently, they serve as a unique observation set in Great Basin woodland and subalpine forest environments and thus provide a new perspective on lapse rates in mountainous terrain.

For example, Dobrowski et al. (2009) compared existing weather station data from the mountains around Lake Tahoe, California very near the Walker Basin. Their study focused on the behavior of near-surface temperature observations relative to modeled estimates of free-atmosphere conditions. Sites

used in the study (*n*=16) had little variation in radiative loading, and were frequently impacted by cold-air pools. The authors concluded that they were only able to observe true environmental lapse rates (at the monthly scale) during the springtime when the boundary layer was well-mixed all the way to the surface, whereas the present study observes environmental lapse rates across all seasons and for sites with both high and low irradiance values. Blandford et al. (2008) compared publically available weather station lapse rates to synoptic patterns in a mountain region in south-central Idaho, with a study area of similar size to the Walker Basin, and similar number of data points (*n*=14). Many of these stations were located on flat topography associated with coniferous forest, and results suggested minimal variability in lapse rates as a result of topographic characteristics other than elevation.

Some studies have deployed temperature microloggers in order to bypass the problems of historic station siting bias when measuring lapse rates. Tang and Fang (2006) did so in China's Qinling Mountains, running one ~25 km transect of 14 sites over a mountain for one year. Their sites were in a wet subtropical climate zone, and therefore were all located within nearly closed canopy forests. Results from their work showed much lower lapse rates for the generally north (~3–6°C km^{-1}) and south (~2–4°C km^{-1}) aspects of Mt. Taibai across all seasons. In this study, actual instrument locations are not described as being controlled for local aspect, but only for the general slopes of the mountain in question. In the Minder et al. (2010) study, a combination of historic weather stations and temporary microloggers was used. However, their study was also in a forested, mesic environment, and additionally did not rely on standardized radiation shielding or deployment height (due to snow) for the micrologger deployments, thus introducing additional uncertainty into the measurements. Siting control for local topography and cold-air flow is unreported in their study, making interpretation of results difficult. Minder et al. (2010) also did not break down micrologger lapse rates by local aspect or diurnal maxima and minima, and only report the annual mean for one year (4.7°C km^{-1}).

Although my study reports monthly lapse rates which are quite steep compared the majority of examples listed above, meeting or exceeding the dry adiabatic rate (9.8°C km^{-1}), particularly on southerly aspects in the warmer months, these kinds of values have been reported for Great Basin mountains before (LaMarche Jr. 1973), as well as in other dry continental mountainous areas (Lundquist et al. 2008).

In conclusion, thermal regimes on typical Great Basin elevated open-canopy woodland slopes were examined across multiple mountain ranges in a large watershed for the influence of elevation and topographic aspect on processes ranging from fine-scale dependence (frost-free season) to broad-scale applicability (seasonal whole-watershed lapse rates), with a focus on eliminating the influence of small-scale inversions and cold-air pools. Relationships of these important topographic variables to these processes were described and quantified within the constraints of the observation period and geographic study design. While all of these topographic/temperature relationships are expressed as linear in nature, it is quite likely that given sufficient sample size and replication across topographic controls, non-linear relationships would emerge, and interactions between other topographic variables would become clearer. Also, because only two seasonal cycles were observed, and both were considered significant drought years that resulted in regionally higher temperatures, extrapolations of these relationships to other regions and climatic settings should be made with caution.

Testing the PRISM daily air temperature gridded product

Because near-surface air temperature in mountain terrain is rarely observed directly, scientists performing landscape-scale analyses often use interpolated models of this and other climatic variables as a substitute for *in-situ* data. Perhaps the most prevalent of these models in the western United States is the gridded PRISM (Parameter-elevation Regression on Independent Slopes Model [*Daly et al.*, 2008])

dataset, which was developed initially in 1991 as an automated way to “map” climate onto the landscape using existing point data (Daly et al. 1994). PRISM has been in development ever since, with a special emphasis on complex terrain and regional climate patterns. Monthly time series of PRISM temperature and precipitation have been publically available at 4 x 4 km resolution for some time, with sub-km spatial resolution products also available on a case-by-case basis. These data have been leveraged for a wide body of scientific work, with examples ranging from ecology (Jacobs et al. 2008; Wiens et al. 2009; Horning et al. 2010; Johnson et al. 2010; Millar and Westfall 2010; Williams et al. 2010) to regional climate (Diaz and Eischeid 2007; McGuire et al. 2012), hydrology (Hamlet et al. 2005; Lundquist, Neiman, et al. 2008; Pederson et al. 2013), palaeo studies (Birkel et al. 2012; Salzer et al. 2014; Saito et al. 2014; Hatchett et al. 2015), topoclimate (Daly et al. 2007; Minder et al. 2010), and even the development of other interpolated climate products (Wang et al. 2006; Hofstra et al. 2009; Rollinson and Kaye 2015). These are just a small sample of the published studies in the literature that have used PRISM as a substitute for *in-situ* climate monitoring observations. Daily time-step data are now available from the PRISM group in response to needs in agriculture and the general trend in scientific fields to improve temporal resolution in process modeling. PRISM offers advantages to local observations in that it has a long temporal coverage (i.e. 1895 to present, depending on the dataset) and mitigates temporary gaps in point data which are common in historical records. Uncertainty in interpolated models varies by geography (e.g. Stoklosa et al. 2015), but is rarely reported in use cases. Direct validation by making observations is often impractical given budget constraints. Because scientific results using PRISM are often presented in the context of projected climate warming (< 10°C), testing the local accuracy of the model in regions and landscapes where error is likely to be greater can give scientists and managers a first-order idea of whether or not their interpretations have additional uncertainty or may even be incorrect.

I collaborated with Dr. Christopher Daly from the PRISM group to perform a case study of topographic temperature model testing using the 16 mountain slope study sites in the Walker Basin. Daily maximum (T_{MAX}) and minimum (T_{MIN}) air temperature estimations from PRISM 30-arc-second (~ 800 m), downscaled 3-arc-second (~80 m), and point-interpolated products were compared to *in-situ* observations to test PRISM for accuracy and to evaluate possible instrumental, topographic, or mechanistic sources of error. In addition, the impacts of model error on examples of ecohydrologic parameters were also explored. The results indicate that PRISM temperatures are generally representative of daily change in observed conditions on semi-arid mountain slopes, but that absolute bias caused by a combination of factors can be significant.

PRISM data and differences from observations

The PRISM Climate Group provided estimates of daily T_{MAX} and T_{MIN} (in °C) for each study site in the Walker Basin (Figure 2; Table 1.1) for nearly two water years (1 Oct 2013 – 1 Sept 2015) at three spatial scales: standard 30 arc-second (~800 m) gridded outputs ($PRISM_{800}$); point-interpolated estimates ($PRISM_{POINT}$); and downscaled 3 arc-second (~80 m) gridded estimates ($PRISM_{80}$) using the PRISM engine on higher-resolution terrain data for the watershed. By generating output at multiple scales, sensitivities of PRISM-derived ecoclimatic estimates to spatial scale in complex terrain were also tested.

Errors in model estimates were calculated using the differences from iButton thermochron observations ($PRISM_{800}$ - *Obs*) for daily T_{MAX} and T_{MIN}. Initial plots of the warm and cool season distributions indicate systematic departures (Figure 14). PRISM underestimates daily T_{MAX} by an average of -1.09°C over all sites and seasons, but the mean bias is close to zero during the winter. Daily T_{MIN} is consistently underestimated (mean = -2.39°C) during all seasons. Across the 16 sites, daily T_{MAX} mean absolute error (MAE) ranged from 1.19–3.75°C, error standard deviation (SD) ranged from 1.30–2.42, r^2 values for the

fit between observations and the model ranged from 0.92–0.97 ($p < 0.001$), and mean bias ranged from -3.73–1.23°C (Table 1.6). The same statistics for daily T_{MIN} have similar ranges; i.e. MAE (1.42–4.10°C), error SD (1.63–2.21), r^2 values [0.91–0.95, ($p < 0.001$)], and overall bias [-4.05–(-0.67°C)] are estimated by PRISM with the same order of accuracy as daily T_{MAX}. Error statistics between T_{MAX} and T_{MIN} at each site are not always similar, suggesting that underlying causes of the model departures may be different for T_{MAX} and T_{MIN}.

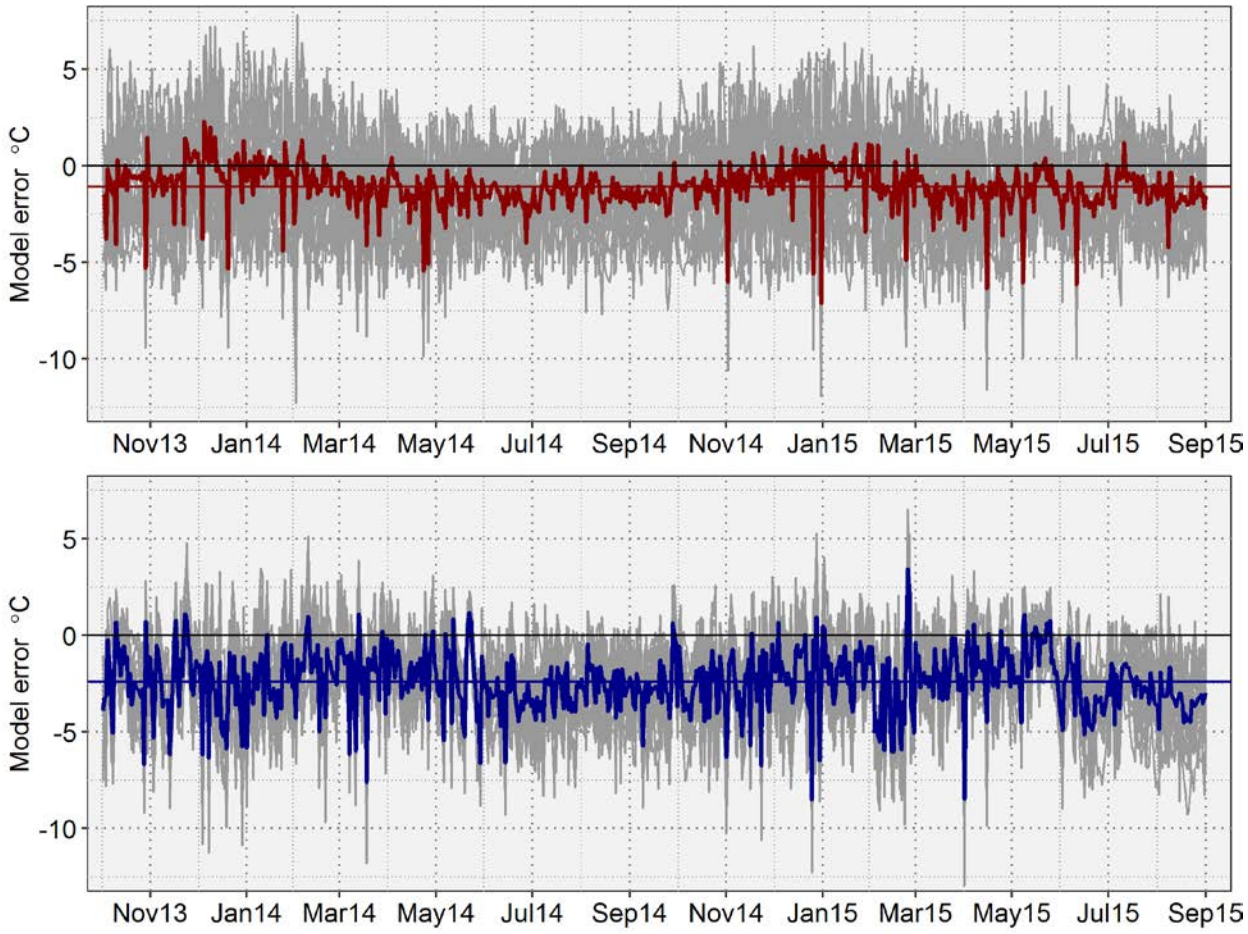

Figure 14: *PRISM - Observations* departures.

Daily model departures (*PRISM*$_{800}$ – *Observations; gray*) for October 2013 – September 2015. Daily T_{MAX} departures are averaged between all 16 sites (top, *red*), with visible seasonal variability and overall slight negative bias. Daily T_{MIN} averages for all sites (bottom, *blue*) show stronger negative bias and a less-pronounced seasonal variation in error.

Table 1.6: PRISM error statistics.
Color shading indicates error groups that resulted from an independent ordination and cluster analysis, shown later in the text and in Figure 16.

***PRISM*$_{800}$ Error Statistics, Daily Values Oct 2013 – Sept 2015**

	T_{MAX} °C				T_{MIN} °C			
Site	**Bias**	**MAE**	**SD**	**r^2 ($p < 0.001$)**	**Bias**	**MAE**	**SD**	**r^2 ($p < 0.0001$)**
Lucky.N	-1.79	2.16	2.05	0.95	-1.46	2.07	2.12	0.92
Lucky.S	-3.71	3.75	1.70	0.95	-3.38	3.44	1.97	0.93
DevGate.N	0.43	1.19	1.51	0.97	-2.63	2.69	1.64	0.94
DevGate.S	-3.73	3.73	1.30	0.97	-3.78	3.80	1.79	0.93
CoreyLow.N	0.37	1.80	2.24	0.93	-1.66	1.90	1.63	0.95
Corey.N	0.45	1.95	2.42	0.92	-0.67	1.42	1.67	0.95
Corey.S	0.65	1.45	1.70	0.95	-1.28	1.75	1.72	0.95
LWalker.N	-2.02	2.13	1.41	0.97	-1.45	1.68	1.94	0.91
Silverado.S	-1.39	1.58	1.31	0.97	-3.08	3.16	1.81	0.94
Silverado.N	-1.43	1.80	1.70	0.96	-2.39	2.48	1.81	0.93
PineGrove.N	-0.60	1.77	2.16	0.94	-3.00	3.07	1.83	0.94
PineGrove.S	-3.48	3.54	1.76	0.96	-2.67	2.75	1.88	0.93
Kavenaugh.N	0.62	1.59	1.89	0.94	-1.69	2.19	2.08	0.91
Lundy.S	-0.63	1.48	1.72	0.94	-1.65	2.09	2.03	0.91
WalkerCyn.N	1.23	1.87	2.19	0.94	-4.05	4.10	2.17	0.92
WalkerCyn.S	-2.36	2.52	1.84	0.95	-3.36	3.42	2.21	0.91
Averages								
Overall	-1.09	2.14	1.81	0.95	-2.39	2.62	1.89	0.93
T_{MAX} Group 1	-2.11	2.44	1.69	0.96	-2.62	2.79	1.94	0.93
T_{MAX} Group 2	0.63	1.64	1.99	0.94	-1.99	2.34	1.82	0.94
T_{MIN} Group 1	-0.47	1.79	1.89	0.94	-1.53	1.95	1.88	0.93
T_{MIN} Group 2	-1.70	2.49	1.72	0.96	-3.24	3.30	1.91	0.93

Potential model error sources

Several factors could contribute to the biases in PRISM daily T_{MAX} and T_{MIN}; therefore each potential source of error was investigated: 1) observational methods; 2) model scale; and 3) model processes related to source data and topography.

Accuracy of deployed sensors

Testing of the iButton/Gill shield deployment is described above and rules out the observational methods as a likely source of bias (Figure 4). Two separate sensor types were compared to the iButton system as deployed in this study, and the iButton measurements compare closely with both. The 25th and 75th percentiles of the iButton error are within the ±0.6°C factory error range of the Campbell HMP-60 temperature probe. Comparisons of both the iButton and Campbell probe to a Type-T thermocouple wire show a low bias for T_{MIN} and a high bias for T_{MAX}, which, given the low thermal mass of the thermocouple wire compared to conventional air temperature measurement instruments makes sense.

Scaling Test

Because most of the sites are located on steep slopes, model scale could be an important source of error. Daily PRISM T_{MAX} and T_{MIN} at three different model scales (*PRISM*$_{800}$, *PRISM*$_{POINT}$, and *PRISM*$_{80}$) were compared to observations. No systematic shifts were observed in model bias, error standard deviations, or correlation with observations by changing model scale (Figure 15). This indicates that model departures from observations are, on average, not tied to scalar issues, even in very steep topography.

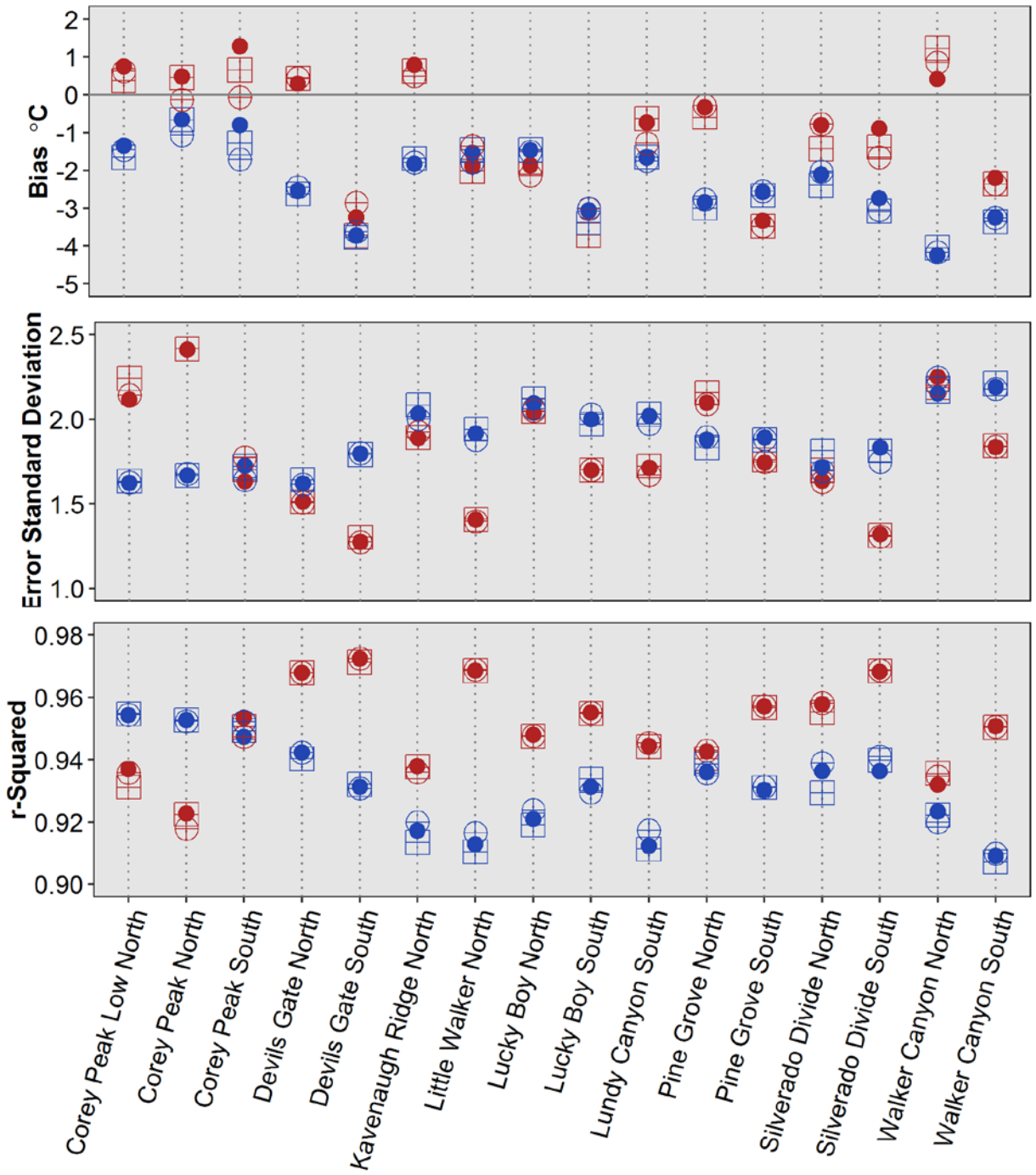

Figure 15: PRISM scaling statistics.

Tests of PRISM scale compared error statistics from the standard 800 m grid product ($PRISM_{800}$; *squares*) with point interpolations ($PRISM_{POINT}$; *solid dots*) and downscaled 80 m grids ($PRISM_{80}$; *open circles*) across all 16 sites.

Topographic variables: cluster analysis and ordination

The PRISM temperature interpolation algorithm relies heavily on statistical relationships between air temperature and physiography to make spatially explicit predictions. Depending on the topographic representativeness of regional weather station sites that contribute to PRISM, as well as calibration of the adaptive portions of the model itself, it is possible that specific topographic features could contribute more to model error than others. To explore this hypothesis, several topographic characteristics for each site were used in an ordination and cluster analysis of PRISM error [Table 1.2 and accompanying text; Table 1.7; (Guisan et al. 1999; Riley et al. 1999; Böhner and Antonić 2009)].

Table 1.7: Topographic variables and relationships to PRISM error.

Variable	Description	T_{MAX} Significance		T_{MIN} Significance		Reference
		r^2	p	r^2	p	
Elev	Elevation of 10 m DEM	0.156	0.334	**0.847**	**0.001**	
Slope	Slope steepness	0.352	0.064	0.135	0.381	
Asp	Aspect, degrees	0.019	0.884	0.291	0.100	
TPI	Topographic Position Index	**0.520**	**0.004**	0.078	0.611	Guisan et al. 1999
TRI	Terrain Ruggedness Index	0.378	0.053	0.132	0.389	Riley et al. 1999
DAH	Diurnal Anisotropic Heating Index	**0.791**	**0.001**	0.013	0.916	
StdH	Standardized Height	0.158	0.328	**0.517**	**0.009**	Böhner and Antonić 2009; Böhner and Selige 2006
SlopH	Slope Height	0.167	0.304	0.367	0.046	
NormH	Normalized Height	0.288	0.116	0.222	0.187	
MSP	Mid-Slope Position	0.362	0.053	0.311	0.089	
VllyD	Valley Depth	**0.526**	**0.006**	0.010	0.946	
TRASP	Topographic Radiation Index	**0.811**	**0.001**	0.028	0.832	Roberts and Cooper 1989

Hierarchical clustering with the Ward2 minimal-variance implementation (Murtagh and Legendre 2014) was used first to group sites by similar error characteristics based on Euclidean distance calculations. Two distinct groups existed for both daily T_{MAX} and T_{MIN} errors based on evaluation of silhouette plots generated using the same Euclidean distance calculations (Rousseeuw 1987). These groups were not identical in terms of their member sites (Figure 16, bottom cluster plots).

To assess interaction and significance of the topographic indices (which are not independent variables), each site's T_{MAX} and T_{MIN} errors were evaluated in two-dimension ordination space by using non-metric multidimensional scaling (NMDS; Oksanen et al. 2015). NMDS is an ordination method which allows comparison of pairwise dissimilarities between variables in low-dimensional space using rank-based correlation (as opposed to linear correlation methods used in principal components analysis or principal coordinates analysis). It accommodates variables with unknown distributions and removes unit distances (losing the absolute magnitude of ordination distance but retaining relative positions of variables). In this manner, topographic variables that are physiographically related but are associated with different atmospheric mechanisms can still be evaluated and grouped for relative influence on PRISM error in the same dimensional space. This aids in interpretation of topoclimatic mechanisms which may influence PRISM error, such as insolation or large-scale convergence.

NMDS is an iterative algorithm which requires successive ordinations (beginning with a randomized placement within *n* dimensions specified) to be compared to actual pairwise dissimilarities until the difference between the two ("stress") is minimized. Stress values of 0.1 or below are considered fair ordination fits. Stress plots of ordination runs for the topographic and PRISM error data indicated that two dimensions were acceptable (Appendix 1). NMDS results using the package *vegan* (Oksanen et al. 2015) with the open-source R software (R Development Core Team 2015) for T_{MAX} PRISM error were as follows: non-metric $R^2 = 0.999$, stress = 0.037, indicating an excellent fit using Euclidean distances as in the cluster analysis. NMDS ordination of T_{MIN} PRISM error resulted in a non-metric $R^2 = 0.993$, with stress = 0.086, a "fair" fit. We can interpret this as T_{MAX} PRISM error having a reasonably strong association with some individual or more likely, groups, of topographic variables that influence error more on some sites than others. T_{MIN} error, on the other hand, may not be as strongly associated with distinct topographic features. Vectors for each topographic variable were fit to the T_{MAX} and T_{MIN} error

ordinations as representations of predictor significance using the *envfit* function in the R package *vegan*, aiding interpretation of the NMDS results (Figure 16, top ordination plots).

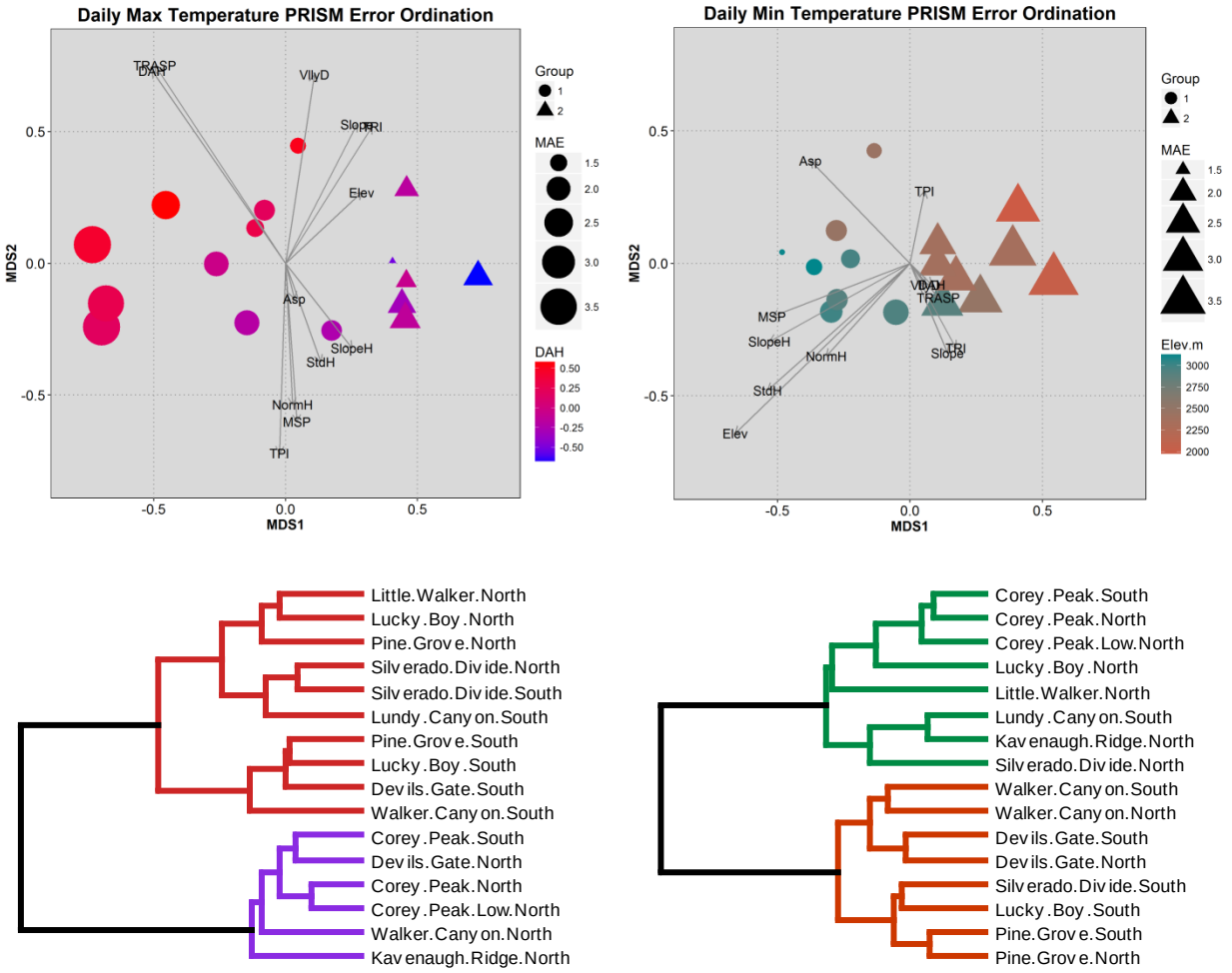

Figure 16: Ordination & cluster plots from topographic variable analysis.

Results from cluster analysis are plotted for T_{MAX} (bottom left) and T_{MIN} (bottom right), indicating which site error chacteristics are more related to each other. For T_{MAX}, cluster groups are partitioned by aspect/radiative exposure as well as elevation. For T_{MIN}, sites are clustered by a combination of elevation and geographic location (not a test parameter). Ordination of PRISM error on each site from NMDS is plotted in two dimensions for T_{MAX} (top left) and T_{MIN} (top right), indicating site relationships to topographic variable vectors (*arrows*) and significance (*arrow length*), as well as site MAE (*symbol size*), cluster group (*symbol type*), and most significant variable (*symbol color*). Clearly, the topographic characteristics of the sites are not independent, and gradients of MAE and clusters do not align directly with any one variable. However, this serves as a visualization tool to aid interpretation of cluster partitioning as well as significance of DAH and Elevation for T_{MAX} and T_{MIN} respectively.

Variables that were significantly associated with PRISM T_{MAX} error (tested using randomized permutations n = 999 in the package *vegan*, Table 1.7) were the indices DAH (r^2 = 0.791, p = 0.001), TRASP (r^2 = 0.811, p = 0.001), VllyD (r^2 = 0.526, p = 0.006) and TPI (r^2 = 0.520, p = 0.004). Because DAH and TRASP are closely related surface heat-loading factors, and VllyD and TPI are both measures of local prominence, we can associate these topographic features with the amount of hillslope directly associated with the study sites absorbing, reflecting, and re-radiating heat during the daytime. Using the same tests, PRISM T_{MIN} error was most strongly associated with elevation (r^2 = 0.847, p = 0.001), and standardized height (r^2 = 0.517, p = 0.009). These topographic factors, per-site MAE, and cluster groups are visualized in ordination plots (Figure 16). These results indicate that the mechanisms associated with PRISM departures from observations are tied to real processes associated with geographic location and topography.

Impacts to estimates of ecohydrologic variables

In order to evaluate effects of model error on ecohydrologic variables commonly calculated from temperature data, three use cases were examined.

2014 frost-free season

The 2014 frost-free season (FF14; the period between the last spring and first autumn frosts) was calculated using both the observed data and the model outputs. PRISM correctly captured the last and first frosts of FF14 at 12 of 16 sites (Figure 17). In only one case did the $PRISM_{80}$ and $PRISM_{POINT}$ downscaled data improve the FF14 estimate.

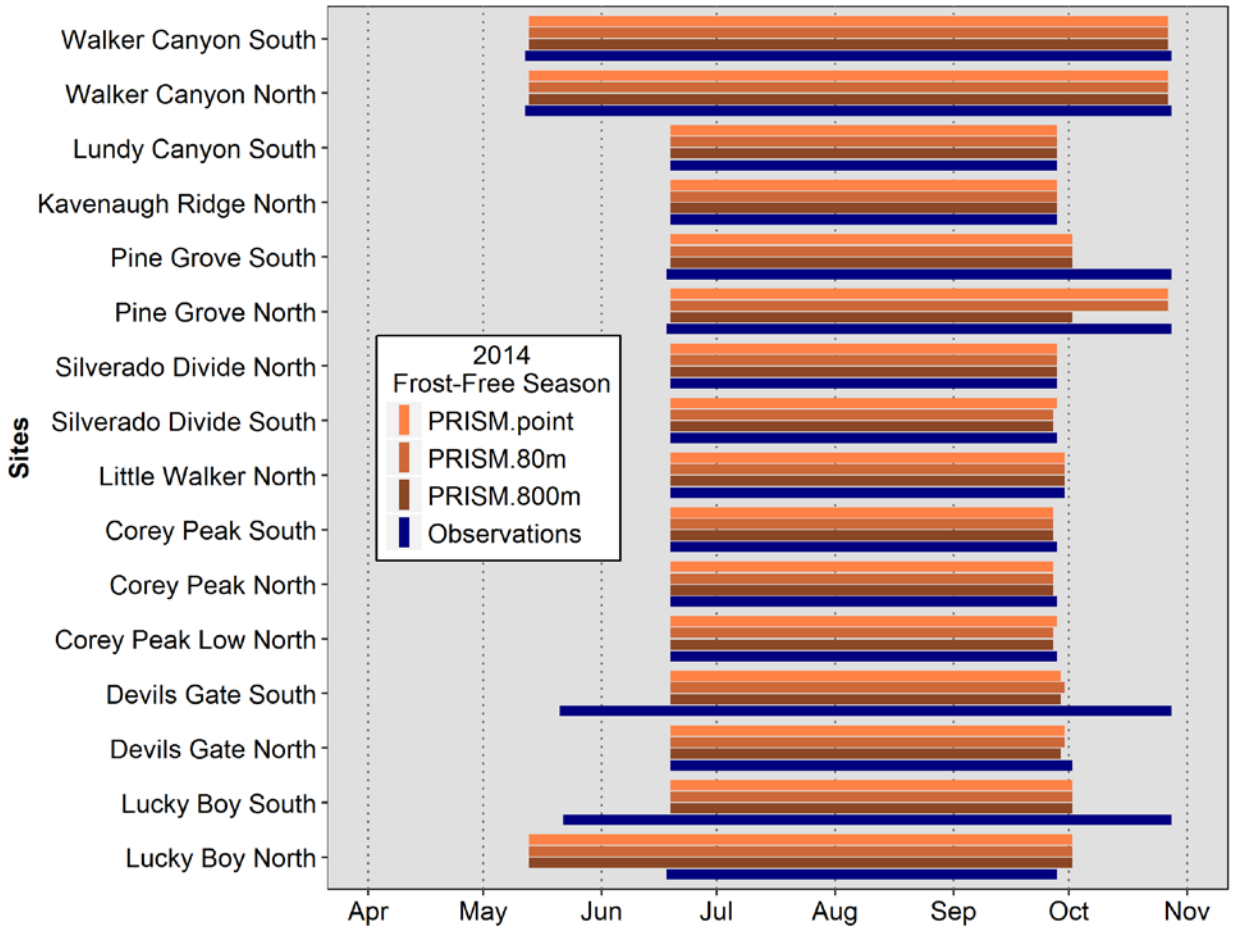

Figure 17: The observed 2014 frost-free season and PRISM estimates of the same.

Precipitation as snow

The fraction of precipitation falling as snow (P_{SNOW}) was estimated using the following empirical model of frozen/liquid fractions developed in a previous study of high-resolution meteorological data across a mountain watershed (Daly et al. 2007):

$$P_s = -0.1667T_m + 0.6667, 0 \leq P_s \leq 1,$$

where P_s is the proportion of daily precipitation as snowfall and T_m is the daily mean temperature in degrees Celsius. If T_m is -2.5°C or less, P_s = 1, and if T_m is 4°C or above, P_s = 0.

Precipitation values from the daily PRISM 30 arc-second precipitation product were obtained for all 16 study sites and then partitioned according to this relationship with air temperature. Although this snow-fraction model was developed in a different climatological region than the Walker Basin, given that this is strictly a test of relative estimates between observed temperatures and PRISM, using it in this scenario is not problematic.

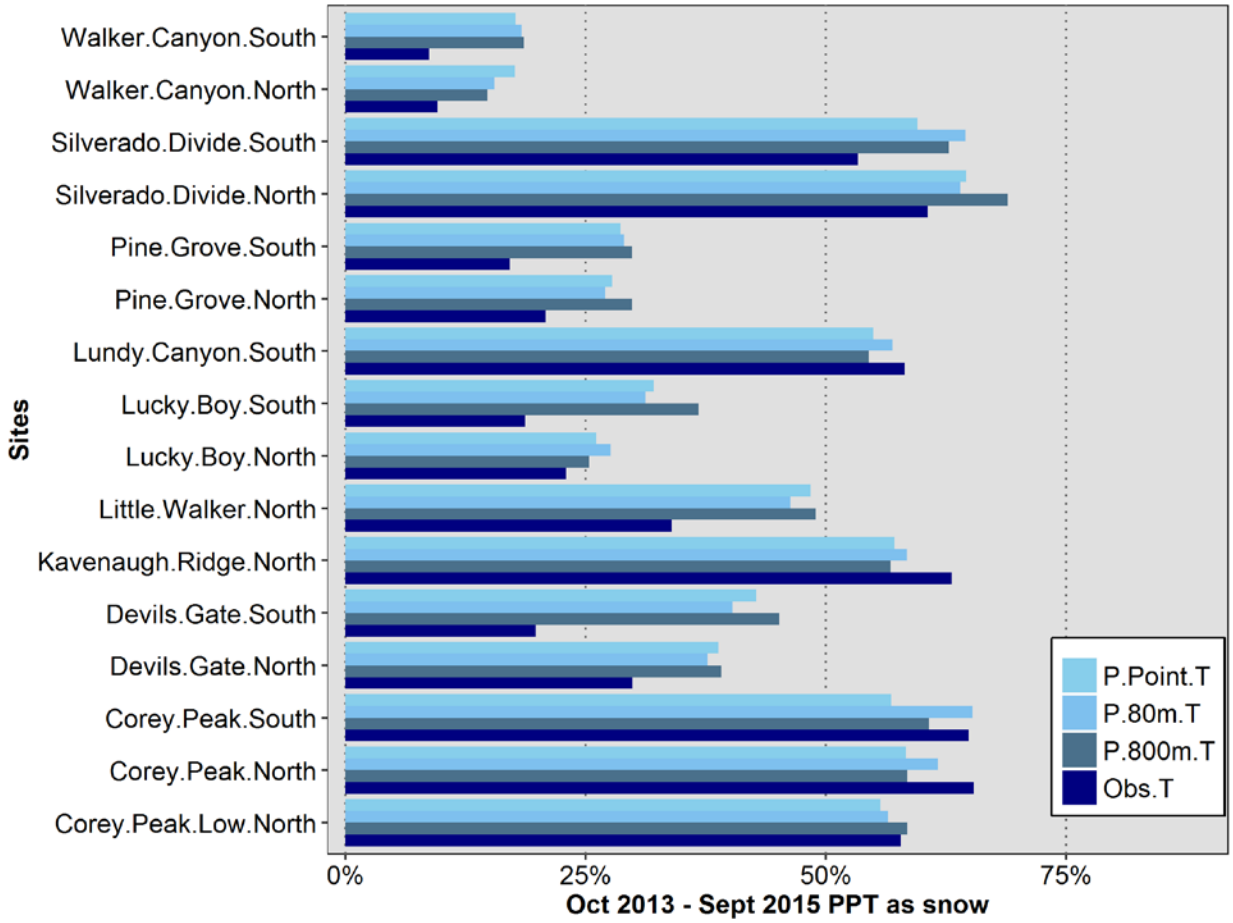

Figure 18: Testing precipitation as snow.

The fraction of precipitation falling as snow was estimated by using PRISM precipitation values for each site and applying the observed temperatures as well as PRISM-estimated temperatures to partition the phases.

Figure 19: Testing growing degree-days.

Three spatial scales of PRISM daily data as well as observations are used to estimate thermal sums on the study sites. In this case, growing degree-days (base = 5°C) are shown for Jan – Sept seasons in years 2014 (top) and 2015 (bottom). GDD5 or thermal sums of similar types are often incorporated in ecological niche and snowmelt models.

PRISM's estimates of P_{SNOW} were similar to observation-driven estimates across many of the sites (Figure 18). However, in general P_{SNOW} was overestimated by PRISM and the relative fraction of this error is substantially higher at lower-elevation sites. Increasing the resolution of the PRISM model did not noticeably improve the accuracy of P_{SNOW} estimates.

2014 and 2015 heat sums

Growing degree-days (GDD) for the intervals Jan 1 – Sept 1 in both years were compared between the observations and model outputs. As expected given the consistent cool bias in both T_{MAX} and T_{MIN}, PRISM underestimated GDD at all sites in both years (Figure 19). Once again, model scale had little to no impact on accuracy of estimates. Most of the sites experienced between 200 and 400 more degree-days in each year than estimated by PRISM. These differences would be significant for both snowmelt and plant growth applications of the data.

Summary and discussion on PRISM error, SNOTEL, and ecohydrological impacts

Consistently high r^2 values at all sites between observations and PRISM temperatures from the daily 30 arc-second product demonstrate that the model approximates day-to-day temperature variability in open woodland environments well, and that the response of the model to changing atmospheric conditions at the watershed scale is generally correct (Table 1.6). The most notable error for PRISM on these study sites is a cool bias in daily T_{MAX} at 10 of 16 sites and T_{MIN} at all 16. Surprisingly, changing model scale by an order of magnitude had no consistent effect on results. Relationships to site topography and different cluster populations for T_{MAX} and T_{MIN} instead suggest mechanistic sources of model departures.

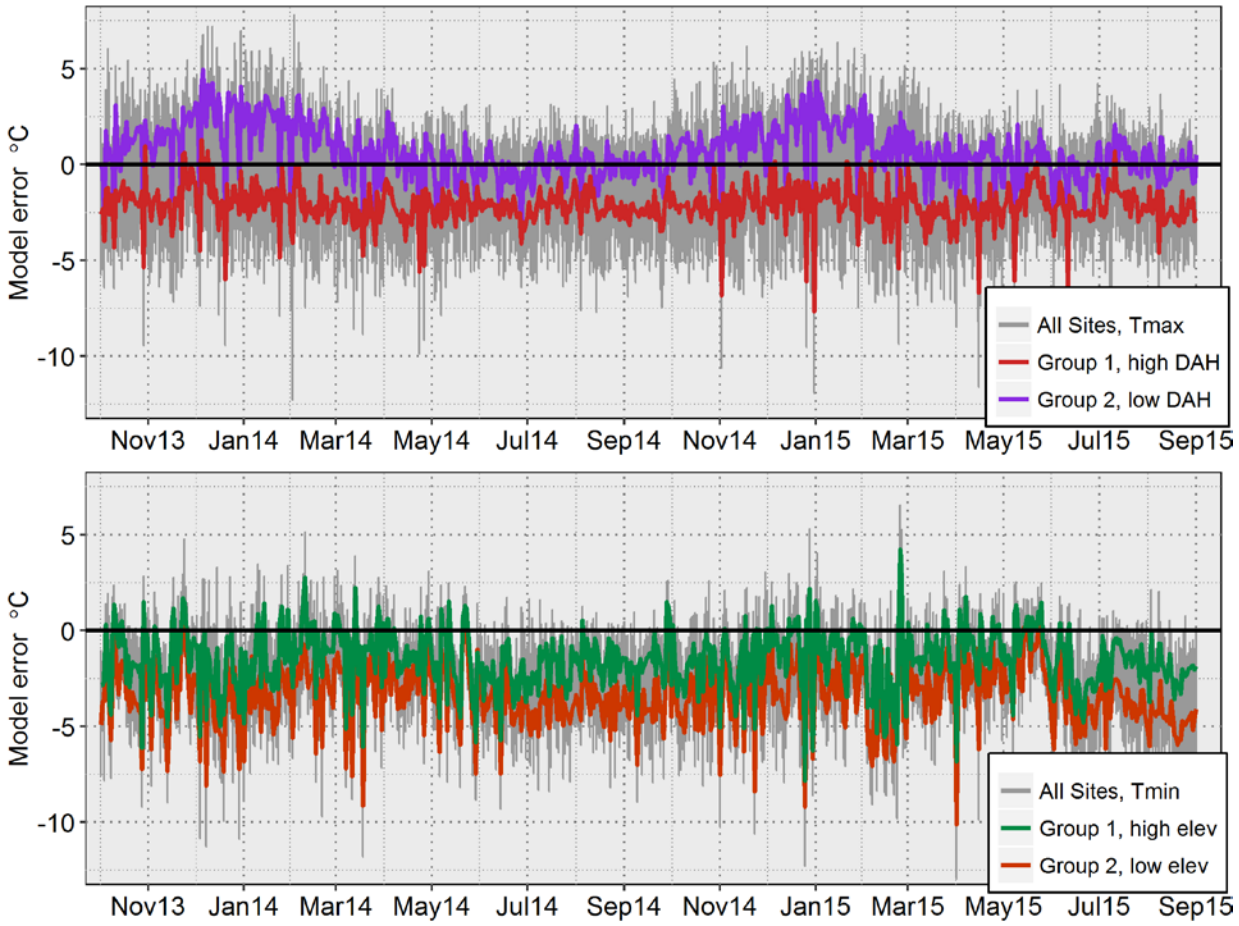

Figure 20: Model departures (*PRISM*$_{800}$ - *Observations*) with separate cluster means.

PRISM daily T_{MAX} errors are shown for all 16 sites (*gray*) with means for cluster groups 1 & 2 (top). Behavior of these clusters is visually quite different in terms of absolute and seasonal bias. This result is strongly aligned with the association of radiative loading indices with T_{MAX} error (seasons with lower sun angle result in greater relative departure, including wintertime overestimation of T_{MAX} at sites with less incident radiation). Daily T_{MIN} error cluster groups (bottom) do not show terribly different behavior, and are differentiated only by a mean bias offset. This result would agree with a spatial or elevational bias in the model given the locations and types of source data stations in the watershed.

Topographic Mechanisms of Error

Diurnal radiation loading is associated strongly with modes of model error in estimating true daily T_{MAX} on open woodland mountain slopes, followed secondarily by relative topographic position (Table 1.7). This means that daytime heating of the ground surface and associated reflection and re-radiation of energy into the near-surface air is operating in a way on the study sites which is not accurately reflected in the PRISM source data or the model's topographic adjustments. It is possible that incorrect

assumptions of local lapse rates confound this error, but the ordination results point to a strong contribution of heat-loading as opposed strictly to elevation (Figure 16). T_{MAX} is consistently underestimated at sites in Group 1 which have high DAH/TRASP values (Figure 20, *top*), whereas T_{MAX} is overestimated in winter and reasonably accurate in summer at sites within Group 2 (Figure 20, *bottom*). These groups are primarily split between sites with high and low radiative loading (DAH/TRASP; Table 1.6), and PRISM's treatment of these groups during the cool season approaches 5°C error on average (Figure 20). The relationship between daily temperature extremes and incident solar radiation is well known (Bristow and Campbell 1984; Thornton and Running 1999), and the interactions of radiation with geography, land cover, slope, and aspect have also been explored in the context of complex terrain (McCutchan and Fox 1986; Bolstad et al. 1998; McCune and Keon 2002; Bennie et al. 2008). These mechanisms can be applied in gridded models with local calibration data obtained at relatively high spatial resolution (e.g. *Daly et al.*, 2007; *Holden et al.*, 2015), and it is clear that the kinds of mountain slopes represented in this study require specific study for calibration and ultimately should be treated differently in the model.

In the case of T_{MIN} departures, there is no consistent seasonal pattern; rather, PRISM has a cool bias in T_{MIN} at all sites regardless of cluster group or season. There were no significant topographic factors associated with these errors besides elevation (Table 1.7). There are almost no regional PRISM source stations in sites that minimize cold-air pooling in the same way that the study sites do (Figure 2). Valley-bottom decoupling from upper air during stable nighttime conditions is a notable feature of Great Basin topography, and cold-air pools at both large and small scales have been documented as regularly-occurring events in the region (Billings 1954; Wells and Shields 1964; Wells 1983; Dobrowski et al. 2009). Cold-air pooling in general remains a challenge for temperature modeling in mountain environments, given that the frequency and depth of pools is dependent on regional climatology, local airflow

responses, and seasonal surface-atmospheric energy exchanges of individual watersheds (e.g. Whiteman 1982; Bell and Bosart 1988; Lundquist et al. 2008; Daly et al. 2010; Lareau and Horel 2014; Holden et al. 2015). Thus, PRISM's estimates of T_{MIN} on open slopes are most likely contaminated by the impact of cold-air pooling around the mostly valley-bottom stations that contribute to the model.

SNOTEL and PRISM in the Walker Basin

A common source of upper-elevation data for PRISM in the western U.S. is the SNOTEL network. The Walker Basin is no exception – there are eight SNOTEL stations within or nearby the watershed, and these dominate the local mid- and upper-elevation data contributions to the model (Figure 2). The topographic siting of these stations therefore becomes an important factor in the performance of PRISM and other gridded models in the region. Because the SNOTEL network is designed to measure snow hydrology variables near the headwaters of major streams and rivers (Serreze et al. 1999; Schaefer and Paetzold 2000), the stations are frequently associated with upper-elevation montane forests, but typically are situated such that they are not thermally representative of woodland slopes, but rather flats or even depressed topography. Accordingly, it is likely that the SNOTEL stations in and around the Walker Basin experience air conditions with canopy-influenced reduction of radiation and increased cooling as well as more stable, frequent flow of cool air during nighttime conditions. These features make the SNOTEL sites a prime suspect in the PRISM departures in this study, particularly T_{MIN} bias, due to local siting characteristics rather than systematic instrumental error.

Oyler et al. (2015) recently determined that changes in SNOTEL temperature sensing hardware and processing practices could introduce a warm bias into the network. While station metadata are still being analyzed to determine which locations are affected by this bias, reported shifts in T_{MIN} are on the order of ±1.5°C. It is possible that the SNOTEL stations in the Walker are also affected by this bias during

the study period. However, the presence of this bias should not result in *under-prediction* of temperature by PRISM, but rather *over-prediction*, which is clearly not the case in this study.

Applications and use of PRISM in mountain ecohydrology

Several contemporary scientific, conservation, and policy-related projects in or near the Walker watershed integrate gridded temperature data as part of their efforts (Lopes and Allander 2009; Millar and Westfall 2010; Mejia et al. 2012; Knick et al. 2013; Millar et al. 2013; Millar et al. 2014; Saito et al. 2014; Hatchett et al. 2015; Millar et al. 2015). These tests of the $PRISM_{800}$ temperature product and downscaled derivatives highlight both strengths and weaknesses of PRISM and similar models in mountain terrain, particularly the proportionally-large areas that are comprised of elevated slopes. Studies using PRISM to estimate frost-free periods in these zones may well be accurate in their conclusions, as first and last frost days in the Great Basin are most likely tied to transitional-season synoptic events which are interpolated well by PRISM. Research that seeks to partition precipitation as well as build/melt snowpacks may be subject to greater error if local calibration is not provided. While PRISM and observed temperatures at high-elevation sites generally resulted in similar partitioning of rain/snow, this was definitely not true at hydrologically-crucial mid- and lower-elevation sites ("snowline"). If degree-day calculations are being used in snowmelt or ecological niche models, local bias of PRISM introduces significant error. Thus, researchers focused on organisms and processes that are sensitive to small changes in thermal conditions may discover that accurate conclusions on elevated slope features will require local observations over full seasonal cycles for model calibration purposes. This is becoming a more common practice, although the method of *in-situ* measurement remains critical to reduce or eliminate bias, particularly for daily T_{MAX}.

Chapter 2 Partitioning liquid and frozen precipitation from automated hourly sensor measurements: The Gage-Difference Method

Background and motivation

Precipitation is one of the most critical environmental inputs for many ecosystems at both short and long timescales. The arrival of water on the landscape and its subsequent impact on the local hydrologic cycle is a process that is of first importance to measure consistently over time for a wide range of scientific and resource management purposes, and has been recognized as such by developed societies for thousands of years (Strangeways 2010). In particular, monitoring the nature of precipitation in orographic catchment zones (mountains) and water-limited environments (arid to semi-arid geography) remains a challenging and necessary endeavor (e.g. Hayes et al. 1999; Schwinning and Sala 2004; Bales et al. 2006; Jones et al. 2009; Stewart 2009; Rasmussen et al. 2012; Yatagai et al. 2012). There are several reasons why improving the quality of precipitation data, especially in mountains, is important and necessary. Recording precipitation inputs (volume, intensity, phase, location, etc.) provides daily-to-seasonal information for water users to plan and partition storage and distribution activities. Geographical climatologies and estimates of long-term regional trends in climate depend on the quality of precipitation records, which are notorious for missing or bad data. Watershed modeling relies on the accuracy of precipitation observations in order to provide useful outputs related to flooding, regional water balance, impacts to ecology, erosion, and numerous other applications. The issue of changing climate is especially important. Projections of retreating snowlines in the western U.S. under future warming scenarios abound, with a primary assumption being that the air temperature during precipitation events will be warmer, altering the elevational distribution of snow in favor of rain (e.g. Knowles and Cayan 2004; Barnett et al. 2005). Future scenarios of this nature are only testable as

hypotheses if records of precipitation phase (i.e. rain or snow) exist on a per-event basis that can be tied back to synoptic and boundary layer controls, and if monitoring of this phase distribution continues into the future.

In-situ observations of precipitation will always be necessary as a primary record source, for model calibration and validation, and for fine-scale geographic discrimination of hydrometeorological processes. Improving the quality of such observations by adding instantaneous phase (rain/snow/ice/mixed) discrimination is a practice that has leveraged methods ranging from simple visual observer reporting (WMO 2008) to near-surface temperature/atmospheric models (Feiccabrino and Lundberg 2008; Marks et al. 2013), and even optical (Huang et al. 2015) and radar measurements (Lundquist et al. 2008). These methods vary in their quantitative, spatial, and temporal resolutions, and not all are easily adapted to automated continuous field measurements. Ideally, a combination of all of these technologies would provide the most accurate *in-situ* data for automated applications (Michaelides et al. 2009); however, adequate optical video or laser sensors are still in development for long-term, fully-automated operation in a low-energy-requirement context (e.g. Löffler-Mang and Joss 2000; Huang et al. 2015; Zhang et al. 2015). Local radar instruments optimized for bright-band detection (and thus estimating the snow line across elevation gradients during storms) are expensive to acquire and operate (M. Dettinger*, pers. comm.*), and snow height measurements using acoustic devices are subject to numerous sources of error when calculating fine-scale (sub-daily) snowfall, especially while events are ongoing (Ryan et al. 2008). Advanced technology solutions at this time are expensive, add to remote station complexity/liability, and are not readily adaptable to existing system designs such as the Snow Telemetry (SNOTEL) network without significant system modifications (e.g. power/processing capacity). Phase discrimination using a combination of snow height, precipitation total, and process modeling has been performed at the sub-daily scale (Avanzi et al. 2014), but this method is specifically

focused on cold-season snowpack modeling and limited in resolution due to, among other things, snow-depth sensor noise.

In response to the scientific need to identify liquid and solid precipitation at an hourly timestep, across seasons, and using low-cost instrumentation, I developed a method of precipitation phase discrimination that uses well-established sensor technologies and system deployment schemes either already in place or easily added to existing infrastructure. This "Gage-Difference" method at the basic level requires only two devices: a precipitation mass weighing sensor (such as are found on most SNOTEL or U.S. Geological Survey precipitation-monitoring sites) and a liquid precipitation sensor (i.e. tipping bucket rain gage, the most common method of automated precipitation monitoring). The Gage-Difference method operates on the principle that at short time scales, the mass weighing sensor retains an instantaneous catch of all the measurable precipitation [minus undercatch due to external sources i.e. wind and wetting loss, (Legates and DeLiberty 1993; Goodison et al. 1998)] while the tipping bucket sensor only records measurable *liquid* precipitation (minus a similar undercatch component). In most circumstances, tipping bucket gages record substantially less than a mass-collection gage at all timescales if the phase is solid or mixed-phase precipitation due to evaporative and wind losses, leading to problems with winter and transition-season precipitation totals reported from stations which only employ these gage types in environments where snowfall is common (Rasmussen et al. 2012; Savina et al. 2012). This phenomenon is especially true when the instrument is unheated, which is a common deployment configuration in all but the most extreme environments. Therefore, examining the difference in catch between the two gage types when co-located, while making adjustments for minor differences in general undercatch and instrument accuracy, can result in reasonable estimates of whether precipitation is in solid or liquid form during a given event.

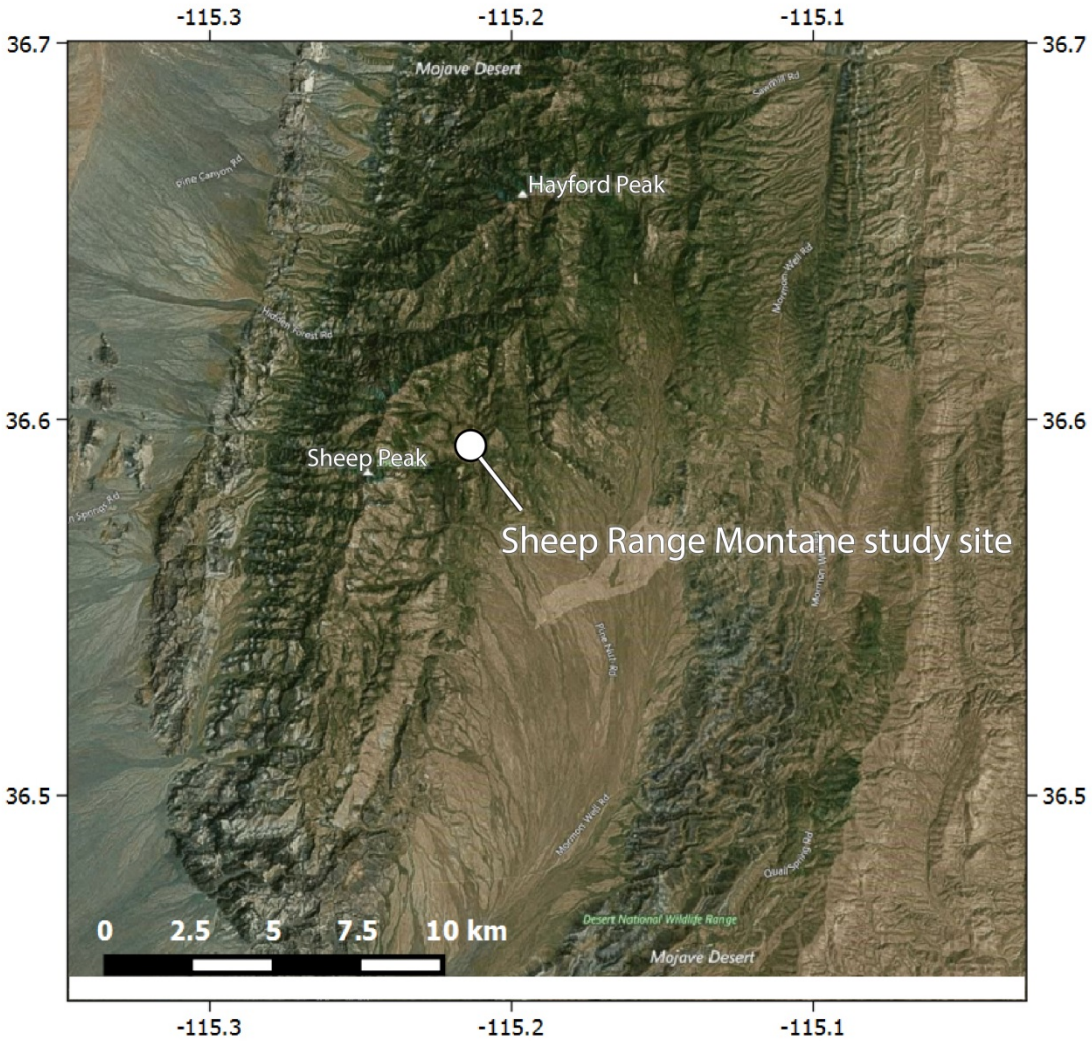

Figure 21. Sheep Range map (see Figure 1 for overview).

Data

Testing and development of the Gage-Difference method (GDM) was performed using instruments deployed as part of the Nevada Climate-ecohydrological Assessment Network (NevCAN; Mensing et al. 2013). These modern micro-meteorological stations are positioned in the semi-arid Great Basin region of North America, where winter and transitional-season snowfall is a significant component of the annual water budget (Welch et al. 2007), yet is not measured across the majority of the mountains in the region (NRCS 2015). While nine of the 12 stations in the network possess both gage types, for

purposes of describing the GDM the procedure is limited herein to the Sheep 4 station in a montane environment in the Sheep Range of Nevada (Figure 21). This station is located within the Great Basin-Mojave Desert climatic zone, and experiences wintertime snowfall as well as summertime convective "monsoon" precipitation of varying intensities. Because of the geographic location, anomalous warm events in the wintertime are also possible, bringing the potential for rain during seasons when it is not expected. This allows the method to be tested across a range of temperature, humidity, and precipitation conditions, and an evaluation of whether the GDM can detect out-of-season frozen precipitation events (such as hail) which would be beyond the range of typical temperature/atmospheric models.

Instruments and siting

Meteorological data from 16 March 2011 – 30 January 2016 were used for the method development and evaluation, an interval of 1782 days or 4.88 years. Automated data collection was performed using scientific-quality electronic sensors attached to a Campbell Scientific CR3000 datalogger programmed to specifications used by the Western Regional Climate Center (WRCC). The datalogger nominal scan interval was 3 seconds, with maximum, minimum, average, and standard deviation statistics for each measurement variable being retained at 1-minute and 10-minute intervals. The sensor used for the mass weighing measurements was the Geonor T-200B all-weather precipitation gage, hereafter referred to as the "Geonor" gage (Figure 22).

Figure 22. The Geonor T-200B precipitation mass weighing sensor.

This gage design uses a vibrating-wire load sensor to monitor the mass of liquid in a bucket protected by a cover with a 200 cm^2 orifice. A single hinged Alter-type passive wind shield was used to decrease wind-related undercatch (Alter 1937; Rasmussen et al. 2012), and the entire gage and shield assembly was mounted to a steel pipe pedestal set in concrete with the gage opening at the 2 m height above ground level. The sensor used for the tipping bucket measurements was a Hydrological Services model TB4 with

Figure 23. The Hydrological Services TB4 tipping bucket rain gage.

a 200 mm orifice, fine-mesh debris screen, and 0.254 mm tip resolution; hereafter referred to as the "TB" gage. This gage was mounted at 1.5 m height above ground level with no additional wind shielding (Figure 23).

The NevCAN Sheep 4 station is located in a semi-arid woodland at a mid-elevation (2280 m) in the Sheep Range of southern Nevada (Figure 21). The local site is a small forested knoll set within a larger ridge/canyon system with higher elevations in all directions, a fairly protected site but not subject to canyon-bottom air movement or temperature anomalies. Trees immediately adjacent to the monitoring station are mature individuals reaching 20 m in height. General canopy density is medium, and understory density is low (Figure 24).

Figure 24. Sheep 4 site conditions.

Site conditions are typical of semi-arid montane forests, with large dominant conifers and scattered sub-dominant conifers and shrubs.

The gages are located in two separate canopy openings, approximately 25 m apart. The station was installed in March 2011 by the NevCAN team and has been in continuous operation to-date. Seasonal servicing of the sensors occurred during each calendar year, with calibration checks on both the weighing sensors and tipping bucket gages.

Data characteristics

Data collected at 1- and 10-minute intervals were transmitted in near-real-time via a terrestrial wireless network to the Nevada Research Data Center (NRDC; McMahon et al. 2011; Dascalu et al. 2014) and subsequently WRCC (WRCC 2016) where they were ingested into databases and archived. Additionally, hourly daylight imagery from a tower-mounted digital network camera was automatically acquired and

archived at the NRDC to assist in visual checking of data anomalies and quality control. Raw 10-minute precipitation data were manually checked and corrected for calibration events, and reviewed for obvious anomalies. Tipping-bucket data are continuous for the entire analysis window (16 March 2011 – 30 January 2016). Geonor data are continuous for the same timeframe, except for the interval 16 August 2012 – 29 November 2012 (105 days), where the sensor was damaged from a nearby lightning strike and associated transient high voltages.

Although automated correction and quality control (QC) algorithms exist for weighing sensors such as the Geonor (Nayak et al. 2010), which are subject to positive and negative drift on all timescales, these procedures are designed for daily timestep summation and are not suitable for sub-daily instantaneous comparison with another gage as the Gage-Difference application calls for. After manual correction for calibration events, data were subjected to supervised QC procedures and Gage-Difference processing using the R package for statistical analysis, version 3.2.3 (R Development Core Team 2015).

The Gage-Difference Method

Steps in development of the GDM included:

1) Precipitation data pre-processing and QC for field calibration events, anomalous values, and evaluation of sensor noise.
2) Identification of “event days” where precipitation above minimal threshold amounts occurred.
3) Identification of “event hours” within event days where precipitation values are evaluated compared to noise and drift in sensor values.
4) Evaluation of catch difference between the gages during the summertime where precipitation should be liquid except hail events.

5) Identification of the relative percentage difference in catch between the two gages for each event hour.

6) Assignment of precipitation phase “frozen”, “mixed”, or “liquid” based on relative differences between the gages for each event hour.

7) Summation of the daily precipitation totals and the percent daily value of each phase using the Geonor catch as the final total.

8) Review of atmospheric data associated with each phase.

9) Review and cross-check of anomalous phase assignments (such as summertime frozen precipitation).

10) Subject to further correction and refinements, such as phase-specific wind-related undercatch, as desired.

A general process flowchart for the GDM can be found in Appendix 2.

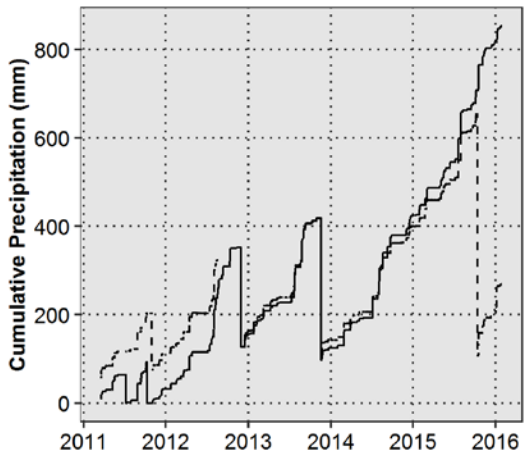

Figure 25. Raw cumulative precipitation data.

Cumulative 10-minute precipitation data for both Geonor (*dashed*) and TB (*solid*) gages after correction for calibration events, but prior to conversion to incremental values and removal of calibration resets (visible as vertical lines).

Figure 26. Hailstorm on 1 August 2012.

Visual checking of anomalous data is useful for detecting real phenomena such as this 30+mm summertime hailstorm in 2012. GDM is capable of identifying these out-of-season frozen precipitation events.

Pre-processing (calibration, anomaly, and noise evaluation)

After manual correction of the raw 10-minute data for seasonal calibration events, the cumulative catch values of each gage (Figure 25) were converted to increment values such that precipitation increment P_I for a given timestep t is equal to the difference between the present cumulative observation P_C and the previous:

$$P_{I(t)} = P_{C(t)} - P_{C(t-1)}$$

Next, 10-minute increments of both gages were examined for non-calibration anomalies exceeding likely maximum precipitation intensity. At this stage, only one event was examined in detail (1 August 2012), where at approximately 1330 hours local time, the tipping bucket recorded a 10-minute catch of 19.81 mm, while the Geonor recorded a catch of 30.5 mm for the same time interval. Further examination of the 1-minute data showed that at 1322 hours local time, a 1-minute catch of 6.7 mm was recorded by the Geonor, with additional catches of 4.9 mm and 4.6 mm during the next two minutes. The tipping bucket maximum 1-minute catch during this event was 2.54 mm. Query of the visual record revealed a hail event (Figure 26), which could easily explain the total undercatch in the tipping bucket due to hydrometeor rebound as well as sublimation from the TB4 funnel surface. This initial investigation indicated that undercatch anomalies associated with frozen precipitation can occur in summer.

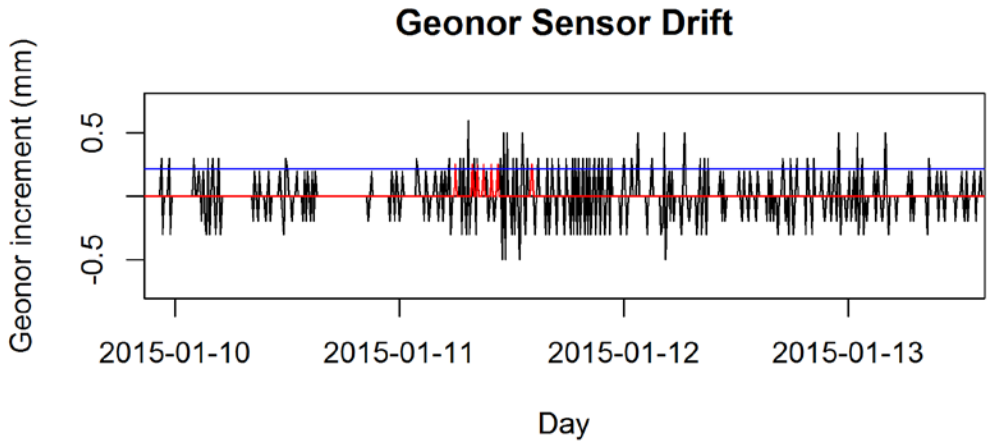

Figure 27. Geonor sensor drift.

Geonor sensor drift is pronounced at short timescales at amounts equivalent to less than 1 mm. This is not an uncommon phenomenon for mass weighing sensors, but it does present a level of complication for data quality control. There is no discernable pattern in the drift, as it is a combination of environmental and electrical factors, but at longer timescales (days) it sums to zero. These 10-minute Geonor readings (*black*) are contrasted with low-intensity tips of the TB4 gage (*red*). The long-term average of the vibrating wire frequency (*blue*) is used instead of the instantaneous values to identify days which experience real precipitation of 1 mm/day or greater.

Finally, noise in the Geonor vibrating wire sensor was evaluated for drift at various timescales. The sensor at Sheep 4 was found to drift around zero up to 0.6 mm using instantaneous 10-minute Geonor increment values (Figure 27). This would be very problematic if precipitation were evaluated at intensities < 4 mm hr^{-1} on any given day. However, the vibrating wire sensor frequency in Hz was also logged as an average of the 3-second datalogger scans (rather than instantaneous value) for 1-minute and 10-minute periods, giving a much smoother indicator of drift, no more than 2 Hz/day typically around a long-term (multi-day) mean. Therefore, a combination of the average sensor frequency and the instantaneous mass was used to identify actual precipitation events during all seasons at first the daily and then the hourly level in an iterative process.

GDM processing steps

Daily trends in sensor frequency were used to identify hourly events, which were then used to assign precipitation phase. The percentage breakdowns of precipitation phase were then re-applied to daily total precipitation (including low-intensity events) as a final step. Post-GDM processing such as wind-based undercatch calculations may be applied afterwards for each percentage amount based on phase identification. Summertime events when most or all of the events would be liquid were used to assess the performance of the GDM in identifying precipitation events in general, as well as potential differences in undercatch between the two gages.

Event days

Days with actual precipitation events were identified as days which experienced significant (~0.75 mm) positive change in Geonor baseline, were not field calibration days, and had either a positive tipping bucket measurement (≥ 0.254 mm) or a net 1 mm/day positive increment in Geonor catch. This is expressed using the following automated algorithm:

$$Day = Event\ Day$$

IF

$$(Freq_{\max(day)} - Freq_{\min(day)}) \geq 2\ Hz$$

AND

$$\left(Freq_{\mathrm{mean}(day)} - Freq_{\mathrm{mean}(day-1)}\right) \geq 0\ Hz$$

AND

$$\left\{\left[\left(\sum_{day} G_{mm} > 0\right) AND \left(\sum_{day} TB_{mm} > 0\right)\right] OR \left[\sum_{day} G_{mm} > 1\right]\right\}$$

Where *Freq* is the vibrating wire sensor frequency, G_{mm} is the Geonor gage increment catch in mm, and TB_{mm} is the tipping bucket increment catch in mm. Days meeting this requirement were classified as "event" days and were included in further analysis. Because day-to-day evaporation loss from the Geonor gage is less than 0.75 mm/day due to the application of mineral oil in the post-calibration charge (a common practice during maintenance of bulk-catch gages), potential daily losses from evaporation were negligible when developing this algorithm.

A total of 215 days out of 1782 in the analysis window were classified as "event" days using this process, or ~12%.

As a check of this process for omission of real events, summer days classified as "non-event" were examined for tipping bucket catch. Over the June – September window for 2011 – 2015 (except the 16 August 2012 – 30 September 2012 period when the Geonor sensor was non-functional), positive tipping bucket catch was recorded on 29 different days not classified as "event" days, with a minimum of 0.254 mm/day, a mean of 0.561 mm/day, a maximum of 1.02 mm/day, and a grand total of 16.26 mm. Total tipping bucket catch for this time period was 708.4 mm, indicating that the "event" day algorithm effectively identifies events which involve more than 1 mm/day catch, and cumulative error was only 2.3%.

The primary reason why "event" days cannot be determined solely by the tipping bucket catch is due to wintertime snow falling into the gage funnel but not tipping the sensor until sometime (up to many days) later, when the sun melts the snow. This would result in errors of adding events on the wrong days, which are even less desirable than omitting low-intensity precipitation from the analysis and would make it difficult to use daily-timestep temperature-based phase discrimination algorithms to refine or verify results.

Event hours

Once days with precipitation events were positively identified, further refinement of the precipitation identification algorithm was continued at the hourly level (*n* = 5160). Precipitation data were aggregated from 10-minute to 60-minute totals. Geonor sensor noise was evaluated at the hourly level for the distribution of departures. Because the drift in the sensor is centered on zero, the distribution of the drift is symmetrical, and the characteristics of negative drift are roughly equivalent to positive drift (although not temporally mirrored; Fig. 7). A check of the Sheep 4 sensor drift during "event" days indicated a sharp reduction of hourly departures between magnitudes 0.4 mm and 0.5 mm (72 and 12 negative occurrences exceeding each threshold, respectively). The maximum negative hourly departure was 0.8 mm (3 occurrences). The number of positive hourly departures exceeding 0.5 mm during event days was 524. Therefore, it was decided to set the detection threshold at 0.5 mm hr^{-1} precipitation intensity. The precipitation increment for each hour during an "event" day was set to the value indicated by the Geonor increment for that hour, provided that this value exceeded the detection threshold of 0.5 mm. This can be expressed using the following automated algorithm:

$$P_{EventDay(hr)} = G_{mm(hr)}$$

IF

$$\left[G_{mm(hr)} > 0.5\right]$$

ELSE

$$P_{EventDay(hr)} = 0$$

where $P_{EventDay(hr)}$ is the hourly precipitation and $G_{mm(hr)}$ is the recorded hourly Geonor increment in mm.

Gage differences

The instantaneous hourly difference between the two gages is then calculated:

$$P_{G-TB(hr)} = P_{EventDay(hr)} - TB_{mm(hr)}$$

where $P_{G\text{-}TB(hr)}$ is the hourly difference in recorded precipitation between the two gages in mm and $TB_{mm(hr)}$ is the recorded hourly TB increment in mm.

In order to identify gross differences in catch between the two gages due to location, shielding, and environmental drivers of undercatch (e.g. local wind velocity, wetting loss, and so forth), the instantaneous catch values were evaluated on "event" days during the monsoon season (July – August). Raw 10-minute increment values for both G_{mm} and TB_{mm} during each event day were compared, as well as hourly aggregates (Figure 28, Figure 29). For July – August in all years, liquid events between 1.5 mm hr^{-1} and 60 mm hr^{-1}, the tipping bucket catch met or exceeded 85% of the Geonor catch. At the 10-minute scale this relationship was also true for almost all events. For events less than 1.5 mm hr^{-1}, the inter-sensor noise increased dramatically. The combination of sensor resolution, potential wind/wetting loss differences, and Geonor sensor noise makes the comparison complicated at small precipitation amounts, but the tipping bucket does not inherently catch less than the Geonor during non-snow events in this case. The relative undercatch performances of the gage openings during snow events is impossible to measure, given that the tipping bucket will almost always undercatch snowfall by significant percentages because the snow must first melt, pass through a screen, and then tip the sensor.

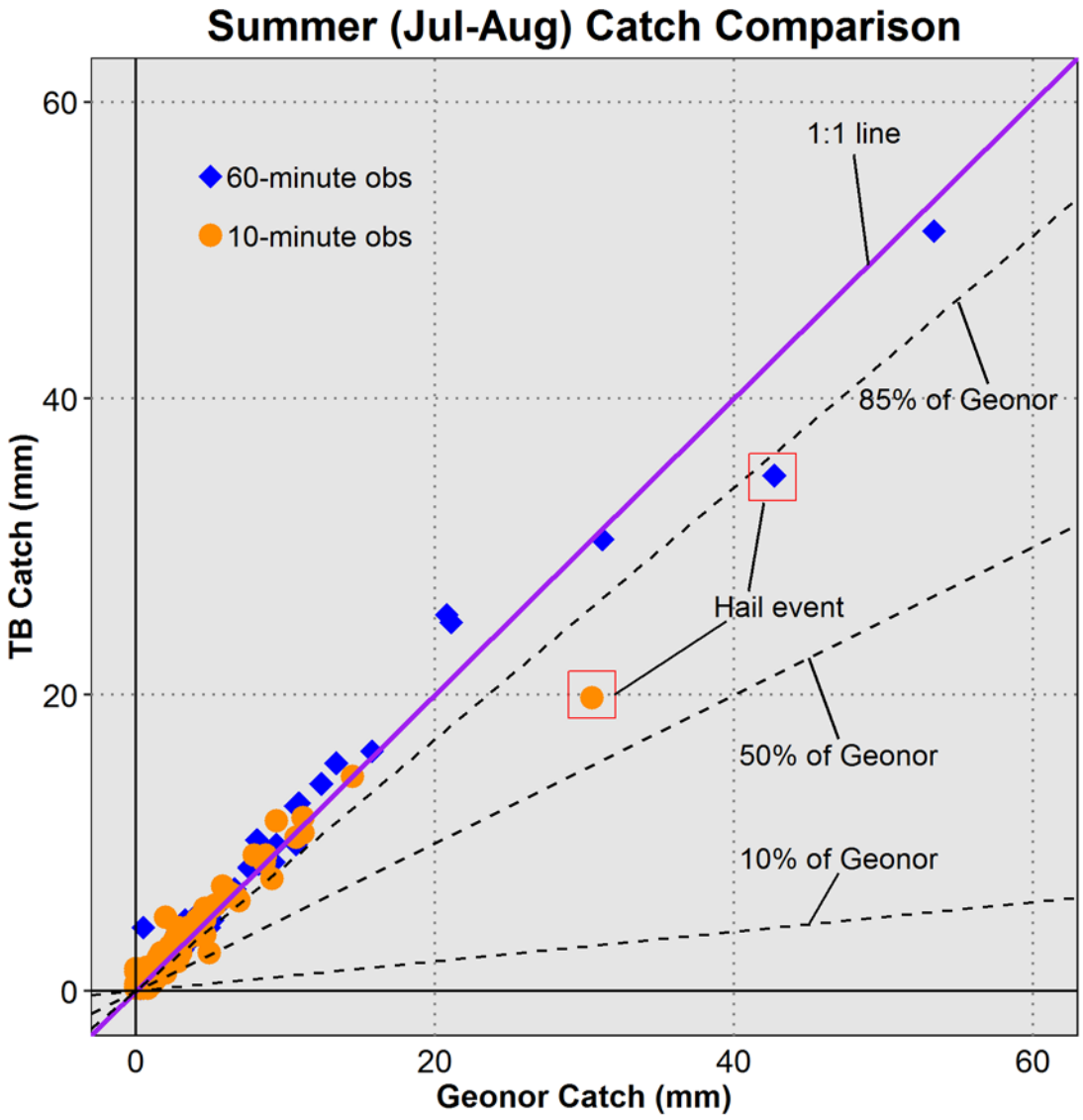

Figure 28. Summertime gage comparison.

Comparison of the Geonor and TB gages during summertime seasons. Relative gage catch during larger liquid events is very close to identical, as the data points closely track the 1:1 line.

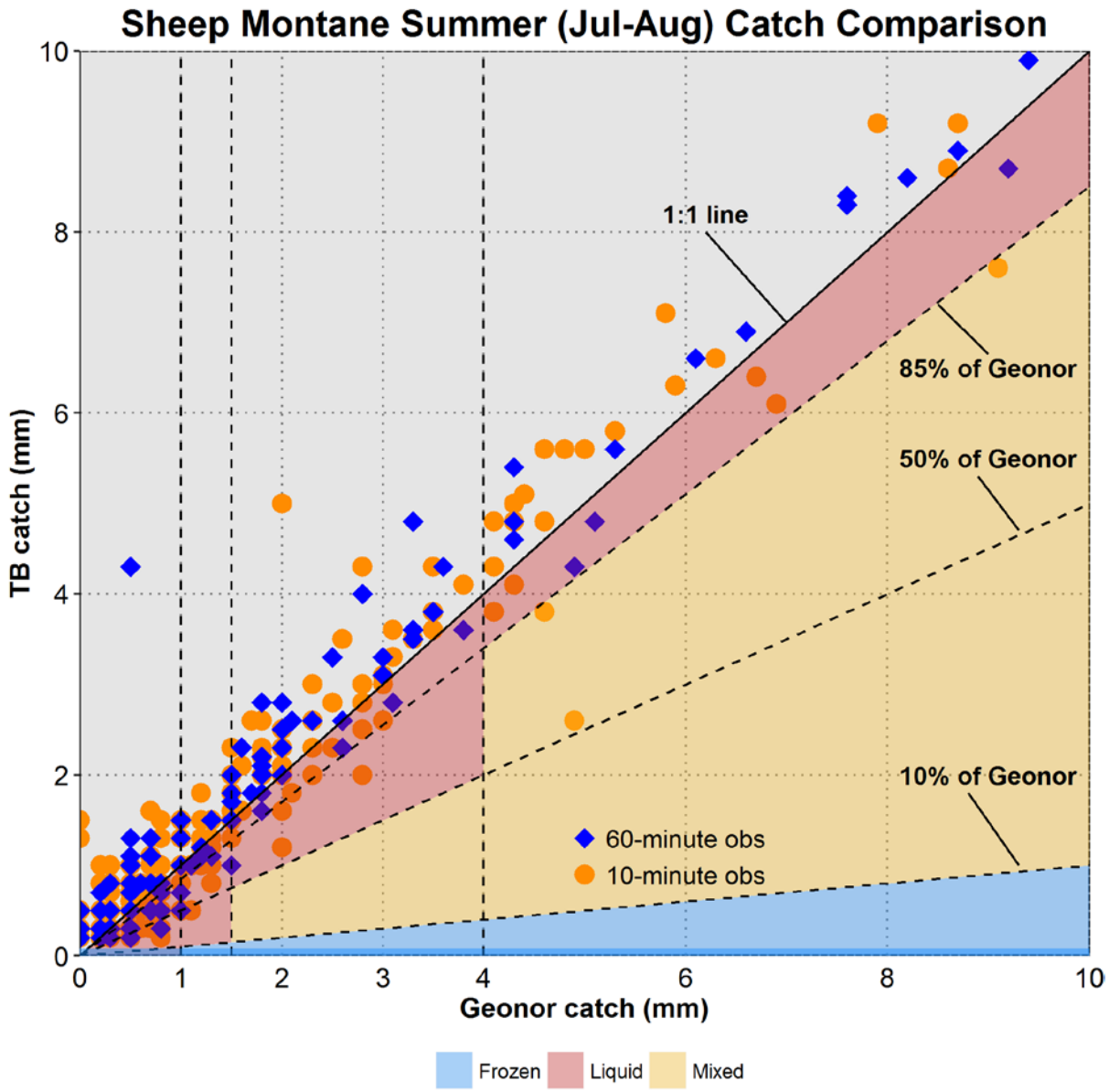

Figure 29. Summertime gage catch, smaller events.

Relative gage catch during smaller events was more widely distributed, probably a function of noise due to wetting loss, sensor resolution, and other factors. GDM filter settings for “liquid”, “frozen”, and “mixed” are shown. These were based on qualitative assessment of the relative gage performance during the warm (non-snow) season.

Precipitation phase assignment

Finally, the phase of each precipitation event was assigned at the hourly scale using the relative differences in catch between the Geonor and the tipping bucket gages, regardless of the season and local atmospheric conditions. Categories used were “frozen”, “mixed”, and “liquid”. These were determined in the following manner:

$$IF\ \left(P_{EventDay(hr)} > 0\right)\ AND\ \left(TB_{mm(hr)} = 0\right);\ P_{EventDay(hr)} = Frozen$$

ELSE

$$IF\ \left[\left(P_{EventDay(hr)} > 1\right)\ AND\ \left(TB_{mm(hr)} > 0\right)\right]\ AND\ \left[\frac{TB_{mm(hr)}}{P_{EventDay(hr)}} \leq 0.10\right];\ P_{EventDay(hr)} = Frozen$$

ELSE

$$IF\ \left[\left(4 > P_{EventDay(hr)} > 1\right)\ AND\ \left(TB_{mm(hr)} > 0\right)\right]\ AND\ \left[\frac{TB_{mm(hr)}}{P_{EventDay(hr)}} < 0.50\right];\ P_{EventDay(hr)} = Mixed$$

ELSE

$$IF\ \left[\left(4 > P_{EventDay(hr)} > 1.5\right)\ AND\ \left(TB_{mm(hr)} > 0\right)\right]\ AND\ \left[\frac{TB_{mm(hr)}}{P_{EventDay(hr)}} \geq 0.50\right];\ P_{EventDay(hr)} = Liquid$$

ELSE

$$IF\ \left[\left(P_{EventDay(hr)} \geq 4\right)\ AND\ \left(TB_{mm(hr)} > 0\right)\right]\ AND\ \left[0.10 < \frac{TB_{mm(hr)}}{P_{EventDay(hr)}} < 0.85\right];\ P_{EventDay(hr)} = Mixed$$

ELSE

$$IF\ \left[\left(P_{EventDay(hr)} \geq 4\right)\ AND\ \left(TB_{mm(hr)} > 0\right)\right]\ AND\ \left[\frac{TB_{mm(hr)}}{P_{EventDay(hr)}} \geq 0.85\right];\ P_{EventDay(hr)} = Liquid$$

ELSE

$$IF\ \left(P_{EventDay(hr)} \leq 1\right)\ AND\ \left(TB_{mm(hr)} > 0\right);\ P_{EventDay(hr)} = Liquid$$

These statements make a number of conservative assumptions to avoid misclassification, and are based on the qualitative assessment of the actual gage pair. For instance, low-intensity snowfall at warmer temperatures is likely to get categorized as liquid or mixed, given the noise in gage-catch differences at these precipitation rates. Because the timescale is hourly, it is possible that significant mixed-phase precipitation will actually get classified as liquid if the actual surface temperature is above freezing and the hydrometeors are not blown away from or out of the tipping bucket catch funnel. Low-noise sensors or scientists only interested in high-intensity events could certainly adjust the timesteps and filter settings depending on the investigative question and desired direction of filter bias/assumptions.

Thus, the results of the GDM as described at the NevCAN Sheep 4 site err on the side of classifying low-intensity events as liquid rather than mixed or frozen. Because the GDM relies on mechanical differences between ice and liquid water to classify events as frozen, events classified as such during times when neither instrument is broken or malfunctioning are either positively frozen or anomalies caused by non-precipitation mass addition to the Geonor gage such as woody debris or animal intrusion, both of which are unlikely given the gage design and would be detected upon seasonal servicing of the gage.

Results for the Sheep montane woodland site

Application of the GDM to precipitation data from the NevCAN Sheep 4 station resulted in clear distinctions between cold and warm seasons in terms of precipitation phase classified independently from temperature (Figure 30). To get a first-order verification of the validity of the GDM phase partitioning, comparisons against atmospheric conditions typically used in rain/snow partitioning models were performed.

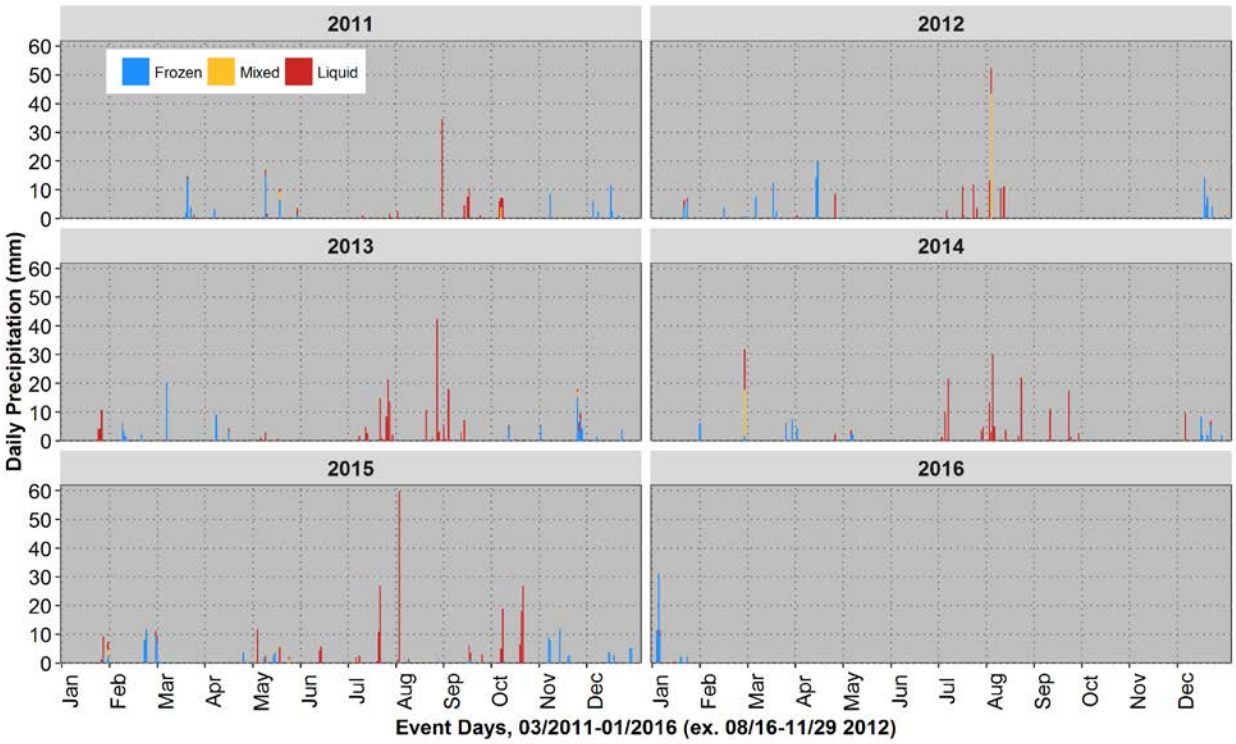

Figure 30. Precipitation classifications for the study period.

All classified events for the entire study period are shown as a stacked bar plot, clearly separating warm from cool seasons. The August 2012 hail event shows up as "mixed", due to the rapid melting of ice in the TB orifice. However, the results seem to indicate that the GDM works well for all but the very low-intensity events.

Testing against atmospheric relationships

The most common atmospheric conditions used to estimate whether precipitation falls as rain or snow are temperature thresholds using dewpoint temperature T_d, dry-bulb temperature T_{db}, and wet-bulb temperature T_{wb} (in °C; e.g. Feiccabrino and Lundberg 2008; Lundquist et al. 2008; Marks et al. 2013). Observations at Sheep 4 of hourly average T_{db} and percentage relative humidity *RH%* using sensors at the 2 m height were used to estimate T_d and T_{wb} using the following equations from Stull (2011) and Lawrence (2005):

$$T_{wb} = T_{db}\tan^{-1}\left[0.151977(RH\% + 8.313659)^{1/2}\right] + \tan^{-1}(T_{db} + RH\%) - \tan^{-1}(RH\% - 1.676331) + 0.00391838(RH\%)^{3/2}\tan^{-1}[0.023101(RH\%)] - 4.686035$$

$$T_d = T_{db} - \left(\frac{100 - RH\%}{5}\right)\left(\frac{T_{db} + 273.15}{300}\right)^2 - 0.00135(RH\% - 84)^2 + 0.35$$

Distributions of classified hourly events (regardless of volume) were examined for all seasons against each measure of air temperature (Figure 31).

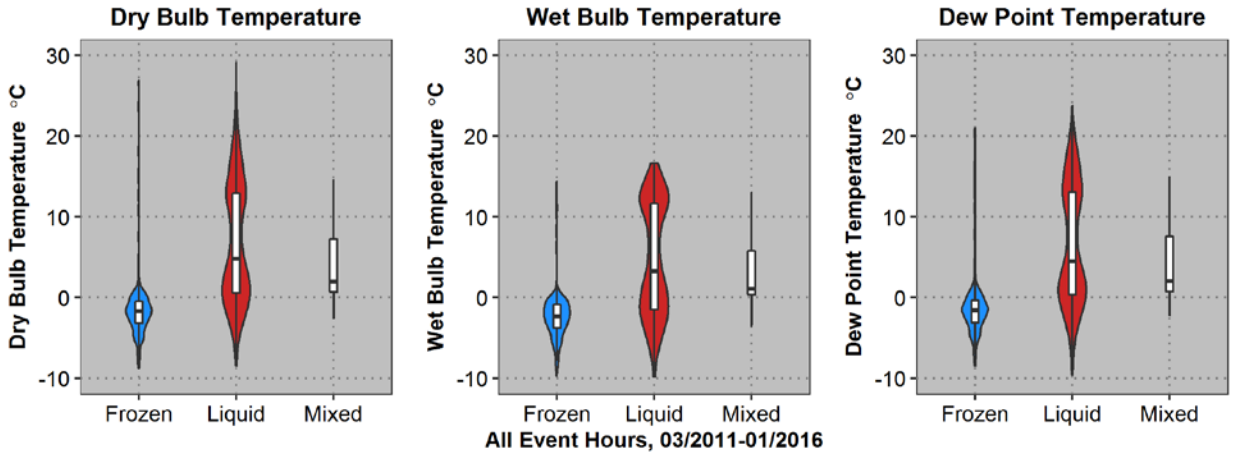

Figure 31. Distributions of classified events *versus* temperature.

Violin plots of classified events and associated air temperatures. The plot areas are scaled by event counts, and represent the kernel densities (distributions) of classified hourly events, regardless of amount of precipitation. Frozen events are certainly clustered below 1°C, with a handful of outliers which may represent either small hail or else near-trace summer events which evaporated in the TB orifice before accumulating enough mass to tip the sensor. The spread of liquid events at near-freezing or lower temperatures is representative of both the sensor noise/misclassification issue at very low precipitation rates, as well as the tendency of near-surface air temperature as not being precisely representative of air conditions higher up, and the fact that snow can occur within wide windows of near-surface temperature (Marks et al. 2013).

The distribution of frozen events is within expected temperature conditions, with a few outliers which either represent out-of-season events such as hail, or trace-level precipitation which is lost to evaporation (wetting loss) while accumulating in the tipping bucket orifice prior to filling the sensor with the required amount to register a tip (~0.254 mm). Liquid events are shown to have a bimodal

distribution, which is not surprising given the bimodal seasonality of the Great Basin/Mojave transition region. The number of events occurring below 0°C is reflective of the numerous near-trace occurrences that are classified as liquid rather than frozen due to the limitations of the Geonor sensor noise. Figure 32 plots the hourly precipitation total by phase against hourly mean temperature. A distinct cutoff of T_{db} ≤ 1.5°C emerged for classification of frozen precipitation, with 98% of total volume occurring at or below this threshold (Figure 32). The 98% thresholds for T_{wb} and T_d were 0.5°C and 1.8°C respectively. All classifications of liquid events below T_{db} = 1°C were of low volume (< 1.3 mm), with 98% of the volume of liquid precipitation occurring when T_{db} > -0.7°C.

These T_{db} thresholds are consistent with results from other empirical studies, where "all snow" thresholds vary from T_{db} < -2°C (Feiccabrino and Lundberg 2008), to T_{db} < -1°C (Tarboton and Luce 1996; Endrizzi et al. 2014), and even T_{db} < 0°C under certain humidity circumstances (Fuchs et al. 2001), while "all rain" thresholds can range from T_{db} > 0°C to T_{db} > 4°C (Lundquist et al. 2008). Great Basin and Mojave climatology is such that snowfall occurs across a variety of synoptic conditions, and the Sheep Range is no exception. These results (Figure 32, *bottom*) do not align well with Marks' et al. (2013) observation of an all-snow threshold of T_d ≤ 0°C for a large December snow event in Idaho. However, their observations of all-snow wet bulb temperatures of T_{wb} ≤ 0.25°C correspond very closely with the Sheep 4 results, which show a sharper temperature cutoff for positively-identified frozen events (Figure 32, *middle*).

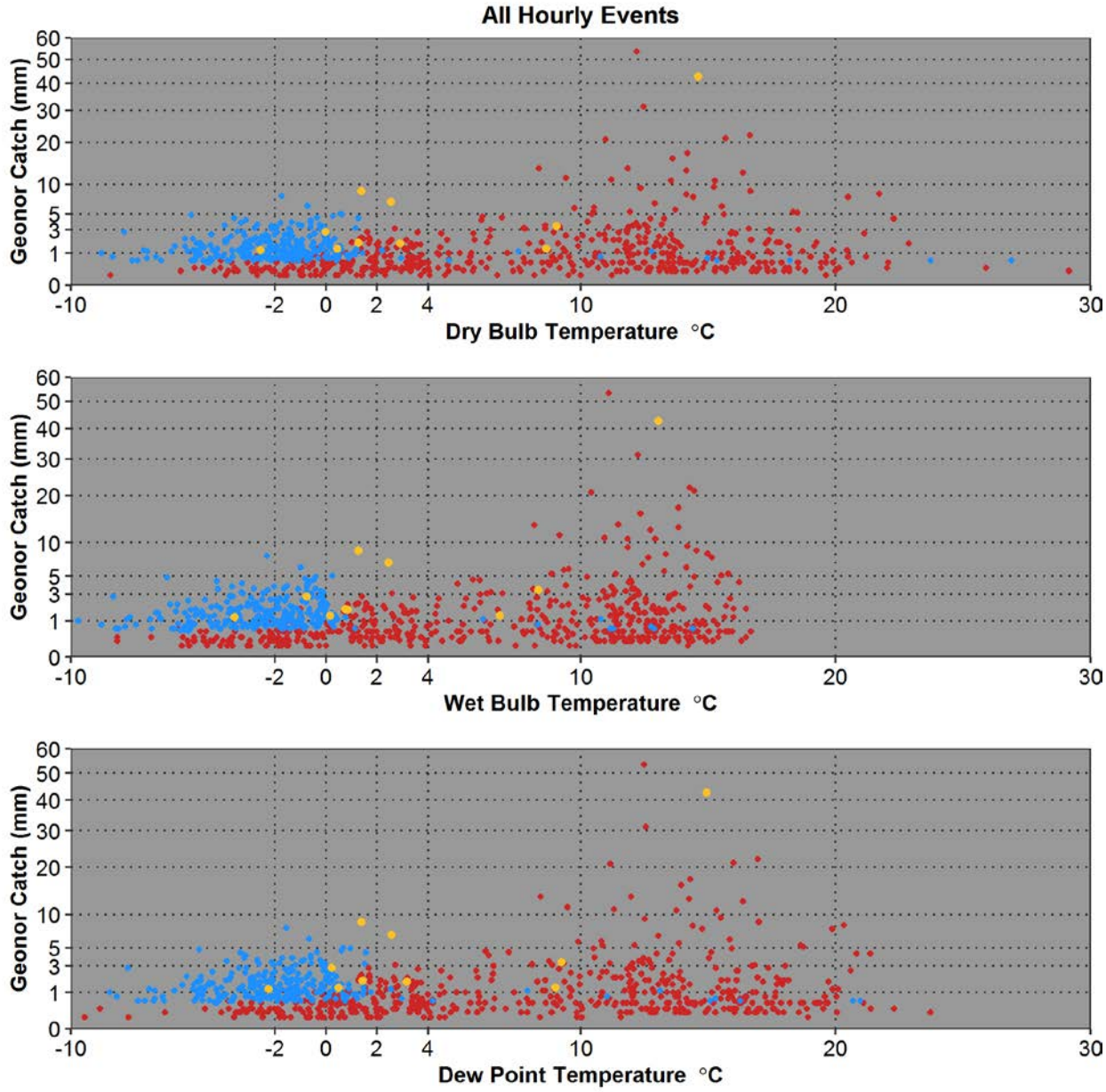

Figure 32. Point clouds of classified events *versus* temperature.

Hourly event totals by classification and temperature. Frozen events (*blue*) are clearly restricted to temperature thresholds consistent with other studies. Only low-intensity events are classified as liquid (*red*) under typical "all snow" temperature thresholds. This reflects the GDM filter configuration in this study set to err on the side of near-trace classification as liquid rather than frozen to avoid Geonor noise-driven misclassification of snow. The few frozen outliers above 2°C, along with the handful of mixed events (*yellow*) are events which would be investigated as potential out-of-season hailstorms.

Conclusions and future applications

This study describes a new method of discriminating precipitation phase between liquid and solid precipitation at hourly timescales. Studies and models using snow depth (e.g. Marks et al. 2013; Avanzi et al. 2014) and temperature thresholds (e.g. Feiccabrino and Lundberg 2008) rely on methods which either require coarse aggregation (≥ daily) or are subject to sensor and event type error at low precipitation intensities. The GDM is a simple solution which does not depend on any atmospheric data for initial filtering (although this could be added *post-hoc* to improve accuracy at low precipitation rates), and leverages common sensors with low power requirements. Hourly precipitation rates of > 1 mm^{-1} water equivalent were reliably classified as frozen precipitation even with conservative filter settings. Hydrologically-important out-of-season frozen (hail) events in warm desert environments were flagged as "mixed" events rather than liquid. The GDM could easily be adapted to SNOTEL observation sites with the addition of a sub-$1000 tipping bucket gage to complement the bulk-catch gages already in place, and no additional power supplies would be required. Very fine-scale phase discrimination could be accomplished using weighing technologies with less sensor drift than the Geonor vibrating wire device, or refinement of the datalogger signal processing procedure.

Given the ease of implementation and low cost, future phase-discrimination investigations using *in-situ* automated observation should incorporate the GDM to help refine atmospheric-, snow-height-, and disdrometer-based methods as well as assist with cross-sensor quality control. Use of the GDM for warm-season hail detection would also not be difficult to incorporate into crop-insurance and hazards networks. Existing mountain climate observatories frequently field both sensor types, and could modify data processing practices using the GDM to classify precipitation phase on an event-by-event basis, ultimately leading to more accurate input data for hydrological models and long-term assessment of changes in the snow-rain ratio across gradients as a test of warming-effect hypotheses.

Chapter 3 Character and impacts of precipitation across Great Basin gradients

Overview and study sites

This investigation leverages a recently-established valley-mountain network of monitoring stations (the Nevada Climate-ecohydrological Assessment Network; NevCAN) located in two Great Basin mountain ranges (Figure 1, Figure 21, Figure 33, Snake and Sheep ranges; Mensing et al. 2013b) to examine multiple years of precipitation across a steep elevational gradient and the subsequent impacts to seasonal soil moisture as a proxy of plant-water availability and recharge timing. Sap flow data from montane conifers in the Snake Range as well as the Sheep Range, a comparative site at the Great Basin/Mojave transition, are used to assess conifer response to various precipitation modes and seasonality. Results include the seasonal partitioning of precipitation across the main Great Basin vegetative zones during a dominant regional drought pattern, relative amounts of snow versus rain in each zone, the subsequent response of soil moisture, and potential adaptations of conifers to shifts in precipitation seasonality and character.

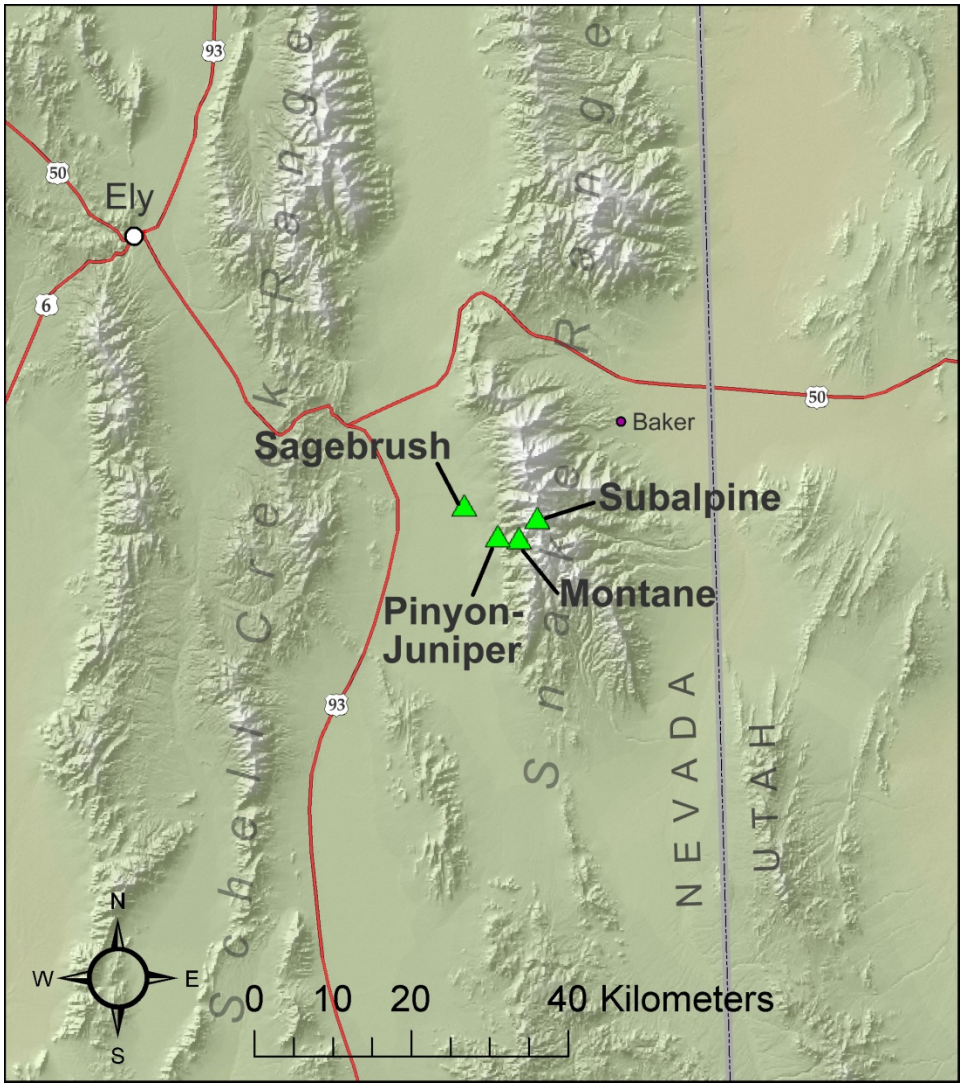

Figure 33. Snake Range site locations (see Figure 1 for overview).

Beginning in 2010, the NevCAN climate monitoring stations were constructed in eastern and southern Nevada as part of an NSF-EPSCoR (National Science Foundation Experimental Program to Stimulate Competitive Research) infrastructure building grant. The Snake Range region has a winter/spring-dominated climatology (Nevada climate division 02), while the Sheep Range regional climatology sees a very dry springtime due to its location on the Great Basin-Mojave Desert boundary (Nevada climate division 04). The space between the two (Nevada climate division 03) experiences fairly even seasonality, as does the region just to the east (Utah climate division 01; Figure 34; climatologies derived

from full network estimated precipitation climate divisional data, McRoberts and Nielsen-Gammon 2011). All divisional climatologies reflect the tremendous variability in almost all months, with the inter-quartile range of the 120-year record spanning more than 50% of the monthly average in many cases. Because both mountain ranges are near the borders of their respective climate divisions, it is likely that they experience a combination of the nearby divisional precipitation regimes.

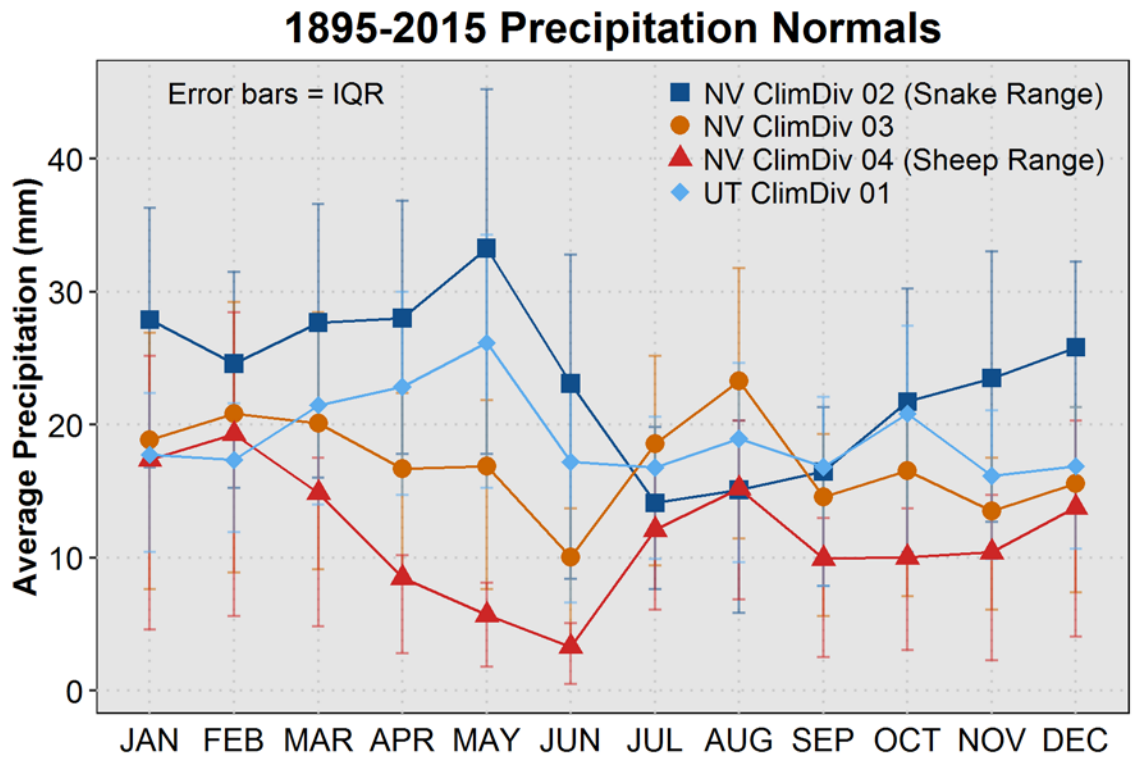

Figure 34. Long-term precipitation climatologies for the region.

Long-term precipitation climatologies for the regions containing the study areas. The 25th and 75th percentiles are displayed as error bars, hinting at the tremendous interannual variability in hydrological inputs that characterizes the intermountain west.

The stations in the Snake Range were located in a manner to reflect near-surface meteorological, precipitation, soils, and vegetation conditions within the dominant Great Basin vegetative/topographic zones of “Sagebrush”, “Pinyon-Juniper”, “Montane”, and “Subalpine”, a classification adaptation of Billings (1951) and Charlet (2007). For this study, data from stations in these four zones are analyzed

across a local elevational gradient from 1800 – 3300 m in the Snake Range (SR; Figure 33, Figure 35), and one station in the Sheep Range (SH) "Montane" zone at 2300 m is also included as a latitudinal comparison point.

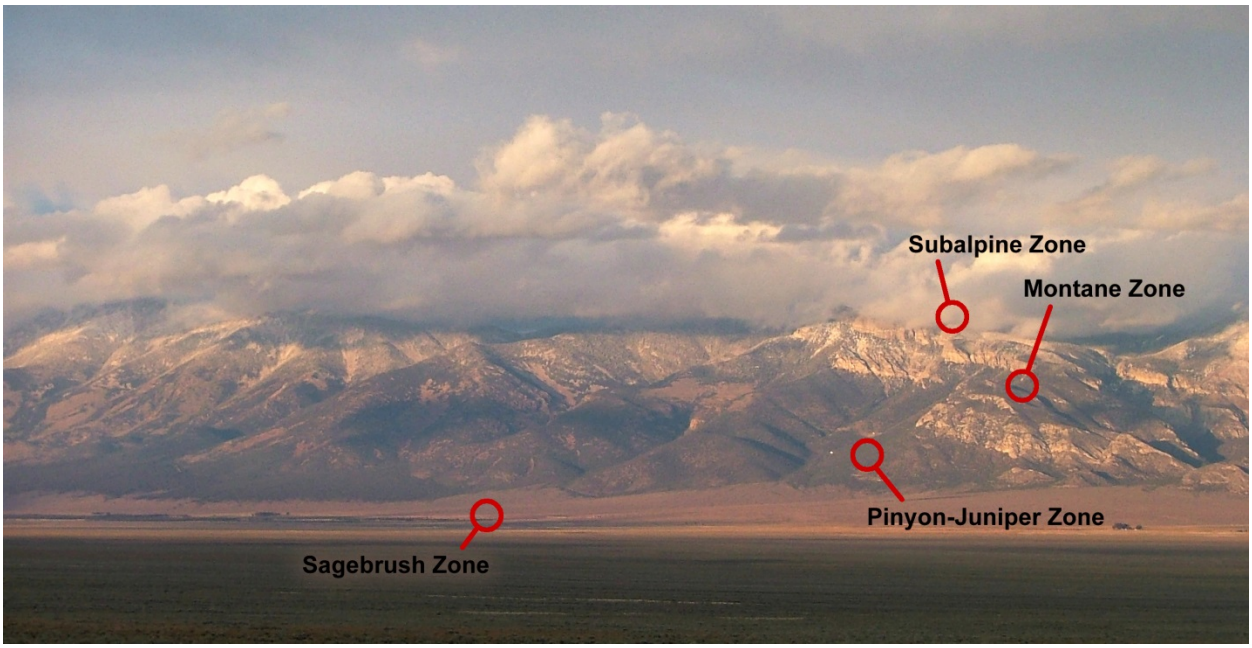

Figure 35. Snake Range study sites and elevation gradient.
Study sites in Spring Valley and on Mt. Washington in the Snake Range, Nevada.

Management of the stations and systems is through a cooperative arrangement between three Nevada System of Higher Education (NSHE) institutions: the University of Nevada, Reno (UNR), the Desert Research Institute (DRI), and the University of Nevada, Las Vegas (UNLV). Seasonal inspections and annual sensor audits are conducted onsite to improve Quality Assurance (QA) and reduce data gaps. Raw data are retrieved from datalogger systems via a terrestrial wireless high-speed digital network to the Nevada Research Data Center (NRDC; Dascalu et al. 2014) where they are archived and distributed to WRCC for independent QC, processing and storage. Because the purpose of this study was to use "raw" sensor data to partition rain and snow, all processing began with the lowest-level data, i.e. "Level 0" (ESIP Envirosensing Cluster 2016), with no previous QC applied.

Meteorological sensors and dataloggers are mounted on 10 m aluminum towers in accordance with WRCC weather station deployment protocols (Figure 36). Sensors are controlled by Campbell Scientific CR3000 dataloggers programmed to WRCC specifications using a nominal 3-second scan interval and recording statistics such as maximum, minimum, average, standard deviation, or sample values for each sensor at 10-minute timeframes (the raw data resolution used in this study). Vegetation sensors are controlled by Campbell Scientific CR1000 dataloggers running 30-second scan and recording sap flow sensor values every 10 minutes. Bulk-catch precipitation gages consist of Geonor model T-200B (referred to hereafter as "Geonor" gages) weighing sensors and are mounted away from the meteorological towers on separate concrete bases. These gages incorporate passive Alter-type wind shielding to reduce undercatch. Liquid-catch gages of the tipping bucket type consist of Hydrological Services model TB4 (hereafter referred to as "tipping bucket" gages), and are mounted on the sides of the towers or on short extension arms without wind shielding. Hourly daylight images are automatically acquired using Canon point-tilt-zoom (PTZ) cameras controlled by software running at NRDC, requiring a functional network connection at the top of each hour. By combining observations from multiple sensor types and systems, a consistent picture of precipitation-related conditions on these sites can be assembled. Anomalies in one sensor data stream can be investigated in a supervised Quality Control (QC) process using independent sensors as well as daylight imagery, reducing observation error and allowing for inclusion of real events (such as extreme precipitation intensity) that might otherwise be filtered out as noise.

Figure 36. Weather station configuration.

The weather stations used in this study are based on 10 m aluminum towers and typical Campbell Scientific equipment for the sensor packages. Shown is the site in the Snake Range “Subalpine” vegetation zone, located at 3350 m on a southern aspect and surrounded by spruce and pine species. More station photographs may be found in Appendix 3.1.

Assembly of precipitation data

Prior to analysis, precipitation data from each site were acquired, quality-controlled, and processed using procedures partially described in Chapter 2 as well as additional methods to follow. The Gage-Difference Method (GDM) was applied to partition hourly precipitation into "frozen", "mixed", or "liquid" form. Precipitation data were then corrected for wind-driven undercatch prior to monthly and seasonal analysis. Timeframes with missing meteorological data due to sensor failure or other problems are shown in Table 3.1. There were only two data gaps larger than one day within the interval of calendar years 2012–2015, and so this was chosen as the primary analysis window for comparative studies across the sites. The total number of 10-minute precipitation observations held in common across all five sites was 193,499.

Table 3.1. Data timeframes by site.

	Snake Range (SR)				Sheep Range (SH)
	SR Sagebrush	**SR Pinyon-Juniper**	**SR Montane**	**SR Subalpine**	**SH Montane**
Start	2010/07/01	2011/05/27	2011/07/26	2011/08/01	2011/03/16
End	2016/01/15	2016/01/29	2016/01/29	2016/01/29	2016/01/29
	Days with significant missing meteorological data				
2010	none	n/a	n/a	n/a	n/a
2011	03/29, 06/11-06/15, 10/08-10/12, 11/02-11/03	none	none	09/15-09/28	none
2012	none	none	none	none	08/16-11/29
2013	none	none	none	none	none
2014	06/09-06/21	none	none	none	none
2015	none	none	none	none	none
2016	none	none	none	none	none

Uniform settings for the GDM phase-classification filter were applied across all sites in order to provide comparability (Appendix 3.2). Filter settings were chosen in an attempt to reduce misclassification at all sites while retaining the best resolution of lower-intensity events. Performance of the classification settings was assessed using the percentage of frozen events falling under given temperature thresholds.

During development of the GDM (Chapter 2), the estimated wet bulb temperature T_{WB} was considered the best atmospheric indicator of precipitation phase transition, and therefore T_{WB} was used in the filter performance assessment at all sites.

A diagnostic value of T_{WB} < 0.5°C was compared to the empirical cumulative distribution of events classified as "frozen" as a function of T_{WB}, and the percentage of events and volume falling under that threshold was determined for the study period at each site (Table 3.2; Appendix 3.3). Except for the Snake Range Sagebrush site, all threshold values for the GDM settings used were high (> 95%), and the distribution breakpoints coincident with the diagnostic T_{WB} threshold, indicating high confidence in phase discrimination even at lower intensity levels. Additional descriptive/diagnostic charts regarding the partitioning are available in Appendices 3.4 and 3.5.

Table 3.2. Frozen classifications occurring at T_{WB} < 0.5°C.

Site	% volume	% events
SR Sagebrush	87.2	84.1
SR Pinyon-Juniper	98.0	97.3
SR Montane	95.8	95.1
SR Subalpine	96.1	95.2
Sheep Montane	98.5	96.4

After precipitation data were partitioned in this manner, wind-based undercatch correction for Alter-shielded gages was performed using published equations for each classified precipitation phase derived from World Meteorological Organization gage intercomparision studies (Yang, B. Goodison, et al. 1998):

$$K_{ss} = 100 \times exp(-4.606 + 0.036 \times v_a^{1.75})$$

$$K_{ms} = \frac{1}{1.010 - 0.0562 \times v_a}$$

$$K_{rs} = 100 \times exp(-4.606 + 0.041 \times v_a^{0.69})$$

where v_a is wind speed in m s^{-1} at the gage orifice and the factors *K* are applied as multiplication coefficients to precipitation values. *K* subscripts indicate rain (*r*), mixed (*m*), and snow (*s*) under Alter-shielded (*s*) conditions.

Wind speeds were obtained from R.M. Young Wind Monitor sensors, which measure wind direction and velocity. This probe was mounted at the 10 m height at each station to avoid excess near-surface turbulence, which is not the same height as the precipitation gage orifices (these vary from 1.7 to 3 m above ground to accommodate different maximum snowpack heights). Therefore, a wind velocity adjustment was made using a power-law model described in empirical studies of near-surface (≤ 10 m) wind speeds (Justus and Mikhail 1976; Chen et al. 1998). Turbulence from differing vegetation heights alters the wind height/velocity relationship at each station, but no empirical data from the sites exist to make these further refinements to fitting parameters. The model used to adjust wind velocity for precipitation catch correction was the following:

$$u = u_{10}\left(\frac{Z}{10}\right)^{b_2}$$

where u is the corrected wind speed at some height Z between 0 and 10 m from the ground, u_{10} is the wind speed at 10 m above ground, and b_2 is an exponential term that depends on surface roughness and air stability.

It is likely that the term b_2 fluctuates significantly in mountain terrain because of the unstable flow of air past vegetation during typical mountain storm events. Previous research generally places b_2 between 0.1 and 0.6 (see literature summary in Chen et al. 1998). A conservative value of 0.25 was chosen for this

parameter and applied across all stations, as a lower value is more applicable at higher wind speeds (Justus and Mikhail 1976), such as those encountered during frontal passage and similar storm events. These adjustments were made recognizing that this model and linear correction approach is only an approximation of the true wind velocity at the gage orifice height at each location. The overall effect of this adjustment is to reduce the wind velocity number by about one-third, which in turn reduces the amount of estimated precipitation undercatch by the Alter-shielded Geonor gages compared with uncorrected 10 m wind data.

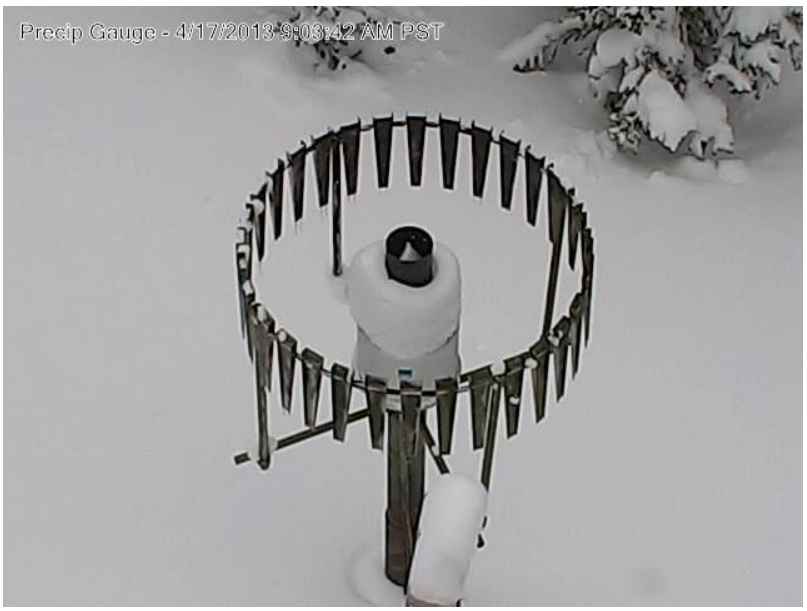

Figure 37. Snow bridging at high elevation.

Snow bridging caught on camera at the Subalpine study site. A partial plug of snow had accumulated on the sidewall of the Geonor gage orifice and did not fall into the weighing sensor until later in the day when solar radiation increased.

No attempt was made to correct for wetting losses, evaporation, or other factors. The Geonor gages were charged with a combination anti-freeze/mineral oil solution to mitigate evaporation as much as possible, and wetting losses are generally assumed to be minimal (e.g. < 5%; Legates and Willmott 1990), although specific to gage type as well as precipitation mode/intensity (Yang et al. 1998; Rasmussen et al. 2012). The location of the Geonor gages at each site, as well as typically low maximum

snow depths, ensured that precipitation overcatch due to migrating snow blowing into the orifice is most likely non-existent.

All precipitation values after classification were derived from shielded Geonor mass-weighing sensors rather than tipping buckets. While these gage types have their own sources of bias (see Chapter 2 and discussion in Rasmussen et al., 2012), wind-based undercatch correction was considered to be sufficient for purposes of comparing relative precipitation amounts between sites. Because the Geonor orifices on these sites are unheated due to power limitations, it is possible that freezing or bridging snow in the orifice could contribute to undercatch or false timing of precipitation at the hourly level during extremely cold events or rapid warm-cold transitions during high-intensity events. Indeed, during the QC process such an event was observed when a significant hourly precipitation catch was recorded during a time of lower humidity and sunlight at the upper-elevation Subalpine site in the Snake Range (Figure 37). Appendix 3 contains additional diagnostic and descriptive data used during the QC/correction process.

For subsequent analyses that involve comparisons between precipitation phases, only precipitation meeting or exceeding 0.7 mm hr^{-1} intensity (post wind-correction) is considered, given filter cutoffs set for during the GDM partitioning procedure. This ensures that relative amounts of liquid *versus* frozen and mixed classifications are comparable and not unduly biased towards the liquid category.

Mean monthly precipitation

Mean monthly precipitation was summed from the QC'd, phase-classified, and wind-corrected Geonor gage data exceeding 0.7 mm hr^{-1} (Table 3.3). Because lower-intensity events are not included in these totals, an attempt was made to assess first-order differences between all precipitation and precipitation at or above 0.7 mm hr^{-1}, as snow precipitation in some regions of the world is dominated by events of 1

mm or less (Zhang et al. 2015). In order to provide "official" total monthly, seasonal, or annual catch comparable to a reporting government agency, event-by-event expert correction must be performed and site-specific estimates of gage performance and undercatch developed through supervised *in-situ* testing. These activities are beyond the scope of this work. However, after applying semi-automated QC checks for sensor resets and other major anomalies, an approximation of the relative contribution of low-intensity precipitation events can be made in this case by taking the monthly difference in catch between the filtered and the summed raw data (positive and negative sensor noise included). The comparison is performed prior to wind correction, because phase classification is required for application of the proper correction equation, and high-resolution phase classification can only take place by using the filtered data in the GDM process described earlier.

Table 3.3. Mean monthly precipitation, 2012-2015.

3.A Corrected classified events, mm ≥ 0.7 mm hr^{-1}												
Site	**Jan**	**Feb**	**Mar**	**Apr**	**May**	**Jun**	**Jul**	**Aug**	**Sep**	**Oct**	**Nov**	**Dec**
Sagebrush	6.3	9.7	4.6	10.2	20.1	2.8	21.8	41.8	29.6	17.6	10.8	22.1
P-J	12.2	17.7	14.7	23.4	32.1	5.5	29.6	39.2	38.7	27.5	13.0	31.7
Montane	25.7	27.8	29.9	43.5	46.1	7.4	37.4	44.8	44.7	35.2	26.4	46.5
Subalpine	40.2	41.8	49.8	69.3	71.6	12.2	53.4	56.7	54.7	46.9	46.7	75.3
Sheep*	11.4	16.0	24.8	18.8	9.6	2.7	52.2	72.5	19.0	21.1	18.2	21.3
3.B Uncorrected classified events, mm ≥ 0.5 mm hr^{-1}												
Sagebrush	5.6	9.3	4.1	8.4	18.9	2.6	19.9	37.5	27.8	16.7	9.4	17.2
P-J	11.9	17.3	13.0	21.5	31.0	5.2	27.9	37.3	37.3	26.1	13.1	30.9
Montane	22.3	24.7	27.0	39.6	43.6	7.0	36.1	42.7	43.4	33.9	22.5	42.8
Subalpine	31.9	34.1	41.0	56.0	63.5	11.7	49.8	53.2	51.4	41.3	35.4	61.8
Sheep*	11.1	15.0	18.3	14.8	8.9	2.5	50.0	68.6	18.1	20.4	15.2	17.4
3.C Uncorrected raw Geonor catch (not QC'd by event), mm												
Sagebrush	9.1	12.1	7.2	10.2	21.7	2.8	21.8	38.4	29.8	19.2	12.0	19.8
P-J	16.5	21.0	18.1	23.7	34.5	5.6	28.6	38.3	39.4	29.8	17.5	38.9
Montane	29.5	30.4	31.0	42.4	50.1	6.7	35.3	42.4	46.0	37.8	29.6	54.7
Subalpine	33.7	36.5	39.5	56.3	69.3	11.5	50.5	52.3	54.6	45.3	41.4	73.1
Sheep*	14.9	19.4	19.7	16.3	11.2	2.3	51.5	71.1	18.7	22.3	18.4	23.6
3.D Percent difference, Raw-Uncorrected												
	Δ%	Δ%	Δ%	Δ%	Δ%	Δ%	Δ%	Δ%	Δ%	Δ%	Δ%	Δ%
Sagebrush	38.5	23.1	43.1	17.6	12.9	7.1	8.7	2.3	6.7	13.0	21.7	13.1
P-J	27.9	17.6	28.2	9.3	10.1	7.1	2.4	2.6	5.3	12.4	25.1	20.6
Montane	24.4	18.8	12.9	6.6	13.0	-4.5	-2.3	-0.7	5.7	10.3	24.0	21.8
Subalpine	5.3	6.6	-3.8	0.5	8.4	-1.7	1.4	-1.7	5.9	8.8	14.5	15.5
Sheep*	25.5	22.7	7.1	9.2	20.5	-8.7	2.9	3.5	3.2	8.5	17.4	26.3
SR Mean	24.0	16.5	20.1	8.5	11.1	2.0	2.6	0.6	5.9	11.1	21.3	17.8

*Sheep Montane site missing corrected precipitation data from 16 Aug to 29 Nov 2012

Table 3.3 contains mean monthly precipitation across 2012–2015 for each site, with section 3.A representing the corrected classified events used in the remainder of these analyses. Section 3.B contains the values resulting from the GDM filter but prior to wind correction, and 3.C contains the uncorrected raw summations of the Geonor sensor data. The percentage difference of the values in 3.B and 3.C are shown in section 3.D. The final row indicates the mean monthly percentage difference, which can be interpreted as the mean fraction of uncorrected precipitation not accounted for by the GDM filtering procedure. While these differences vary highly from site-to-site, it is evident that the mean differences are much higher in the winter (17–24%) than in the summer (2–6%). The amount of error strictly associated with sensor noise in the Geonor during summer as opposed to winter is not estimated here, but raw plots of the Geonor 10-minute data suggest that there can be times when the noise amplitude is large (Appendix 3). Another potential source of error in the raw data is long-term electro/mechanical sensor drift (positive or negative) that is not included in the GDM event-by-event classification and summation.

Taking these unknowns into account and reviewing the range of individual station differences (Table 3.D), it could be estimated that typical low-intensity precipitation amounts are 15–30% of the monthly winter totals, and 2–8% of the monthly summer totals, with transition seasons seeing numbers in between these ranges. This may be a generous estimate, as the higher percentage differences noted at the lower elevation sites are most likely results of individual low-intensity storm events, and there are only four years of data to work with. Because monthly totals at lower elevations are much lower than those at high elevation, single longer-duration events with lower intensity could easily change the monthly differences given four years of data. For instance, the intensity-duration-frequency curves for nearby Baker, Nevada (estimated by the National Weather Service from long-term precipitation observations) place a 6-day 0.5 mm hr^{-1} event as reoccurring every 2 years (Appendix 3.6; NOAA-NWS

2016), a total volume equivalent to 2–3 times wintertime monthly normals (Figure 34). Given that this study's observations were taken during a timeframe recognized as a significant drought period in the western U.S. (Swain 2015), the low numbers given in Table 3.3 are probably not unusual as individual storm effects on the total are amplified by general drought conditions.

The SN Subalpine winter difference between classified events and raw catch is substantially lower than the other two mountain sites (Table 3.D). This is indicative of either a systematic change in precipitation intensities at very high elevations (unlikely), or a mechanistic error source. The raw sensor data plot (Appendix 3) illustrates that winter sub-daily noise in the SN Subalpine sensor is more variable than the other sites, although these should still sum to 0 in the long term. Another likely cause of this departure is the confirmed orifice bridging events during significant snowfall events at SN Subalpine (Figure 37). One side effect of the bridging is that more snow is lost out of the orifice due to wind eddies because it is not immediately falling to the bottom and melting in the antifreeze pre-charge. If these occur often enough, the gage will undercatch even more than normal and light, minimal accumulation snow from low-intensity periods during the overall storm event is more susceptible to loss (Rasmussen et al. 2012). This in turn would cause the winter totals of low-intensity events to decline, and the relative difference to the filtered/classified totals would shrink accordingly.

Overall, the greater percentage of lower-intensity precipitation appears to occur in the winter, and thus during frozen events. This phenomenon must therefore be taken into account when assessing the breakdown of frozen versus liquid or mixed precipitation at an annual scale. Undercatch resulting from processing methods (e.g. < 0.7 mm hr^{-1} filter cutoffs), however, should not significantly impact a month-by-month analysis of the relative fractions of precipitation phase between the stations across the elevation gradient.

Total classified monthly precipitation

In order to assess the relative character of the years used in the observations, total monthly precipitation was graphed for both the corrected/classified events and the raw sensor catch (Figure 38). The difference between the two is not great, and the impact on month-to-month patterns is negligible. Overall, the annual patterns during this drought period seem to oscillate between seasonal patterns of nearby climate divisions. First, the observed seasonal patterns contrast strongly with the climate division normals for both mountain ranges (Div. 2, Figure 34), with general failures of wintertime precipitation relative to other seasons. For the Snake Range stations, 2012, 2013, and 2014 most resemble NV Division 3, while 2015 seems to match Utah Division 1 with a strong springtime and weak winters. For the Sheep Range site, the NAM season (July-August) remains the primary contributor in all years under otherwise dry conditions.

Notable features include the stormy May of 2015, a dry June across all years, and the appearance of summertime moisture mitigating dry conditions. Examination of the December–May six-month precipitation departures from normal indicate that 2012–2014 were drier than normal, while 2015 was slightly above average (Appendix 3.7; NOAA-NCDC 2016). July-August-September precipitation for 2012–2014 appears to be higher than the climatological normal in relative terms, indicating stronger summertime moisture flow into the region during otherwise drier years. Because these “drought” years are not “normal” where regional seasonal precipitation is concerned, assessment of annual soil moisture curves and response of shallow soil moisture to different precipitation episodes becomes relevant. Of particular interest in this regard is the monthly/seasonal fraction of frozen precipitation at each site, and associated observations of seasonally available soil moisture at each site. Monthly precipitation totals and their seasonal patterns do not necessarily tell us 1) if that precipitation was frozen or liquid, or 2) if that precipitation was “effective”, that is, did it serve to recharge the local soil moisture adequately to

mitigate overall drier conditions for local ecology during the springtime growing season as well as the summer and fall timeframes.

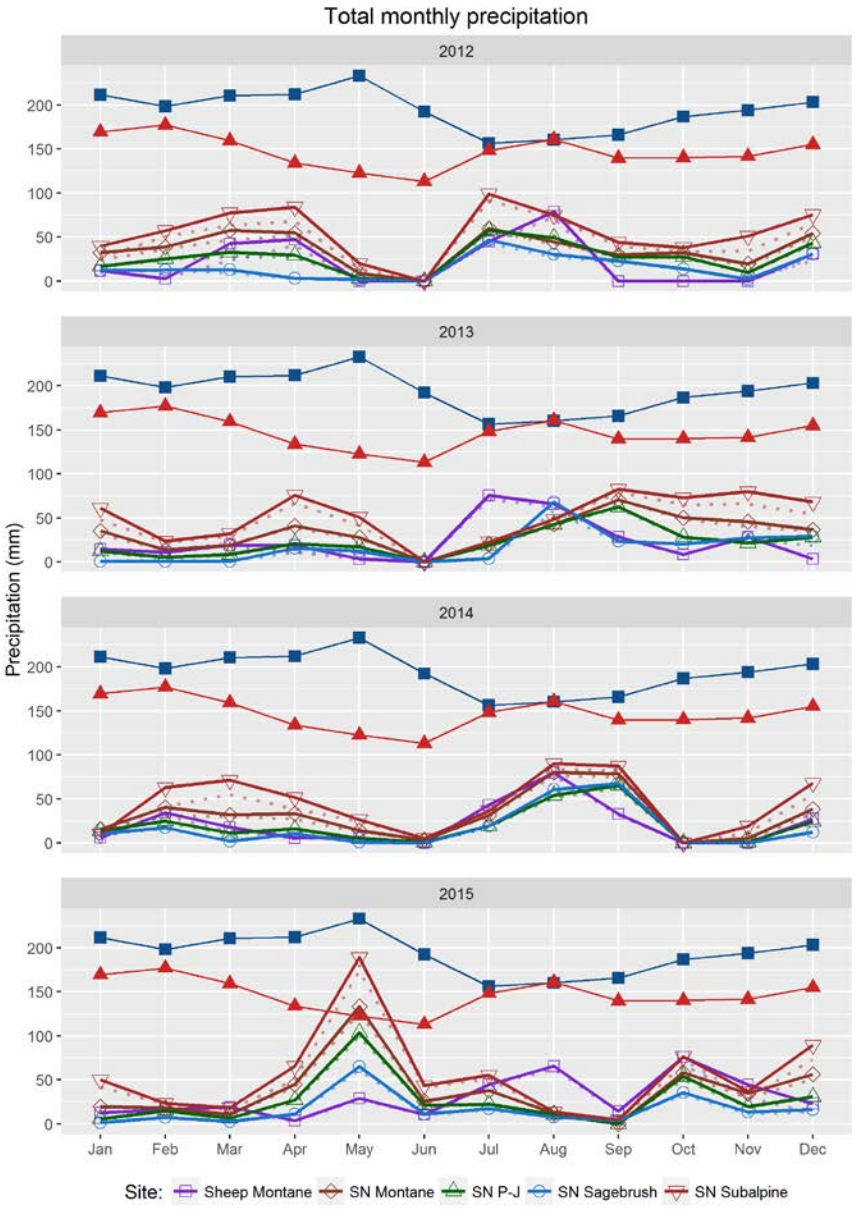

Figure 38. Total monthly precipitation, by year.

Total monthly precipitation at the Snake Range sites is shown for the corrected/classified precipitation data (*solid lines*) as well as the uncorrected raw gage catch (*dotted lines*). The annual patterns (except for 2015) diverge significantly from the divisional climatology in Figure 34, indicating that these were not "normal" years. The 120-year means from NV climate divisions 02 (*solid blue squares*) and 04 (*solid red triangles*) are overplotted as dimensionless indices for pattern comparison in each year. The Sheep Montane site is missing precipitation data from 16 Aug 2012 to 29 Nov 2012.

Fractions of frozen precipitation across the gradient

Estimates of the percentage of total precipitation occurring in frozen form for each month in the years 2012–2015 show high variability across the elevation gradient (Figure 39), although the general trend is definitely an increasing fraction with elevation as would be expected in a mid-latitude mountain environment (Table 3.4).

Table 3.4. Monthly mean percent (%) frozen precipitation, 2012-2015

Site	Jan	Feb	Mar	Apr	May	Jun	Jul	Aug	Sep	Oct	Nov	Dec	Overall
Sagebrush	74.3	46.4	66.5	18.4	1.6	0.0	2.5	2.4	3.5	15.2	52.7	62.8	19.0
P-J	92.2	71.2	84.0	54.8	31.6	0.0	0.0	2.5	3.2	13.9	80.3	91.0	36.7
Montane	98.5	100.0	95.6	92.7	66.4	3.6	5.5	6.9	9.1	43.9	98.2	97.9	58.7
Subalpine	100.0	97.9	100.0	98.1	89.4	21.2	6.9	8.7	13.1	79.5	98.8	100.0	68.7
Sheep M.	37.6	50.6	90.9	79.0	26.7	0.0	0.3	0.9	2.6	9.6	73.1	85.1	27.5

In general, all sites receive frozen precipitation in fall, winter, and spring months, with the June-Sept window being nearly devoid of frozen events during the years of observation. Events classified as frozen during the July-August timeframe are either hail events or small-magnitude misidentifications by the GDM filter due to wetting loss or hydrometeor bounce out of the tipping bucket orifice. Hail events classified as “mixed” are certainly visible (dashed lines, Figure 39). These patterns can be examined in greater detail using the daily classified precipitation totals in Appendix 3.8. Annual patterns in the frozen/liquid ratio for the two upper-elevation sites in the Snake Range are generally similar. The Pinyon-Juniper site sometimes follows the seasonal pattern of the upper sites, and sometimes that of the lower Sagebrush site. There are similarities between the two lower Snake Range sites and the Sheep Range site. The Sagebrush site is the only true valley basin location (Figure 35), and therefore does not experience orographic effects that modify precipitation processes on the mountain block. This site sees substantially less precipitation in frozen form (19.7% overall) than the other sites (Table 3.4), but

examination of the lower-intensity totals in Table 3.3 suggests that perhaps this site sees a greater fraction of low-intensity precipitation in Dec-Jan-Feb-Mar, which would more than likely occur as snow and be missed in the classified totals. It certainly receives less frozen precipitation during the transition seasons.

Of particular interest is the May-June transition, where the mountain sites see a sharp decrease in the frozen fraction, and the month of October, where the frozen fraction varies year-to-year on the mountain sites. This variable behavior in transition-season precipitation character suggests a high level of control that synoptic conditions can exert in the Great Basin on an interannual basis, and brings up questions of how local snowpack conditions, shallow soil moisture, and vegetation growth all respond to such variability. In order to broadly evaluate interactions, observations are scaled to daily values in order to review all four years in some detail, and then individual timeframes of interest are examined using hourly data.

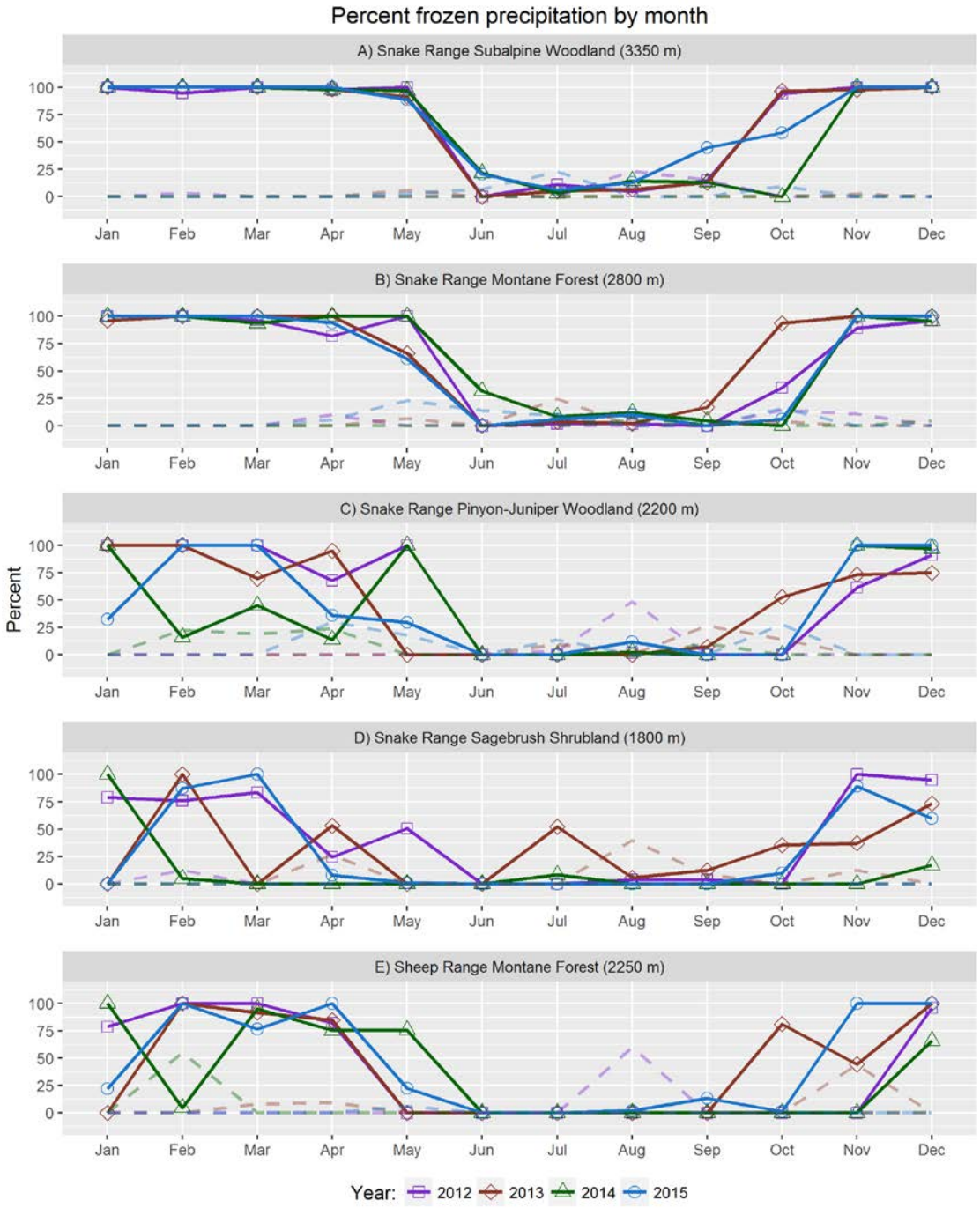

Figure 39. Frozen percentages of monthly precipitation.

Percentage of total monthly precipitation classified as “frozen” for each site during the 2012 – 2015 timeframe. “Mixed” classification is shown as dashed lines. Low elevation sites see a significantly lower proportion of frozen precipitation than the upper-elevation sites. Summertime hail events show up as frozen and mixed, are highly localized, and do not impact one station more than the others within this timeframe.

Daily ecohydrologic patterns across the gradient

In order to assess the interaction of precipitation, soil moisture, and atmospheric conditions at each site, observations of shallow soil moisture, relative humidity, and snowpack presence were added to the temperature and precipitation observations. At the Snake Range Subalpine, Snake Range Montane, and Sheep Range Montane sites, dominant vegetation species (trees) were instrumented with sap flow sensors recording the relative sap velocity at hourly intervals. This array of sensors and information provides a detailed picture of how precipitation impacts near-surface ecohydrology under different seasonal conditions.

Description of observed variables

Shallow soil moisture was measured using buried electronic probes at a range of depths and orientations. Volumetric water content (VWC) for the soil located between probe tines is reported as a percentage. In 2012, the probes used were Acclima Digital TDT devices; however, these sensors revealed a high failure rate and they were replaced in late 2012 with Campbell Scientific CS-650 time-domain reflectometry (TDR) probes instead. For this study, results are reported from a 10 cm depth horizontally-oriented probe at each site. Because the soil structure and horizon depths are significantly different between sites across the gradient, the shallow, horizontally-oriented probe was judged to be the most indicative of rapid response of soil moisture to seasonal processes and thus useful for relative comparisons across different sites. In 2015, 2014, and 2013, these data are continuous except for a 2-week gap in June 2014 at the Snake Range Sagebrush site. In 2012, data are continuous except for gaps in October-December when the sensors were replaced and a settling time for the new installation was allowed. The Acclima sensor at the SR Sagebrush site was non-functional in 2012, so data are not available until November. Data from the Acclima sensors in 2012 were standardized to fit the distributions of the Campbell sensors at each site for comparability purposes. Rough estimates of VWC

at field capacity (VWC_{FC}) and permanent wilting point (VWC_{PWP}) can be made for each site by alternatively examining the long-term mean VWC during wintertime snow cover or during the non-growing season (maximum drainage) and the lowest VWC values in the driest portions of the growing season (maximum plant use), although actual VWC_{PWP} varies with potential evapotranspiration (Denmead and Shaw 1962).

Vapor pressure deficit (VPD; the difference between the saturated vapor pressure at a given temperature and the actual amount of saturation) was calculated at hourly intervals using the air temperature and relative humidity measurements with the following equation:

$$VPD = 0.611\ exp\left[\frac{17.27T}{(T + 237.3)}\right] \times \left[1 - \frac{RH}{100}\right]$$

where *VPD* is expressed in kPa, *T* is air temperature (dry bulb) and *RH* is relative humidity in percent (Howell 1995). For all sites, air temperature and relative humidity were measured at the 2 m height above ground; however, the 2 m sensor at the SR Pinyon-Juniper site experienced occasional problems and these temperature data were substituted using measurements taken at the 10 m height (resulting in a more narrow diurnal range between daily maximum and minimum and a slight reduction in estimated daily VPD). All temperature sensors used were Type-T thermocouple wires installed in 6-plate Gill-type passive radiation shields and attached to Campbell CR3000 dataloggers with on-board calibrated temperature references.

Snowpack presence was determined by evaluating daily images of the ground surface above the soil moisture probes, and delineating the wintertime window between snowpack establishment and melt-off (coverage longer than 7 days). Short-term snow coverage which melted off within a week from early or late storms was not included in these date windows.

Sap flow data were obtained by applying the Granier thermal dissipation probe (TDP) technique, which uses a combination of passive and heated electrical probes to measure movement of xylem sap in plant stems (Granier 1987). While sap flow measurements are often applied in a water-balance context (e.g. Granier et al. 2000; Wilson et al. 2001; Williams et al. 2004), they are also useful indicators of plant activity in terms of transpiration and water stress when combined with basic atmospheric and soil measurements (Pataki et al. 2000; Burgess et al. 2001). Sap flow sensors were installed on sub- and co-dominant mature trees (not saplings) at the Snake Range Subalpine, Snake Range Montane, and Sheep Range Montane sites with some replication across trees and species, but not enough to perform comprehensive whole-plant water capacitance or estimate stand-level transpiration (Burgess and Dawson 2008); rather, these installations were performed at the "pilot" scale, to get a first-order assessment of tree growth activity across a variety of locations and in species that have not been studied in this fashion within the Great Basin. Conversion of raw sap flow sensor measurements to velocity in mm sec^{-1} can be accomplished using the empirically-derived Granier (1987) equation

$$Q_S = 0.119\left(\frac{\Delta T_0 - \Delta T}{\Delta T}\right)^{1.231}$$

where Q_S is velocity in mm sec^{-1}, ΔT is the sensor value (the difference in passive and active probe temperatures), and ΔT_0 is the maximum daily value of ΔT, which is assumed to be zero sap flow. Ranges of values reported in sap flow literature vary substantially, and are usually evaluated over very short timescales (e.g. days). Because of potential long-term changes in conductivity of tree tissues surrounding the TDP probes and uncertainties related to intra-species and stem radius replication (Nadezhdina et al. 2002), very low-flow or reverse-flow conditions (Burgess et al. 2001), and probe separation (Köstner et al. 1998), sap flow data are presented in either daily difference form ($\Delta T_0 - \Delta T$; greater differences indicate higher maximum velocities) or in raw hourly ΔT values. Maintaining these

forms should be sufficient for purposes of reviewing sensor and tree behavior in a relative sense over long time series, as well as instantaneous comparisons to other variables.

Storm event identification

Because this investigation is expressly interested in highlighting impacts of precipitation on near-surface processes, multiple temporal resolutions must be considered. The scope of this study is concerned with hourly-to-seasonal effects, and precipitation arrives via storm events that can last from minutes to days. Accounting for storm "pulses" as single contributing units is a prominent conceptual model in semi-arid ecology (e.g. Weltzin et al. 2003; Chesson et al. 2004; Loik et al. 2004; Schwinning and Sala 2004; Potts et al. 2006). Total storm precipitation amount as well as the intensity at which the bulk of the storm precipitation arrives is closely tied to the balance of runoff, infiltration, and surficial evaporation as a fundamental principle of surface hydrology (Horton 1933). Thus, not all storms (or precipitation characteristics) are equal, hence the concept of "tiered" ecosystem responses to different storm mechanisms which are subsequently filtered by local soil conditions (Reynolds et al. 2004).

Depending on the science question and scale of interest, "effective" precipitation is not strictly dictated by precipitation amount, but also includes information on infiltration as opposed to runoff (Yevjevich 1967). The number of variables when directly calculating "effective", or locally-infiltrating, precipitation is substantial, including hillslope length, surface roughness, surface vegetation, local soil hydrological conductivity, saturation/infiltration curves for the soil column, current saturation, rainfall rate, and so forth (Dunne et al. 1991). However, it is also common to infer effective precipitation using empirical data from measurements of the precipitation, runoff, and infiltration processes themselves (Beven 2011). This study does neither in the modeling sense, but instead qualitatively assesses the impacts of each precipitation event to specific measured variables at each site. Following this line of investigation,

"storm" events were classified as those time intervals where all days receiving precipitation were grouped into the same "storm" as long as the days were immediately adjacent. This grouping scheme also allowed for intra-storm gaps of one non-precipitation day, because of the intensity-selection bias of the GDM filter. In this fashion, each significant precipitation "event" is identified that should have discrete impacts on the local ecohydrology. Weighted mean storm intensity was calculated for each grouped "storm" event by taking each hour with measured precipitation during the event, weighting that value using its percentage of the storm total, and summing the weighted values. The resulting weighted average provides a representative estimate of the hourly precipitation rate associated with the bulk of the storm's rain or snowfall.

Evaluation of daily ecohydrology across the gradient

The ecoclimatic variables of daily air temperature, VPD, shallow soil VWC, wintertime snow cover, precipitation phase and amount, and weighted mean storm intensity are shown in Figure 40–Figure 48, first by each study site for 2012–2015 and then across sites for each year. In this manner, temporal as well as spatial/elevational dimensions can be evaluated.

Following the daily data summaries are specific "case study" examples of processes and interactions that were identified as being of ecohydrologic relevance and until this study were either unobserved directly (relative daily drought stress between mountain conifer species) or entirely unknown (the effects of hail storms on mid-drought tree stress at the Mojave transition). Hourly data in each case study show how diurnal cycles of temperature, VPD, and precipitation by phase are related to soil VWC and sap flow by species. These mechanisms can easily be placed in seasonal context by referring to the annual plots of daily data. The variables of sap flow and VPD were plotted as indices in the case studies rather than in engineering units.

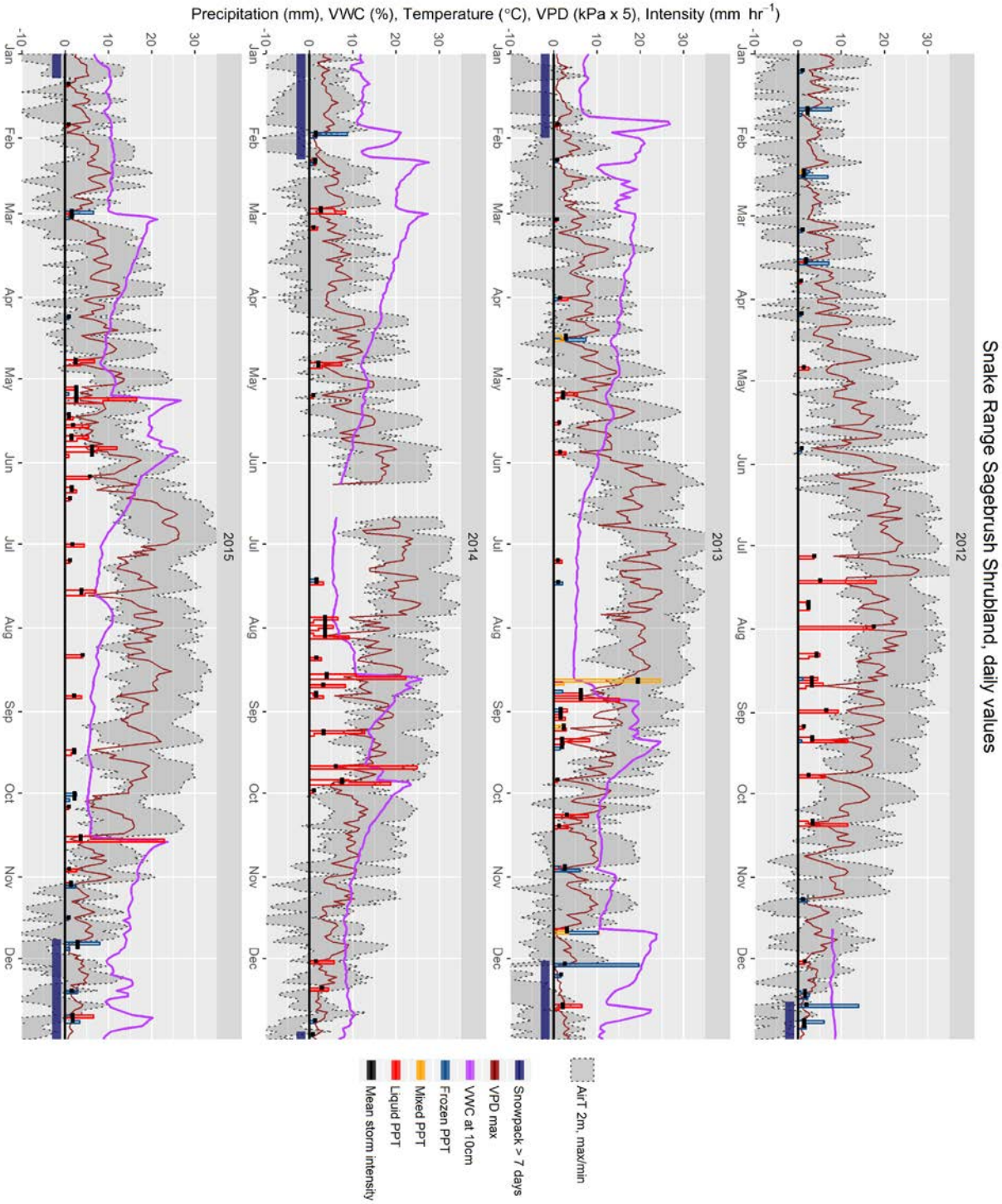

Figure 40. Timeseries of observed ecohydrologic variables at the SR Sagebrush site.

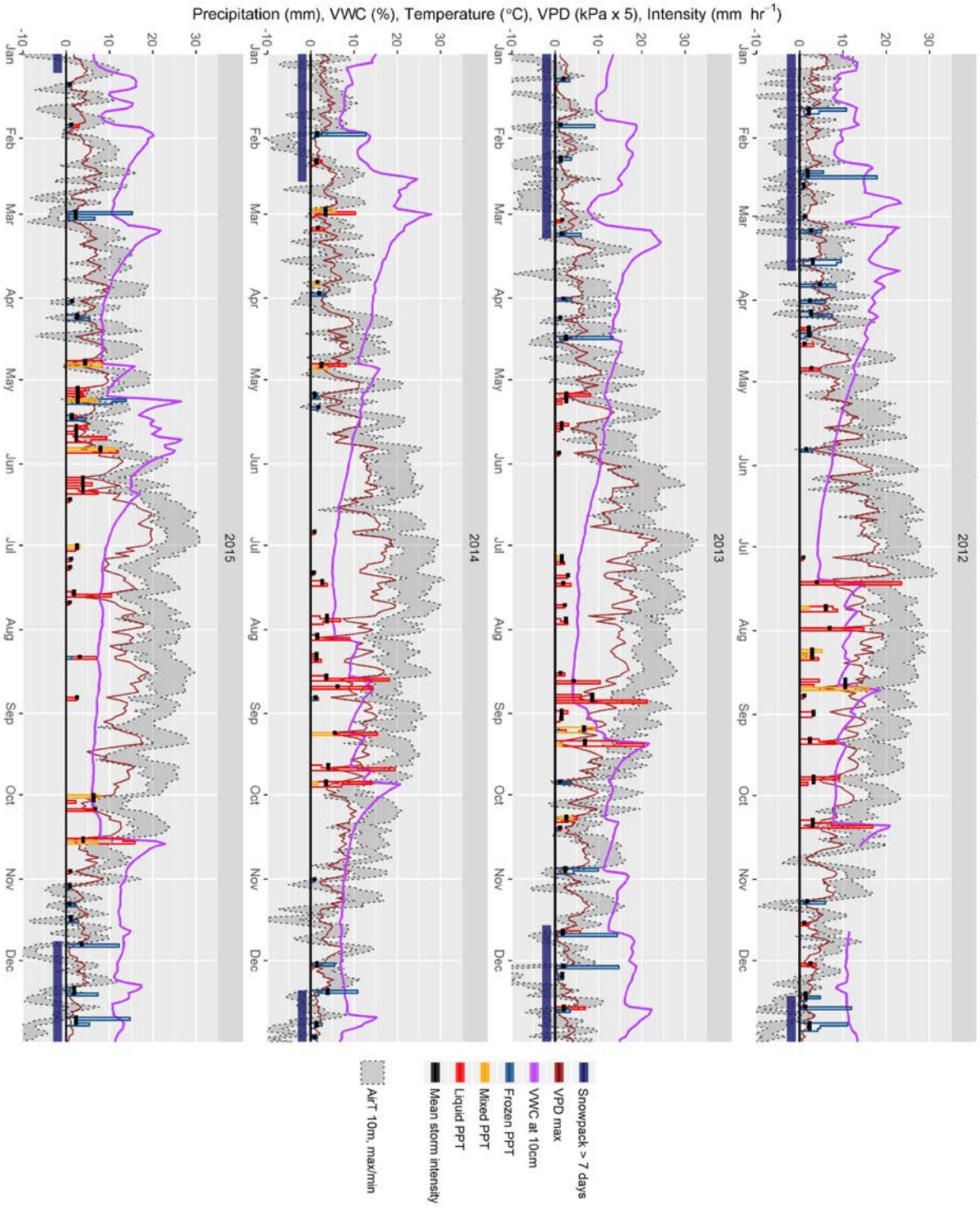

Figure 41. Timeseries of observed ecohydrologic variables at the SR Pinyon-Juniper site.

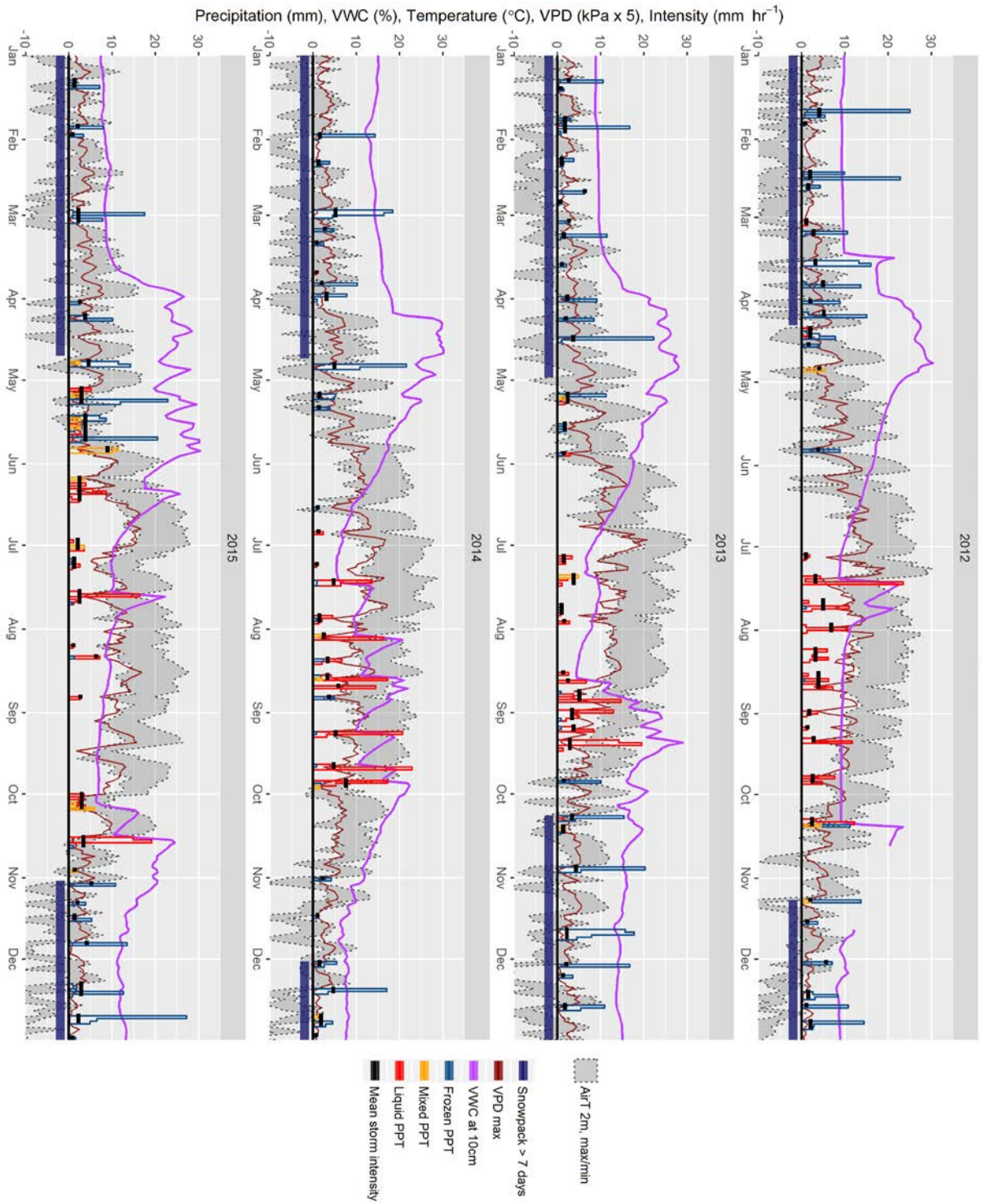

Figure 42**.** Timeseries of observed ecohydrologic variables at the SR Montane site.

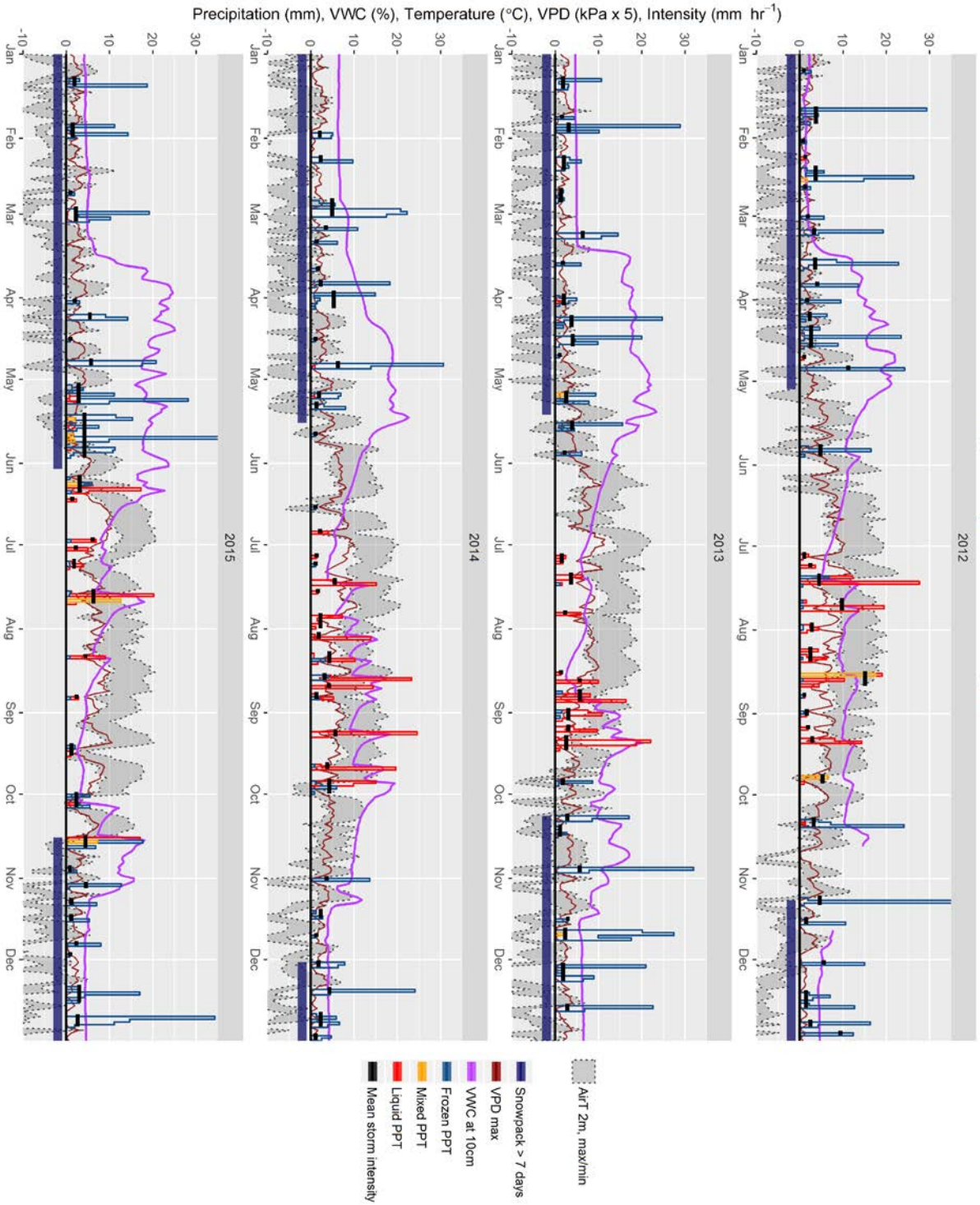

Figure 43**.** Timeseries of observed ecohydrologic variables at the SR Subalpine site.

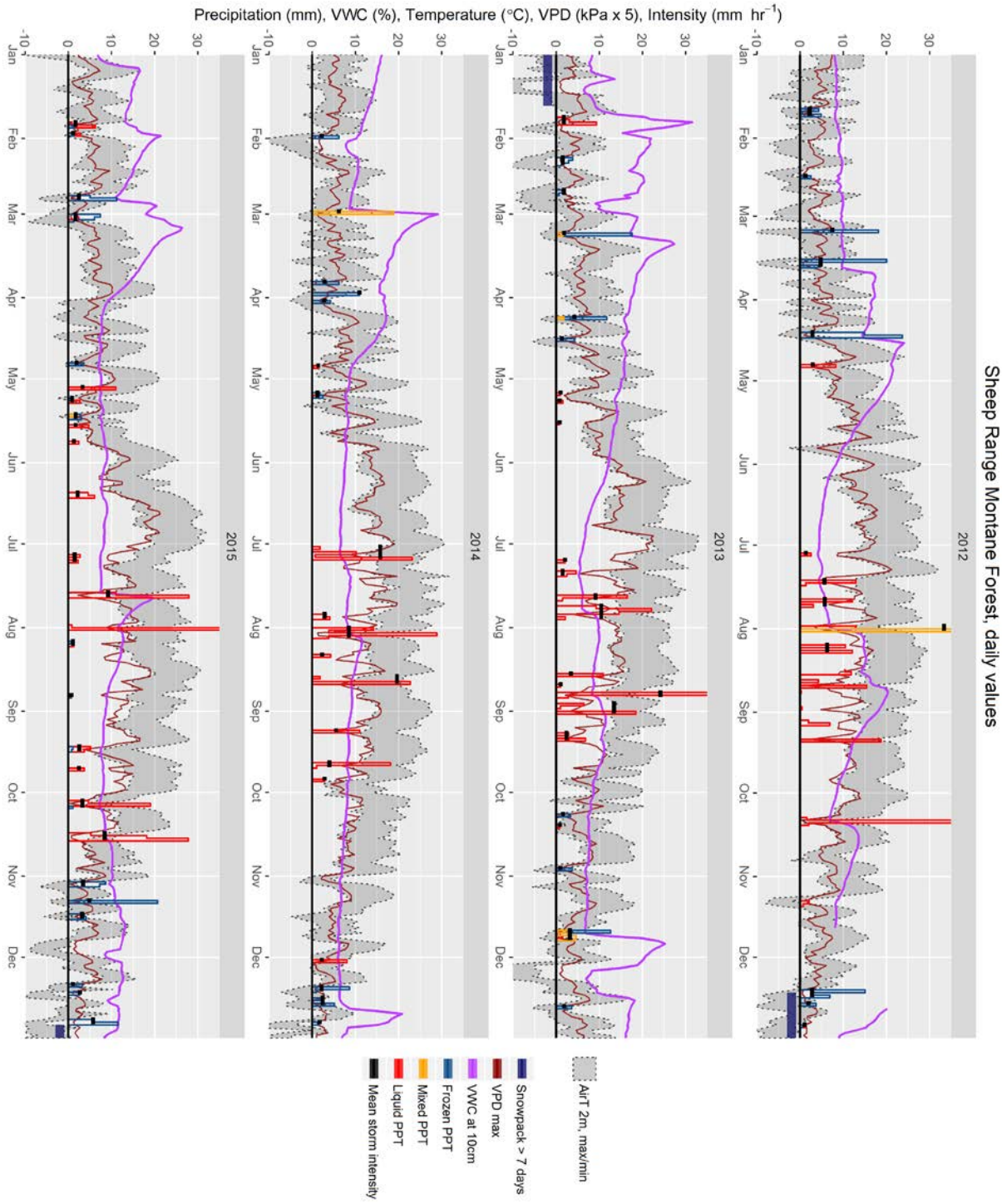

Figure 44. Timeseries of observed ecohydrologic variables at the Sheep Montane site.

Precipitation from 16 Aug to 29 Nov 2012 is substituted as the raw tipping bucket catch and therefore was not classified or included in storm summaries.

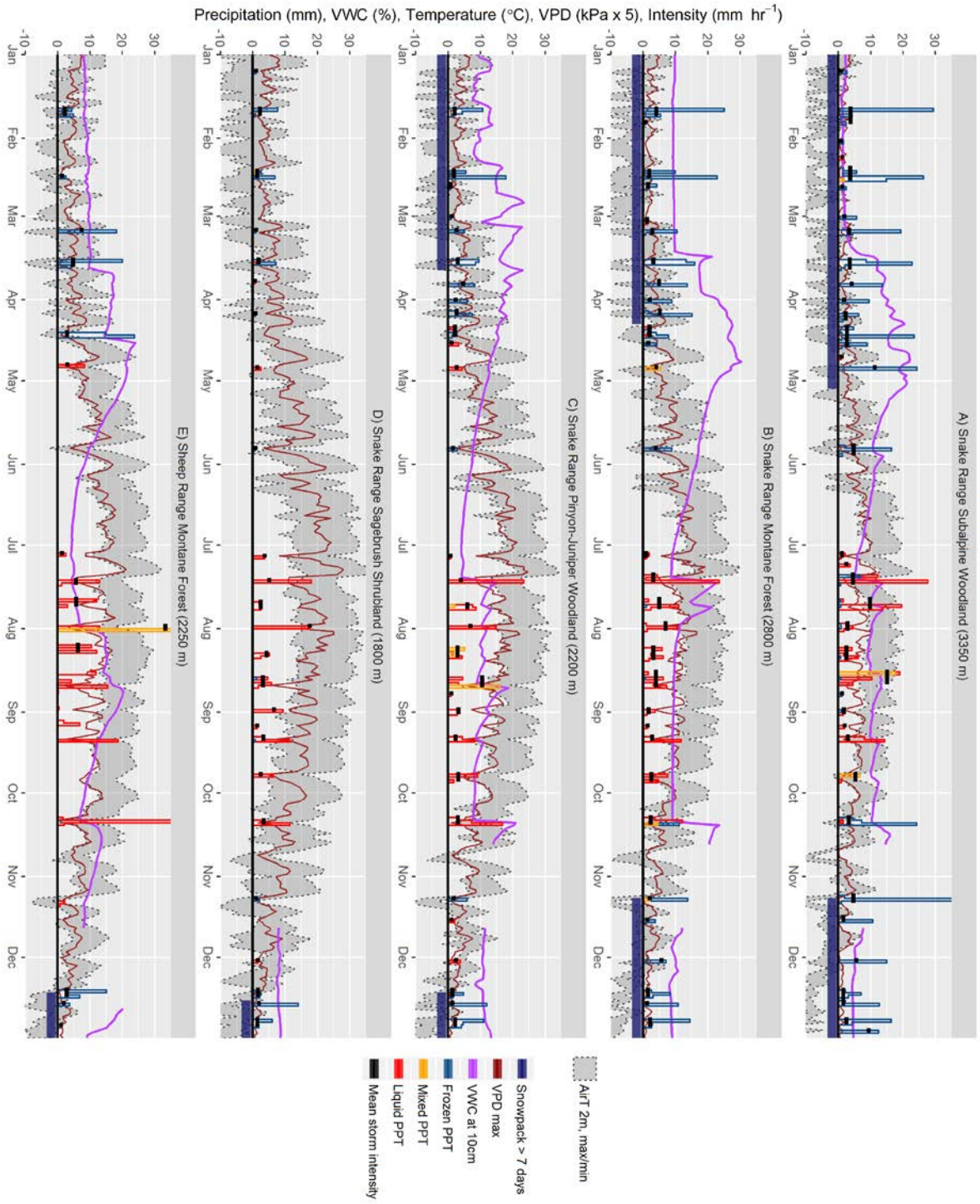

Figure 45. Timeseries of observed ecohydrologic variables at all five sites during the year 2012.

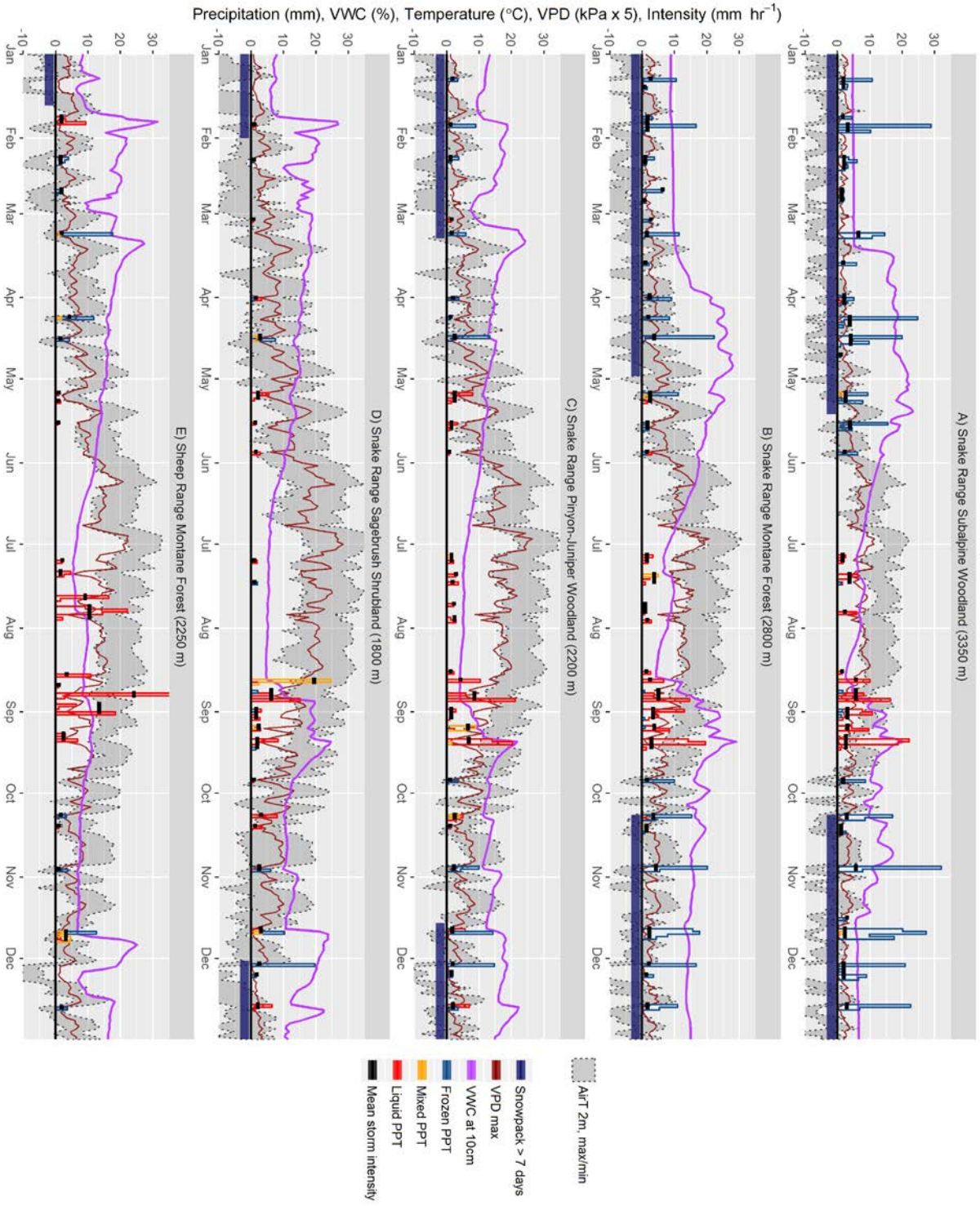

Figure 46**.** Timeseries of observed ecohydrologic variables at all five sites during the year 2013.

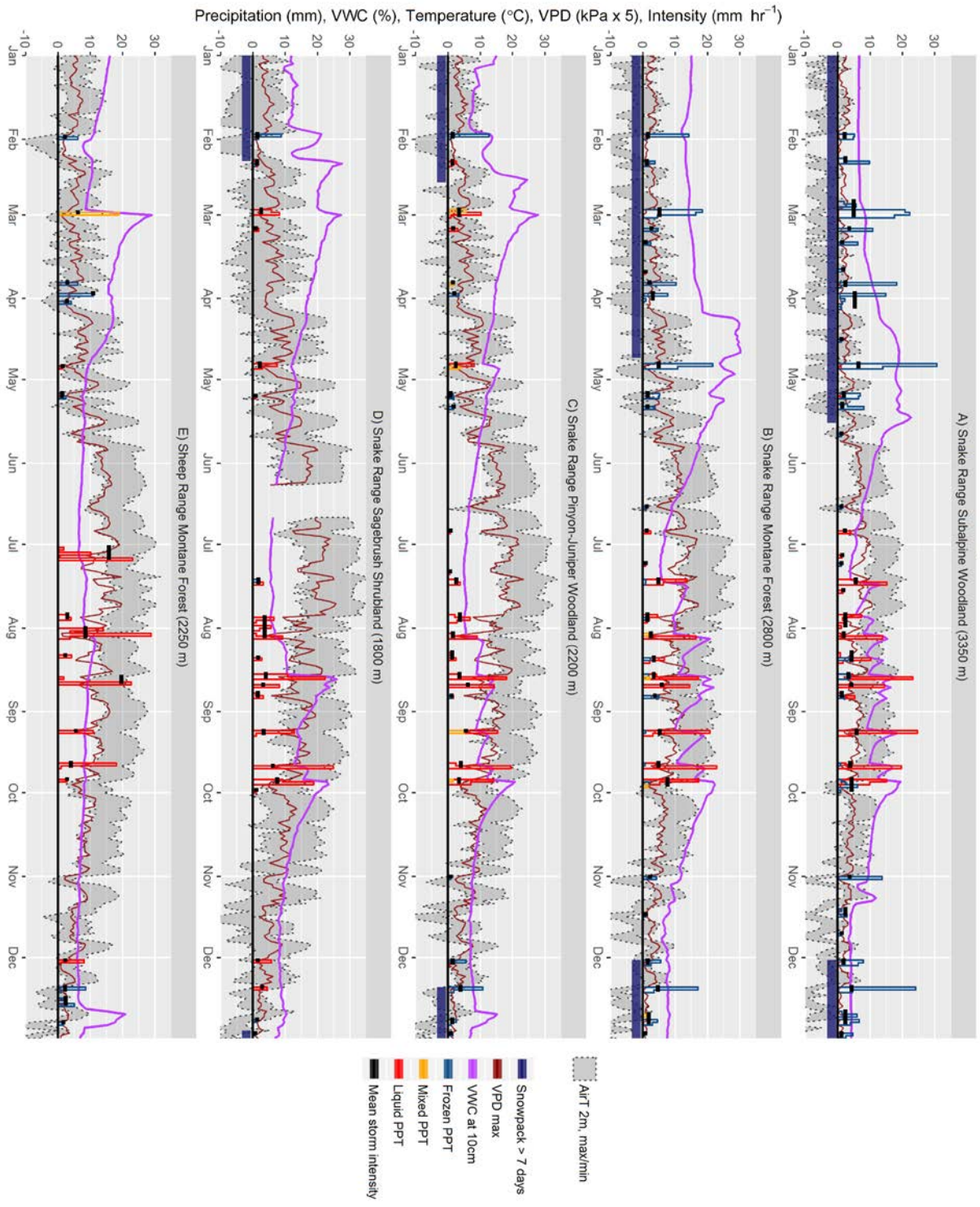

Figure 47**.** Timeseries of observed ecohydrologic variables at all five sites during the year 2014.

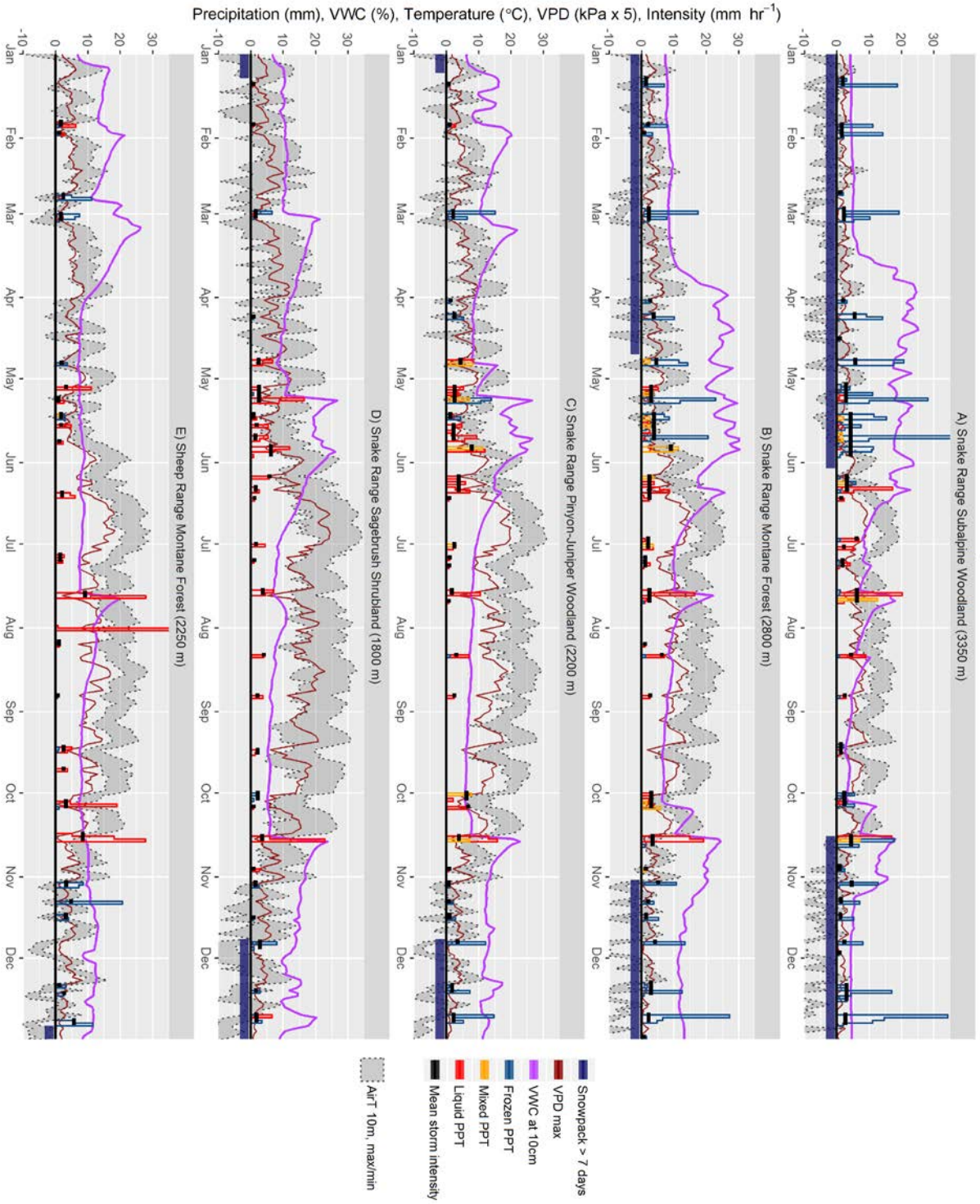

Figure 48**.** Timeseries of observed ecohydrologic variables at all five sites during the year 2015.

Snake Range Sagebrush

For the SR Sagebrush site (Figure 40), soil moisture data are not available during 2012 due to a sensor malfunction, and there is also a short data gap in June 2014 due to battery failure. Notable features of this 4-year interval include different precipitation seasonality each year. Persistent snow cover was not present in early 2012, and there were only 3 significant storms occurring prior to July. Summer storms separated by about 1 week punctuated July–September 2012, presumably mitigating what otherwise was a very dry year. In 2013, snow cover was present in January, a remnant of a mid-December storm that persisted due to lower temperatures. Spring 2013 was only lightly punctuated by precipitation, but enough water arrived to prolong reductions of soil VWC. June and July of that year were extremely dry (as evidenced by the shallow soil moisture curve) right up until an intense storm event in August deposited over 20 mm of liquid equivalent in one hour. This was a mixed rain/hail event that was flagged by the GDM filter and confirmed with hourly imagery (Figure 49). This event only partially affected shallow soil moisture, and it was not until a longer-duration storm of moderate intensity a few days later that sufficient infiltration occurred to recharge soil moisture to springtime levels. Persistent smaller precipitation events throughout September coupled with lower VPD during this period maintained high soil VWC going into Fall 2013.

Figure 49. Mixed rain and hail at the SR Sagebrush site.

A mixed rain/hail storm event at the SR Sagebrush site on 20 August 2013 deposited over 30 mm of precipitation in a short period of time. In this image, pooling and runoff are clearly visible, indicative of the "flash-flood" nature of some Great Basin high-intensity storms. The GDM processing filter correctly flagged this event as "mixed" precipitation, not entirely "frozen", and not entirely "liquid", demonstrating the usefulness of the method in capturing unusual precipitation events even during the warm seasons.

Snow cover persisted into February 2014, in spite of a warm rain event in late 2013 that partially melted the snowpack. Soil VWC in 2014 peaked in March with one spring storm making an impact to delay maximum drying by roughly 2 weeks. Summer rains arrived in late July, and recharged soil VWC significantly. No snowfall occurred in late 2014. Temperatures stayed elevated starting in early 2015 exacerbating a dry winter with only a single major storm in March. The soil VWC outlook for 2015 was very bleak until a wet May materialized; however a very warm June with persistently high VPD quickly erased gains and a relatively hot and dry summer followed until a large rain storm in October. Overall, precipitation at this site occurs at moderate to low intensity (< 5 mm hr^{-1}) that improves soil VWC in all seasons, with infrequent high-intensity (> 10 mm hr^{-1}; two in four years) events that are not particularly effective due to runoff rather than infiltration. For instance, the 20 August 2013 storm totaled 39.4 mm (31% liquid, 19.5 mm hr^{-1} weighted mean intensity), which was 19% of the annual total (203 mm) of classified events. That storm raised the 10 cm soil VWC from 5% to 9% in 2 days, whereas the very next storm (23.9 mm total, 91% liquid, 6.3 mm hr^{-1}) raised the VWC from 8% to 19% over 3 days (Figure 50).

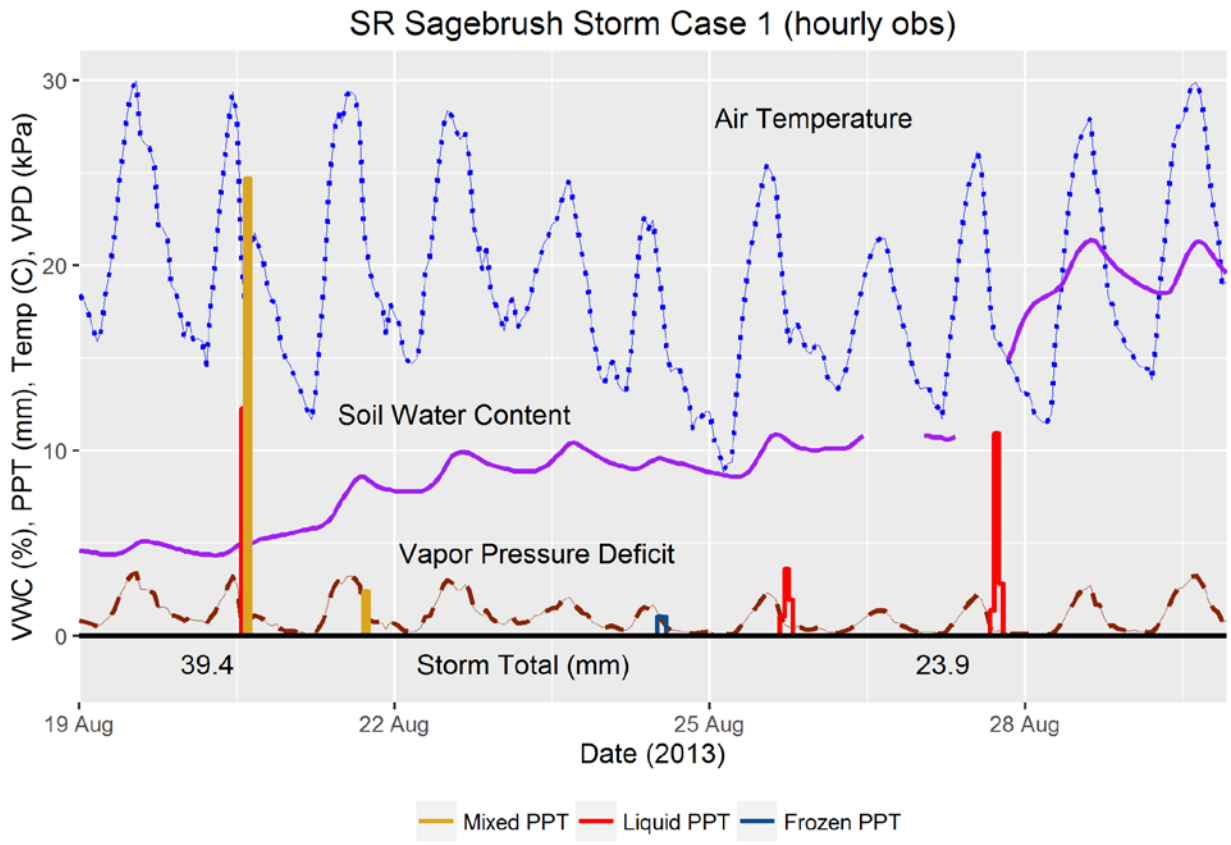

Figure 50. Sagebrush site Case 1.

Two subsequent storms at the SR Sagebrush site had vastly different impacts on soil moisture, primarily due to the differences in intensity. The mixed hail storm of 20 August contained enough rain early in the event to melt the hail on contact, allowing it to contribute to runoff (Figure 49).

Snake Range Pinyon-Juniper

During 2012, the SR Pinyon-Juniper site (Figure 41) started the year with several winter and spring storms which kept soil VWC elevated until April. A dry April-May-June sequence ended in July when the soil VWC was approaching the apparent VWC_{PWP}. Weekly storm events maintained soil moisture throughout the late summer and fall, and low temperatures allowed snow cover to remain until March 2013. Drying in spring 2013 happened more slowly than in 2012, with several minor storm events and reduced VPD prolonging bottoming out of the soil VWC curve. A wet late summer continued into a wet fall, with soil VWC remaining high until a warm, dry January 2014. A cold snap in February 2014

prolonged snowmelt in an otherwise warm winter, and a warmer March storm set the soil VWC peak for the year. Small storms mitigated the drop in soil VWC during the April-May-June window, and it was not until August 2014 that significant precipitation arrived. High temperatures and VPD quickly dried shallow soils between large, moderate-intensity events in August-September, and a dry October-November rapidly allowed the soil VWC to approach the apparent VWC_{FC} point. Only one snow event of significant volume/intensity occurred in December 2014 to February 2015, although the large soil VWC response and lower VPD sequence in late January 2015 indicates that perhaps a persistent low-intensity event occurred between January 14-20 that was not picked up by the precipitation data processing filter (Figure 51). A substantial snow storm in March 2015 was followed by elevated temperatures which rapidly dried soils to levels unseen in the previous three March-April timeframes. Nearly continuous storm activity in May peaked the soils VWC in advance of the driest summer of the four years observed, which was not mitigated substantially until mid-October.

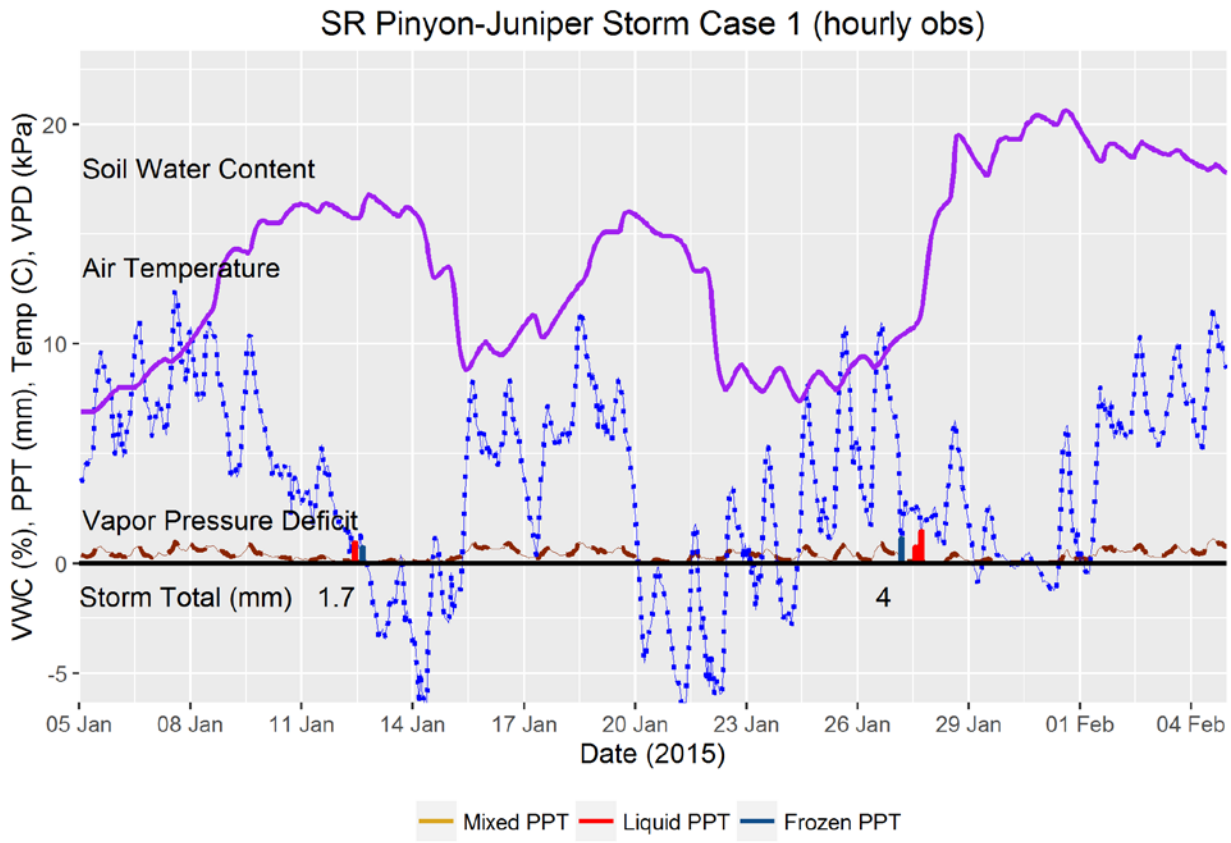

Figure 51. SR Pinyon-Juniper site Case 1.

During the dry winter of 2014-2015, unmeasured or dramatically under-estimated low-intensity precipitation events (< 0.5 mm hr^{-1}) may have combined with low VPD to provide additional soil VWC recharge, as measured storm events were very small and there was no snow cover melting at the time to otherwise recharge the shallow soil column.

Snake Range Montane

Assessment of precipitation/VPD/VWC/vegetation interaction and storm effectiveness is greatly enhanced at the SR Montane site, as several trees on site were instrumented to monitor sap flow in the outer xylem stem tissues, with data spanning 2013–2015. Species included in this study were *Pinus flexilis* (PIFL; limber pine), *Cercocarpus ledifolius* (CELE; mountain mahogany), *Abies concolor* (ABCO: white fir), and *Pseudotsuga menziesii* (PSME; Douglas-fir). The first two species are commonly found at mid and high elevations in major Great Basin mountain ranges, whereas ABCO and especially PSME are

generally restricted to distributions in the central-eastern portions of the region (Charlet 1996), associated with Rocky Mountain ecoclimatic influences.

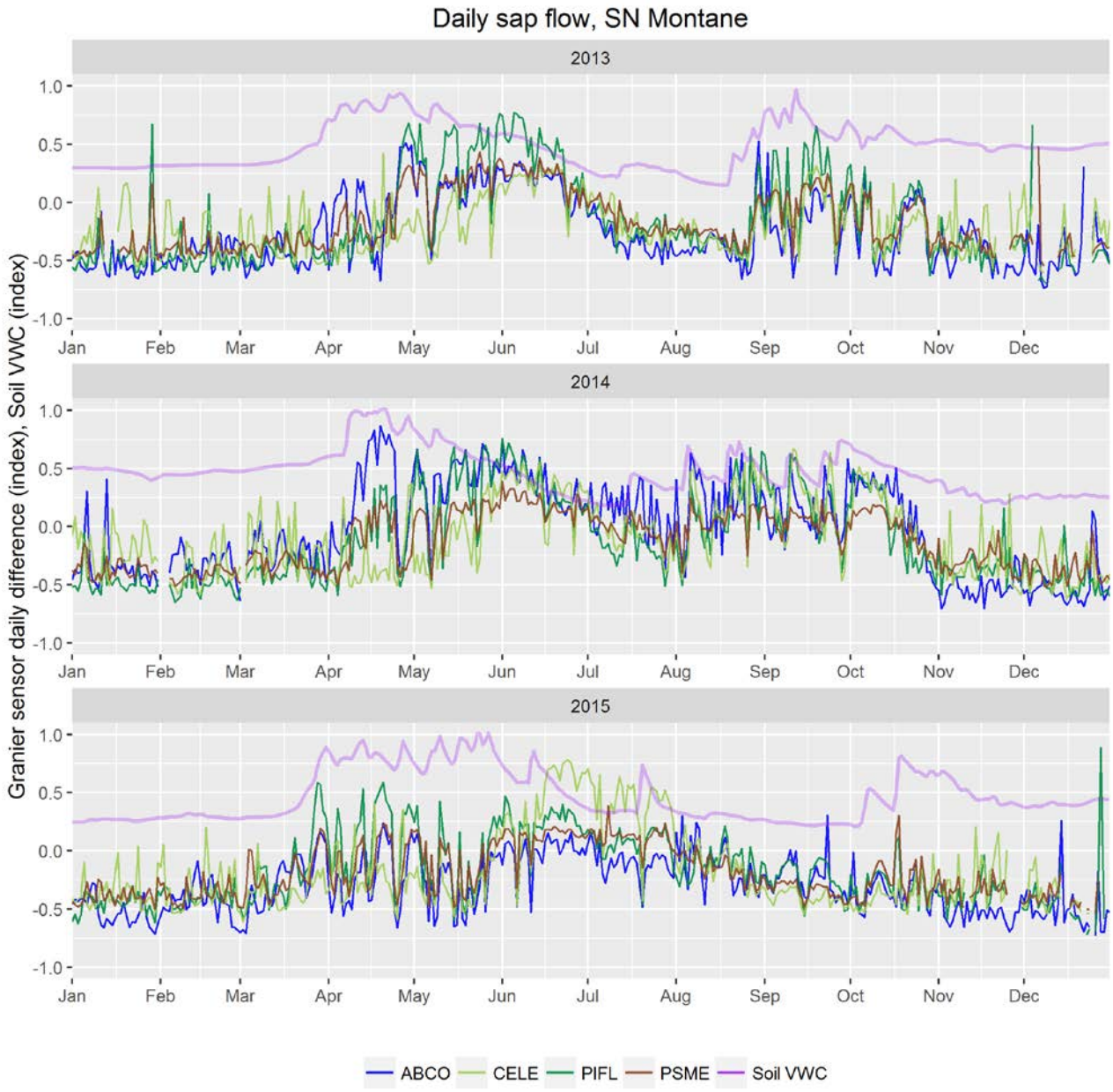

Figure 52. SR Montane sap flow by year.

Maximum daily temperature differences in the Granier probe data are indicative of higher sap velocity. The measurements from individual probes were combined as means for each species (ABCO *n*=2, PIFL *n*=2, CELE *n*=3, PSME *n*=2), converted to daily differences (Granier probe differential hourly $°C_{MAX} - °C_{MIN}$), and standardized for comparison. Soil VWC is shown as an index, and is the same curve shown in Figure 42. ABCO hourly data were particularly noisy due to problems with sensors, and were not used in further analysis.

The SR Montane site (Figure 42) differs strongly from the two lower-elevation sites in the sense that snow cover occurs in all years and persists through much of the winter. Shallow soil VWC peaks in the spring during snow melt, and drops precipitously as temperature and VPD are already quite high in June. Snow storms occur through May in all years, although 2012 was limited in this regard. Each summer within the observation period had very different precipitation and shallow soil moisture regimes. Overall, the sap flow trends closely follow this soil moisture curve (Figure 52), but the trees do not always have the same seasonal response. For example, in 2013 and 2014, sap flow ramps up in the spring as soil VWC from the melting snowpack peaks, declines as the warm season progresses and soil dries, and then has a secondary response to influx of late summer precipitation that persists into October in accordance with the available soil moisture. In 2015, sap flow is generally lower, but has initial responses early in the season that are suppressed by the cool, wet storms during May. Consistent flow begins after May, but tapers off for the rest of the year and does not respond significantly to the moisture arriving in October, even though in previous years active sap flow was present in the same month. The primary difference here is that September in the previous years was wet, while in 2015 it was not.

A detailed examination of processes occurring during the late summer of 2013 demonstrates relief of drought stress by storms which improve soil VWC and subsequent restart of sap flow by the local trees (Figure 53). Prior to the storm on August 20, the shallow soil VWC was at the lowest point in the 4-year record (4.0%; 08-18-2013), one indication of the highest drought stress measured. Successive storms brought rain to the site which increased the VWC to pre-summer levels. Sap flow did not occur prior to the storm of August 27-28, whereas afterwards a substantial sap velocity increase took place during daylight hours throughout the stormy September period. This sap flow restart was coincident with initial reductions in daily VPD and increases in soil VWC above 15%.

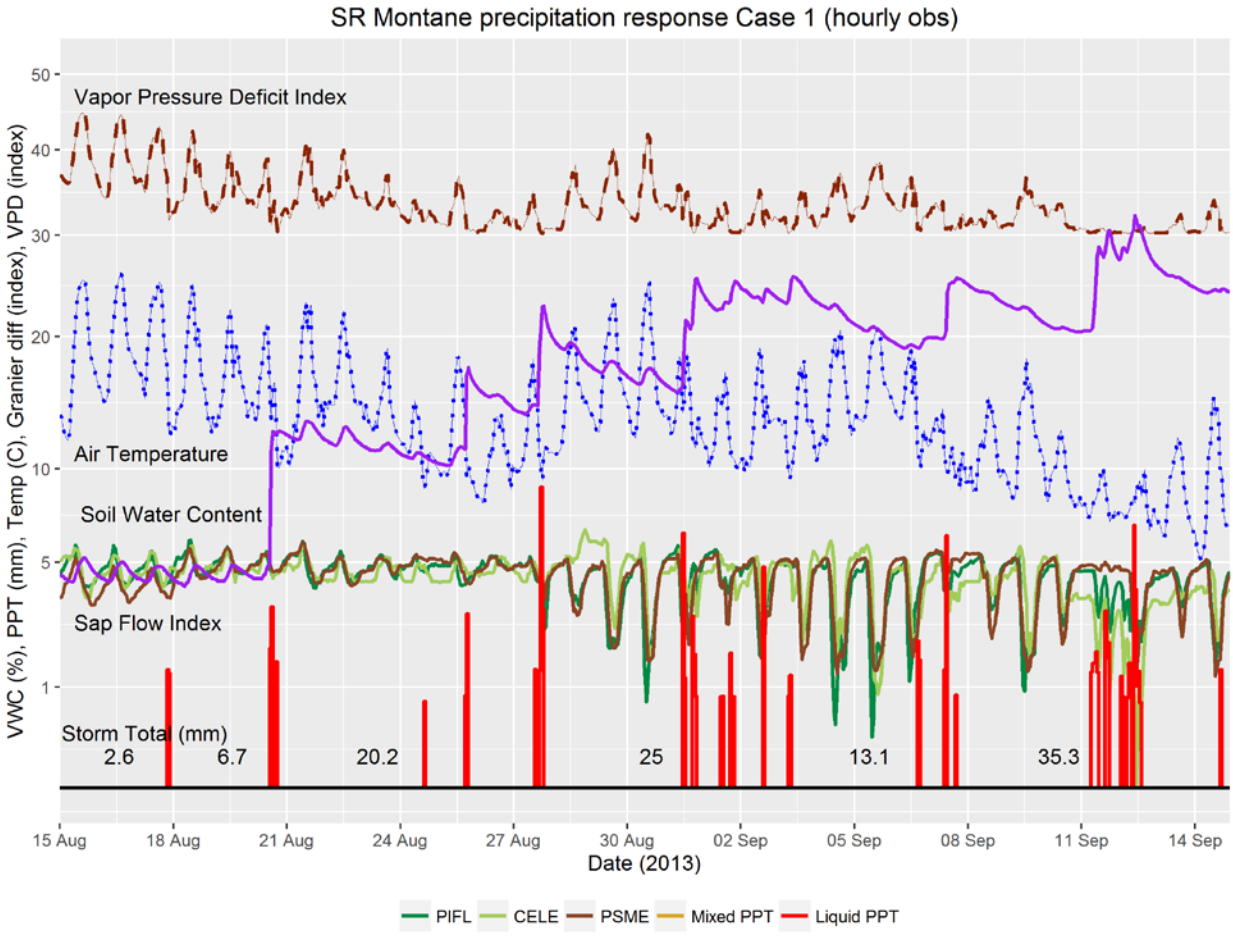

Figure 53. SR Montane site Case 1.

Tree sap flow response to late summer storms is shown after soil VWC is brought up to spring levels following the lowest point of VWC observed on the site in the 2012-2013 period. VPD and sap flow are shown as dimensionless indices. Lower values of the sap flow index are representative of higher sap velocity. The y-scale is non-linear to improve visual clarity.

A second case of interesting tree behavior is in October 2014, when active sap flow occurred well into the fall season and then precipitously dropped off by November 1. Following a very wet summer, sap flow remained elevated near spring levels, although storm events and associated low VPD (and cloudiness) temporarily reduced daytime sap velocities. After the final storm in September, October remained warm and dry, with temperatures rarely approaching 0°C (Figure 54). Soil VWC tapered steadily down during this time to 10%, although nowhere near maximum drought levels of 4%. Sap flow remained high until mid-October, when it began to reduce in diurnal amplitude following two days of

colder temperatures. By the end of the month, significant sap flow ceased for the three species shown after another 2-day cold event, even though subsequent temperatures remained above freezing, VPD remained elevated, and soil VWC remained above 10%.

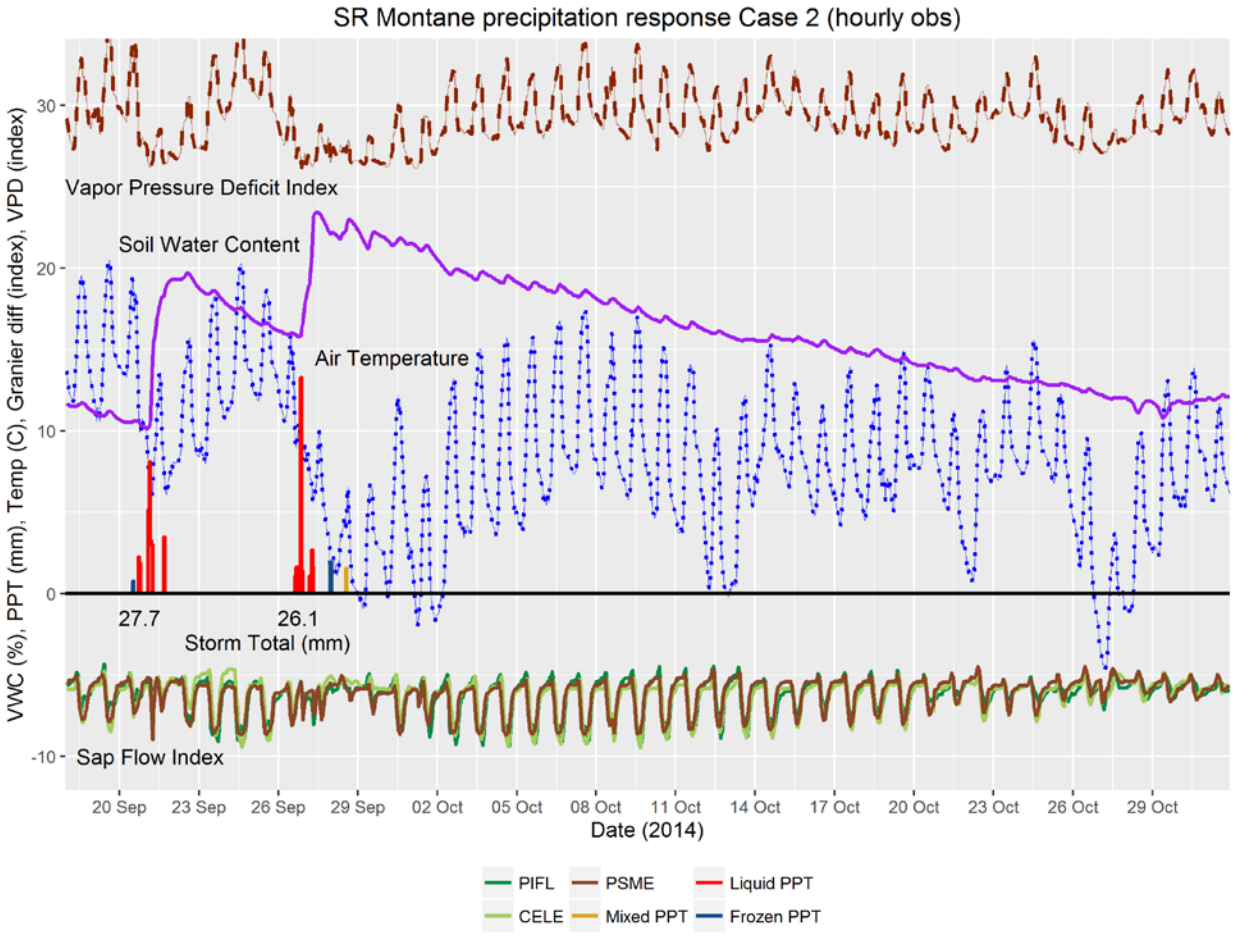

Figure 54. SR Montane site Case 2.

October 2014 showed strong sap velocities in multiple species on the SR Montane site in response to seasonally warm temperatures and adequate soil moisture.

Finally, May 2015 is examined. In the two previous Mays, sap velocities were high. A sustained cold storm sequence interrupted early-season sap flow occurring in the conifers but not in the *Cercocarpus* (Figure 55). Once the stormy period was past, sap flow commenced immediately with the rise of VPD and air temperatures. This continued until August, when velocities dropped due to reductions in VWC

and elevated VPD (Figure 42, Figure 52). The soil VWC was not replenished during August-September, and sap flow remained generally low until the end of the year. It is worth noting that the relative velocity of sap flow in CELE was sustained at a higher level than in previous years during the June-August 2015 interval.

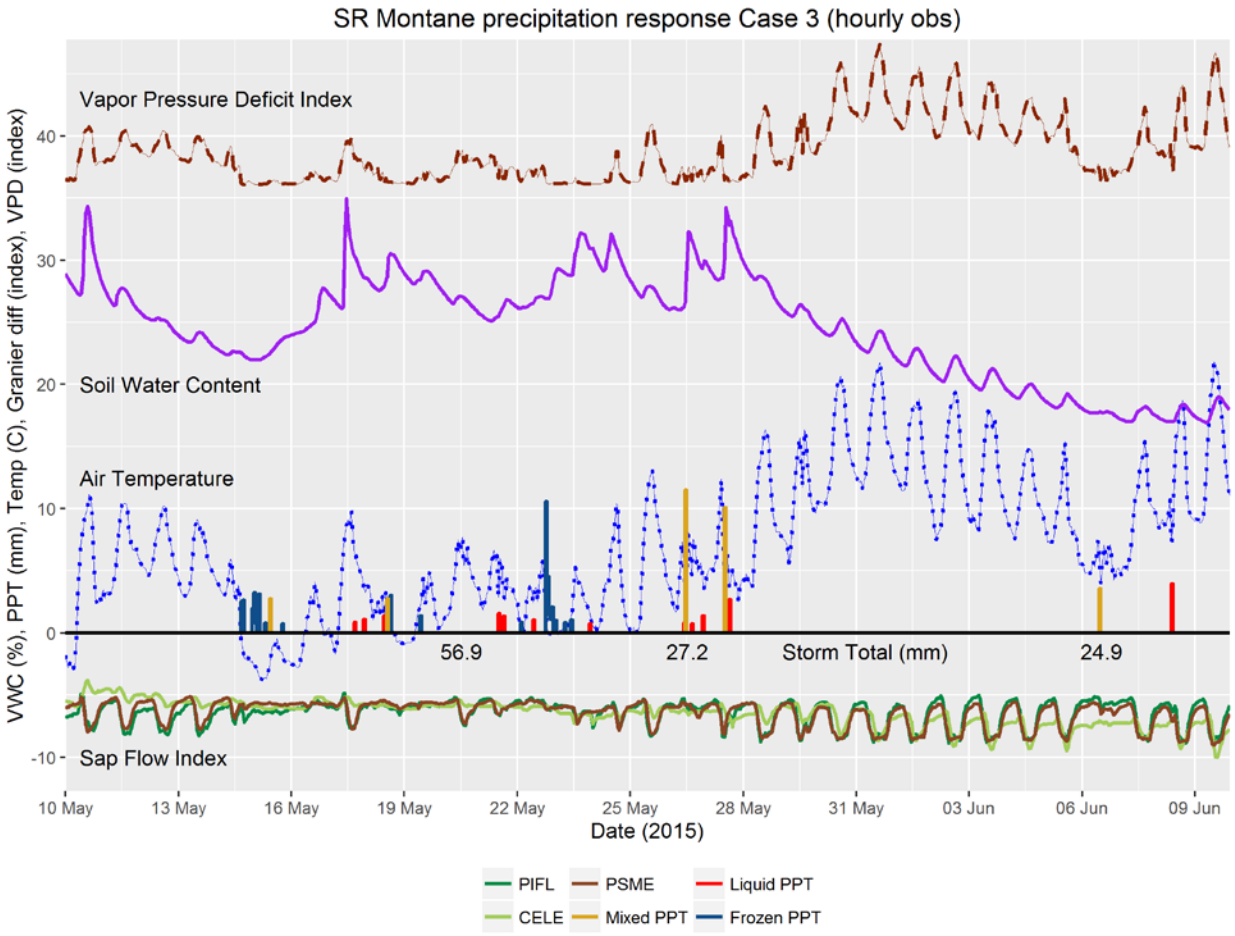

Figure 55. SR Montane site Case 3.

The stormy May 2015 interval halted spring conifer sap flow for nearly two weeks. At the end of the storm sequence, mountain mahogany sap flow started for the year along with the resumption of limber pine and Douglas-fir activity. This was to be the peak of the conifers' sap flow season for the year, as no substantial precipitation relief of summer dryness materialized (Figure 52).

Snake Range Subalpine

The SR Subalpine study site represents a unique set of scientific observations, in that it provides comprehensive high-resolution sensor data for several seasons from a Great Basin bristlecone pine (*Pinus longaeva*; PILO) woodland. It is one of very few instrumented high-altitude sites in the region, and has a wider range of sensors and instruments than probably any other subalpine-zone climatological research site in the Great Basin. Constructing and maintaining such a site is a major accomplishment, especially as the data are remarkably complete and free of major gaps.

This site's precipitation and soil moisture record is similar to the SR Montane site, as it has persistent snow cover in winter months during the observation period, experienced significant summer moisture in 2012–2014, and had a dry late summer in 2015. The nature of precipitation events appears to be more dynamic at this site compared to the others in the Snake Range, due to the length of the snowfall season, notable summer hail events, and the fact that some storms appear to deposit significantly more precipitation at this site (Figure 42, Figure 43, Figure 45, Figure 46, Figure 47, Figure 48).

Sap flow monitoring sensors were installed in the summer of 2012 on three non-old-growth *Pinus flexilis* (two co-dominant mature, one subdominant) and four non-old-growth *Pinus longaeva* (co-dominant), commonly co-occurring east-central Great Basin high-elevation conifers (Charlet 1996). The response of these two species to precipitation under regional drought conditions is of particular interest. These two species are considered to be strongly drought adapted and moisture dependent, and the sap flow within each season seems to be closely tied to soil moisture conditions during May to October (Figure 56).

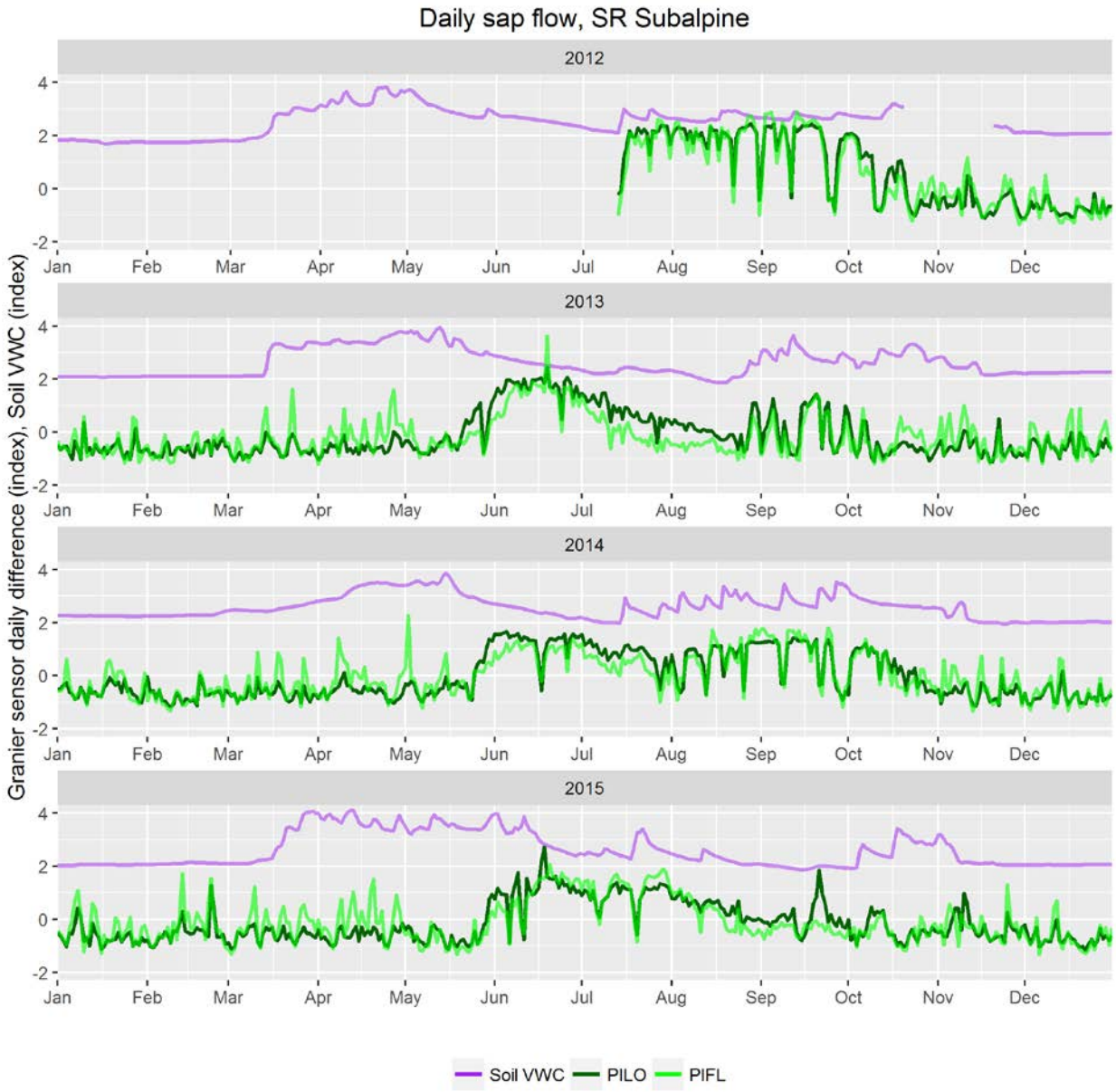

Figure 56. SR Subalpine site sap flow.

Sap flow in two prominent Great Basin conifer species is shown in comparison with shallow soil moisture data. Seasonality in regards to sap flow onset appears to be synchronous across 3 years, but late-season sap flow is different in every year. While the two species appear to respond in a similar manner, precise timing and magnitude of sap flow during high-stress periods (e.g. summer 2013) differs.

Between the sap flow and precipitation regime, several features of interest are evident which improve our knowledge of high-elevation systems in the Great Basin. First, there is the phenomenon of summer precipitation events that occur as hail storms. Two substantial events of this nature occur during the four years of observation; the first in August 2012, and the second in July 2015. While there was probably hail associated with other summer events during the time period, these stand out because of the volume and amount of the storm total that fell as ice rather than rain. The storm in August 2012 was particularly intense, with nearly 40 mm of precipitation falling within a 2-hour window (Figure 57). This single event raised the soil VWC from 10% to 14%, but did not immediately impact sap flow as previous storms in July had already raised the moisture from the seasonal low point (Figure 43). However, this recharge amount extended elevated summertime soil moisture (and high sap flow rates) until the next large event in mid-September.

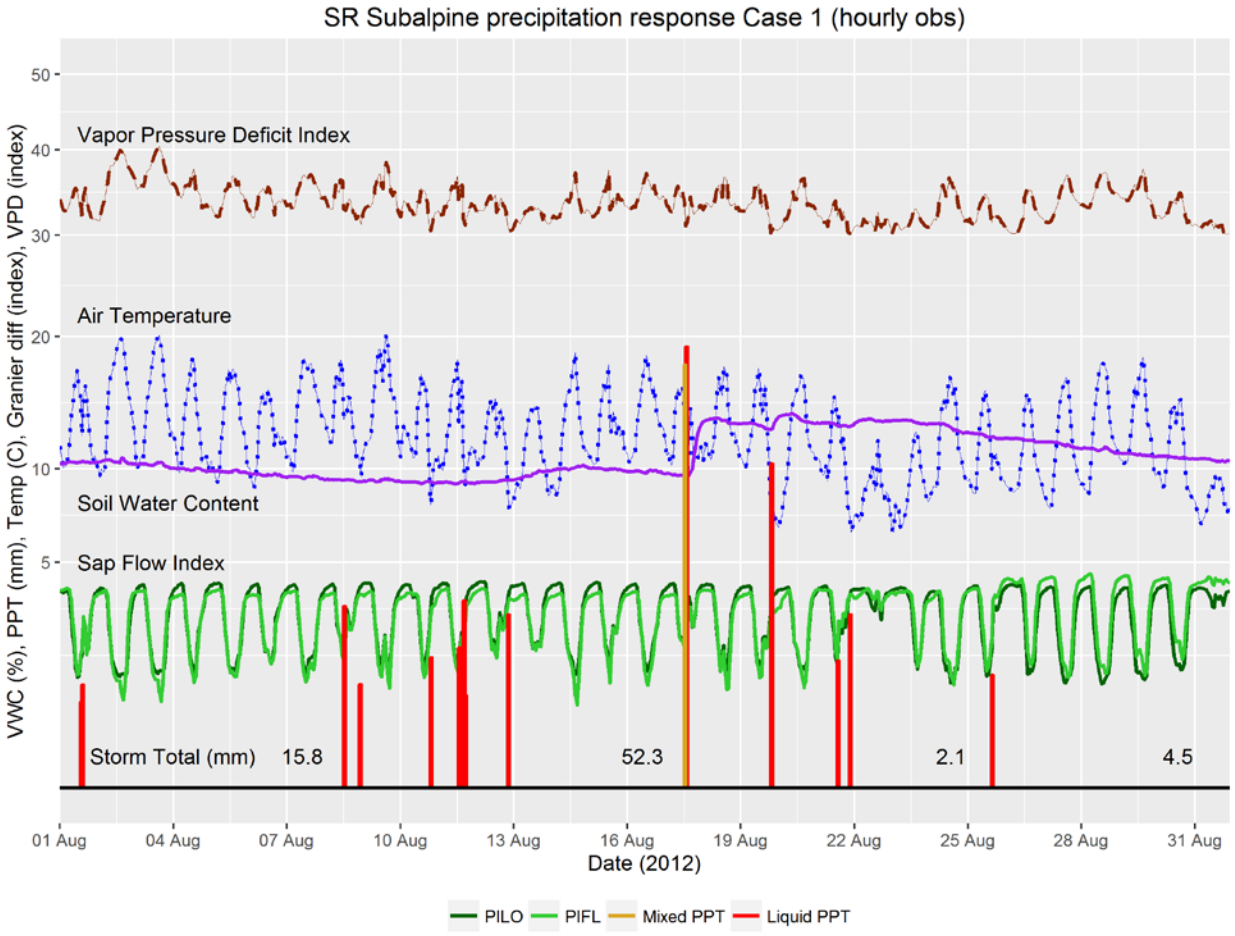

Figure 57. SR Subalpine site Case 1.

The highest-intensity hourly precipitation event during the observational period at the SR Subalpine site occurred as a mixed rain-hail storm in August 2012. While the 5-day storm total was 52.3 mm, the initial event deposited almost 40 mm of liquid equivalent in two hours. The impact to the soil moisture for this event was much higher than adjacent events (note: non-linear scale), presumably because even though this intensity-duration-amount combination should have resulted in substantial runoff, the form of the precipitation as ice allowed for additional infiltration as it melted over several hours (see Figure 58).

Figure 58. The August 2012 hail storm at the SR Subalpine site.

A strong summer hail storm deposited nearly 40 mm of liquid equivalent, which did not immediately melt and run off, but persisted for several hours and provided a much greater proportion of effective soil VWC recharge than if this same intensity-duration event had been 100% rain. The elevated VWC persisted for multiple weeks afterwards, with subalpine conifer sap flow responding with seasonally-high flow rates through September (Figure 56).

Another prominent feature of these data is the persistence of sap flow in the conifers until well into the fall season, as long as September soil VWC is elevated. Both species respond to late-summer precipitation and warm temperatures even after cold storms in September-October (Figure 59). Several

cm of snow fell in mid-October 2012, and in less than one week completely melted under warmer temperatures after the storm (Figure 60). While sap flow slowed considerably at this time, the diurnal changes in velocity persisted for another week before temperatures dropped substantially.

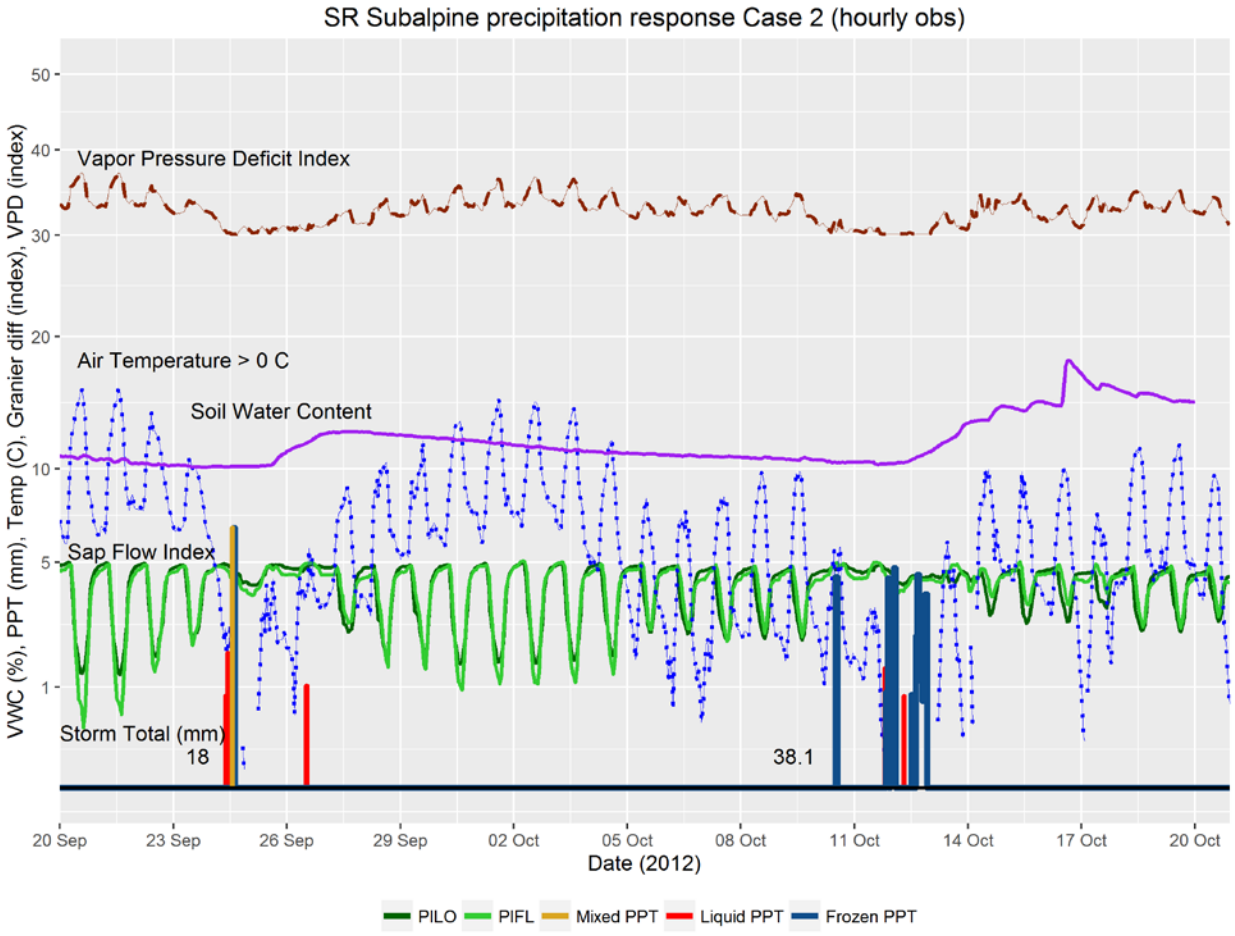

Figure 59. SR Subalpine site Case 2.

Late-season sap flow at high altitude is observed in both PILO and PIFL, even between cold storms. Directly after this sequence, a short cold event occurred with daytime high temperatures near -10°C (Figure 43).

Figure 60. October 2012 snowstorm at the SR Subalpine site.

A fall season snowstorm melted within a few days as temperatures remained between 0–10°C afterwards. The conifer daytime sap flow continued on the 15th and persisted for another week.

The third interesting interaction between climatological inputs, soil VWC, and sap flow is the pattern that occurs during the minimum shallow soil VWC (or, peak moisture stress) during the growing season. Even though these years were considered to be part of a major "drought" sequence in the region, demonstrable moisture stress on the conifers only occurred on the SR Subalpine site twice – during August 2013 and September 2015. It is also possible that this happened in July 2012, but sap flow data used in this study did not begin until just after this time. In both cases as drying shallow soil VWC passes through the 5-6% threshold, a noticeable decoupling of diurnal sap flow occurred between limber pine and bristlecone (Figure 61, Figure 62). In the 2013 case, high VPD coupled with rapid soils drying was

associated with a reversal of daily sap flow amplitude in PIFL during an approximately 3-week period in August. PILO, on the other hand, slowed the daytime sap velocity during this period but never fully ceased or reversed. A series of rain events recharged the soil moisture, and by 29 August both species exhibited elevated sap velocities even while VPD and daytime high temperature were lower than previously (Figure 61).

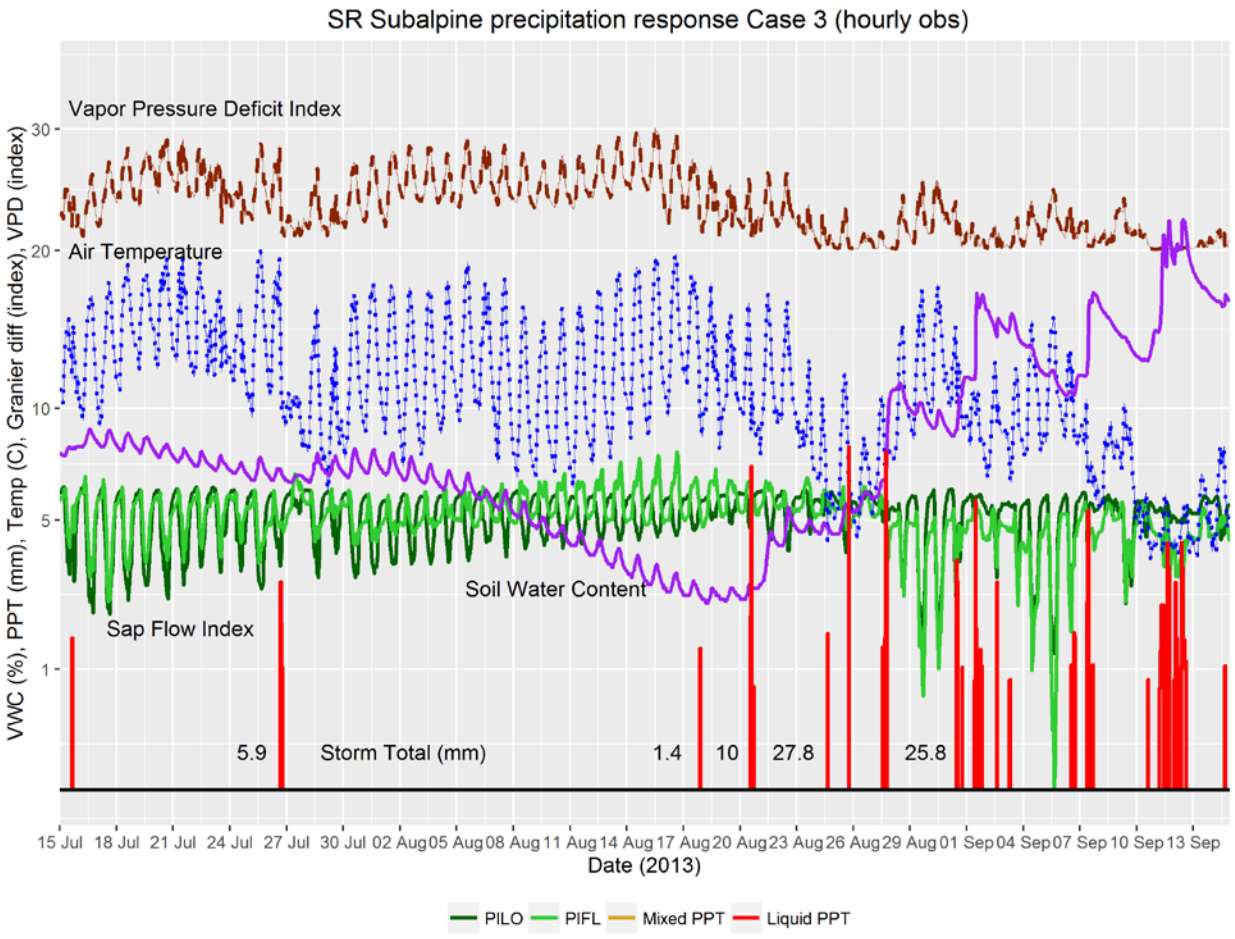

Figure 61. SR Subalpine site Case 3.

Data from August 2013 indicates high stress levels on both conifer species, with daytime sap flow slowing significantly in bristlecone pine and coming to a complete stop in limber pine during the day.

The water-stress sequence in 2015, however, lasted for approximately four weeks. Similarly, elevated VPD and air temperatures accelerated soil drying, and a small storm event of 3.7 mm precipitation failed

to mitigate decoupling of diurnal species sap flow activity. PIFL diurnal sap flow patterns once again reversed during the final week of the stress sequence, and PILO daily flow nearly ceased. A multi-day storm event that totaled 4.5 mm only raised the shallow VWC by 2 percentage points, but it was enough for PILO to restart sap flow and actually increase velocity for a few days before it tapered off again, while PIFL sap flow still indicated zero or negative daytime flow. A sudden cold storm brought 19.5 mm of snow, after which both species resumed an abbreviated diurnal pattern for a short time (Figure 62).

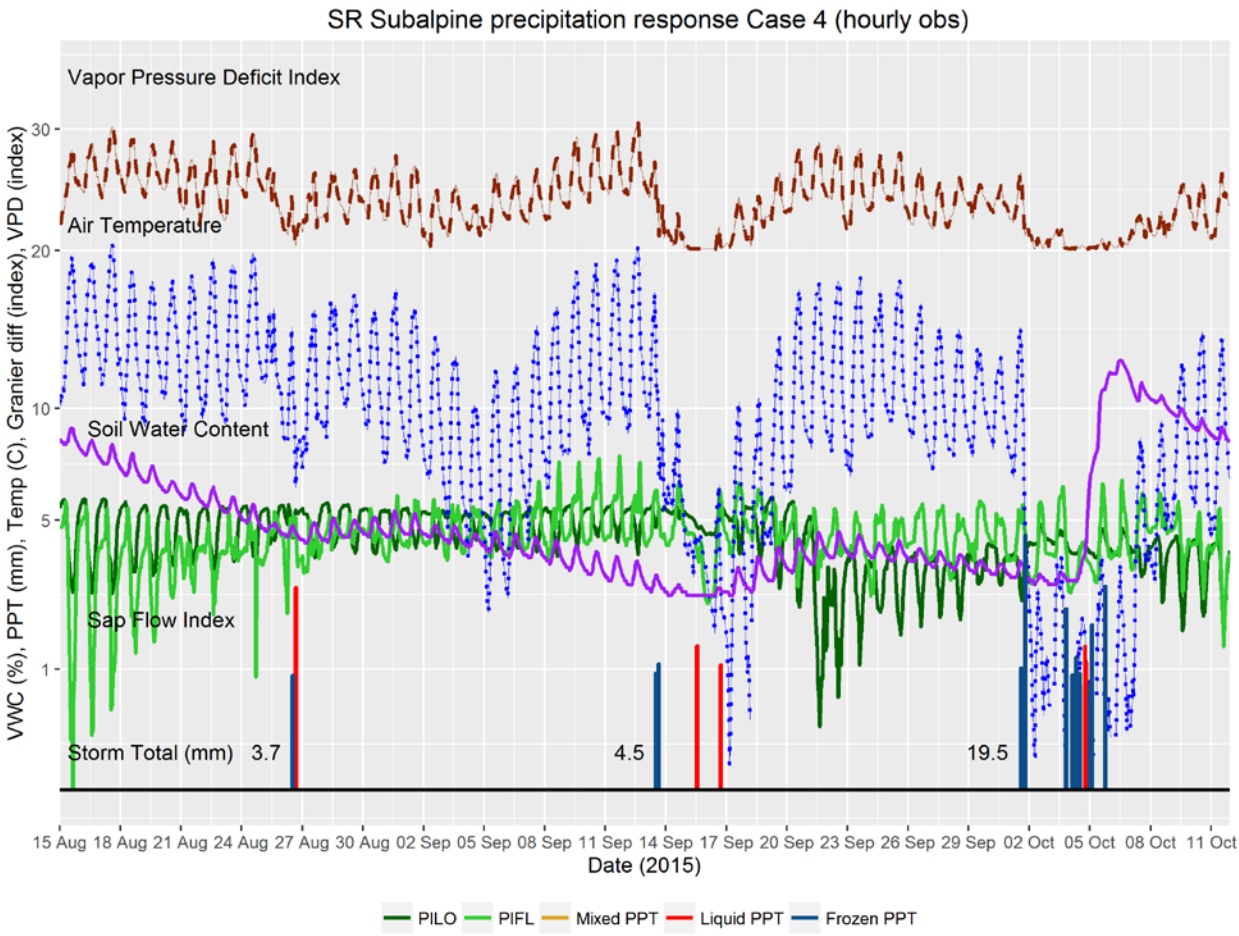

Figure 62. SR Subalpine site Case 4.

Another high-stress period on the SR Subalpine site is indicated during September 2015. Similar to the 2013 sequence, PIFL daily sap flow patterns halted or reversed prior to PILO as soil VWC decreased.

One common theme in the three complete years of sap flow data is the onset of sap flow, which occurs at approximately the same time (late May). This time frame is somewhat coincident with rises in temperature and the disappearance of snow cover in open, generally unshaded areas (Figure 43, Figure 56).

Sheep Range Montane

The clear winter-summer seasonality observed in the Snake Range is somewhat suppressed at the Sheep Range Montane site (Figure 44). While there are certainly cool and warm seasons, there is no persistent winter snow cover that the other tree-covered sites experienced during the same observation period. Soil moisture therefore is the product of individual storms or stormy periods. “Effective” precipitation at the Sheep Range site is also clearly much less than annual or monthly totals would indicate, due to high run-off and evaporation ratios. Many of the storms that occur are in the warmer seasons, and involve higher hourly intensities than the storms seen in the Snake Range. Therefore, even if daily precipitation totals are high, the effect on the shallow soil VWC is minimized because of runoff. Frozen precipitation, on the other hand, contributes much more proportionally to VWC than liquid events. In fact, only one purely-liquid storm event raised the shallow soil VWC more than 10%, whereas frozen and mixed events were responsible for the rest of the large increases in VWC in all seasons (Figure 44). Sap flow during the years of observation was extremely restricted compared to the Snake Range, and the data are quite noisy. However, several important features are illuminated when comparing xylem activity to the meteorological observations.

Figure 63. Sheep Montane site sap flow.

Relative sap flow and shallow soil moisture plotted for the Sheep Montane site indicates a dual spring-summer response regime, and that single events that quickly add moisture to the soils column can result in substantial responses in summer. The July-August 2012 data are from a separate sensor installation that was destroyed in a lightning strike, and therefore are not scaled the same as the rest of the dataset.

Sap flow was monitored in two mature, co-dominant *Pinus ponderosa* (PIPO; ponderosa pine) and four mature, co-dominant *Pinus monophylla* (PIMO; singleleaf pinyon pine). The original installation was short-lived, as a direct lightning strike destroyed the sap flow monitoring system after one month of

operation in August 2012. These four weeks of data, however, provided critical information on the response of the trees to precipitation in the middle of a notorious drought year. Subsequent years of sap flow data indicate an opportunistic response behavior to even small changes in soil VWC. An examination of the soil VWC and sap flow data across all years reveals that contrary to the Snake Range, the shallow soil moisture at the Sheep Range remained at or below the "plant available water" threshold (or approximate VWC_{PWP}) for much of the observation period (Figure 44, Figure 63).

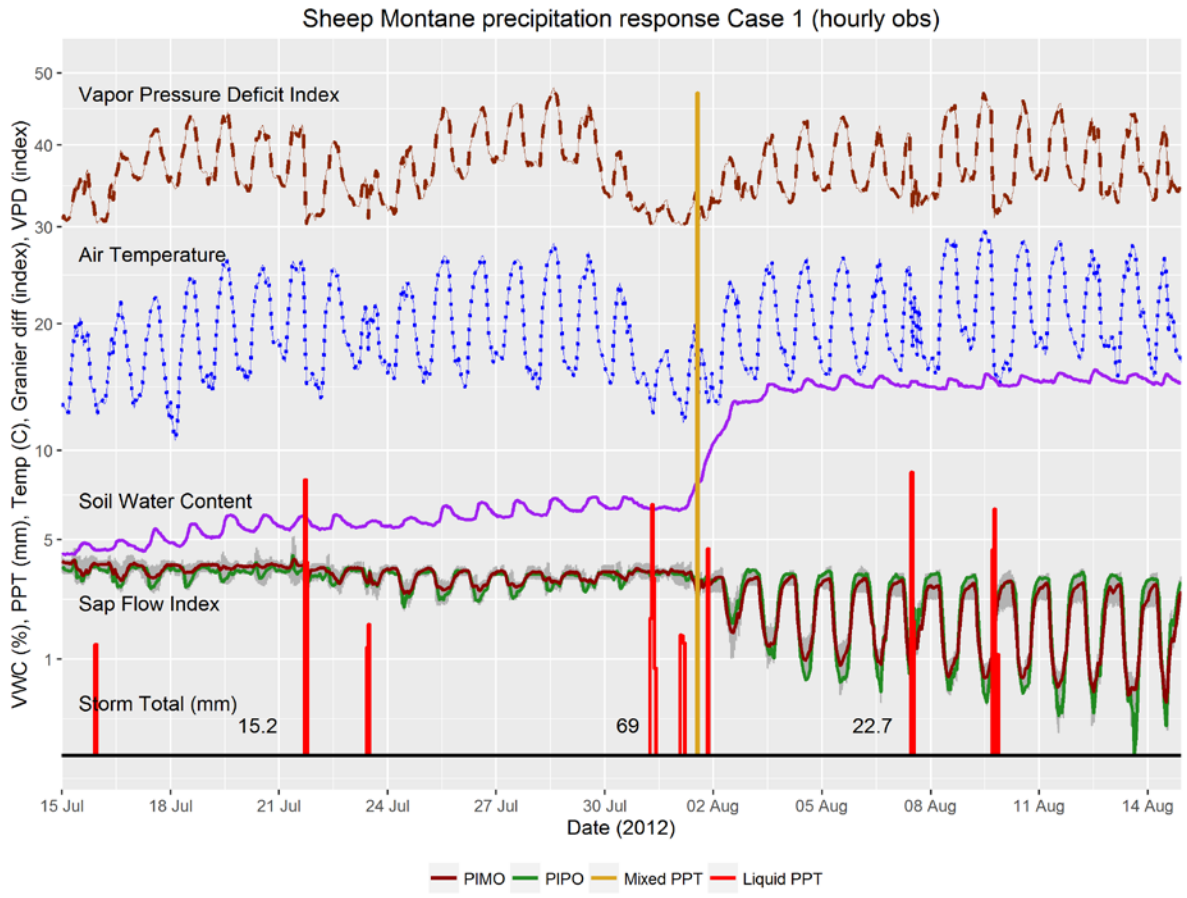

Figure 64. Sheep Montane site Case 1.

A mixed rain/hail storm in 2012 is the only precipitation event in July-August to have a substantial and immediate impact on shallow soils VWC. Over 45 mm of liquid equivalent fell within one hour, and similar to the hail storm at the Snake Range Subalpine site did not completely run off or evaporate, but provided infiltration over several hours.

One of the more substantial summer soil VWC recharge events during the observational period was caused by a high-intensity hail storm (47.1 mm hr^{-1}) that had immediate infiltration effects and restarted nearly dormant sap flow in both species (Figure 64, Figure 65). Comparable incidents to the August 2012 hailstorm occurred in July 2015, when two different storms each deposited similar amounts of precipitation but with very different rainfall intensities. The first storm on 20 July had a storm total of 39 mm, but the maximum hourly intensity was 14.2 mm hr^{-1}. The second storm totaled 63.7 mm, but had a maximum hourly intensity of 57.3 mm hr^{-1}, similar to the August 2012 storm (Figure 66).

Both the 2015 storms were effectively 100% liquid, but each had very different effects on soil moisture. The total recharge effect of the 2012 storm after 2 days was a 7.9% VWC increase. The first 2015 storm increased VWC by 12.2% after two days, but the second storm had no immediate effect at the 10 cm level. Instead, the soil VWC at this depth remained in a steady state for the following days. These three storms show that the character of precipitation events strongly dictates the impact to shallow soil VWC at the Sheep Range site.

Figure 65. August 2012 hail event at Sheep Montane.

The hail event of 1 August 2012 was flagged as a "mixed" event by the GDM, and was confirmed by camera imagery. The top of the TB-4 tipping bucket rain gage is shown, with hailstones from the event still slowly melting in the orifice.

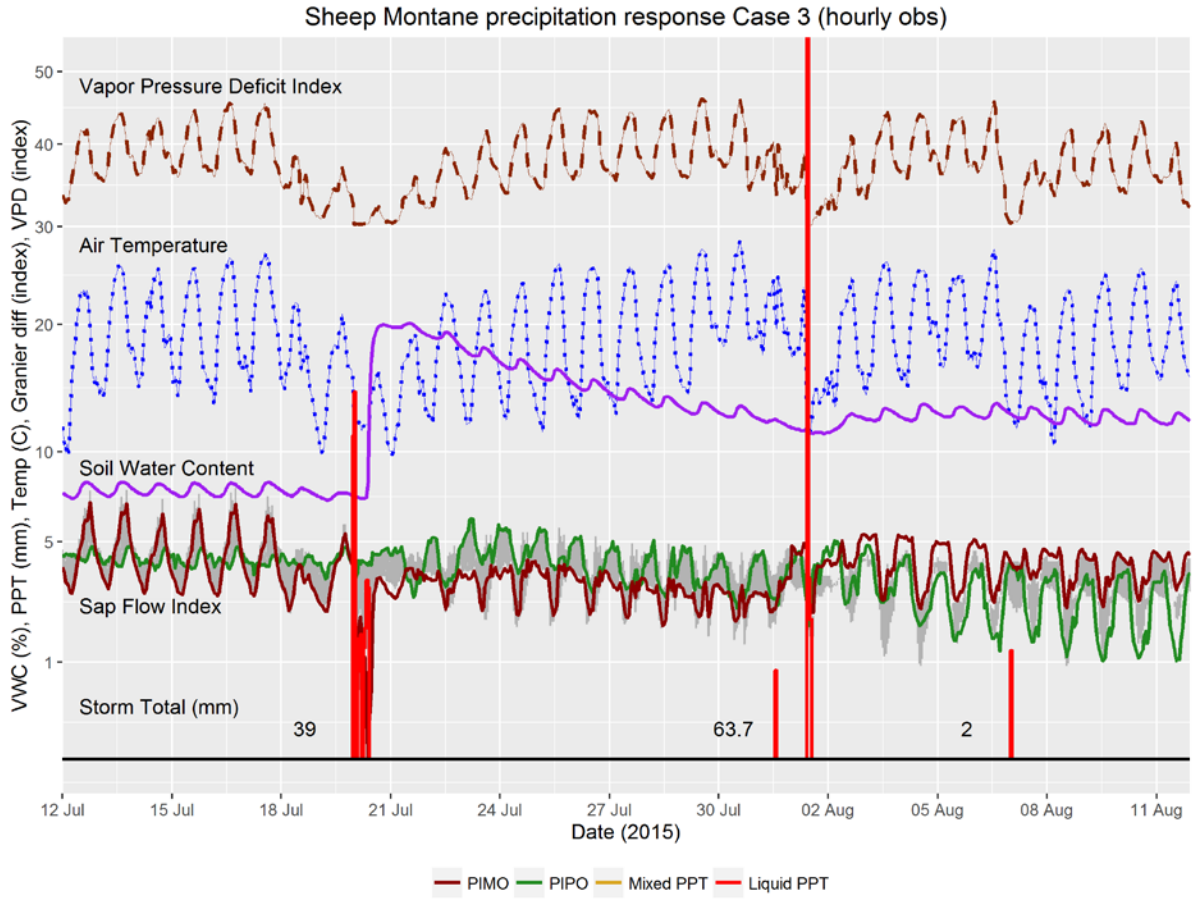

Figure 66. Sheep Montane site Case 2.

Two additional high-volume storms in 2015 had very different effects on soil VWC due to the arrival rates. Coincidentally, the high-intensity precipitation on 1 August was similar to the storm of 2012, and upon review of imagery had some hail mixed with the rain but not enough to accumulate and slowly melt.

Summary

Four years of sub-hourly ecohydrological observations were presented from four study sites that represent the valley-to-mountain gradient of vegetative zones in the central Great Basin region of the United States, as well as a representative site from the lower montane environment within the Great Basin/Mojave Desert transition. These data were analyzed to extract the character of precipitation events, which ultimately control the seasonal water budgets of these zones. Subsequent responses of rooting depth soil moisture and sap flow activity in dominant vegetative species at the three higher-

elevation sites were compared to these precipitation events, and seasonal patterns described. Specific interactions at sub-daily resolution were highlighted, showing examples of cause-and-effect processes which have not been previously observed in this region. These processes have implications for ecological studies of these species, working concepts of seasonal water balances, and projections of climate adaptation.

Seasonality of precipitation under regional "drought"

Because the four years of observation were coincident with prevailing regional drought, this provided an opportunity to examine processes under potential changes in seasonality. Indeed, monthly distributions of precipitation during the period proved to be quite different than long-term "normals". In the Great Basin, interannual variability is quite significant, both during the modern period (Redmond and Koch 1991) and inferred from palaeorecords (e.g. Hughes and Funkhouser 2003; Strachan et al. 2012). Coarser-resolution palaeoecological data suggest that long-term shifts between seasonal circulation regimes are also possible (e.g. Wigand and Nowak 1992; Holmgren et al. 2010). This is due partially to the region functioning as a transition zone between longer-term oscillations in large-scale circulation (Cayan 1996; Wise 2010), and that relatively few storms have proportionally large impacts on any given season.

Each year of the study period exhibited slightly different seasonal patterns; however, the dominant theme in three of the four years (2012, 2013, and 2014) proved to be a two-season mode of precipitation with significant summer storm events balancing relatively dry winters, which contrasts with the overall long-term climatology. Summer storm events in the south-central Great Basin are most commonly associated with the North American Monsoon (NAM) seasonal pattern, which transports high

amounts of water vapor into the American Southwest during the July–September period (Higgins et al. 1997; Means 2013).

Convective activity from daytime solar insolation during these months generates active thunderstorms, which serve as the main precipitation mechanisms. Consequently, precipitation events during the summer would be expected to be spatially disjunct and highly variable in intensity and duration. Analysis of storm intensity by season and site location confirms that storms in winter exhibit lower hourly precipitation rates than spring and summertime events, and that summer intensities are more variable (Figure 67). A one-way analysis of variance (ANOVA) on log-transformed storm intensity (Snake Range sites only, binned together) by season indicates that the difference between seasonal storm intensities (in particular, summer and winter) during drought conditions is significant [$F(3, 458) = 11.14$, $p < 0.0001$].

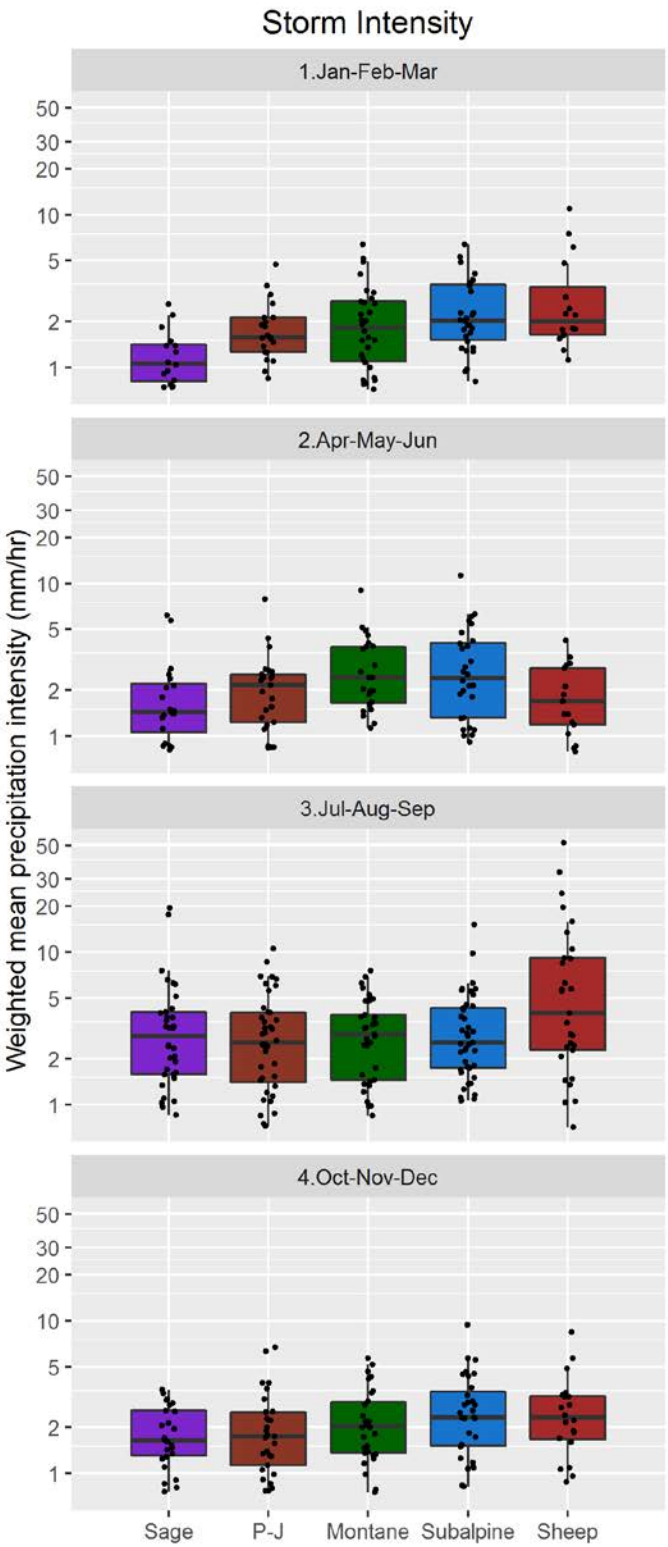

Figure 67. Seasonal storm intensities.
Distributions of seasonal storm intensities for all years are shown for each site. There is a clear relationship with elevation for the four sites in the Snake Range during the colder seasons.

Convective activity from daytime solar insolation during these months generates active thunderstorms, which serve as the main precipitation mechanisms. Consequently, precipitation events during the summer would be expected to be spatially disjunct and highly variable in intensity and duration. Analysis of storm intensity by season and site location confirms that storms in winter exhibit lower hourly precipitation rates than spring and summer events, and that summer intensities are more variable (Figure 67). A one-way analysis of variance (ANOVA) on log-transformed storm intensity (Snake Range sites only, binned together) by season indicates that the difference between seasonal storm intensities (in particular, summer and winter) during drought conditions is significant [$F(3, 458) = 11.14$, $p < 0.0001$].

Influence of topography

Topographic gradients play a critical part in

the spatial distribution and phase of precipitation during most storm events. This is particularly evident during non-summer seasons, and is due to a combination of orographic enhancement, boundary layer fluxes, low-level wind patterns, and temperature lapse rates that are driven by individual storm characteristics (Kirshbaum and Smith 2008; Minder et al. 2008; Lundquist et al. 2010; Minder et al. 2011; Luce et al. 2013). Year-by-year visual comparisons of daily precipitation values across sites show that the relationship between precipitation and elevation varies by storm (Figure 45, Figure 46, Figure 47, Figure 48). The percentage of precipitation as "frozen" during the observational period was significantly higher for the two upper-elevation sites in the Snake Range (58.7% and 68.7%) than the two lower sites (19.0% and 36.7%; Table 3.3).

In addition, the weighted mean hourly storm intensity is directly related to elevation during non-summer seasons. A one-way ANOVA on log-transformed storm intensity (for non-summer seasons) across the Snake Range sites indicates that the difference in hourly precipitation intensity between elevational zones is significant [$F(3, 306) = 7.85$, $p < 0.0001$]. As the spatial separation of the sites is minimal (8.9 km total separation, Figure 33) and all are located on the western gradient of the same mountain range, the primary geographic dissimilarity metric is elevation (1500 m total separation; Figure 35).

Summer storm intensity does not differ significantly by site, and the monthly precipitation totals appear to vary by elevation only in a minor fashion during this season, with considerable variation (Figure 38). The GDM analysis flagged multiple instances of high-intensity summertime "mixed" events, which were confirmed to be hail storms. None of these events (during daylight hours) at the lower-elevation sites left visible ice on the ground within one hour after the event, whereas the events at higher elevations had hailstones which persisted for more than one hour (Appendix 3.9). Cooler temperatures and

perhaps greater percentages of ice rather than liquid during high-elevation hail events assist in longer melting times and thus higher shallow soils infiltration rates.

Opportunistic behavior in Great Basin trees

A significant ecohydrological observation of this study was the seasonally opportunistic xylem sap flow (a proxy for transpiration) behavior of the dominant trees on upper-elevation sites in both ecoregions in response to effective precipitation inputs, and very late-season activity even above 3000 m. The departures in precipitation seasonality from a winter-dominated regime during 2012, 2013, and 2014 resulted in two "seasons" of peak rooting-depth soil moisture in each year. Tree transpiration responded accordingly for continuous time periods (weeks) for PILO, PIFL, ABCO, PSME, CELE, PIPO, and PIMO in the late summer, extending elevated sap velocities well into October in most cases. By contrast in 2015, a wet May–June in the Snake Range suppressed VPD and shortened the transition from spring into a dry summer. Sap flow activity at the SR sites declined from a peak in June and, except for very short instances in some species, did not exhibit the dual-season behavior of the previous three years (Figure 52, Figure 56). At the Sheep Range in 2015, sap flow response was mixed between trees/species, as soil VWC was at minimal levels for the majority of the warm season with only one effective storm to provide drought relief (Figure 48, Figure 63). These observations highlight the importance of summer monsoon activity in the central Great Basin in relieving winter-season drought for mountain ecological communities, as well as impacts of July–September soil moisture on tree transpiration activity and the balance of resources that influence the following year's growth.

Mountain conifers in the western United States are generally associated with winter, snow-dominated precipitation seasonality, and primary growth processes occur during the June–July window, although photosynthesis and associated activities can occur across a range of seasons (Fritts 1976). This is

particularly true in the semi-arid regions of the Southwest. In a study by Adams and Kolb (2005), an intermountain conifer species assembly similar to the Snake Range showed growth sensitivity to spring and summer water stress at both high- and low-elevation sites near the southern edge of their distributions in a dry, monsoon-influenced mountain environment, although the effects of previous-year conditions were not evaluated. Williams and Ehleringer (2000) found that trees adapted to predictable monsoonal precipitation (such as *Pinus edulis*; PIED) make significant use of shallow soil moisture in September as long as they are located in a geographical zone where the monsoon makes a regular contribution, but that use of this seasonal water drops off as the geographic predictability of the monsoon is reduced. This geographic shift in response begs the question of phenotypical adaptation, and a recent study of PIPO genetics (Potter et al. 2013; Potter et al. 2015) showed that in the central and southern Great Basin there was a gradient of differences in the genetic markers analyzed. Similar studies have not been performed for the other conifers mentioned here, but it would be interesting to see if PILO or PIFL had similar differentiating markers across geographical space. In one of the only examples of direct instrumentation and continuous phenology observation of high-altitude conifers in the Great Basin, Fritts (1969; 1976) observed that *Pinus longaeva* in the White Mountains of California experienced radial increment growth in the basal stem during the June–July period, and that significant diurnal oscillations in dendrograph readings (a proxy for sap flow activity) persisted into August during 1962, 1963, and 1964. Unfortunately, the study only covered these summer months, so tree activity and response to environmental conditions outside of this window remained unknown. The Fritts study was repeated in 2007 and 2008, with similar results, but once again the observations were only made during the June–August timeframe (Hallman and Arnott 2015). Similar early dendrograph work on mid- and low-elevation conifers in the southwest suggest that significant diurnal sap flow can occur in PIPO, PSME, and PIED from March to October on semi-arid sites (Fritts et al. 1965).

Observation of this same type of seasonally opportunistic behavior near the treeline and at higher latitude is critical to our understanding of the adaptability of these central Great Basin conifer communities. Peaks of late-summer sap flow activity were observed in August–September indicating use of monsoonal moisture to maintain respiration and photosynthetic activities. High sap flow rates extending into October even at a near-treeline site such as the SR Subalpine location seems to run the risk of cell cavitation due to freezing conditions, which is a real limitation for high-altitude tree growth (Körner 2012). LaMarche and Mooney (1972) suggested that the Snake Range populations of *Pinus longaeva* were not as adapted to summer and fall drought as those in the White Mountains, and thus more susceptible to winter desiccation. Much more work on the physiology and biogeographic distinctions of Great Basin conifers remains to be done, but these contrasts bring into question whether the Snake Range trees have rooting and water-use strategies that are adapted to mitigate wintertime precipitation failures and springtime drought by exploiting frequent monsoon activity, even at the risk of early-season extreme-cold events. It is also possible that the southern topographic exposure of the SR Subalpine study site supports this season-extending behavior due to higher amounts of direct solar radiation. This hypothesis is partially supported by examples of lower-elevation PILO populations in seemingly warm and minimal-snowfall environments across the south-central Great Basin, with a distinct absence of PIFL in these same stands (Charlet 1996). Of particular interest in this study's observations from the SR Subalpine site are the empirical differences between the relative VWC_{PWP} thresholds for PILO and PIFL. Diurnal sap flow activity between the two species is very similar overall (Figure 56); however, at times of greatest water stress PIFL appear to close stomata during the day at an earlier point in time than PILO do. This is visible in Figure 61 and Figure 62 as a reversal of the diurnal peak in sap flow. None of the peak water stress points (lowest soil VWC during elevated atmospheric VPD) see a complete daytime shutdown in PILO sap flow. PIFL, on the other hand, exhibits a greater sensitivity to moisture stress under these same conditions. Bristlecone pine possess characteristically

smaller growth increments and generally denser xylem structures than limber pine (LaMarche 1969), which would improve cavitation resistance and aid in the adaptation to water stress (Hacke and Sperry 2001) that characterizes the species and its geographic distribution. What is currently understood about the biogeographic history of south-central Great Basin conifers certainly points to a long timeframe of regional adaptation (Charlet 2007; Cole et al. 2013; Potter et al. 2015). The distribution of PILO, ABCO, PSME, and PIPO in particular across this region strongly suggests a tie to monsoonal geography and warmer temperatures (van Devender and Spaulding 1979; Charlet 1996; Potter et al. 2013). Direct observations of these opportunistic processes across diverse seasonal patterns assists in interpreting both genetic and palaeoclimatic records.

The roles of snow and frozen precipitation

Snow plays a significant role in annual ecohydrological processes in Great Basin mountains, even in times of regional drought and very low April 1 snowpack (Appendix 3.10). In the Snake Range, the three mountain-block sites (Pinyon-Juniper, Montane, and Subalpine) experienced some period of snow cover longer than seven days during the winter in each year. The percent of monthly precipitation classified as "frozen" was at or near 100% for November to April for the two Snake Range upper-elevation sites in all four years. The subsequent delay in soil moisture peak as the snowpack melted each year provided the primary conifer growing season (April–June at the SR Montane site, and June–July at the SR Subalpine site) with soil moisture levels above the apparent VWC_{PWP} for almost the entire season in each case.

Snow at the SR Pinyon-Juniper, SR Sagebrush, and Sheep Range Montane sites was much more variable as a percentage of total precipitation during the winter (Figure 39), although when it did occur it seemed to impact soil VWC more substantially than rain events of similar magnitude. It is difficult to speculate on how warm-season water balances would change if winter snow events were reduced to a minimum,

as summer precipitation dramatically augmented the light winters in the Snake Range. It seems, however, that even "low snow" years such as 2012, 2013, and 2014 brought enough to maintain local conifer populations at mid- to high-elevation sites. This study does not explore the nature of vegetative competition and relative rooting depth of the species on each site, but the preliminary conclusions from seasonal and case-study sap flow measurements indicate that the instrumented species can have different times of sap flow peak relative to one another, somewhat driven by the soil VWC and likely other variables such as soil temperatures and remnant shaded snow.

Frozen precipitation during the summer (i.e. hail) had a demonstrable effect on conifer sap flow at the SR Subalpine and Sheep Range sites compared to 100% liquid events of comparable magnitude. Although these events would seem to be rare, the fact that this four-year study observed multiple examples of this phenomenon indicates that, during seasons of elevated convective activity, high-intensity hail events may be an effective mechanism at relieving summer drought stress on mountain sites. It is important to note that current methods of automated weather monitoring and historical weather data from such sites do not differentiate between rain, snow, and hail, or the difference in "effective" precipitation between a 50 mm hr^{-1} hail event versus the same falling as rain. These results highlight the importance of quantifying storm totals, durations, intensities, and most importantly precipitation phase in order to gain insight into seasonal ecological climate response when both weather and ecology are monitored in a water-limited context.

Precipitation at the Mojave transition

The Sheep Range in particular seemed to benefit the most from snow at short-term timescales, as rain events were typically higher in intensity and generated much more runoff rather than infiltration. Soils at the Sheep Range site seemed to respond best to snow/ice, and then to medium intensity to low-

intensity/long-duration liquid events. High-intensity events at the Sheep Range seemingly did not improve soil moisture conditions proportionally, and therefore the use of monthly or seasonal total precipitation catch as a proxy for "effective" precipitation does not seem accurate. Indeed, Reynolds at al. (2004) argue that simply using daily precipitation events as-is and not grouping by storms or taking into account antecedent and post-storm soil moisture over-generalizes the "pulse-reserve" ecological modeling paradigm in arid and semi-arid ecosystems. While the Reynolds et al. study was essentially a coarse meta-analysis of three different desert ecoregions and did not address the issue of individual storm intensity, their findings of 1) summer rainfall being less effective for plant productivity (and by proxy, soil VWC recharge) and 2) the majority of daily rainfall events being smaller, and by themselves not very "effective" generally agree with results at the Sheep Range site. Their statement about the chances of "persistent" rainfall in the Mojave Desert being much lower in the summer does not match storm results from the Sheep Range Montane site, where summer storms (with hourly precipitation exceeding 0.5 mm uncorrected catch) were the longest of the four seasons (2.2 days mean Jul-Aug-Sep storm duration). The fact that the Sheep Range site is a mountain site may alter the nature of both winter and summer storms compared to the weather stations in the region situated in the low-elevation hot desert.

Conclusions

This four-year study of precipitation across a Great Basin mountain gradient with comparison to the Mojave transition reveals concurrent ecohydrologic processes at a level of spatiotemporal detail which has not been previously possible in the region. Combining precipitation phase, storm characteristics, winter snowpack, rooting-depth soil moisture, air temperature, vapor pressure deficit, and tree sap flow at sub-daily resolution into a single study over several continuous seasons provides new insights into the relative impacts of hydroclimatic inputs on Great Basin mountain communities. A more complete

understanding of what “seasonal variability” actually looks like in the Great Basin will aid environmental research from a conceptual standpoint as well as an operational one if future study designs are implemented using these data. During regional drought conditions, the seasonality of precipitation in the Snake Range was altered from the long-term normals, with summer (Jul-Aug-Sept) storms contributing much more to the annual totals during 2012, 2013, and 2014 than the more “normal” year of 2015. All four years were considered to be regional “drought” years, but water stress at middle and upper elevations on the mountains did not appear extreme if soil VWC and tree sap flow are reasonable indicators. This demonstrates the buffering effect of high elevation on semi-arid ecological populations from drought due certainly to lower temperatures and VPD, but perhaps even more because of large changes in precipitation character in montane and subalpine zones compared to lower elevations. Two dominant modes of precipitation seasonality were observed during the study period: one that includes mild winters from the snowfall perspective but with significant summer effective moisture, and a second mode where spring precipitation is very high and the summer is dry. The long-term effects of each of these seasonal modes are difficult to gage, but these observations reinforce the concept of the Great Basin as a seasonally dynamic region with opportunistic and adaptable ecology. In addition, the role of mountain topography in the context of precipitation is highlighted, which contributes to concepts of ecological refugia during extended periods of drought or increased temperatures. Results from the comparative Sheep Range site in a Mojave Desert montane transition zone show that this is indeed a site which is subject to extreme water stress, as well as failure of multiple seasons of precipitation. Because high-resolution measurements of climate variables in mountains of this region have not been made until relatively recently, it is difficult to say if the conditions observed are sustainable for the sizable conifer populations there, especially at the lower extents of the montane conifer distribution. However, it is clear that the few snow storms which occurred during the study period had a substantial role in elevating shallow soil moisture to levels useful to the conifers.

Future studies should examine the spatial distributions, depths, and patterns of soil moisture from a micro-site perspective, to examine whether conifers at these locations exhibit different seasonal strategies tied to individual tree rooting depths, local competitive dynamics, and shading/persistence of snow and moderation of soil temperatures.

Chapter 4 An approach to sensor-based observation in mountains

Data quality: a challenge

Technological advances have facilitated the acquisition of new environmental data in quantities not previously feasible (Hart and Martinez 2006; Krause et al. 2015). Examples of these new modalities are visible at coordinated-funding scales such as the NEON project and others (Schimel et al. 2007; Chorover et al. 2012; Collins and Childers 2014), as well as grassroots-level networking similar to the scale of this study (Baldocchi et al. 2001; Richardson et al. 2007; Weathers et al. 2013; Vanderbilt et al. 2015). However, data from observation networks designed for a single application (such as municipal weather or SNOTEL) are often leveraged for other purposes (such as PRISM), which can be a cause of unexpected or even undetected bias in scientific conclusions (Dai et al. 2006; Daly 2006; Oyler et al. 2015). The results from this study highlight how significant knowledge gaps that persist in ecohydrological observations of mountain environments can be addressed by improving the quality and diversity of data collected. As this work has demonstrated, a critical concept that must be integrated as mountain system science moves forward is comprehensive gradient monitoring. Not far behind gradient study in importance is the integration of modern technologies and best practices for remote data acquisition and management.

Data gaps and otherwise non-continuous datasets persist in long-term climatic records. Ground observations are notorious for possessing large gaps or intermittent records that can be difficult to fill if the spatial density of stations is low (Peck 1997; Jeffrey et al. 2001; Mitchell and Jones 2005). Historic observations made on a daily basis by human operators often have multiple changes in location and setting over time to accommodate urbanization and other setting shifts. Furthermore, “permanent” instrumented platforms located in challenging environments have major issues with missing data due to

equipment failures and associated problems. Contributing factors include inadequate systems design, poor quality installations, and lack of regular human access (ESIP Envirosensing Cluster 2016). Moreover, instruments in remote locations are not always provided a means of remote access via radio telemetry systems, meaning that issues with sensors or power systems are not recognized until a periodic site visit or even worse, during post-processing and analysis of the data. Thus, records from mountain regions are much more likely to be incomplete or of poor quality, making scientific interpretation and meta-analysis challenging or even erroneous (e.g. Laternser and Schneebeli 2002; Stewart 2009).

Methodological opportunities in study design

Stepping outside our topographic niche

Expanding study designs to include observations across a range of topographic, vegetation, and elevation gradients enables ground-truthing and improvement of distributed landscape process models as demonstrated in this study and others (Lookingbill and Urban 2003; Anderson-Teixeira et al. 2011; Li et al. 2013; Krofcheck et al. 2014; Vitale 2015; Holden et al. 2015). Gradient observations can provide more comprehensive datasets to address a wider range of science questions, as the dataset from the Snake Range indicate. Designing studies to not only facilitate primary science questions, but also consider the broader impacts (e.g., meta-analyses, management practices, and socio-ecological applications) will change the impact and visibility of *in-situ* observations in mountains.

Uniformity & standards for siting

Regionally “representative” observations for different climate variables in mountains are ideally not all taken in the same geographic location. In order to monitor precipitation, for example, instruments need to be placed in zones with lower wind speeds and decreased wind shear so that rain and snow can fall more directly into the gage opening. Thus, gages at upper elevations are typically located in

topographically-protected sites in forested valleys or depressions, such as most SNOTEL sites (Schaefer and Paetzold 2000). Because atmospheric conditions can vary significantly between sheltered and exposed sites, observations such as temperature from such microclimatically disparate locations can disagree substantially (Gallo 2005) and influence modeling efforts, as the comparisons in Chapter 1 between PRISM and open slope temperatures in the Walker Basin demonstrated.

Figure 68. Differences in siting.

Both of these sites in the Snake Range are located in the "Subalpine" vegetative zone, but the first one (top) is sited in a concave high valley setting, whereas the second (bottom) is sited on a gentle mountain slope more typical of the subalpine zone in the Great Basin. The first is highly shaded, has much denser vegetation, and can retain snow cover much longer than the second even though it is at a slightly lower elevation (the photographs were taken within one day of each other). Treating these sites as equally representative of ecohydrologic conditions for this vegetation zone would be most unwise, although they may represent two ends of a spectrum.

For instance, if a science question is focused on precipitation across elevation, siting conditions for instruments must be kept as uniform as possible across individual mountain gradients, in order to make comparative results robust. Future instrumentation and network design would ideally be guided by widely-accepted protocols that account for differences in site environments that cannot be standardized to the World Meteorological Organization (WMO) ideal for weather stations. Slope, aspect, soil type, vegetation characteristics, and wind and sun exposure impact the microclimate and must be considered when comparing multiple sites within and across networks (Figure 68, and as represented in the noise between study sites in Chapter 1).

Applying technology for efficacy

Technology is key in the transformation of mountain science. Besides the plethora of environmental sensor applications, the ability to set up real-time or near-real-time telemetry of data is crucial for maintaining data quality and minimizing gaps in the record. The most effective of these technologies at this point in time utilize standard bi-directional Transmission Control Protocol/Internet Protocol (TCP/IP). The reasons for this are many, notably that TCP/IP is inherently error correcting, eliminating data corruption during transmission. Moreover, the use of TCP/IP based technologies allows: 1) data to be efficiently transferred offsite for redundancy; 2) immediate detection and remote troubleshooting of equipment related failures; 3) remote device configuration and control; and 4) any number of TCP/IP enabled devices connected to the network (Gubbi et al. 2013). In particular, the use of TCP/IP cameras is gaining traction to not only visually monitor climatic conditions, but also to track biodiversity (e.g., species occurrence and population size, vegetation phenology; Richardson et al. 2007). Because TCP/IP networking is such a prolific technology, there are many options available for extending this telemetry via satellite or 100+ km terrestrial wireless connections (ESIP Envirosensing Cluster 2016). The stations in the Snake and Sheep Ranges, as well as the testbed station in the Walker Basin all leverage this technology.

Long-term costs of maintaining remote observation systems such as the Snake and Sheep Range sites can be mitigated by the use of these digital networking technologies. Because technician time and associated travel expenses are the most costly part of maintaining field-based infrastructure, the ability to remotely diagnose problems and plan site visits is important from a budgetary perspective (ESIP Envirosensing Cluster 2016). Remote control of field devices such as cameras, heater units, relay panels, dataloggers, and so forth can allow scientists or technicians to manage equipment operation during adverse environmental conditions when physical access would be difficult or dangerous. Furthermore,

automated image capture from field-based TCP/IP cameras can assist in remote inspection and sensor data Quality Assurance and Quality Control (QA/QC) as demonstrated in Chapters 2 and 3. For example, the gap in Geonor and sap flow data at the Sheep Range Montane site (Figure 44, Figure 63) was caused by a direct lightning strike to the site that was discovered immediately thanks to real-time telemetry of data. I was able to access the site to inspect equipment soon afterwards and repair or replace most of the faulty equipment before winter.

Integrating a "cyberinfrastructure" into sensor-based observation planning is essential, as expertise in digital data communications, management, and processing has become a crucial part of multidisciplinary science (Atkins 2003; McMahon et al. 2011; Michener et al. 2012). Cyberinfrastructure for field science requires individuals with technological skill sets that include datalogger programming, digital network management, wireless-microwave communications, database administration, application development, and data QA/QC. Ideally, the workflow for acquiring, managing, processing, and tracking environmental data from a modern observation site should be a seamless integration of software and domain experts, but implementation of such a system in small-scale environmental science remains a challenge due to cost and technical requirements (Jones et al. 2015; ESIP Envirosensing Cluster 2016).

Figure 69. Datalogger and wiring box for the Snake Range Subalpine sap flow sensor system.

This complex system requires attention to detail and technical expertise to plan, acquire, assemble, configure, and maintain. There are several single points of failure that could halt operation of the entire system. This hardware must survive being buried in snow for a substantial portion of the year, as well as handle summer exposure to intense thunderstorms, high-altitude solar radiation, and potential animal disturbance. Primary science data acquisition using automated methods in remote mountain environments is challenging and requires expertise and preparation beyond typical short-lived installations.

Best practices in systems engineering

Good observational science using automated methods will only result from conscientious planning and attention to technical detail. Construction of sites like those in the Snake and Sheep Ranges is part of a lengthy and involved process that has the potential to end in failure-prone instrumentation and poor-quality data (Figure 69). Engineering the scientific packages and support systems such as the power

supply, structure, and telemetry is best addressed early on in the planning stages (Figure 70; ESIP Envirosensing Cluster 2016).

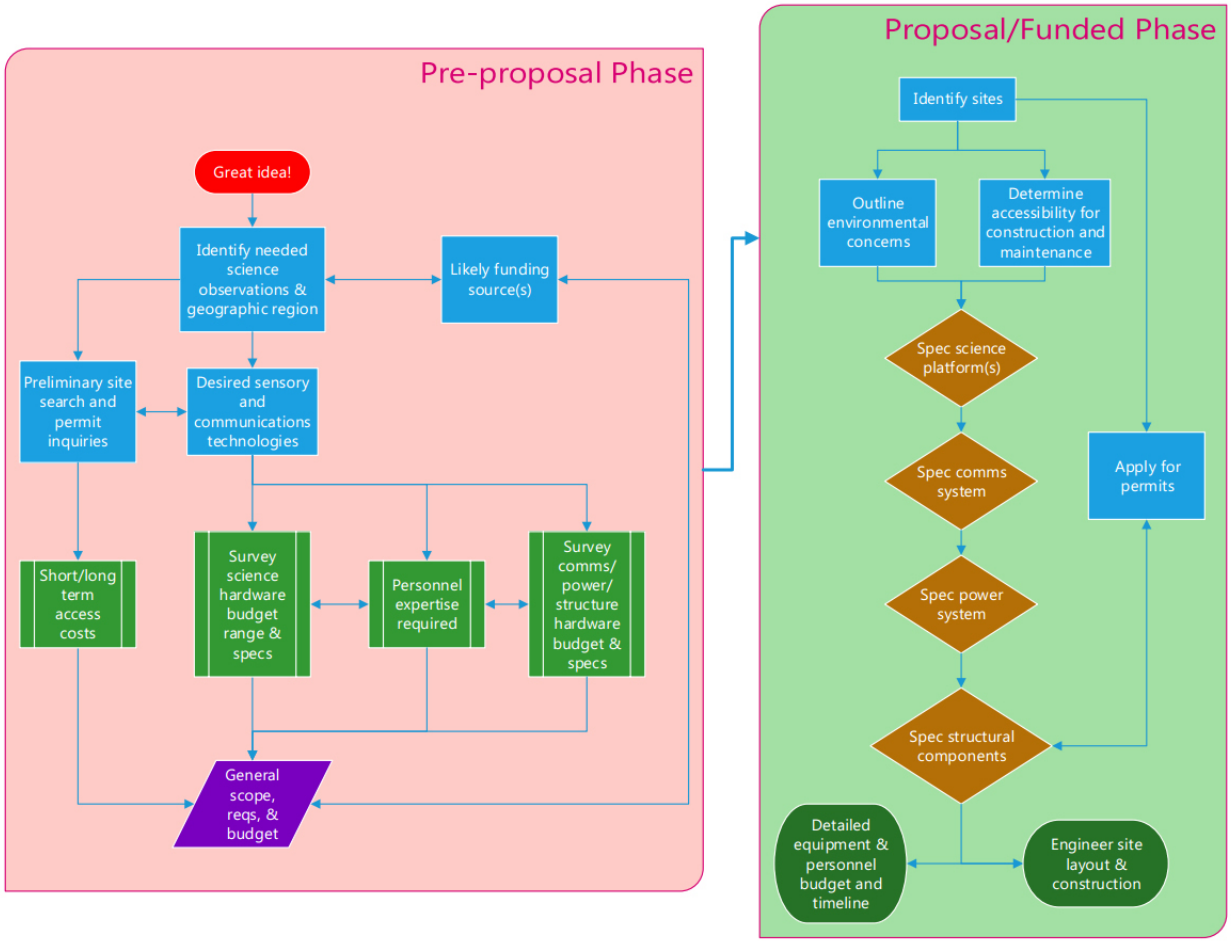

Figure 70. Sensor deployment flowchart.

This flowchart depicts the decision-making process that should be followed prior to field deployment of sensors regardless of project scale or objectives. High-quality long-term data come from installations that have been carefully considered.

A design philosophy that maximizes capacity, redundancy, and modularity helps increase future flexibility when additional sensors need to be added, or unanticipated environmental materialize. This philosophy can be applied to the sensor systems, structure and layout of the deployment, power generation and storage, and communications links.

Conclusions

By moving forward with a consistent and reasonably uniform monitoring strategy for mountain ecosystems, the scientific community has the opportunity to address knowledge gaps by improving existing systems, extending existing networks, and/or establishing new ones. This study advocates an approach of making gradients, uniformity, and proven technologies the central themes with “best practices” as the philosophical approach. Development of truly effective ecohydrological process models that are relevant at multiple scales will occur through an evolutionary process of knowledge-based testing, evaluation, and improvement of interpolative techniques (Daly et al. 2002; Hijmans et al. 2005; Holden et al. 2015), and these themes are an excellent basis from which to proceed.

Overall summary and conclusions

Original contributions of this work

This work presents new collections of climate and ecohydrological data from mountain environments in the Great Basin, USA. These observations were made following protocols that are directly comparable to worldwide standards of weather and climate monitoring; however, the topographic distributions of these observations are unique for the region, and provide an unprecedented level of visibility into Great Basin mountain climate processes at the sub-hourly to multi-seasonal scales. New insights into the performance of the popular PRISM climate model were obtained for terrain categories that comprise a large portion of Great Basin mountain landscapes. A simple method of instantaneous partitioning of precipitation by phase based on *in-situ* mass measurements was introduced. Distribution of storm-by-storm rain and snow, as well as precipitation intensity, was quantified for four years across the primary Great Basin vegetation zones on a large elevation gradient. Responses of shallow soil moisture and tree sap flow activity to different seasonal regimes within a deep regional drought period were reported, demonstrating that summer moisture can make a significant impact in reducing the effects of relatively dry winters and regionally-elevated temperatures on shallow-rooting vegetation. High-altitude Great Basin bristlecone pines were observed (using xylem flow as the indicator) to sustain daytime respiratory activities during drier conditions than neighboring limber pines, confirming their greater resilience to drought and warming conditions. Multiple montane and subalpine tree species located in the central Great Basin were observed to maintain positive daytime xylem flow activity into late October if August-September moisture was present, indicating a significant monsoon-season adaptation well north of the accepted North American Monsoon primary region of influence. Ecohydrology at the Great Basin/Mojave Desert transition zone was observed to be seasonally variable, with storm precipitation totals not providing an accurate indication of “effective” precipitation and soil water recharge in a

montane environment. Instead, the timing, rate, and phase (rain, snow, or hail) of precipitation made a difference in shallow soils infiltration and subsequent conifer xylem activity. The design and implementation practices developed over the course of this study for automated monitoring in remote mountain environments resulted in an unusually large collection of highly consistent and gap-free year-round observations.

Practical implications

Insight gained from this work has direct application to past, current, and future scientific activity in the Great Basin and temperate mountain environments in general. Controlling observations for cold-air pooling and topographic category allows empirical development of strong relationships between elevation and temperature-related variables at the large watershed scale, but current observational data are not properly capturing this. Studies that use the PRISM dataset to model thermal sums or estimate precipitation as snow, for instance, may dramatically underestimate the true heat accumulation or overestimate mid-elevation snowfall across large portions of Great Basin watersheds. Existing monitoring networks which field both mass-collection and tipping bucket precipitation gages could produce a phase-discrimination dataset using a version of the Gage-Difference Method tailored for their specific hardware and data characteristics. Adding one gage type or the other to existing networks for this data product would be advantageous in areas where the snowline is dynamic (such as the slopes of the Sierra Nevada), or in places where hailstorms are frequent and otherwise difficult to quantify. Studies of high-elevation conifers in the western U.S. can use the observations of xylem response during drought conditions to infer relative adaptive strategies and refine study designs related to these species' distributions, potential phylogenetic differentiation, and seasonal growth behavior. Regional summaries of "drought" can use the information on shallow soil moisture conditions and summer relief to refine perceptions of seasonal drought and moisture stress across mountain gradients

in the Great Basin. Ecohydrological studies that use the "pulse-reserve" paradigm for estimating impact of sub-seasonal precipitation on semi-arid ecosystems would benefit significantly from *in-situ* measurements of soil moisture given that storm events (and thus their impacts) in the Great Basin differ in volume, intensity, and phase over very short distances in mountain environments. Detailed insight into complex ecohydrological processes is achieved using a combination of observations at high temporal resolution, topographic diversity, and data completeness. These goals are all achieved using methodological practices developed and demonstrated in this work when designing and implementing technology-based observation networks.

Future work

Given the breadth of the data resulting from this work, the follow-up investigative possibilities are numerous and diverse in discipline. The most immediately useful further analyses of these data would be to:

1) Evaluate other temperature products such as Daymet (Thornton et al. 2012) and TopoWX (Oyler et al. 2014) in a similar manner to the test of PRISM in the Walker Basin;

2) Compare local *versus* watershed-scale temperature anomalies with specific synoptic mechanisms such as persistent cold-season high pressure and advancing cold fronts in the transition seasons;

3) Develop corrections for PRISM data in the Walker watershed on topography similar to the instrumented sites and evaluate the impacts of these corrections to existing hydrological or ecological models in the area;

4) Refine the Gage-Difference Method with additional processing steps that incorporate basic atmospheric data in an effort to improve the low-intensity storm classifications, and test the GDM

using data from a sensor-diverse environment such as one of the prominent snow-oriented research laboratories to investigate weaknesses such as orifice bridging and weighing-sensor noise;

5) Apply a refined GDM to the study sites in the Snake and Sheep Ranges, with filter settings specifically tuned for the nuances of each site's sensor behavior in different seasons;

6) Evaluate storm characteristics (phase, intensity, volume, subsequent soil moisture or snow depth impact) across the Snake Range gradient in light of each storm's synoptic origins;

7) Investigate the tree-by-tree responses of xylem sap flow activity within species to multiple soil moisture depths, with consideration of their relative positions on the landscape, competitive interaction, and potential rooting depths; and

8) Compare iButton deployment data with co-located in-canopy temperature measurements to evaluate the differences in daily maximum and minimum temperature values using each method.

Valuable continuation work that may require more sophisticated study designs include:

1) Expand the Walker Basin temperature study to include a wider range of topographic categories, including ridges and valleys, as well as add measurements of relative humidity, incident radiation, and wind velocity;

2) Investigate the GDM with disdrometer observations, multi-height wind velocity, different gage orifice configurations, and areal measurements of snow accumulation and snow water-equivalent (SWE);

3) Increase replication of tree instrumentation along with soil moisture and temperature monitoring on the sunny and shaded sides of each tree, such that multiple sap flow sensors per tree and several

trees per species per site would provide a more accurate picture of variability in the measurements and thus interpretation of results;

4) Combine additional sap flow and soil properties measurements with gas exchange measurements from tree foliage during specific timeframes, such as warm winter interludes, peak summer drought, and peak sap velocity; and

5) Set up long-term monitoring of air temperature, relative humidity, and multi-depth soil moisture and temperature across *Pinus longaeva* populations in the Great Basin.

Of course, the most obvious thing to do in the future is to analyze the same data streams from these study sites in subsequent years, so as to include a wider range of seasonal climates. The fact that it is likely that these data streams will persist for years at similar quality levels for future comparability underscores the value in long-term thinking at the study design and systems engineering stages. Much research funding supports individual investigators for three-year periods focused on individual questions of specific scientific interest. The conclusions and datasets highlighted in this work would not have been possible using the typical single-PI approach, and demonstrate instead the need to follow an interdisciplinary methodology focused on long-term success rather than short-term results. This mindset was best described by Dr. John Wehausen, a longtime researcher of bighorn sheep population ecology:

> "Treat theory as a human abstraction that has a high probability of being incorrect; instead, give primacy to data…the devil is almost always in the details and better data can make a huge difference. Be prepared to devote a long time if you want an adequate understanding at a system level. Be open to the possibility that variables you never considered may be very important, relegating a lot of previous research to little more than a preliminary study. Finally, there is no substitute for spending a great deal of time in the field…[to think about] what

> variables might be important. Unfortunately, most research I see begins with an inadequate problem analysis." *Quote from an interview in* Mountain Views Newsletter (Millar 2013)

Undoubtedly, given high temporal and topographic climate variability of the region, the most scientifically-valuable observations in present-day Great Basin ecosystems are those which can be made repeatedly over years to decades, are located with specific topography in mind (Valleys? Ridges? Slopes?), and are obtained using clearly-described practices that can be evaluated for methodological bias (such as instrument configuration). The Great Basin already has a rich history of research in the natural sciences, and holds tremendous potential for additional insight into the complexity of climate and ecohydrological processes in semi-arid regions. If we are prepared to apply new technologies and approaches that build on previous work and emphasize long-term observation, fresh and exciting discoveries are sure to be made and future challenges will be matched with informed decision-making.

References

Adams HD, Kolb TE. 2005. Tree growth response to drought and temperature in a mountain landscape in northern Arizona, USA. *Journal of Biogeography* 32:1629–1640.

Alter JC. 1937. Shielded storage precipitation gages 1. *Monthly Weather Review* 65:262–265.

Anderson-Teixeira KJ, Delong JP, Fox AM, Brese DA, Litvak ME. 2011. Differential responses of production and respiration to temperature and moisture drive the carbon balance across a climatic gradient in New Mexico. *Global Change Biology* 17:410–424.

Andrews ED. 2012. *Hydrology of the Sierra Nevada Network national parks: Status and trends*. Natural Resource Report NPS/SIEN/NRR—2012/500. Fort Collins, Colorado.

Araújo MB, Guisan A. 2006. Five (or so) challenges for species distribution modelling. *Journal of Biogeography* 33:1677–1688.

Atkins DE. 2003. *Revolutionizing science and engineering through cyberinfrastructure: Report of the National Science Foundation blue-ribbon advisory panel on cyberinfrastructure 2003-01*.

Austin AT, Yahdjian L, Stark JM, Belnap J, Porporato A, Norton U, Ravetta DA, Schaeffer SM. 2004. Water pulses and biogeochemical cycles in arid and semiarid ecosystems. *Oecologia* 141:221–235.

Austin MP, Van Niel KP. 2011. Improving species distribution models for climate change studies: Variable selection and scale. *Journal of Biogeography* 38:1–8.

Avanzi F, De Michele C, Ghezzi A, Jommi C, Pepe M. 2014. A processing-modeling routine to use SNOTEL hourly data in snowpack dynamic models. *Advances in Water Resources* 73:16–29.

Baldocchi D, Falge E, Gu L, Olson R, Hollinger D, Running S, Anthoni P, Bernhofer C, Davis K, Evans R, et al. 2001. FLUXNET: A New Tool to Study the Temporal and Spatial Variability of Ecosystem-Scale Carbon Dioxide, Water Vapor, and Energy Flux Densities. *Bulletin of the American Meteorological Society* 82:2415–2434.

Bales RC, Molotch NP, Painter TH, Dettinger MD, Rice R, Dozier J. 2006. Mountain hydrology of the western United States. *Water Resources Research* 42:1–13.

Barnett TP, Adam JC, Lettenmaier DP. 2005. Potential impacts of a warming climate on water availability in snow-dominated regions. *Nature* 438:303–9.

Begert M, Schlegel T, Kirchhofer W. 2005. Homogeneous temperature and precipitation series of Switzerland from 1864 to 2000. *International Journal of Climatology* 25:65–80.

Bell GD, Bosart LF. 1988. Appalachian Cold-Air Damming. *Monthly Weather Review* 116:137–161.

Beniston M, Diaz HF, Bradley RS. 1997. Climatic change at high elevation sites: an overview. *Climatic Change* 36:233–251.

Bennie J, Huntley B, Wiltshire A, Hill MO, Baxter R. 2008. Slope, aspect and climate: Spatially explicit and implicit models of topographic microclimate in chalk grassland. *Ecological Modelling* 216:47–59.

Bentz B, Vandygriff J, Jensen C, Coleman T, Maloney P, Smith S, Grady A, Schen-langenheim G. 2013. Mountain Pine Beetle Voltinism and Life History Characteristics across Latitudinal and Elevational Gradients in the Western United States. *Forest Science* 60:434–449.

Berghuijs WR, Woods RA, Hrachowitz M. 2014. A precipitation shift from snow towards rain leads to a decrease in streamflow. *Nature Climate Change* 4:583–586.

Bergström S, Carlsson B, Gardelin M, Lindström G, Pettersson A, Rummukainen M. 2001. Climate change impacts on runoff in Sweden - Assessments by global climate models, dynamical downscalling and hydrological modelling. *Climate Research* 16:101–112.

Beven KJ. 2011. *Rainfall-Runoff Modelling: The Primer*. John Wiley & Sons.

Billings W. 1954. Temperature inversions in the pinyon-juniper zone of a Nevada mountain range. *Butler University Botanical Studies* 11.

Billings WD. 1951.*Vegetational zonation in the Great Basin of western North America* In: Les bases écologiques de la régénération de la végétation des zones arides. Vol. 9. International Union of Biological Sciences, Series B: Colloquia. p. 101–122.

Birkel SD, Putnam AE, Denton GH, Koons PO, Fastook JL, Putnam DE, Maasch KA. 2012. Climate Inferences from a Glaciological Reconstruction of the Late Pleistocene Wind River Ice Cap , Wind River Range , Wyoming. *Arctic, Antarctic, and Alpine Research* 44:265–276.

Blandford TR, Humes KS, Harshburger BJ, Moore BC, Walden VP, Ye H. 2008. Seasonal and synoptic variations in near-surface air temperature lapse rates in a mountainous basin. *Journal of Applied Meteorology and Climatology* 47:249–261.

Böhner J, Antonić O. 2009. Land-surface parameters specific to topo-climatology. *Developments in Soil Science* 33:195–226.

Böhner J, Selige T. 2006.*Spatial prediction of soil attributes using terrain analysis and climate regionalisation* In: Böhner J, McCloy KR, Strobl J, editors. SAGA - Analyses and Modelling Applications: Göttinger Aeographische Abhandlungen. Vol. 115. p. 13–28.

Bolstad P V, Swift L, Collins F, Regniere J. 1998. Measured and predicted air temperature at basin to regional scales in the southern Appalacian mountains. *Agricultural and Forest Meteorology* 91:161–176.

Brekke L, Thrasher BL, Maurer EP, Pruitt T. 2013. *Downscaled CMIP3 and CMIP5 climate projections: Release of downscaled CMIP5 climate projections, comparison with preceding information, and summary of user needs*. US Department of the Interior, Bureau of Reclamation, Technical Services Center, Denver, Colorado.

Bristow KL, Campbell GS. 1984. On the relationship between incoming solar radiation and daily maximum and minimum temperature. *Agricultural and Forest Meteorology* 31:159–166.

Brohan P, Kennedy JJ, Harris I, Tett SFB, Jones PD. 2006. Uncertainty estimates in regional and global observed temperature changes: A new data set from 1850. *Journal of Geophysical Research* 111:21.

Burgess SSO, Adams MA, Turner NC, Beverly CR, Ong CK, Khan AAH, Bleby TM. 2001. An improved heat pulse method to measure low and reverse rates of sap flow in woody plants. *Tree Physiology* 21:589–598.

Burgess SSO, Dawson TE. 2008. Using branch and basal trunk sap flow measurements to estimate whole-plant water capacitance: a caution. *Plant and Soil* 305:5–13.

Campbell Scientific, Inc. 2016. HMP60-L: Temperature and Relative Humidity Probe. [accessed 2016 Feb 17]. https://www.campbellsci.com/hmp60

Castelli RM, Chambers JC, Tausch RJ. 2000. Soil-plant relations along a soil-water gradient in great basin riparian meadows. *Wetlands* 20:251–266.

Cayan DR. 1996. Interannual climate variability and snowpack in the western United States. *Journal of Climate* 9:928–948.

Charlet DA. 1996. *Atlas of Nevada Conifers: A Phytogeographic Reference*. Reno: University of Nevada Press.

Charlet DA. 2007. Distribution patterns of Great Basin conifers: implications of extinction and immigration. *Aliso: A Journal of Systematic and Evolutionary Botany* 24:31–61.

Chen YC, Bundy DS, Hoff SJ. 1998. Modeling the Variation of Wind Speed with Height for Agricultural Source Pollution Control. *ASHRAE Transactions* 104.1B:1685–1691.

Chesson P, Gebauer RLE, Schwinning S, Huntly N, Wiegand K, Ernest MSK, Sher A, Novoplansky A, Weltzin JF. 2004. Resource pulses, species interactions, and diversity maintenance in arid and semi-arid environments. *Oecologia* 141:236–253.

Chorover J, Scatena FN, White T, Anderson S, Aufdenkampe AK, Bales RC, Brantley SL, Tucker G. 2012. *Common Critical Zone Observatory (CZO) Infrastructure and Measurements*. http://criticalzone.org/national/infrastructure/a-common-approach-1national/

Cole KL, Fisher JF, Ironside K, Mead JI, Koehler P. 2013. The biogeographic histories of Pinus edulis and Pinus monophylla over the last 50,000 years. *Quaternary International* 310:96–110.

Collins SL, Childers DL. 2014. Long-Term Ecological Research and Network-Level Science. *Eos, Transactions American Geophysical Union* 95:293–294.

Comstock JP, Ehleringer JR. 1992. Plant Adaptions in the Great Basin and Colorado Plateau. *The Great Basin Naturalist* 52:195–215.

Crookston NL, Rehfeldt GE, Dixon GE, Weiskittel AR. 2010. Addressing climate change in the forest vegetation simulator to assess impacts on landscape forest dynamics. *Forest Ecology and Management* 260:1198–1211.

Dai A, Karl TR, Sun BM, Trenberth KE. 2006. Recent trends in cloudiness over the United States - A tale of monitoring inadequacies. *Bulletin of the American Meteorological Society* 87:597–606.

Daly C. 2006. Guidelines for assessing the suitability of spatial climate data sets. *International Journal of Climatology* 26:707–721.

Daly C, Conklin DR, Unsworth MH. 2010. Local atmospheric decoupling in complex topography alters climate change impacts. *International Journal of Climatology* 30:1857–1864.

Daly C, Gibson WP, Taylor GH, Johnson GL, Pasteris P. 2002. A knowledge-based approach to the statistical mapping of climate. *Climate Research* 22:99–113.

Daly C, Halbleib M, Smith JI, Gibson WP, Doggett MK, Taylor GH, Curtis J, Pasteris PP. 2008. Physiographically sensitive mapping of climatological temperature and precipitation across the conterminous United States. *International Journal of Climatology* 28:2031–2064

Daly C, Neilson RH, Phillips DL. 1994. A statistical-topographic model for mapping climatological precipitation over mountainous terrain. *Journal of Applied Meteorology* 33:140–158.

Daly C, Smith JW, Smith JI, McKane RB. 2007. High-resolution spatial modeling of daily weather elements for a catchment in the Oregon Cascade Mountains, United States. *Journal of Applied Meteorology and Climatology* 46:1565–1586.

Dascalu S, Harris Jr FC, McMahon Jr M, Fritzinger E, Strachan S, Kelley R. 2014. An Overview of the Nevada Climate Change Portal. *Proceedings of The 7th International Congress on Environmental Modelling and Software (iEMSs 2014)* 1:75–82.

Denmead OT, Shaw RH. 1962. Availability of Soil Water to Plants as Affected by Soil Moisture Content and Meteorological Conditions1. *Agronomy Journal* 54:385.

Dettinger MD, Cayan DR, Diaz HF, Meko DM. 1998. North-South precipitation patterns in western North America on interannual-to-decadal timescales. *Journal of Climate* 11:3095–3111.

Dettinger MD, Cayan DR, Meyer MK, Jeton A. 2004. Simulated hydrologic responses to climate variations and change in the Merced, Carson, and American River basins, Sierra Nevada, California, 1900-2099. *Climatic Change* 62:283–317.

van Devender TR, Spaulding WG. 1979. Development of vegetation and climate in the southwestern United States. *Science* 204:701–710.

Diamond HJ, Karl TR, Palecki MA, Baker CB, Bell JE, Leeper RD, Easterling DR, Lawrimore JH, Meyers TP, Helfert MR, et al. 2013. U.S. climate reference network after one decade of operations status and assessment. *Bulletin of the American Meteorological Society* 94:485–498.

Diaz HF, Eischeid JK. 2007. Disappearing "alpine tundra" Koppen climatic type in the western United States. *Geophysical Research Letters* 34:1–4.

Diodato N. 2005. The influence of topographic co-variables on the spatial variability of precipitation over small regions of complex terrain. *International Journal of Climatology* 25:351–363.

Dobrowski SZ. 2011. A climatic basis for microrefugia: the influence of terrain on climate. *Global Change Biology* 17:1022–1035.

Dobrowski SZ, Abatzoglou JT, Greenberg J a., Schladow SG. 2009. How much influence does landscape-scale physiography have on air temperature in a mountain environment? *Agricultural and Forest Meteorology* 149:1751–1758.

Douglas MW, Maddox RA, Howard K, Reyes S. 1993. The Mexican monsoon. *Journal of Climate* 6:1665–1677.

Dunne T, Zhang W, Aubry BF. 1991. Effects of rainfall, vegetation, and microtopography on infiltration and runoff. *Water Resources Research* 27:2271–2285.

Easterling DR. 2002. Recent Changes in Frost Days and the Frost-Free Season in the United States. *Bulletin of the American Meteorological Society* 83:1327–1332.

Endrizzi S, Gruber S, Dall'Amico M, Rigon R. 2014. GEOtop 2.0: Simulating the combined energy and water balance at and below the land surface accounting for soil freezing, snow cover and terrain effects. *Geoscientific Model Development* 7:2831–2857.

ESIP Envirosensing Cluster. 2016. Community Wiki Document on best practices for sensor networks and sensor data management, Federation of Earth Science Information Partners. [accessed 2016 Jan 1]. http://wiki.esipfed.org/index.php/EnviroSensing_Cluster

Feiccabrino J, Lundberg A. 2008.*Precipitation Phase Discrimination in Sweden* In: 65th Eastern Snow Conference. Fairlee, VT. p. 239–254.

Fiebrich CA. 2009. History of surface weather observations in the United States. *Earth-Science Reviews* 93:77–84.

Fitzpatrick MC, Hargrove WW. 2009. The projection of species distribution models and the problem of non-analog climate. *Biodiversity and Conservation* 18:2255–2261.

Foley JA, Defries R, Asner GP, Barford C, Bonan G, Carpenter SR, Chapin FS, Coe MT, Daily GC, Gibbs HK, et al. 2005. Global consequences of land use. *Science (New York, N.Y.)* 309:570–574.

Fridley JD. 2009. Downscaling climate over complex terrain: High finescale (<1000 m) spatial variation of near-ground temperatures in a montane forested landscape (Great Smoky Mountains). *Journal of Applied Meteorology and Climatology* 48:1033–1049.

Fritts HC. 1969. *Bristlecone pine in the White Mountains of California, growth and ring-width characteristics*. Papers of the Laboratory of Tree-Ring Research No.4, Tucson.

Fritts HC. 1976. *Tree Rings and Climate*. London: Academic Press.

Fritts HC, Smith DG, Stokes MA. 1965. The biological model for paleoclimatic interpretation of Mesa Verde tree-ring series. *Memoirs of the Society for American Archaeology* 19:101–121.

Fuchs T, Rapp J, Rubel F, Rudolf B. 2001. Correction of synoptic precipitation observations due to systematic measuring errors with special regard to precipitation phases. *Physics and Chemistry of the Earth, Part B: Hydrology, Oceans and Atmosphere* 26:689–693.

Gallo KP. 2005. Evaluation of temperature differences for paired stations of the U.S. Climate Reference Network. *Journal of Climate* 18:1629–1636.

Garratt J. 1994. Review: the atmospheric boundary layer. *Earth-Science Reviews* 37:89–134.

Gleick PH, Chalecki EL. 1999. The impacts of climatic changes for water resources of the Colorado and Sacramento-San Joaquin river basins. *Journal of the American Water Resources Association* 35:1429–1441.

Goodison BE, Louie PYT, Yang D. 1998. *WMO Solid Precipitation Measurement Intercomparison*. World Meteorological Organization.

Graae BJ, De Frenne P, Kolb A, Brunet J, Chabrerie O, Verheyen K, Pepin N, Heinken T, Zobel M, Shevtsova A, et al. 2012. On the use of weather data in ecological studies along altitudinal and latitudinal gradients. *Oikos* 121:3–19.

Graham NE, Hughes MK, Ammann CM, Cobb KM, Hoerling MP, Kennett DJ, Kennett JP, Rein B, Stott L, Wigand PE, et al. 2007. Tropical Pacific - mid-latitude teleconnections in medieval times. *Climatic Change* 83:241–285.

Granier A. 1987. Evaluation of transpiration in a Douglas-fir stand by means of sap flow measurements. *Tree Physiology* 3:309–320.

Granier A, Biron P, Lemoine D. 2000. Water balance, transpiration and canopy conductance in two beech stands. *Agricultural and Forest Meteorology* 100:291–308.

Grayson DK. 2011. *The Great Basin: A Natural Prehistory*. 2nd ed. Berkeley: University of California Press.

Gubbi J, Buyya R, Marusic S, Palaniswami M. 2013. Internet of Things (IoT): A vision, architectural elements, and future directions. *Future Generation Computer Systems* 29:1645–1660.

Guisan A, Thuiller W. 2005. Predicting species distribution: Offering more than simple habitat models. *Ecology Letters* 8:993–1009.

Guisan A, Weiss SB, Weiss AD. 1999. GLM versus CCA spatial modeling of plant species distribution. *Plant Ecology* 143:107–122.

Gurung AB, von Dach SW, Price MF, Aspinall R, Balsiger J, Baron JS, Sharma E, Greenwood G, Kohler T. 2012. Global Change and the World's Mountains— Research Needs and Emerging Themes for Sustainable Development. *Mountain Research and Development* 32:S47–S54.

Hacke UG, Sperry JS. 2001. Functional and ecological xylem anatomy. *Perspectives in Plant Ecology, Evolution and Systematics* 4:97–115.

Hallman C, Arnott H. 2015. Morphological and physiological phenology of Pinus longaeva in the White Mountains of California. *Tree-Ring Research* 71:1–12.

Hamann A, Wang T. 2006. Potential effects of climate change on ecosystem and tree species distribution in British Columbia. *Ecological Society of America* 87:2773–2786.

Hamlet AF, Lettenmaier DP. 2005. Production of Temporally Consistent Gridded Precipitation and Temperature Fields for the Continental United States. *Journal of Hydrometeorology* 6:330–336.

Hamlet AF, Mote PW, Clark MP, Lettenmaier DP. 2005. Effects of temperature and precipitation variability on snowpack trends in the western United States. *Journal of Climate* 18:4545–4561.

Harpold AA, Molotch NP, Musselman KN, Bales RC, Kirchner PB, Litvak M, Brooks PD. 2015. Soil moisture response to snowmelt timing in mixed-conifer subalpine forests. *Hydrological Processes* 29:2782–2798.

Hart JK, Martinez K. 2006. Environmental Sensor Networks: A revolution in the earth system science? *Earth-Science Reviews* 78:177–191.

Hasenauer H, Merganicova K, Petritsch R, Pietsch SA, Thornton PE. 2003. Validating daily climate interpolations over complex terrain in Austria. *Agricultural and Forest Meteorology* 119:87–107.

Hatchett BJ, Boyle DP, Putnam AE, Bassett SD. 2015. Placing the 2012–2015 California-Nevada drought into a paleoclimatic context: Insights from Walker Lake, California-Nevada, USA. *Geophysical Research Letters* 42:8632–8640.

Hayes MJ, Svoboda MD, Wilhite DA, Vanyarkho OV. 1999. Monitoring the 1996 Drought Using the Standardized Precipitation Index. *Bulletin of the American Meteorological Society* 80:429–438.

Haylock MR, Hofstra N, Klein Tank AMG, Klok EJ, Jones PD, New M. 2008. A European daily high-resolution gridded data set of surface temperature and precipitation for 1950-2006. *Journal of Geophysical Research: Atmospheres* 113.

Hengl T, Heuvelink GBM, Tadić MP, Pebesma EJ. 2012. Spatio-temporal prediction of daily temperatures using time-series of MODIS LST images. *Theoretical and Applied Climatology* 107:265–277.

Higgins RW, Yao Y, Wang XL. 1997. Influence of the North American monsoon system on the U.S. summer precipitation regime. *Journal of Climate* 10:2600–2622.

Hijmans RJ, Cameron SE, Parra JL, Jones PG, Jarvis A. 2005. Very high resolution interpolated climate surfaces for global land areas. *International Journal of Climatology* 25:1965–1978.

Hock R. 2003. Temperature index melt modelling in mountain areas. *Journal of Hydrology* 282:104–115.

Hofstra N, Haylock M, New M, Jones PD. 2009. Testing E-OBS European high-resolution gridded data set of daily precipitation and surface temperature. *Journal of Geophysical Research: Atmospheres* 114.

Holden ZA, Swanson A, Klene AE, Abatzoglou JT, Dobrowski SZ, Cushman SA, Squires J, Moisen GG, Oyler JW. 2015. Development of high-resolution (250 m) historical daily gridded air temperature data using reanalysis and distributed sensor networks for the US Northern Rocky Mountains. *International Journal of Climatology*.

Holmgren CA, Betancourt JL, Rylander KA. 2010. A long-term vegetation history of the Mojave–Colorado Desert ecotone at Joshua Tree National Park. *Journal of Quaternary Science* 22:222–236.

Horning ME, McGovern TR, Darris DC, Mandel NL, Johnson R. 2010. Genecology of holodiscus discolor (Rosaceae) in the Pacific Northwest, U.S.A. *Restoration Ecology* 18:235–243.

Horton RE. 1933. The Rôle of infiltration in the hydrologic cycle. *Eos, Transactions American Geophysical Union* 14:1689–1699.

Houghton J. 1979. A model for orographic precipitation in the north-central Great Basin. *Monthly Weather Review* 107:1462–1475

Howell TA. 1995. Comparison of Vapor-Pressure-Deficit Calculation Methods—Southern High Plains. *Irrigation and Drainage Engineering* 121:191–198.

Huang G-J, Bringi VN, Moisseev D, Petersen WA, Bliven L, Hudak D. 2015. Use of 2D-video disdrometer to derive mean density–size and Ze–SR relations: Four snow cases from the light precipitation validation experiment. *Atmospheric Research* 153:34–48.

Hughes MK, Diaz HF. 1994. Was there a "medieval warm period", and if so, where and when? *Climatic Change* 26:109–142.

Hughes MK, Funkhouser G. 2003. Frequency-dependent climate signal in upper and lower forest border tree rings in the mountains of the Great Basin. *Climatic Change* 59:233–244.

Huntington JL, Niswonger RG. 2012. Role of surface-water and groundwater interactions on projected summertime streamflow in snow dominated regions: An integrated modeling approach. *Water Resources Research* 48:1–20.

Integrated M. 2016. DS1922L: iButton Temperature Loggers with 8KB Data-Log Memory. [accessed 2016 Feb 17]. https://www.maximintegrated.com/en/products/digital/data-loggers/DS1922L.html

Jacobs B, Romme W, Allen C. 2008. Mapping "old" vs."young" piñon-juniper stands with a predictive topo-climatic model. *Ecological Applications* 18:1627–1641.

Jakeman AJ, Hornberger GM. 1993. How Much Complexity Is Warranted in a Rainfall-Runoff Model. *Water Resources Research* 29:2637–2649.

Jeffrey SJ, Carter JO, Moodie KB, Beswick AR. 2001. Using spatial interpolation to construct a comprehensive archive of Australian climate data. *Environmental Modelling and Software* 16:309–330.

Johnson RC, Erickson VJ, Mandel NL, St Clair JB, Vance-Borland KW. 2010. Mapping genetic variation and seed zones for Bromus carinatus in the Blue Mountains of eastern Oregon, USA. *Botany-Botanique* 88:725–736.

Jones AS, Horsburgh JS, Reeder SL, Ramírez M, Caraballo J. 2015. A data management and publication workflow for a large-scale, heterogeneous sensor network. *Environmental Monitoring and Assessment* 187:348.

Jones D, Wang W, Fawcett R. 2009. High-quality spatial climate data-sets for Australia. *Australian Meteorological and Oceanographic Journal* 58:233–248.

Justus CGG, Mikhail A. 1976. Height variation of wind speed and distribution statistics. *Geophysical Research Letters* 3:261–264.

Kalma JD, McVicar TR, McCabe MF. 2008. Estimating land surface evaporation: A review of methods using remotely sensed surface temperature data. *Surveys in Geophysics* 29:421–469.

Kimball KD, Weihrauch DM. 2000. Alpine Vegetation Communities and the Alpine-Treeline Ecotone Boundary in New England as Biomonitors for Climate Change. *USDA Forest Service Proceedings* 3:93–101.

Kirshbaum DJ, Smith RB. 2008. Temperature and moist-stability effects on midlatitude orographic precipitation. *Quarterly Journal of the Royal Meteorological Society* 134:1183–1199.

Knick ST, Hanser SE, Preston KL. 2013. Modeling ecological minimum requirements for distribution of greater sage-grouse leks: Implications for population connectivity across their western range, U.S.A. *Ecology and Evolution* 3:1539–1551.

Knowles N, Cayan DR. 2004. Elevational dependence of projected hydrologic changes in the San Francisco Estuary and watershed. *Climatic Change* 62:319–336.

Knutti R, Furrer R, Tebaldi C, Cermak J, Meehl GA. 2010. Challenges in combining projections from multiple climate models. *Journal of Climate* 23:2739–2758.

Körner C. 2012. *Alpine Treelines: Functional Ecology of the Global High Elevation Tree Limits*. Basel, Switzerland: Springer.

Köstner B, Granier A, Cermák J. 1998. Sapflow measurements in forest stands : methods and uncertainties. *Annals of Forest Science* 55:13–27.

Krause S, Lewandowski J, Dahm CN, Tockner K. 2015. Frontiers in real-time ecohydrology - a paradigm shift in understanding complex environmental systems. *Ecohydrology* 8:529–537.

Krofcheck DJ, Eitel JUH, Vierling LA, Schulthess U, Hilton TM, Dettweiler-Robinson E, Pendleton R, Litvak ME. 2014. Detecting mortality induced structural and functional changes in a piñon-juniper woodland using Landsat and RapidEye time series. *Remote Sensing of Environment* 151:102–113.

Kunkel KE, Easterling DR, Hubbard K, Redmond K. 2004. Temporal variations in frost-free season in the United States: 1895–2000. *Geophysical Research Letters* 31:1–4.

LaMarche VC. 1973. Holocene climatic variations inferred from treeline fluctuations in the White Mountains, California. *Quaternary Research* 3:632–660.

LaMarche VC. 1969. Environment in relation to age of bristlecone pines. *Ecology* 50:53–59.

LaMarche VC, Mooney HA. 1972. Recent climatic change and development of the bristlecone pine (P. longaeva Bailey) krummholz zone, Mt. Washington, Nevada. *Arctic and Alpine Research* 4:61–72.

Lareau NP, Horel JD. 2014. Dynamically Induced Displacements of a Persistent Cold-Air Pool. *Boundary-Layer Meteorology* 154:291–316.

Laternser M, Schneebeli M. 2002. Temporal Trend and Spatial Distribution of Avalanche Activity during the Last 50 Years in Switzerland. *Natural Hazards* 27:201–230.

Laternser M, Schneebeli M. 2003. Long-term snow climate trends of the Swiss Alps (1931-99). *International Journal of Climatology* 23:733–750.

Lawrence MG. 2005. The relationship between relative humidity and the dewpoint temperature in moist air: A simple conversion and applications. *Bulletin of the American Meteorological Society* 86:225–233.

Lawrimore JH, Menne MJ, Gleason BE, Williams CN, Wuertz DB, Vose RS, Rennie J. 2011. An overview of the Global Historical Climatology Network monthly mean temperature data set, version 3. *Journal of Geophysical Research: Atmospheres* 116:1–18.

Legates DR, DeLiberty TL. 1993. Precipitation measurement biases in the United States. *Journal of the American Water Resources Association* 29:855–861.

Legates DR, Willmott CJ. 1990. Mean seasonal and spatial variability in gauge-corrected, global precipitation. *International Journal of Climatology* 10:111–127.

Lenoir J, Graae BJ, Aarrestad PA, Alsos IG, Armbruster WS, Austrheim G, Bergendorff C, Birks HJB, Bråthen KA, Brunet J, et al. 2013. Local temperatures inferred from plant communities suggest strong spatial buffering of climate warming across Northern Europe. *Global Change Biology* 19:1470–1481.

Li X, Cheng G, Liu S, Xiao Q, Ma M, Jin R, Che T, Liu Q, Wang W, Qi Y, et al. 2013. Heihe Watershed Allied Telemetry Experimental Research (HiWATER): Scientific Objectives and Experimental Design. *Bulletin of the American Meteorological Society* 94:1145–1160.

Löffler-Mang M, Joss J. 2000. An optical disdrometer for measuring size and velocity of hydrometeors. *Journal of Atmospheric and Oceanic Technology* 17:130–139.

Loik ME, Breshears DD, Lauenroth WK, Belnap J. 2004. A multi-scale perspective of water pulses in dryland ecosystems: climatology and ecohydrology of the western USA. *Oecologia* 141:269–281.

Lookingbill TR, Urban DL. 2003. Spatial estimation of air temperature differences for landscape-scale studies in montane environments. *Agricultural and Forest Meteorology* 114:141–151.

Lookingbill TR, Urban DL. 2005. Gradient analysis, the next generation: towards more plant-relevant explanatory variables. *Canadian Journal of Forest Research* 35:10.

Lopes TJ, Allander KK. 2009. *Water Budgets of the Walker River Basin and Walker Lake , California and Nevada: U. S. Geological Survey Scientific Investigations Report 2009–5157*.

Luce CH, Abatzoglou JT, Holden ZA. 2013. The missing mountain water: slower westerlies decrease orographic enhancement in the Pacific Northwest USA. *Science* 342:1360–1365.

Lundquist JD, Cayan DR. 2007. Surface temperature patterns in complex terrain: Daily variations and long-term change in the central Sierra Nevada, California. *Journal of Geophysical Research* 112:D11124.

Lundquist JD, Minder JR, Neiman PJ, Sukovich E. 2010. Relationships between barrier jet heights, orographic precipitation gradients, and streamflow in the northern Sierra Nevada. *Journal of Hydrometeorology* 11:1141–1156.

Lundquist JD, Neiman PJ, Martner B, White AB, Gottas DJ, Ralph FM. 2008. Rain versus Snow in the Sierra Nevada, California: Comparing Doppler Profiling Radar and Surface Observations of Melting Level. *Journal of Hydrometeorology* 9:194–211.

Lundquist JD, Pepin N, Rochford C. 2008. Automated algorithm for mapping regions of cold-air pooling in complex terrain. *Journal of Geophysical Research* 113.

Marks D, Winstral A, Reba M, Pomeroy J, Kumar M. 2013. An evaluation of methods for determining during-storm precipitation phase and the rain/snow transition elevation at the surface in a mountain basin. *Advances in Water Resources* 55:98–110.

Maule CP, Chanasyk DS, Muehlenbachs K. 1994. Isotopic determination of snow-water contribution to soil water and groundwater. *Journal of Hydrology* 155:73–91.

McCabe GJ, Wolock DM. 1999. General-Circulation-Model simulations of future snowpack in the western United States. *Journal of the American Water Resources Association* 35:1473–1484.

McCune B, Keon D. 2002. Equations for potential annual direct incident radiation and heat load. *Journal of Vegetation Science* 13:603–606.

McCutchan MH, Fox DG. 1986. Effect of Elevation and Aspect on Wind, Temperature and Humidity. *Journal of Climate and Applied Meteorology* 25:1996–2013.

McEvoy DJ, Mejia JF, Huntington JL. 2014. Use of an Observation Network in the Great Basin to Evaluate Gridded Climate Data. *Journal of Hydrometeorology* 15:1913–1931.

McGuire CR, Nufio CR, Bowers MD, Guralnick RP. 2012. Elevation-Dependent Temperature Trends in the Rocky Mountain Front Range: Changes over a 56- and 20-Year Record. *PLoS ONE* 7.

McMahon MJ, Dascalu SM, Harris FC, Strachan S, Biondi F. 2011. Architecting climate change data infrastructure for Nevada. *Lecture Notes in Business Information Processing* 83 LNBIP:354–365.

McMaster GS, Wilhem WW. 1997. Growing degree days: one equation, two interpretations. *Agricultural and Forest Meteorology* 87:291–300.

McRoberts DB, Nielsen-Gammon JW. 2011. A new homogenized climate division precipitation dataset for analysis of climate variability and climate change. *Journal of Applied Meteorology and Climatology* 50:1187–1199.

Means JD. 2013. GPS precipitable water as a diagnostic of the North American monsoon in California and Nevada. *Journal of Climate* 26:1432–1444.

Mejia JF, Huntington J, Hatchett B, Koracin D, Niswonger RG. 2012. Linking Global Climate Models to an Integrated Hydrologic Model: Using an Individual Station Downscaling Approach. *Journal of Contemporary Water Research & Education*:17–27.

Mensing S, Strachan S, Arnone J, Fenstermaker L, Biondi F, Devitt D, Johnson B, Bird B, Fritzinger E. 2013. A network for observing Great Basin climate change. *Eos, Transactions American Geophysical Union* 94:105–106.

Mensing SA, Smith J, Burkle Norman K, Allan M, Norman KB. 2008. Extended drought in the Great Basin of western North America in the last two millennia reconstructed from pollen records. *Quaternary International* 188:79–89.

Messerli B, Ives JD, editors. 1997. *Mountains of the world: a global priority.* Carnforth: Parthenon Publishing Group.

Meyer SJ, Hubbard KG. 1992. Nonfederal Automated Weather Stations and Networks in the United States and Canada: A Preliminary Survey. *Bulletin American Meteorological Society* 73:449–457.

Michaelides S, Levizzani V, Anagnostou E, Bauer P, Kasparis T, Lane JE. 2009. Precipitation: Measurement, remote sensing, climatology and modeling. *Atmospheric Research* 94:512–533.

Michener WK, Allard S, Budden A, Cook RB, Douglass K, Frame M, Kelling S, Koskela R, Tenopir C, Vieglais D a. 2012. Participatory design of DataONE-Enabling cyberinfrastructure for the biological and environmental sciences. *Ecological Informatics* 11:5–15.

Millar CI. 2013. The Long Path Toward Restoration of Sierra Nevada Bighorn Sheep; An Interview with John Wehausen. *Mountain Views: The Newsletter of the Consortium for Integrated Climate Research in Western Mountains* 7:48–51.

Millar CI, Westfall RD. 2010. Distribution and Climatic Relationships of the American Pika (Ochotona princeps) in the Sierra Nevada and Western Great Basin, U.S.A.; Periglacial Landforms as Refugia in Warming Climates. *Arctic, Antarctic, and Alpine Research* 42:493–496.

Millar CI, Westfall RD, Delany DL. 2013. Thermal and hydrologic attributes of rock glaciers and periglacial talus landforms: Sierra Nevada, California, USA. *Quaternary International* 310:169–180.

Millar CI, Westfall RD, Delany DL. 2014. Thermal regimes and snowpack relations of periglacial talus slopes , Sierra Nevada, California, U . S . A . *Arctic, Antarctic, and Alpine Research* 46:483–504.

Millar CI, Westfall RD, Delany DL, Flint AL, Flint LE. 2015. Recruitment patterns and growth of high-elevation pines in response to climatic variability (1883–2013), in the western Great Basin, USA. *Canadian Journal of Forest Research* 45:1299–1312.

Miller RF, Chambers JC, Pyke DA, Pierson FB, Williams CJ. 2013. *A Review of Fire Effects on Vegetation and Soils in the Great Basin Region : Response and Ecological Site Characteristics*. Rocky Mountain Research Station, United States Department of Agriculture, Forest Service.

Minder JR, Durran DR, Roe GH. 2011. Mesoscale controls on the mountainside snow line. *Journal of the Atmospheric Sciences* 68:2107–2127.

Minder JR, Durran DR, Roe GH, Anders AM. 2008. The climatology of small-scale orographic precipitation over the Olympic Mountains: Patterns and processes. *Quarterly Journal of the Royal Meteorological Society* 134:817–839.

Minder JR, Mote PW, Lundquist JD. 2010. Surface temperature lapse rates over complex terrain: Lessons from the Cascade Mountains. *Journal of Geophysical Research: Atmospheres* 115:1–13.

Mitchell TD, Jones PD. 2005. An improved method of constructing a database of monthly climate observations and associated high-resolution grids. *International Journal of Climatology* 25:693–712.

Mock CJ. 1996. Climatic controls and spatial variations of precipitation in the western United States. *Journal of Climate* 9:1111–1124.

Murtagh F, Legendre P. 2014. Ward's Hierarchical Agglomerative Clustering Method: Which Algorithms Implement Ward's Criterion? *Journal of Classification* 31:274–295.

Nadezhdina N, Cermák J, Ceulemans R. 2002. Radial patterns of sap flow in woody stems of dominant and understory species: scaling errors associated with positioning of sensors. *Tree Physiology* 22:907–918.

Nayak A, Chandler DG, Marks D, McNamara JP, Seyfried M. 2010. Correction of electronic record for weighing bucket precipitation gauge measurements. *Water Resources Research* 46:1–6.

Nieto R, Gimeno L, de la Torre L, Ribera P, Gallego D, Garcia-Herrera R, Garcia JA, Nunez M, Redano A, Lorente J. 2005. Climatological features of cutoff low systems in the Northern Hemisphere. *Journal of Climate* 18:3085–3103.

NOAA-NCDC. 2016. National Temperature and Precipitation Maps. [accessed 2016 Jan 1]. http://www.ncdc.noaa.gov/temp-and-precip/us-maps/

NOAA-NWS. 2016. Precipitation Frequency Data Server. [accessed 2016 Jan 1]. http://hdsc.nws.noaa.gov/hdsc/pfds/

Nowak CL, Nowak RS, Tausch RJ, Wigand PE. 1994. Tree and shrub dynamics in northwestern Great Basin woodland and steppe during the late-Pliestocene and Holocene. *American Journal of Botany* 81:265–277.

NRCS. 2015. SNOTEL Sites. *U.S.D.A. Natural Resources Conservation Service*. [accessed 2015 Jul 1]. http://www.nv.nrcs.usda.gov/snow/snotel.html

Oakley NS, Redmond KT. 2014. A climatology of 500-hPa closed lows in the northeastern Pacific Ocean, 1948-2011. *Journal of Applied Meteorology and Climatology* 53:1578–1592.

Oksanen J, Blanchet FG, Kindt R, Legendre P, Minchin PR, Hara RBO, Simpson GL, Solymos P, Stevens MHH, Wagner H. 2015. Package "vegan." [accessed 2015 Jul 1]. https://github.com/vegandevs/vegan

Oyler JW, Ballantyne A, Jencso K, Sweet M, Running SW. 2014. Creating a topoclimatic daily air temperature dataset for the conterminous United States using homogenized station data and remotely sensed land skin temperature. *International Journal of Climatology* 35.

Oyler JW, Dobrowski SZ, Ballantyne AP, Klene AE, Running SW. 2015. Artificial amplification of warming trends across the mountains of the western United States. *Geophysical Research Letters* 42:153–161.

Parish TR. 1982. Barrier winds along the Sierra Nevada mountains. *Journal of Applied Meteorology* 21:925–930.

Pataki DE, Oren R, Smith WK. 2000. Sap flow of co-occuring species in a western subalpine forest during seasonal soil drought. *Ecology* 81:2557–2566.

Pearson RG, Dawson TP. 2003. Predicting the impacts of climate change on the distribution of speces: are bioclimate envelope models useful? *Global Ecology and Biogeography* 12:361–371.

Peck EL. 1997. Quality of hydrometeorological data in cold regions. *Journal of the American Water Resources Association* 33.

Pederson GT, Betancourt JL, McCabe GJ. 2013. Regional patterns and proximal causes of the recent snowpack decline in the Rocky Mountains, U.S. *Geophysical Research Letters* 40:1811–1816.

Pepin NC, Seidel DJ. 2005. A global comparison of surface and free-air temperatures at high elevations. *Journal of Geophysical Research D: Atmospheres* 110:1–15.

Potter KM, Hipkins VD, Mahalovich MF, Means RE. 2013. Mitochondrial DNA haplotype distribution patterns in Pinus ponderosa (Pinaceae): range-wide evolutionary history and implications for conservation. *American Journal of Botany* 100:1562–1579.

Potter KM, Hipkins VD, Mahalovich MF, Means RE. 2015. Nuclear genetic variation across the range of ponderosa pine (Pinus ponderosa): Phylogeographic, taxonomic and conservation implications. *Tree Genetics & Genomes* 11.

Potts DL, Huxman TE, Cable JM, English NB, Ignace DD, Eilts JA, Mason MJ, Weltzin JF, Williams DG. 2006. Antecedent moisture and seasonal precipitation influence the response of canopy-scale carbon and water exchange to rainfall pulses in a semi-arid grassland. *New Phytologist* 170:849–860.

QGIS Development Team. 2015. QGIS Geographic Information System. http://qgis.osgeo.org

R Development Core Team. 2015. The R Project for Statistical Computing. http://www.r-project.org/

Randin CF, Engler R, Normand S, Zappa M, Zimmermann NE, Pearman PB, Vittoz P, Thuiller W, Guisan A. 2009. Climate change and plant distribution: Local models predict high-elevation persistence. *Global Change Biology* 15:1557–1569.

Rango A, Martinec J. 1995. Revisiting the degree-day method for snowmelt computations. *Water Resources Bulletin* 31:657–669.

Rasmussen R, Baker B, Kochendorfer J, Meyers T, Landolt S, Fischer AP, Black J, Thériault JM, Kucera P, Gochis D, et al. 2012. How well are we measuring snow: The NOAA/FAA/NCAR winter precipitation test bed. *Bulletin of the American Meteorological Society* 93:811–829.

Reba ML, Pomeroy J, Marks D, Link TE. 2012. Estimating surface sublimation losses from snowpacks in a mountain catchment using eddy covariance and turbulent transfer calculations. *Hydrological Processes* 26:3699–3711.

Redmond KT, Koch RW. 1991. Climate and streamflow variability in the western United States and their relationship to large-scale circulation indices. *Water Resources Research* 27:2381–2399.

Reinemann SA, Porinchu DF, MacDonald GM, Mark BG, DeGrand JQ. 2014. A 2000-yr reconstruction of air temperature in the Great Basin of the United States with specific reference to the Medieval Climatic Anomaly. *Quaternary Research* 82:309–317.

Reinking RF, Boatman JF. 1986.*Upslope precipitation events* In: Mesoscale Meteorology and Forecasting. American Meteorological Society, Springer. p. 437–471.

Renard B, Kavetski D, Kuczera G, Thyer M, Franks SW. 2010. Understanding predictive uncertainty in hydrologic modeling: The challenge of identifying input and structural errors. *Water Resources Research* 46:1–22.

Reynolds JF, Kemp PR, Ogle K, Fernandez RJ. 2004. Modifying the “pulse-reserve” paradigm for deserts of North America: precipitation pulses, soil water, and plant responses. *Oecologia* 141:194–210.

Richardson AD, Jenkins JP, Braswell BH, Hollinger DY, Ollinger S V, Smith ML. 2007. Use of digital webcam images to track spring green-up in a deciduous broadleaf forest. *Oecologia* 152:323–334.

Riley SJ, Degloria SD, Elliot R. 1999. A terrain ruggedness index that quantifies topographic heterogeneity. *Intermountain Journal of Sciences* 5:23–27.

Roberts DW, Cooper SV. 1989. *Concepts and techniques of vegetation mapping*. General technical report. US Department of Agriculture, Forest Service, Intermountain Research Station (USA).

Robinson DA, Campbell CS, Hopmans JW, Hornbuckle BK, Jones SB, Knight R, Ogden F, Selker J, Wendroth O. 2008. Soil moisture measurement for ecological and hydrological watershed-scale observatories: a review. *Vadose Zone Journal* 7:358–389.

De Rocher TD, Tausch RJ. 1994. Predicting potential transpiration of singleleaf pinyon: an adaptation of the potometer method. *Forest ecology and management* 63:169–180.

Rodriguez-Iturbe I. 2000. Ecohydrology: A hydrologic perspective of climate-soil-vegetation dynamics. *Water Resources Research* 36:3–9.

Roe GH. 2005. Orographic Precipitation. *Annual Review of Earth and Planetary Sciences* 33:645–71.

Rollinson CR, Kaye MW. 2015. Modeling monthly temperature in mountainous ecoregions: importance of spatial scale for ecological research. *Climate Research* 64:99–110.

Rousseeuw PJ. 1987. Silhouettes: A graphical aid to the interpretation and validation of cluster analysis. *Journal of Computational and Applied Mathematics* 20:53–65.

Ryan WA, Doesken NJ, Fassnacht SR. 2008. Evaluation of ultrasonic snow depth sensors for U.S. snow measurements. *Journal of Atmospheric and Oceanic Technology* 25:667–684.

Saito L, Biondi F, Devkota R, Vittori J, Salas JD. 2014. A water balance approach for reconstructing streamflow using tree-ring proxy records. *Journal of Hydrology*.

Salzer MW, Bunn AG, Graham NE, Hughes MK. 2014. Five millennia of paleotemperature from tree-rings in the Great Basin, USA. *Climate Dynamics* 42:1517–1526.

Salzmann N, Nötzli J, Hauck C, Gruber S, Hoelzle M, Haeberli W. 2007. Ground surface temperature scenarios in complex high-mountain topography based on regional climate model results. *Journal of Geophysical Research: Earth Surface* 112:1–10.

Savina M, Schäppi B, Molnar P, Burlando P, Sevruk B. 2012. Comparison of a tipping-bucket and electronic weighing precipitation gage for snowfall. *Atmospheric Research* 103:45–51.

Schaefer G, Paetzold R. 2000.*SNOTEL (SNOwpack TELemetry) and SCAN (soil climate analysis network)* In: Automated Weather Stations for Applications in Agriculture and Water Resources Management: Current Use and Future Perspectives. Lincoln, NE. p. 30.

Scherrer D, Körner C. 2011. Topographically controlled thermal-habitat differentiation buffers alpine plant diversity against climate warming. *Journal of Biogeography* 38:406–416.

Schimel D, Hargrove W, Hoffman F, MacMahon J. 2007. NEON: a hierarchically designed national ecological network. *Frontiers in Ecology and the Environment* 5:59–59.

Schwinning S, Sala OE. 2004. Hierarchy of responses to resource pulses in arid and semi-arid ecosystems. *Oecologia* 141:211–220.

Serreze MC, Clark MP, Armstrong RL, McGinnis DA, Pulwarty RS. 1999. Characteristics of the western United States snowpack from snowpack telemetry (SNOTEL) data. *Water Resources Research* 35:2145–2160.

Singh VP, Woolhiser DA. 2002. Mathematical modeling of watershed hydrology. *Journal of Hydrologic Engineering* 7:270–292.

Spaulding WG, Graumlich LJ. 1986. The last pluvial climatic episodes in the deserts of southwestern North America. *Nature* 320:441–444.

Sperry JS, Hacke UG. 2002. Desert shrub water relations with respect to soil characteristics and plant functional type. *Functional Ecology* 16:367–378.

Stahl K, Moore RD, Floyer JA, Asplin MG, McKendry IG. 2006. Comparison of approaches for spatial interpolation of daily air temperature in a large region with complex topography and highly variable station density. *Agricultural and Forest Meteorology* 139:224–236.

Stewart IT. 2009. Changes in snowpack and snowmelt runoff for key mountain regions. *Hydrological Processes* 23:78–94.

Stoklosa J, Daly C, Foster SD, Ashcroft MB, Warton DI. 2015. A climate of uncertainty: accounting for error in climate variables for species distribution models. *Methods in Ecology and Evolution* 6:412–423.

Strachan S, Biondi F, Leising J. 2012. 550-year reconstruction of streamflow variability in Spring Valley, Nevada. *Journal of Water Resources Planning and Management* 138:326–333.

Strahler AN. 1952. Hypsometric (Area - Altitude) Analysis of Erosional Topography. *Geological Society of America Bulletin* 63:1117–1142.

Strangeways I. 2010. A history of rain gauges. *Weather* 65:133–138.

Stull R. 2011. Wet-Bulb Temperature from Relative Humidity and Air Temperature. *Journal of Applied Meteorology and Climatology* 50:2267–2269.

Swain DL. 2015. A tale of two California droughts: Lessons amidst record warmth and dryness in a region of complex physical and human geography. *Geophysical Research Letters* 42:999–10,003.

Tang Z, Fang J. 2006. Temperature variation along the northern and southern slopes of Mt. Taibai, China. *Agricultural and Forest Meteorology* 139:200–207.

Tarboton D, Luce C. 1996. *Utah energy balance snow accumulation and melt model (UEB)*. Utah Water Research Laboratory.

Tausch RJ, West NE, Nabi A. 1981. Tree age and dominance patterns in Great Basin pinyon-juniper woodlands. *Journal of Range Management* 34:259–264.

Thompson RS, Anderson KH, Pelltier RT, Strickland LE, Bartlein PJ, Shafer SL. 2012. Quantitative estimation of climatic parameters from vegetation data in North America by the mutual climatic range technique. *Quaternary Science Reviews* 51:18–39.

Thompson RS, Anderson KH, Pelltier RT, Strickland LE, Shafer SL, Bartlein PJ, McFadden AK. 2015. *Atlas of relations between climatic parameters and distributions of important trees and shrubs in North America: Revisions for all taxa from the United States and Canada and new taxa from the western United States*. Reston, VA.

Thornton PE, Running SW. 1999. An improved algorithm for estimating incident daily solar radiation from measurements of temperature, humidity, and precipitation. *Agricultural and Forest Meteorology* 93:211–228.

Thornton PE, Thornton MM, Mayer BW, Wilhelmi N, Wei Y, Devarakonda R, Cook R. 2012. *Daymet: Daily surface weather on a 1 km grid for North America, 1980-2008.* Oak Ridge National Laboratory (ORNL) Distributed Active Archive Center for Biogeochemical Dynamics (DAAC) 1.

Thuiller W, Lavorel S, Araújo MB, Sykes MT, Prentice IC. 2005. Climate change threats to plant diversity in Europe. *Proceedings of the National Academy of Sciences of the United States of America* 102:8245–8250.

Vanderbilt KL, Lin C-C, Lu S-S, Kassim AR, He H, Guo X, Gil IS, Blankman D, Porter JH. 2015. Fostering ecological data sharing: collaborations in the International Long Term Ecological Research Network. *Ecosphere* 6.

Van De Ven CM, Weiss SB, Ernst WG. 2007. Plant species distributions under present conditions and forecasted for warmer climates in an arid mountain range. *Earth Interactions* 11:1–33.

Vitale AP. 2015. *Near-surface air temperature in complex terrain: daily predictions of fine-scale (30 m) temperature in the Snake Range, Nevada, USA*. Master's Thesis. University of Nevada Reno.

Viviroli D, Weingartner R. 2004. The hydrological significance of mountains: from regional to global scale. *Hydrology and Earth System Sciences* 8:1017–1030.

Wang SY, Gillies RR, Reichler T. 2012. Multidecadal drought cycles in the great basin recorded by the Great Salt Lake: modulation from a transition-phase teleconnection. *Journal of Climate* 25:1711–1721.

Wang T, Hamann A, Spittlehouse DL, Aitken SN. 2006. Development of scale-free climate data for western Canada for use in resource management. *International Journal of Climatology* 26:383–397.

Warren DL, Cardillo M, Rosauer DF, Bolnick DI. 2014. Mistaking geography for biology: inferring processes from species distributions. *Trends in Ecology & Evolution* 29:572–580.

Weathers KC, Hanson PC, Arzberger P, Brentrup J, Brookes J, Carey CC, Gaiser E, Hamilton DP, Hong GS, Ibelings B, et al. 2013. The Global Lake Ecological Observatory Network (GLEON): The evolution of grassroots network science. *Limnology and Oceanography Bulletin* 22:71–73.

Weiss SB, Murphy DD, Ehrlich PR, Metzler CF. 1993. Adult emergence phenology in checkerspot butterflies: the effects of macroclimate, topoclimate, and population history. *Oecologia* 96:261–270.

Welch A, Bright D, Knochenmus L. 2007. *Water resources of the Basin and Range carbonate-rock aquifer system, White Pine County, Nevada, and adjacent areas in Nevada and Utah*. US Geological Survey Scientific Investigations Report 5261.

Wells PV, Shields LM. 1964. Distribution of Larrea divaricata in Relation to a Temperature Inversion at Yucca Flat, Southern Nevada. *The Southwest Naturalist* 9:51–55.

Wells PV. 1983. Paleobiogeography of Montane Islands in the Great Basin since the Last Glaciopluvial. *Ecological Monographs* 53:341.

Weltzin JF, Loik ME, Schwinning S, Williams DG, Fay PA, Haddad BM, Harte J, Huxman TE, Knapp AK, Lin G, et al. 2003. Assessing the response of terrestrial ecosystems to potential changes in precipitation. *BioScience* 53:941.

Whiteman CD. 1982. Breakup of Temperature Inversions in Deep Mountain Valleys: Part I. Observations. *Journal of Applied Meteorology* 21:270–289.

Wiens J, Stralberg D, Jongsomjit D, Howell C, Snyder M. 2009. Niches, models, and climate change: assessing the assumptions and uncertainties. *Proceedings of the National Academy of Sciences of the United States of America* 106 Suppl :19729–19736.

Wigand PE, Nowak CL. 1992.*Dynamics of Northwest Nevada Plant Communities During the Last 30,000 Years* In: The History of Water: Eastern Sierra Nevada, Owens Valley, White-Inyo Mountains, White Mountain Research Station Symposium. Vol. 4. p. 40–62.

Wigmosta MS, Vail LW, Lettenmaier DP. 1994. A distributed hydrology-vegetation model for complex terrain. *Water Resources Research* 30:1665–1679.

Williams AP, Michaelsen J, Leavitt SW, Still CJ. 2010. Using tree rings to predict the response of tree growth to climate change in the continental United States during the twenty-first century. *Earth Interactions* 14:1–20.

Williams DG, Cable W, Hultine K, Hoedjes JCB, Yepez EA, Simonneaux V, Er-Raki S, Boulet G, de Bruin HAR, Chehbouni A, et al. 2004. Evapotranspiration components determined by stable isotope, sap flow and eddy covariance techniques. *Agricultural and Forest Meteorology* 125:241–258.

Williams DG, Ehleringer JR. 2000. Intra- and interspecific variation for summer precipitation use in pinyon – juniper woodlands. 70:517–537.

Wilson KB, Hanson PJ, Mulholland PJ, Baldocchi DD, Wullschleger SD. 2001. A comparison of methods for determining forest evapotranspiration and its components: Sap-flow, soil water budget, eddy covariance and catchment water balance. *Agricultural and Forest Meteorology* 106:153–168.

Wise EK. 2010. Spatiotemporal variability of the precipitation dipole transition zone in the western United States. *Geophysical Research Letters* 37:1–5.

WMO. 2008. *Guide to meteorological instruments and methods of observation*. World Meteorological Organization, Geneva.

WRCC. 2016. Western Regional Climate Center - WRCC Projects. [accessed 2016 Jan 4]. http://www.wrcc.dri.edu/PROJECTS.html

Yang D, Goodison B, Ishida S, Benson C. 1998. Adjustment of daily precipitation data at 10 climate stations in Alaska: Application of World Meteorological Organization intercomparison results. *Water Resources Research* 34:241–256.

Yang D, Goodison BE, Metcalfe JR, Golubev VS, Bates R, Pangburn T, Hanson CL. 1998. Accuracy of NWS 8" standard nonrecording precipitation gauge: Results and application of WMO intercomparison. *Journal of Atmospheric and Oceanic Technology* 15:54–68.

Yatagai A, Kamiguchi K, Arakawa O, Hamada A, Yasutomi N, Kitoh A. 2012. APHRODITE: Constructing a long-term daily gridded precipitation dataset for Asia based on a dense network of rain gauges. *Bulletin of the American Meteorological Society* 93:1401–1415.

Yevjevich V. 1967. *An objective approach to definitions and investigations of continental hydrologic droughts*. Colorado State University, Fort Collins.

Zhang L, Zhao L, Xie C, Liu G, Gao L, Xiao Y, Shi J, Qiao Y. 2015. Intercomparison of Solid Precipitation Derived from the Weighting Rain Gauge and Optical Instruments in the Interior Qinghai-Tibetan Plateau. *Advances in Meteorology* 2015:11.

Appendix 1

1.1 NMDS stress diagnostic outputs for PRISM daily maximum temperature errors

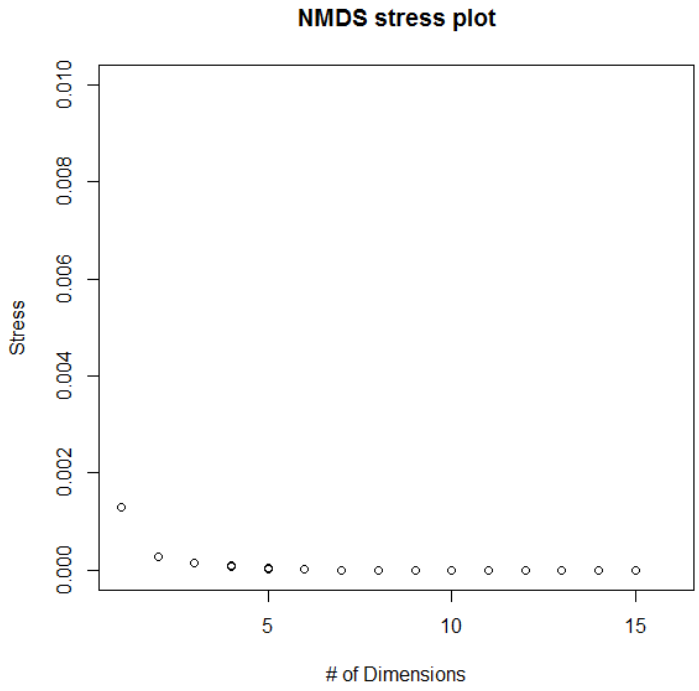

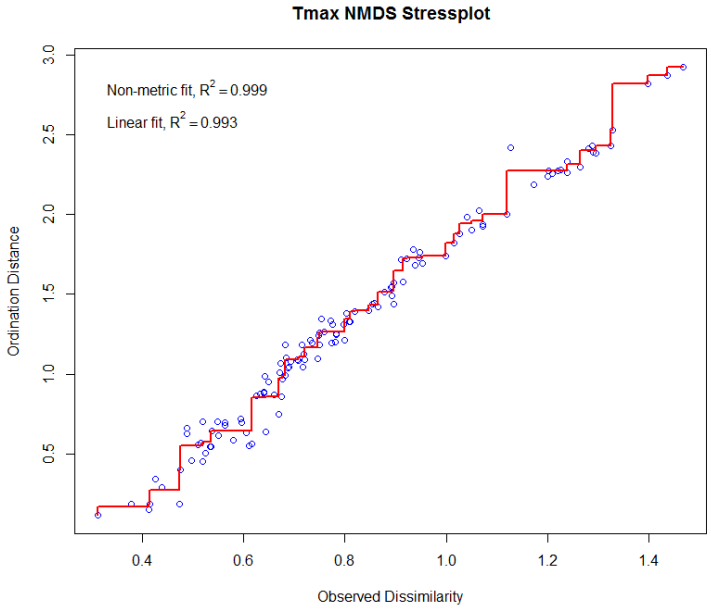

1.2 NMDS stress diagnostic outputs for PRISM daily minimum temperature errors

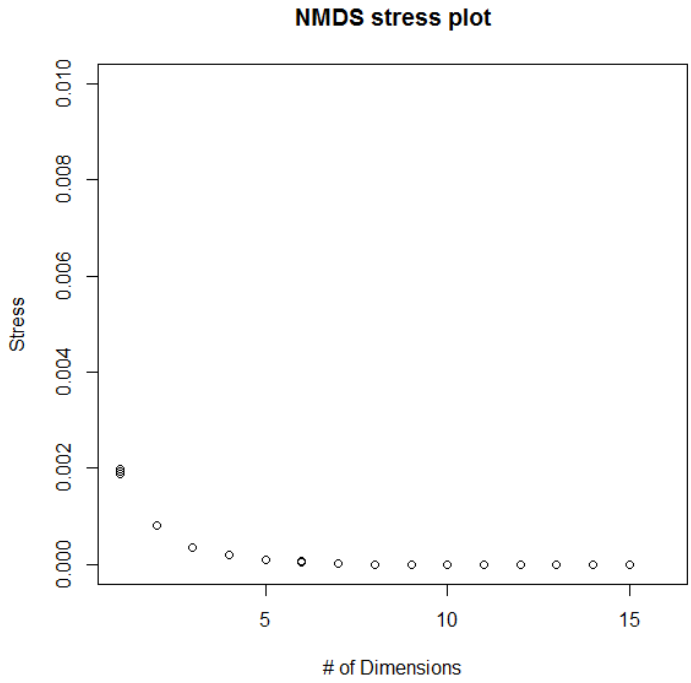

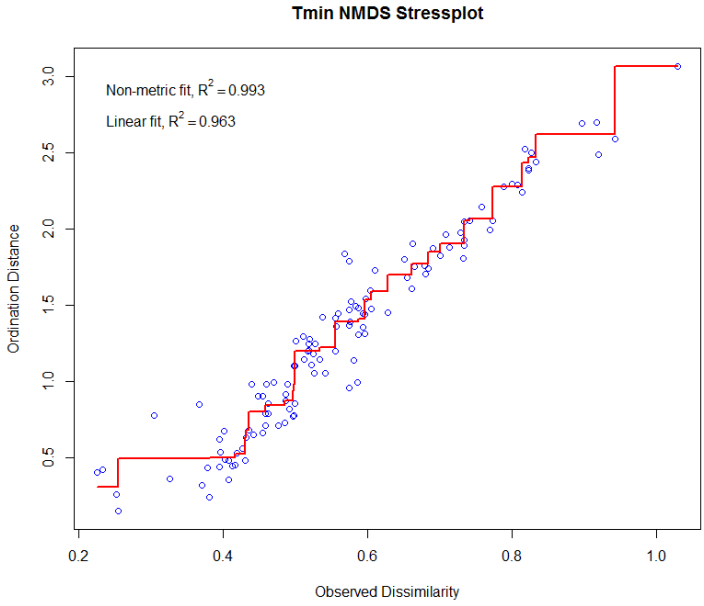

1.3 Sensitivity of absolute PRISM bias to “stormy” days in the Walker Watershed, where “storms” are days fitting the following criteria at the Rockland climate station: average incoming solar radiation < than 140 W/m^2; average wind velocity > 6 m s^{-1}; and average relative humidity > 55%.

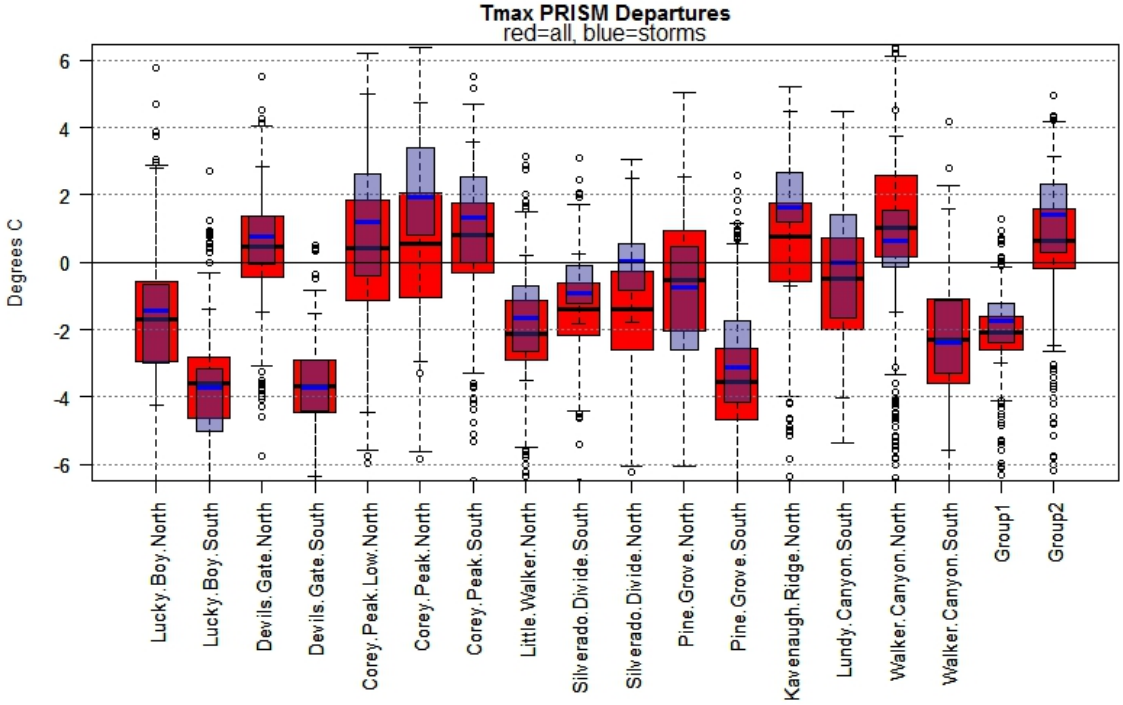

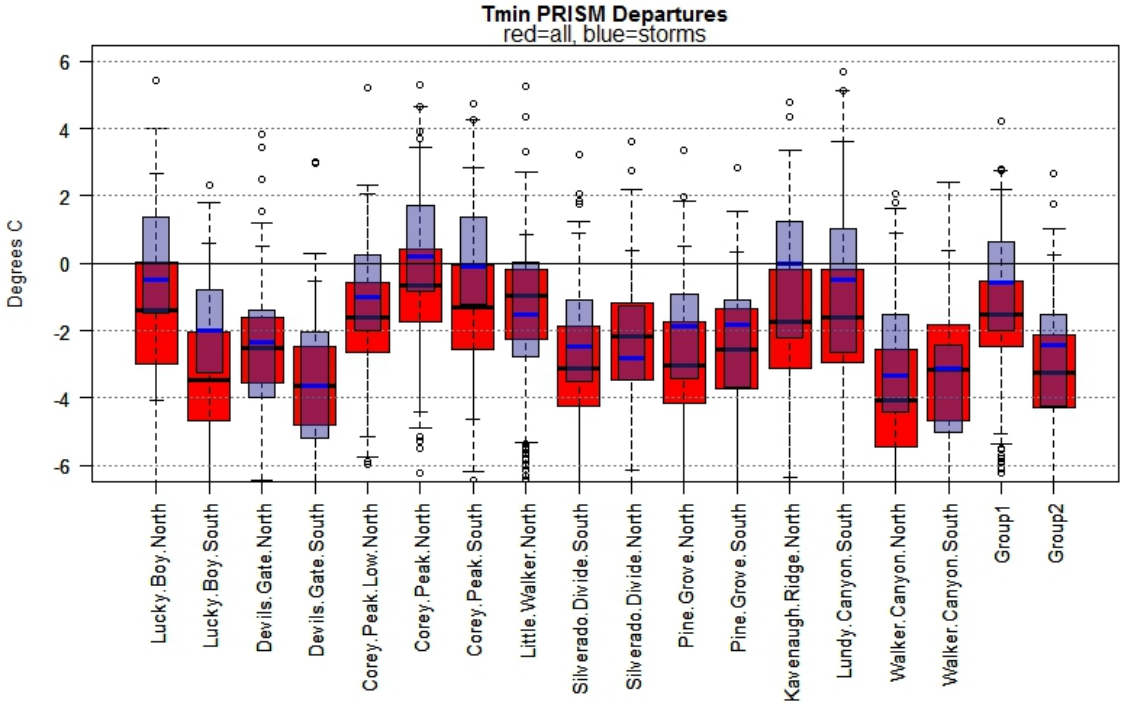

Appendix 2

Raw data from the NevCAN stations can be downloaded from the WRCC website at

http://www.wrcc.dri.edu/GBtransect/

http://www.wrcc.dri.edu/SRtransect/

and from the UNR NRDC at

http://sensor.nevada.edu

2.1 Gage-Difference Method flow chart.

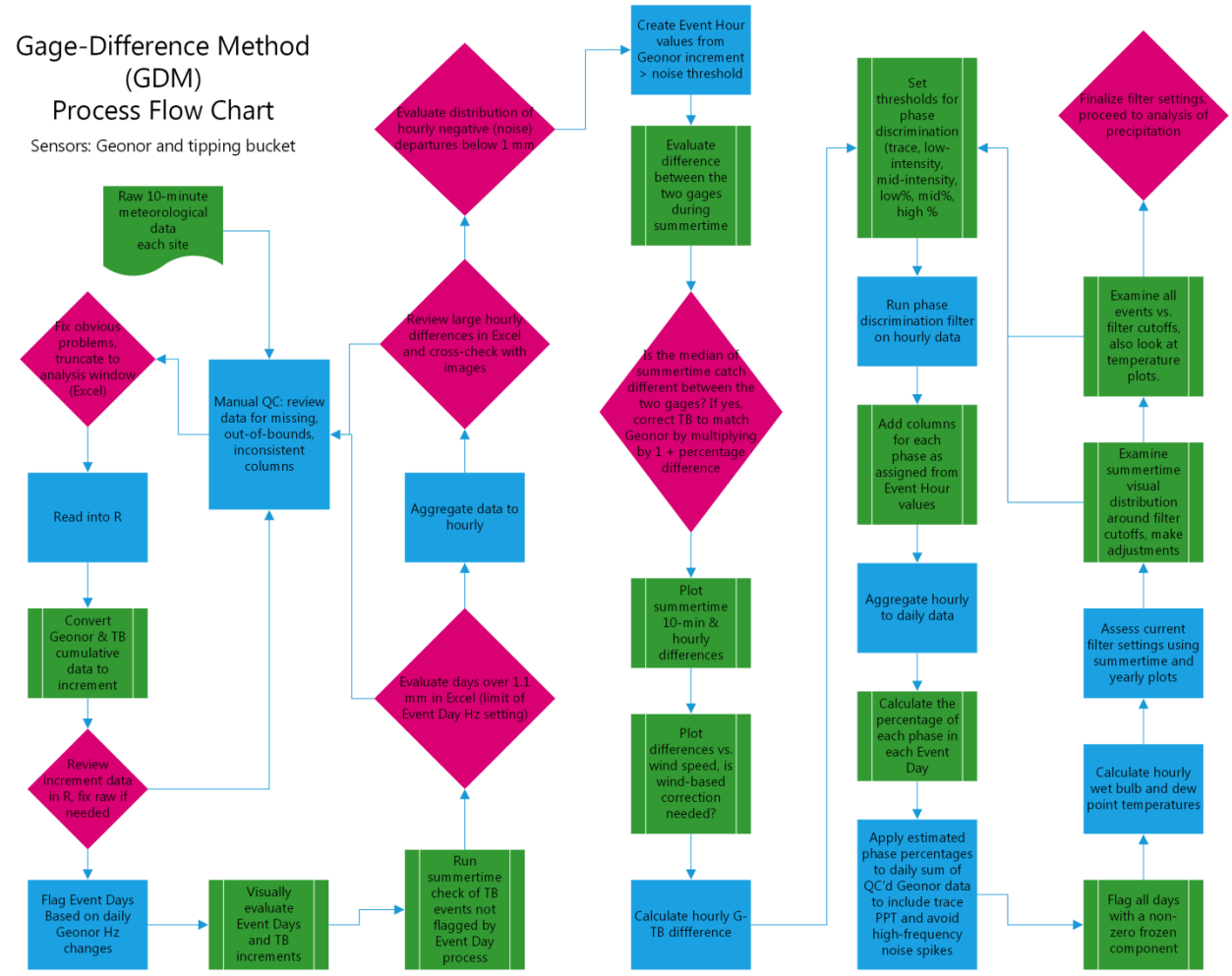

2.2. GDM Event Day flow chart.

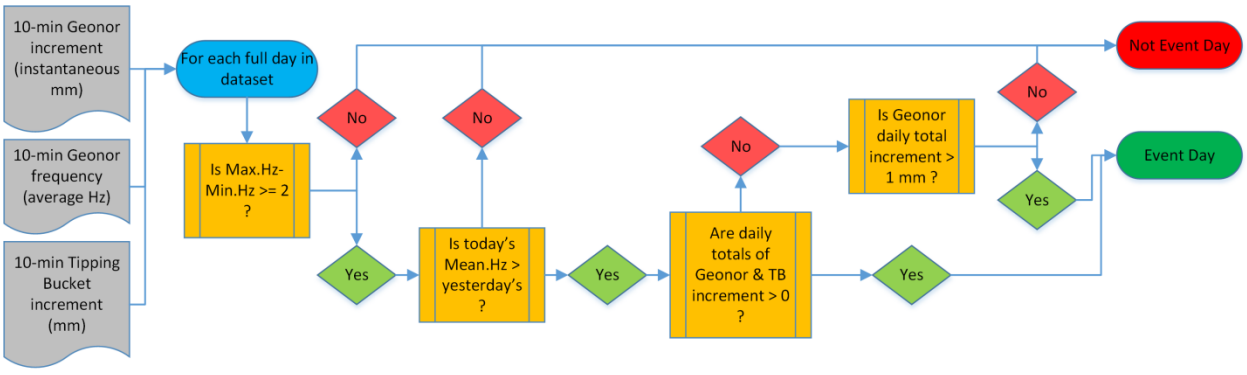

Gage-Difference Method (GDM) Event Day decision filter

Appendix 3

3.1 Observation station photographs

3.1.1: The author performs maintenance on the Snake Range Sagebrush observation station in Spring Valley in 2015. This site differs from the others in the study in the sense that it is not located within the mountain block and therefore is subject to different temperature, wind, and precipitation processes.

3.1.2: The Snake Range Pinyon-Juniper site is located in a relatively young woodland of moderate density and low canopy height (< 8 m). The meteorological tower (left) and Geonor precipitation gage (right) are sited in small clearings.

3.1.3: The Snake Range Montane site is located on a forested limestone ridge within a relatively young mixed-conifer forest. Canopy height of dominant species is at or above the 10 m tower, and a range of understory size classes exists, making for competitive interaction between individuals and species of vegetation.

3.1.4: The Snake Range Subalpine site is situated on a southerly-exposed mild slope at high elevation. The surrounding woodland is a low-density spruce-pine population with dominant canopy heights < 10 m.

3.1.5: The Sheep Range Montane site is located on a small forested knoll within a larger slope/canyon system. The vegetation community is on the margin between a mature ponderosa forest and a pinyon-juniper woodland, so there is a variety of dominant and understory size classes and species.

3.2 Gage-Difference filter configurations

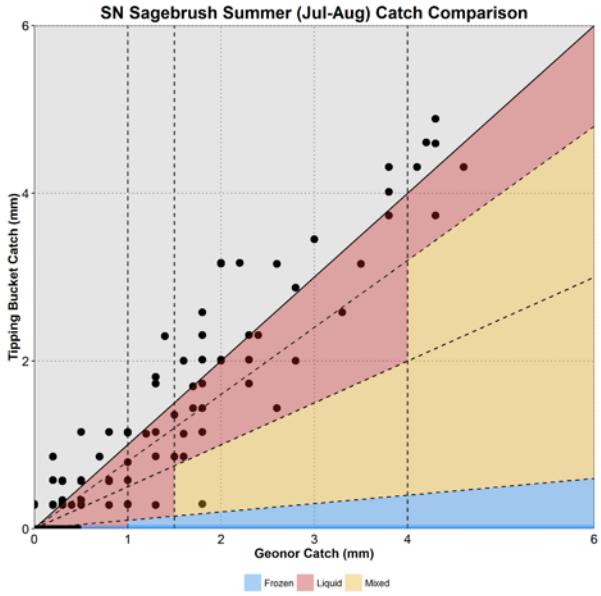

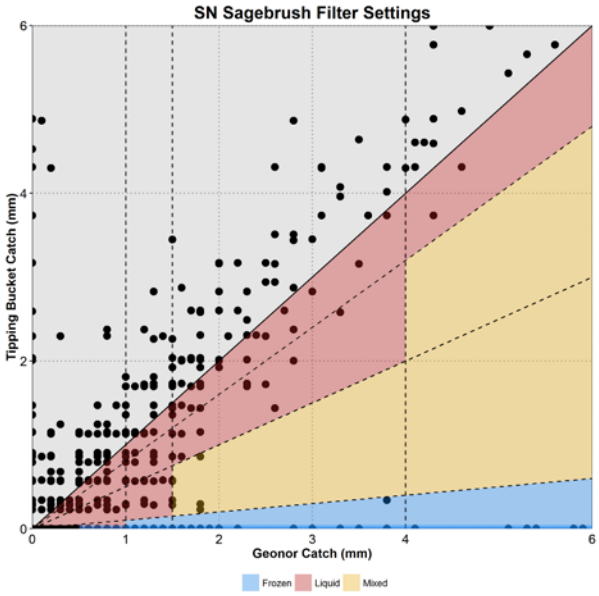

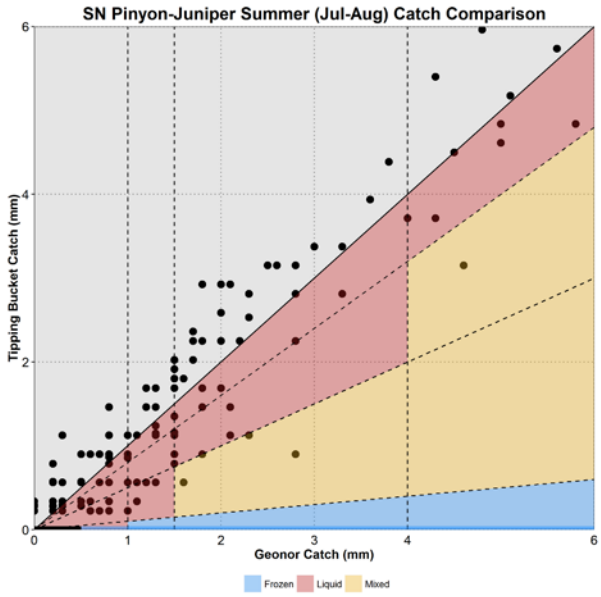

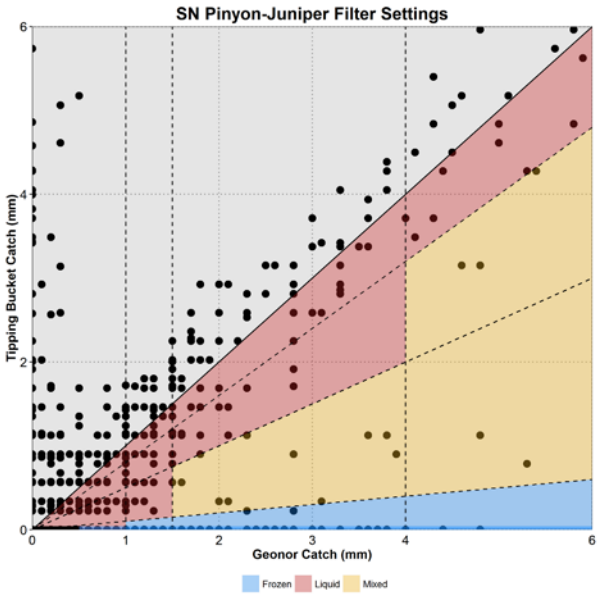

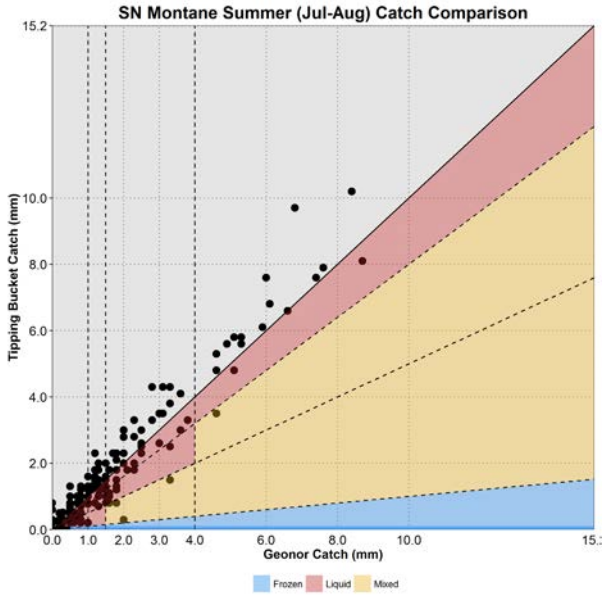
SN Montane Summer (Jul-Aug) Catch Comparison
Tipping Bucket Catch (mm)
Geonor Catch (mm)
Frozen
Liquid
Mixed

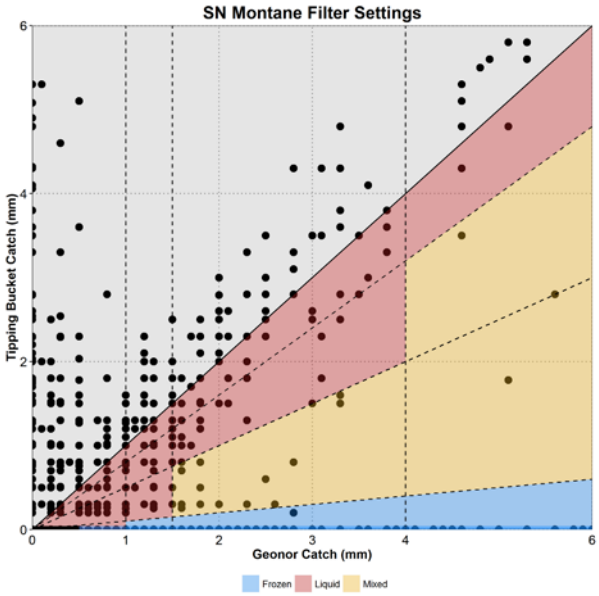
SN Montane Filter Settings
Tipping Bucket Catch (mm)
Geonor Catch (mm)
Frozen
Liquid
Mixed

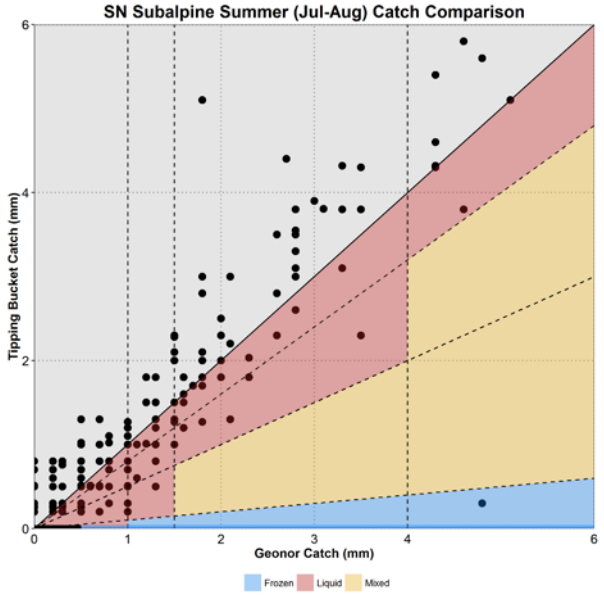
SN Subalpine Summer (Jul-Aug) Catch Comparison
Tipping Bucket Catch (mm)
Geonor Catch (mm)
Frozen
Liquid
Mixed

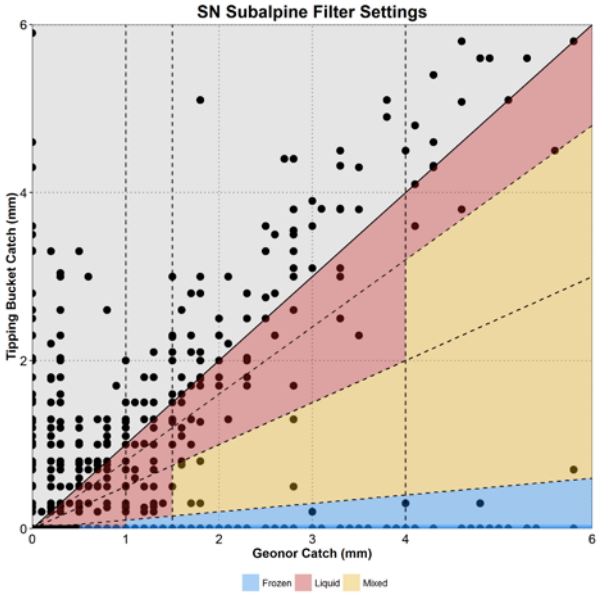
SN Subalpine Filter Settings
Tipping Bucket Catch (mm)
Geonor Catch (mm)
Frozen
Liquid
Mixed

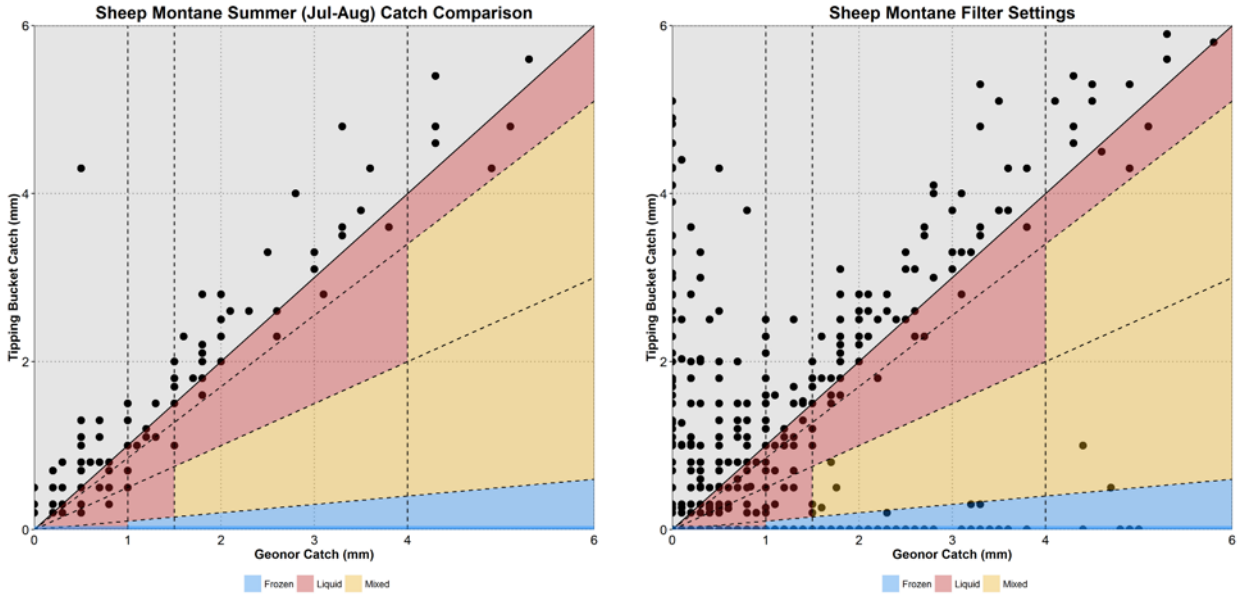

Filter settings are shown with gage catches plotted against each other to illustrate the noise in precipitation catch on a per-event basis. Warm seasons used to set filter thresholds (e.g. July-Aug) are shown with classified events on the left, and settings with all events in all seasons are shown on the right. Graph scale is limited to 6 mm/hr for clarity. GDM filters were set to uniform thresholds for all sites, with a stepped classification based on hourly event amount. Because noise in measured precipitation accuracy is greatest at low intensities, classification of frozen and mixed is only considered reliable above certain intensity thresholds using this method.

3.3 GDM-based phase discrimination comparisons with temperature

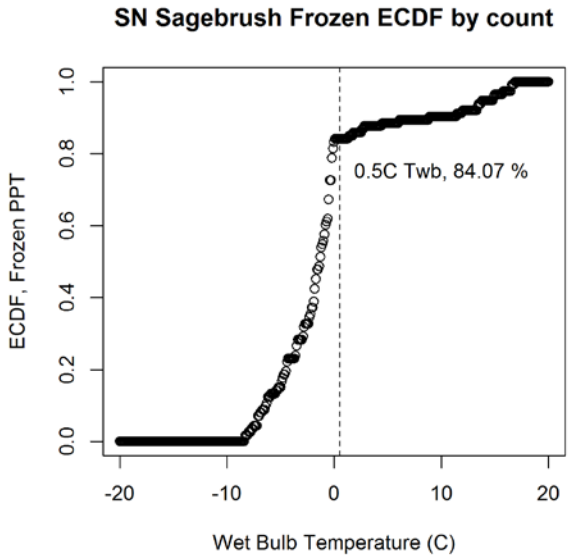

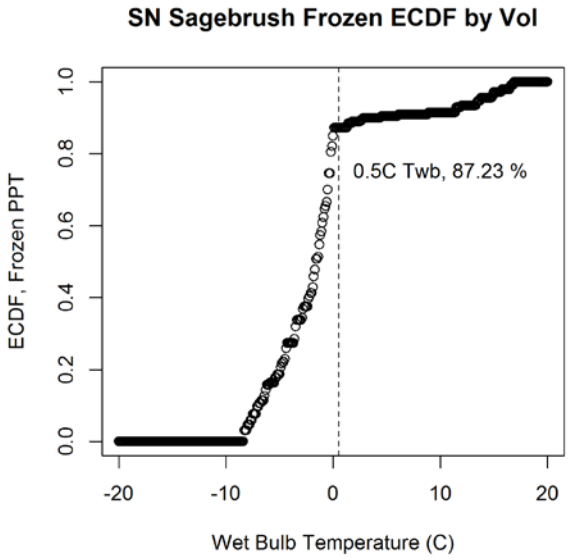

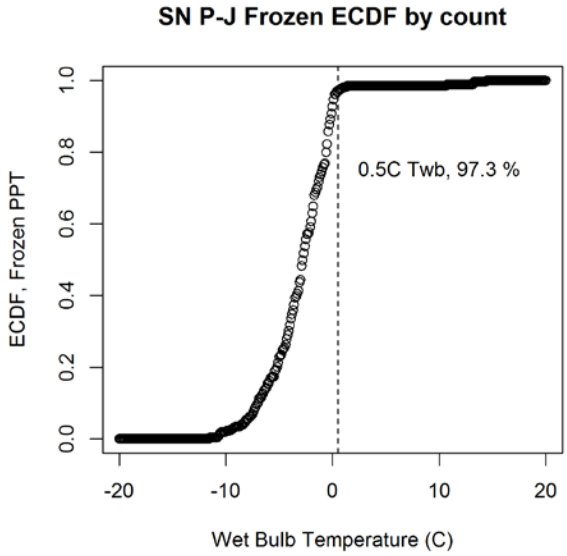

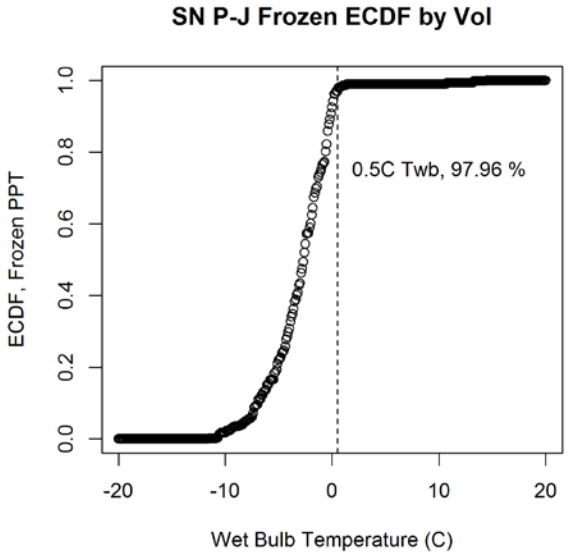

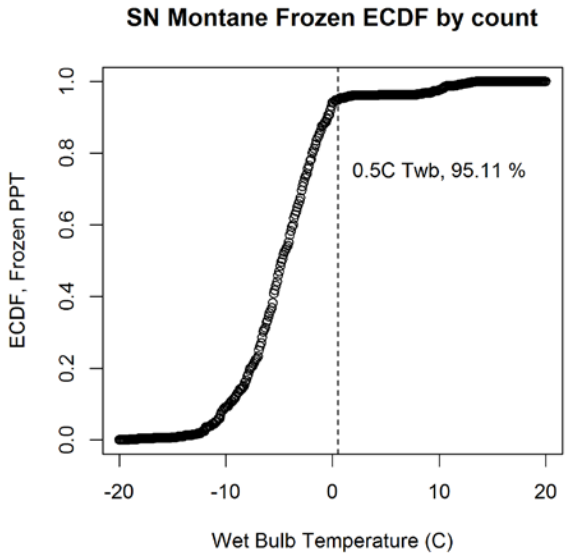
SN Montane Frozen ECDF by count
ECDF, Frozen PPT
0.0
0.2
0.4
0.6
0.8
1.0
0.5C Twb, 95.11 %
-20
-10
0
10
20
Wet Bulb Temperature (C)

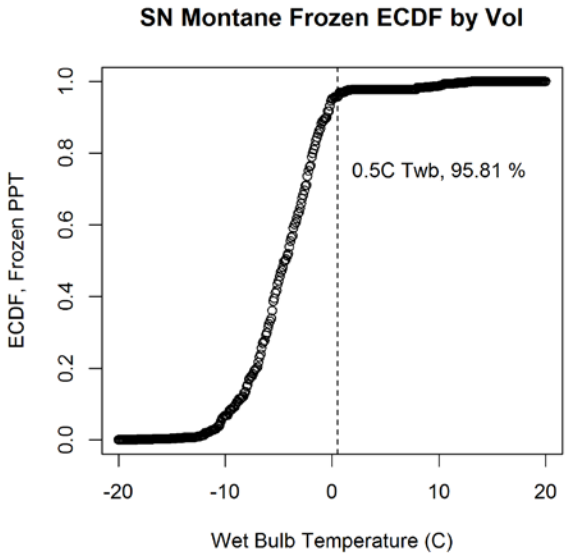
SN Montane Frozen ECDF by Vol
ECDF, Frozen PPT
0.0
0.2
0.4
0.6
0.8
1.0
0.5C Twb, 95.81 %
-20
-10
0
10
20
Wet Bulb Temperature (C)

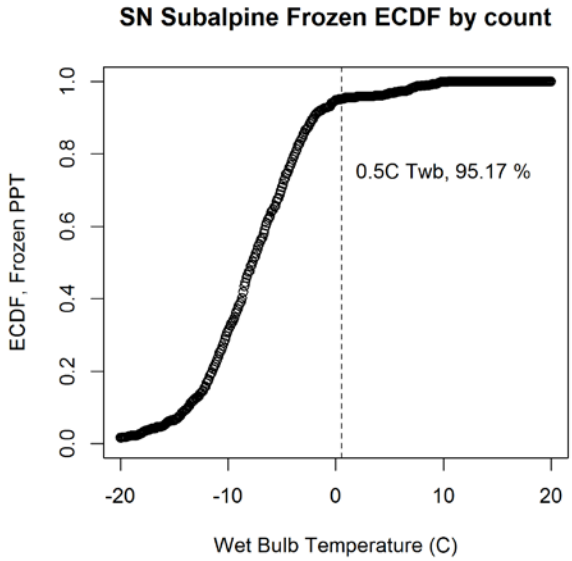
SN Subalpine Frozen ECDF by count
ECDF, Frozen PPT
0.0
0.2
0.4
0.6
0.8
1.0
0.5C Twb, 95.17 %
-20
-10
0
10
20
Wet Bulb Temperature (C)

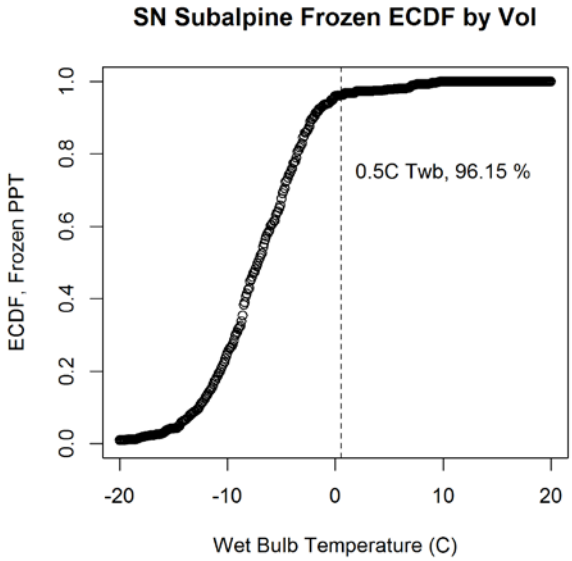
SN Subalpine Frozen ECDF by Vol
ECDF, Frozen PPT
0.0
0.2
0.4
0.6
0.8
1.0
0.5C Twb, 96.15 %
-20
-10
0
10
20
Wet Bulb Temperature (C)

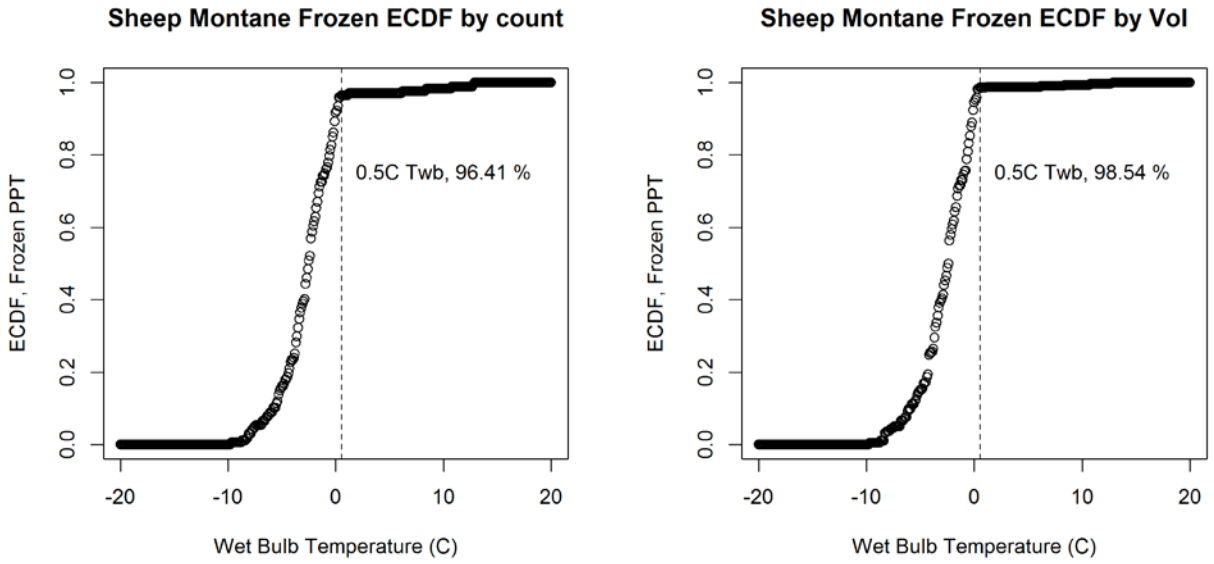

Empirical cumulative distributions of precipitation events (left) and volume (right) classified as frozen as a function of estimated wet bulb temperature. High-percentage cutoffs between 0 and 1°C indicate high confidence in the performance of the GDM filter settings as applied.

3.4 Violin plots of classified precipitation events by site

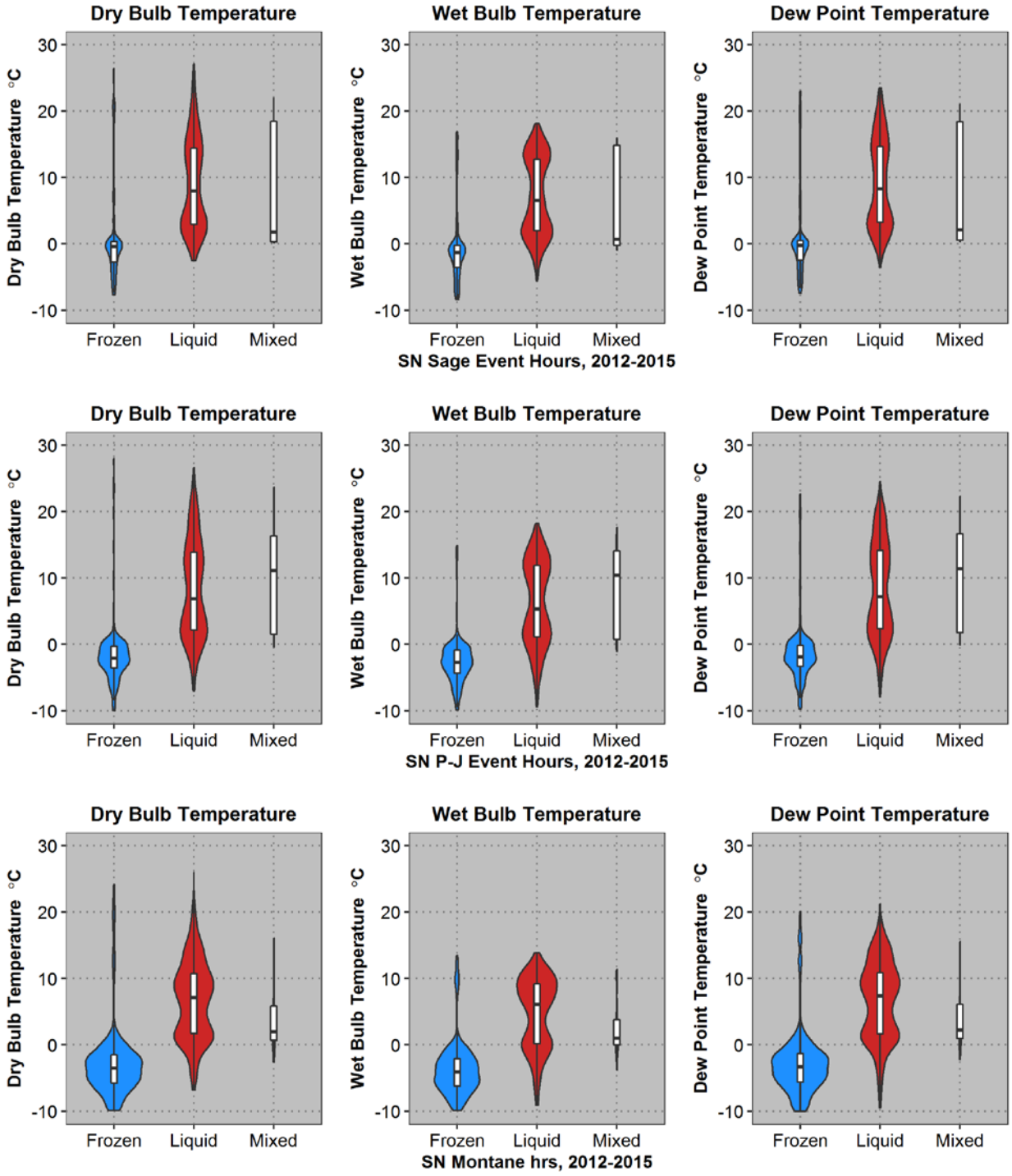

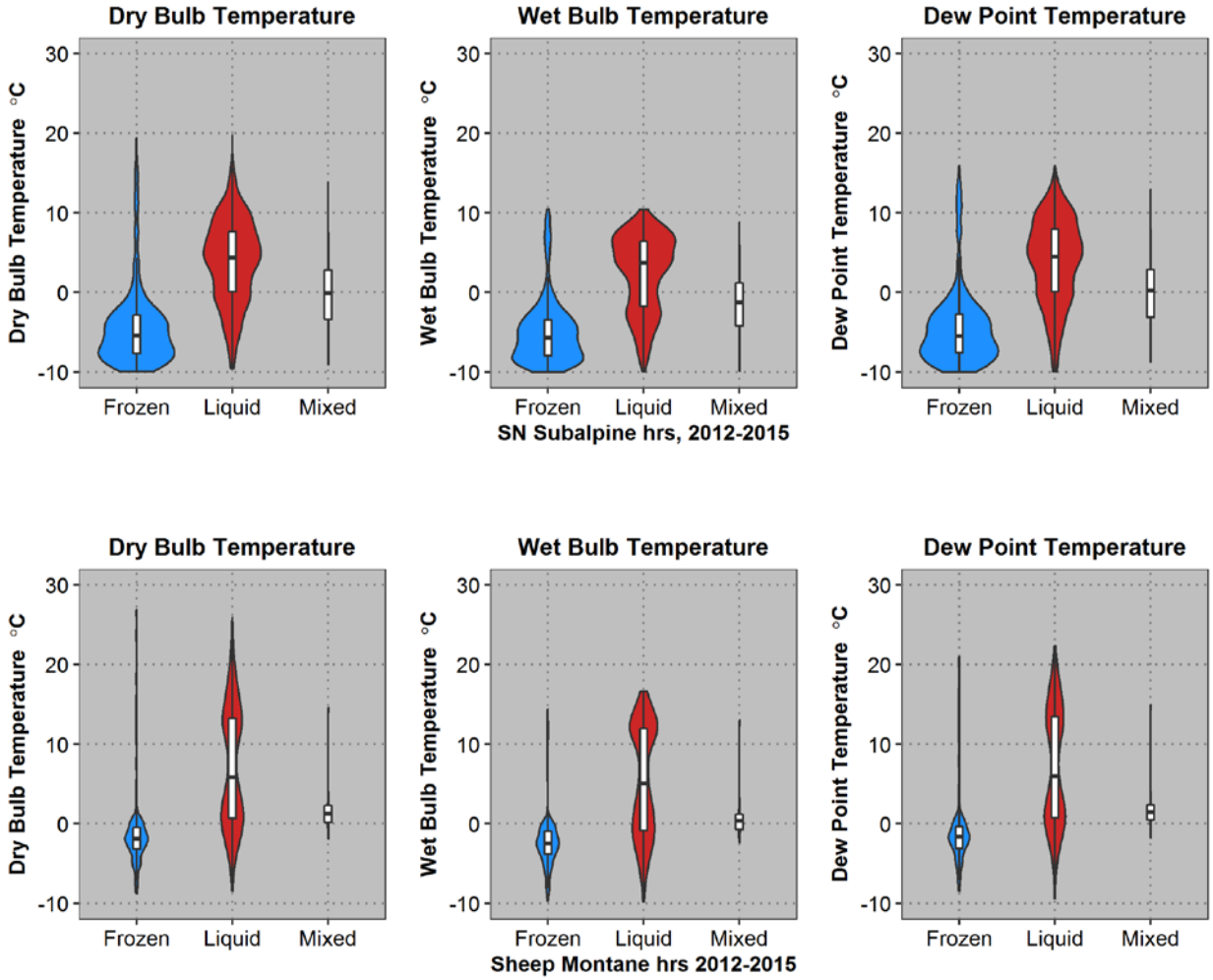

Violin plots indicating distribution characteristics are shown for classified events relative to the measurement of air temperature as well as estimates of wet bulb and dew point temperatures. Liquid classifications are shown as occurring well into the freezing range (< 0°C), due to filter settings which intentionally classify very low intensity events as liquid to avoid misclassification as frozen.

3.5 Plots of all events by catch and temperature

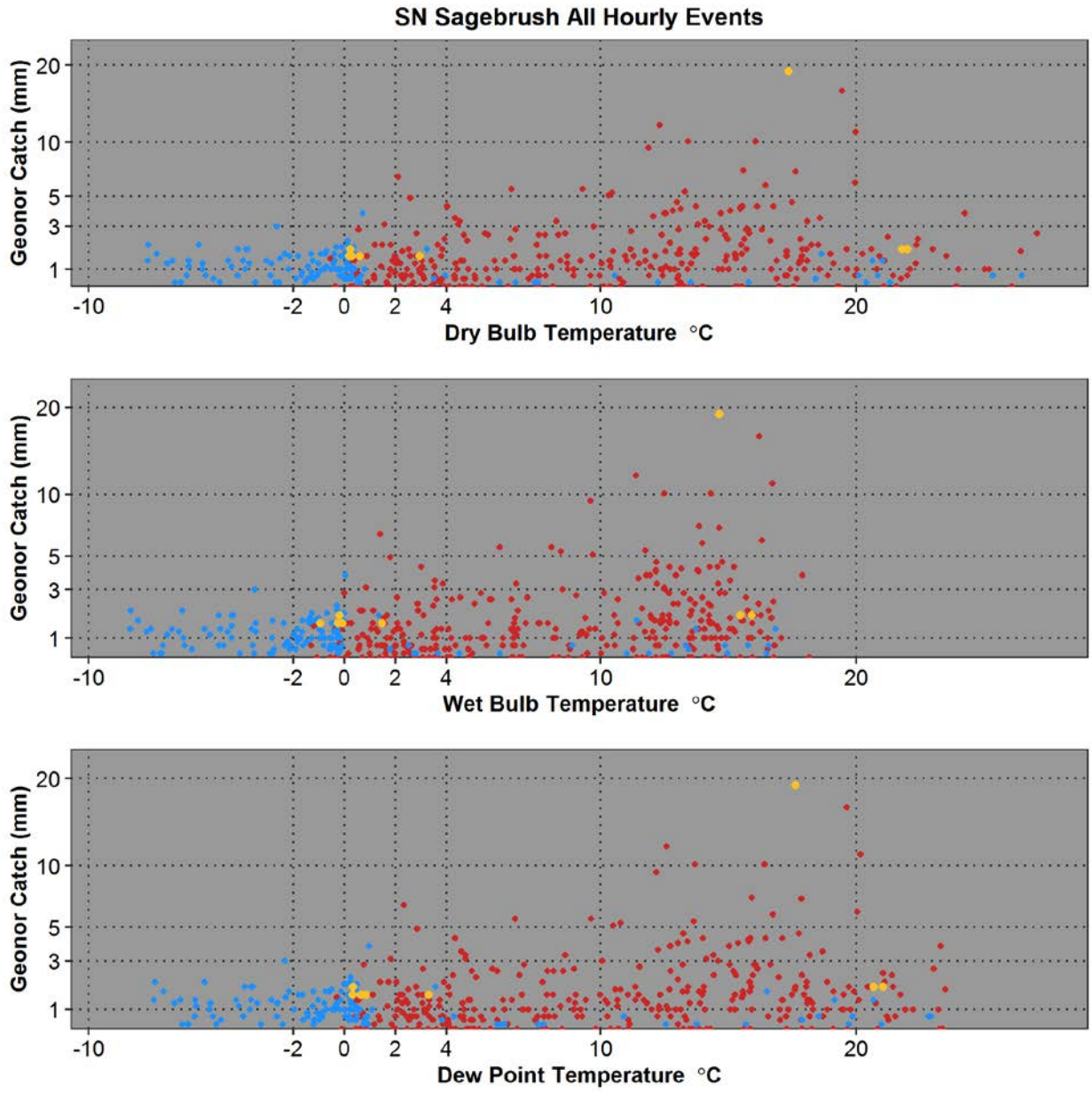

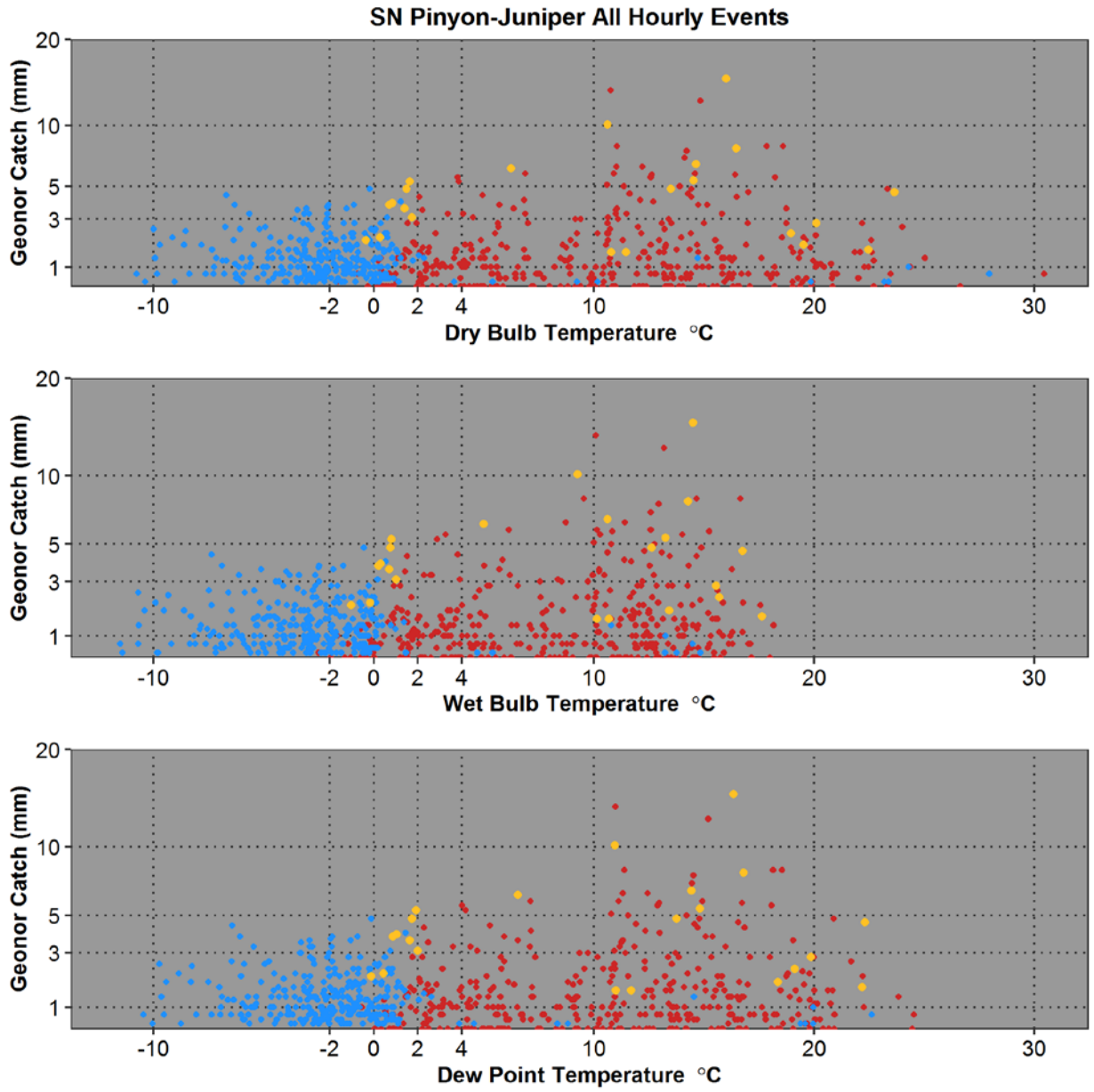
SN Pinyon-Juniper All Hourly Events
Geonor Catch (mm)
20
10
5
3
1
-10
-2
0
2
4
10
20
30
Dry Bulb Temperature °C
Geonor Catch (mm)
Wet Bulb Temperature °C
Geonor Catch (mm)
Dew Point Temperature °C

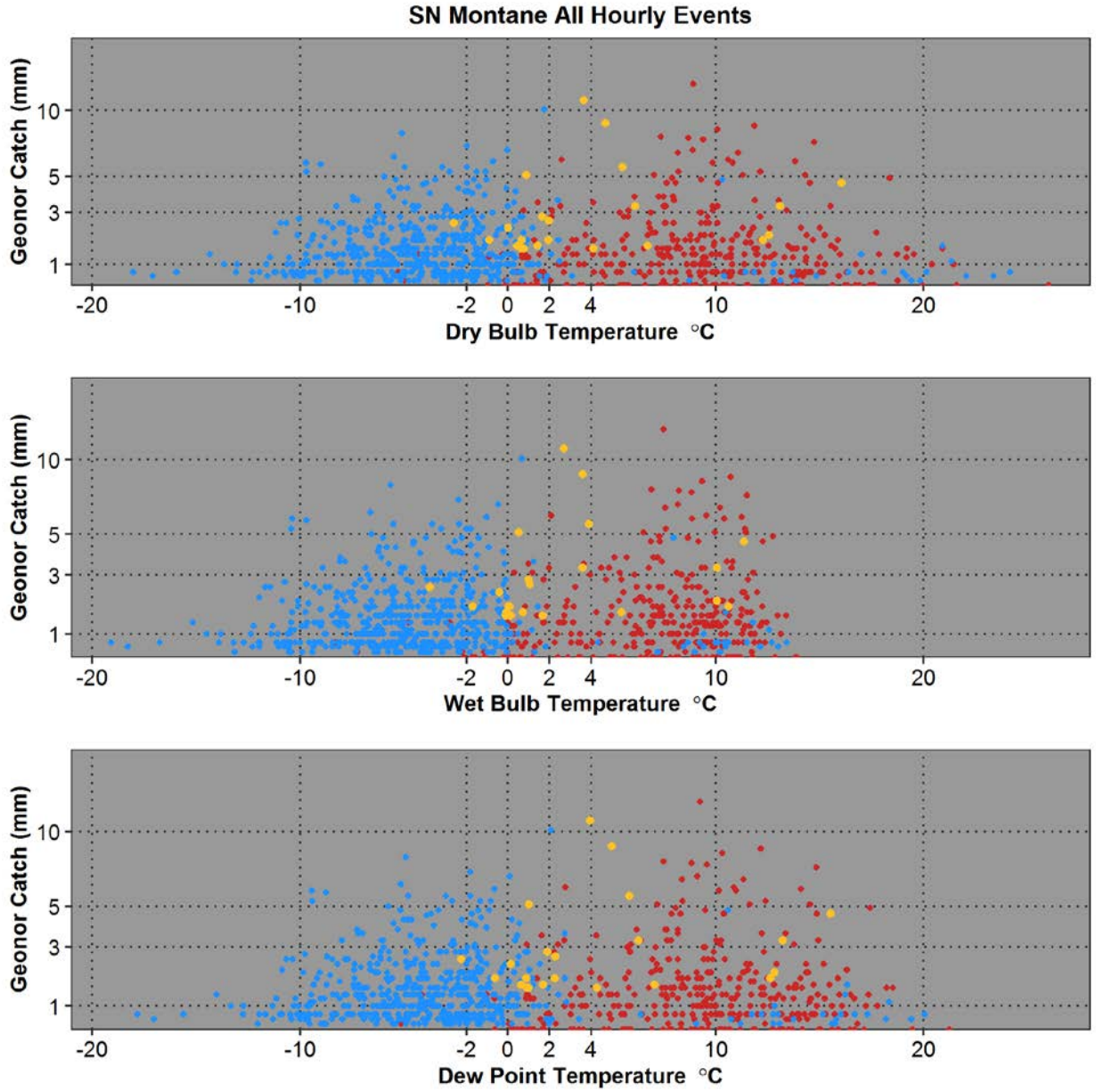
SN Montane All Hourly Events
Geonor Catch (mm)
10
5
3
1
-20
-10
-2
0
2
4
10
20
Dry Bulb Temperature °C
Geonor Catch (mm)
10
5
3
1
-20
-10
-2
0
2
4
10
20
Wet Bulb Temperature °C
Geonor Catch (mm)
10
5
3
1
-20
-10
-2
0
2
4
10
20
Dew Point Temperature °C

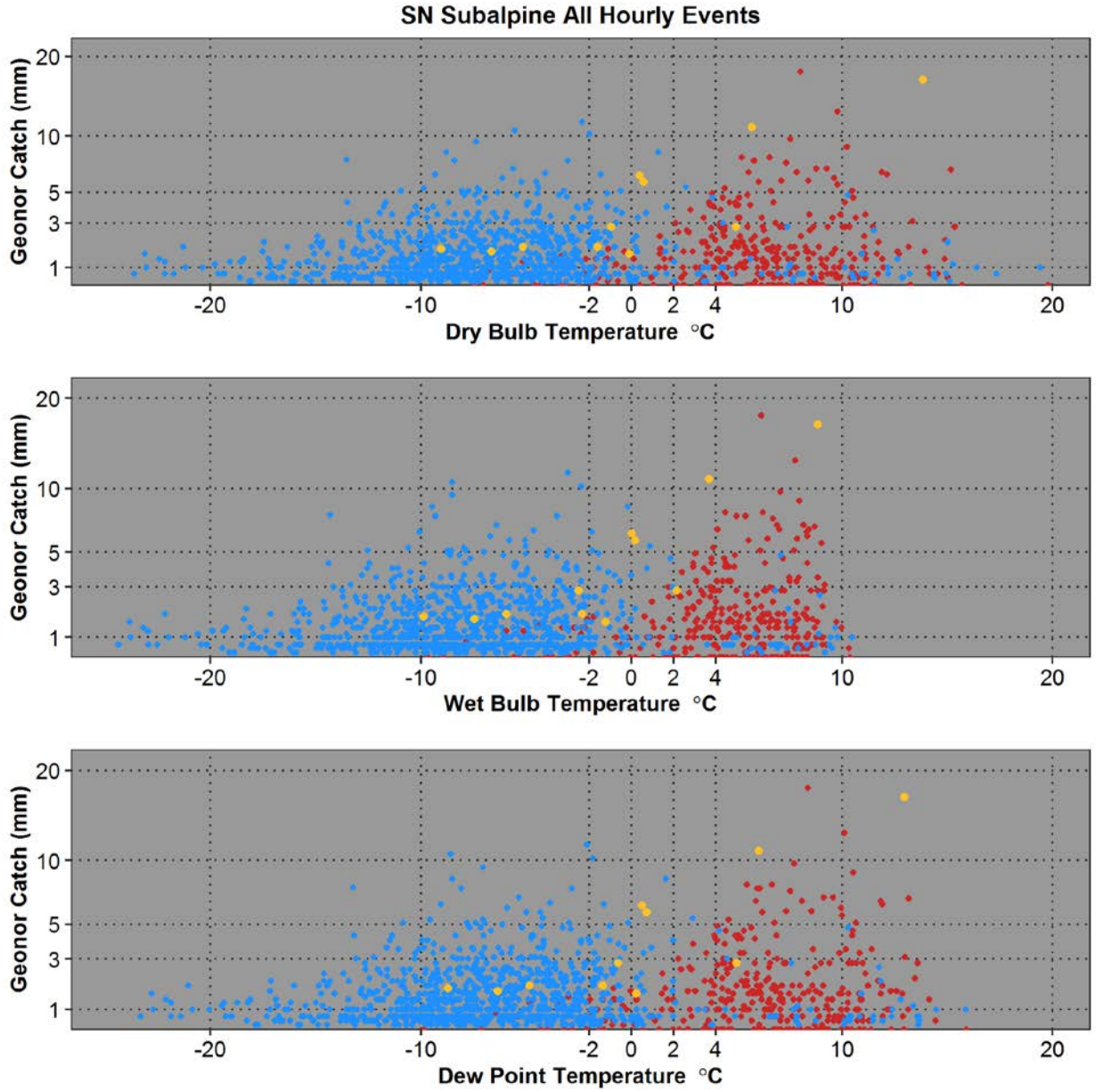
SN Subalpine All Hourly Events
Geonor Catch (mm)
20
10
5
3
1
-20
-10
-2
0
2
4
10
20
Dry Bulb Temperature °C
Wet Bulb Temperature °C
Dew Point Temperature °C

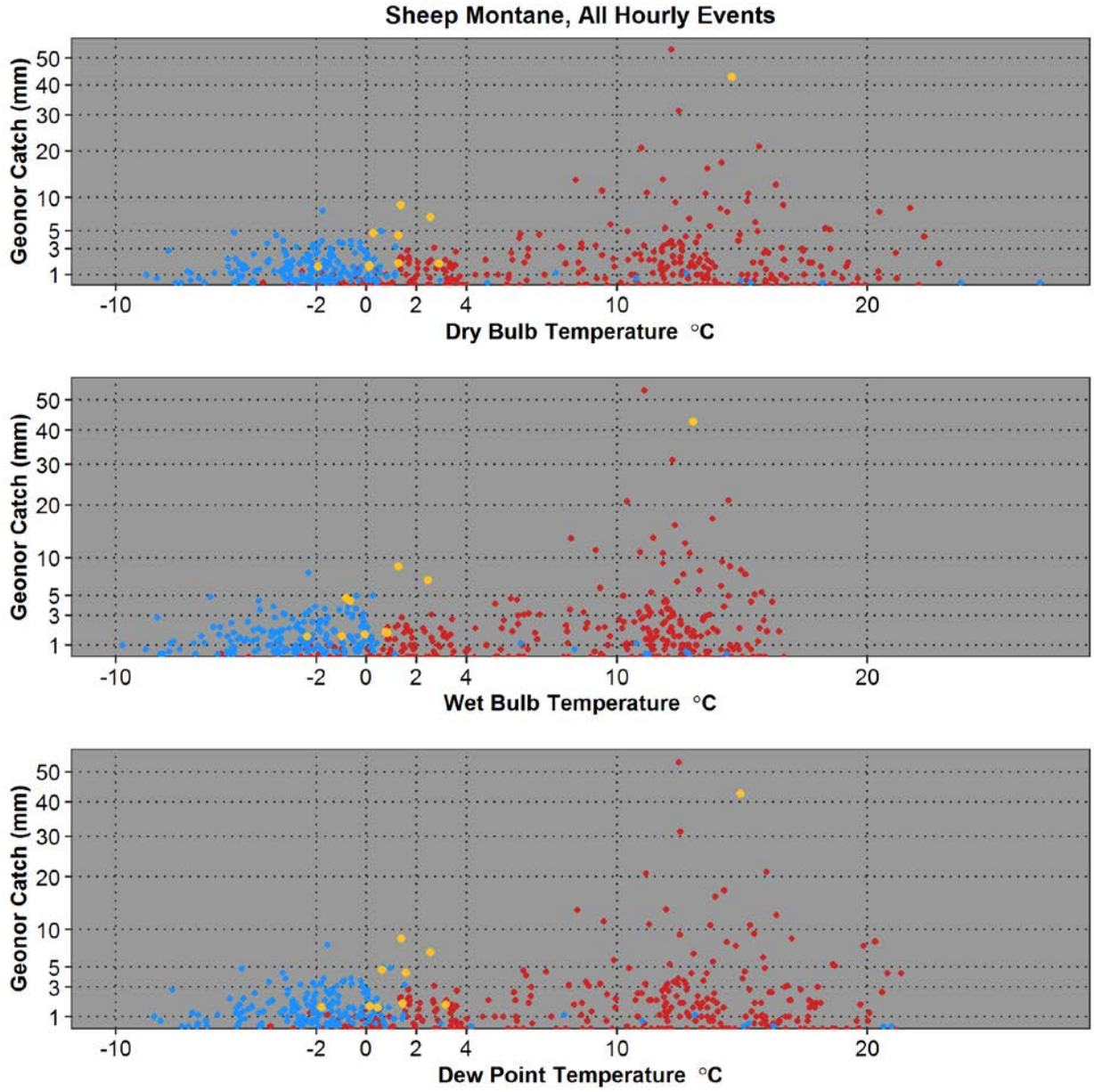

All hourly precipitation classifications (e.g. > 0.5 mm hr^{-1}) are shown in raw catch numbers prior to correction. Potential modes of misclassification can be hypothesized based on phase, the catch level, and associated temperatures. For instance, lower-intensity events (< 1 mm hr^{-1}) are subject to greater misclassification due to amplified differences in wetting losses and evaporation between gages.

3.6 NWS regional intensity-duration-frequency curves

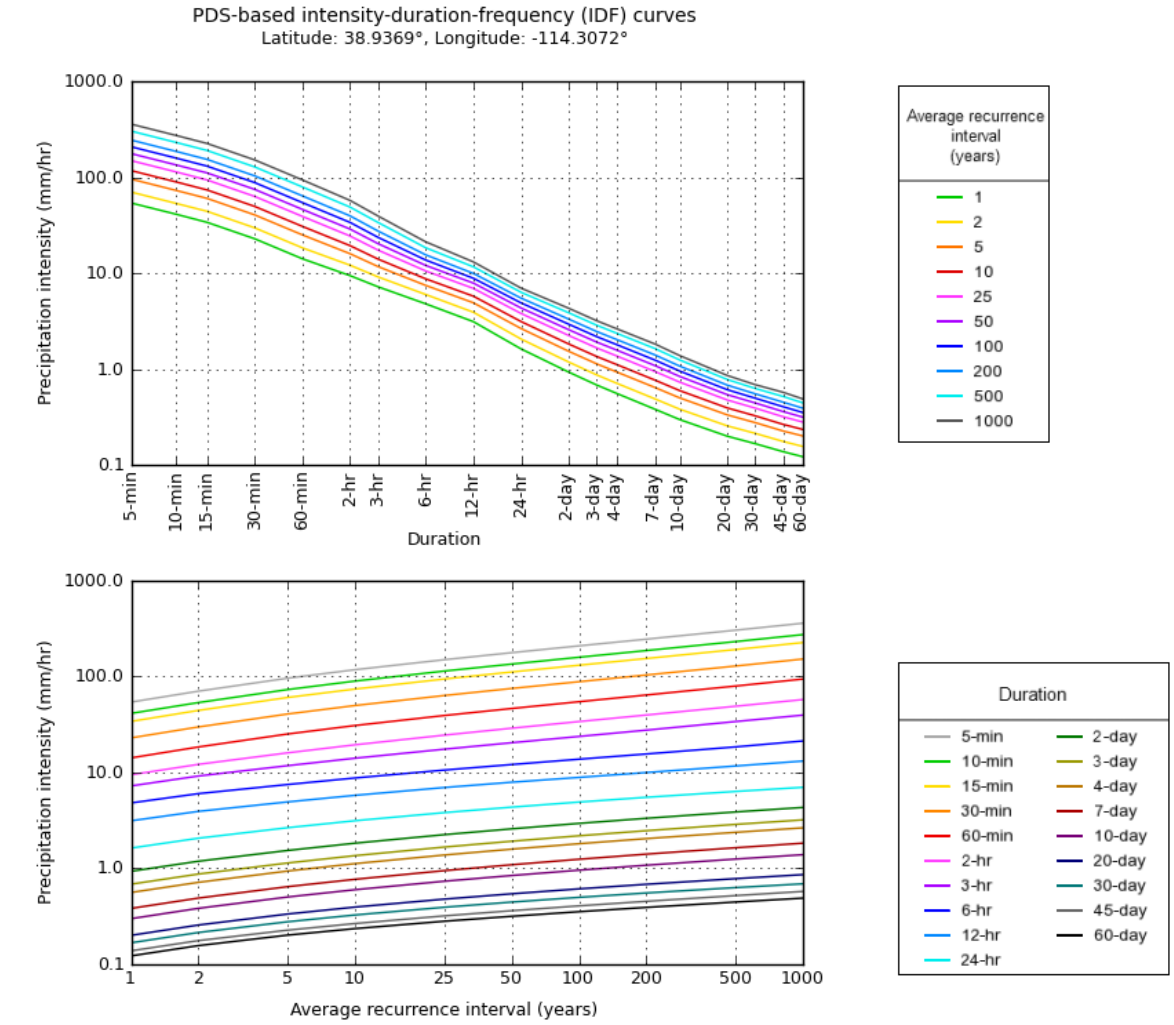

3.7 NCDC climate division 6-month precipitation anomalies by year

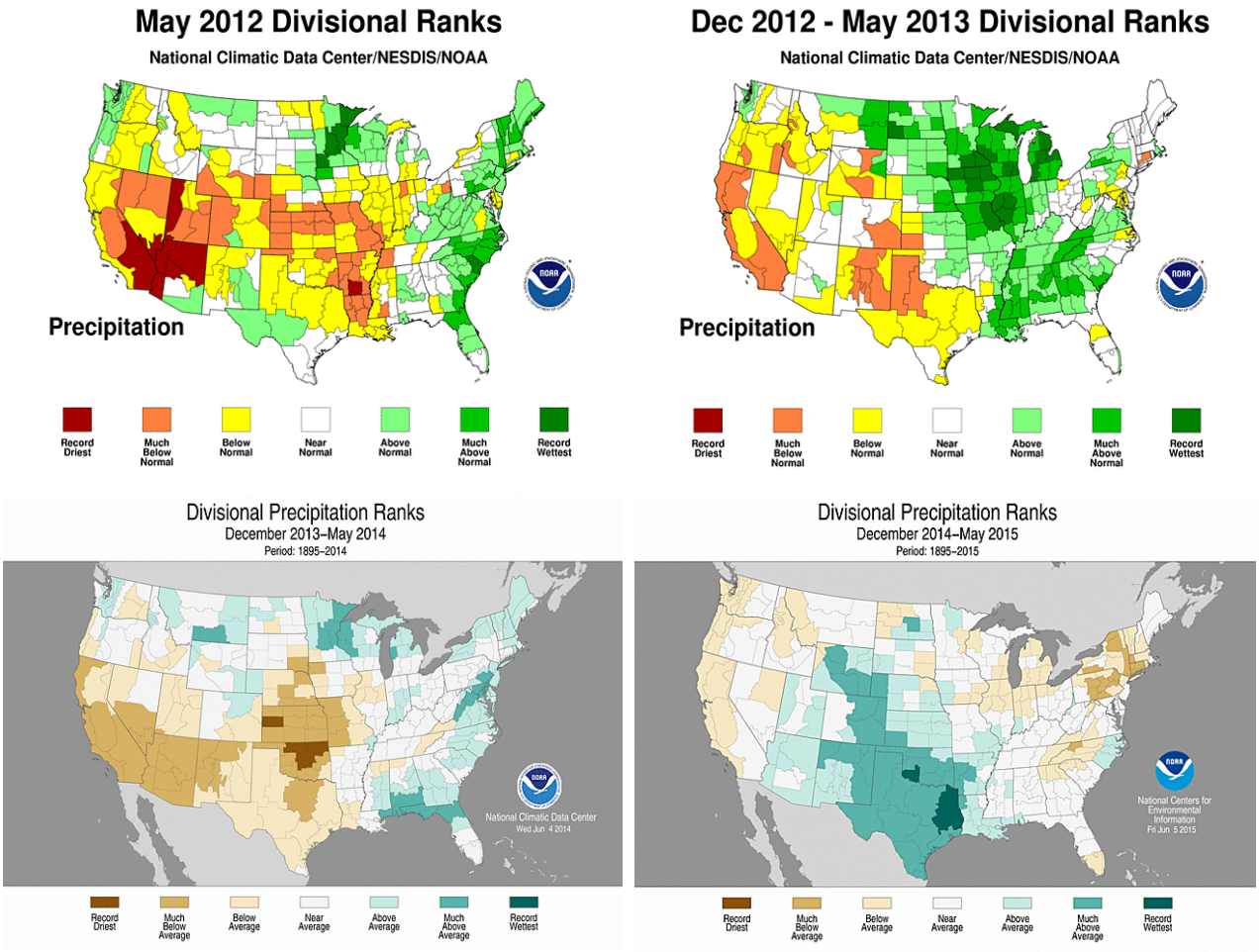

Precipitation departures from climate divisions normals are shown for the Dec–May periods of 2012–2015. Three of the four years of observation were drier than normal from the precipitation standpoint, with 2012 being a very dry year for all divisions associated with this study.

3.8 Daily classified uncorrected precipitation totals

Daily precipitaiton totals (uncorrected for wind undercatch) are shown by phase as stacked bars.

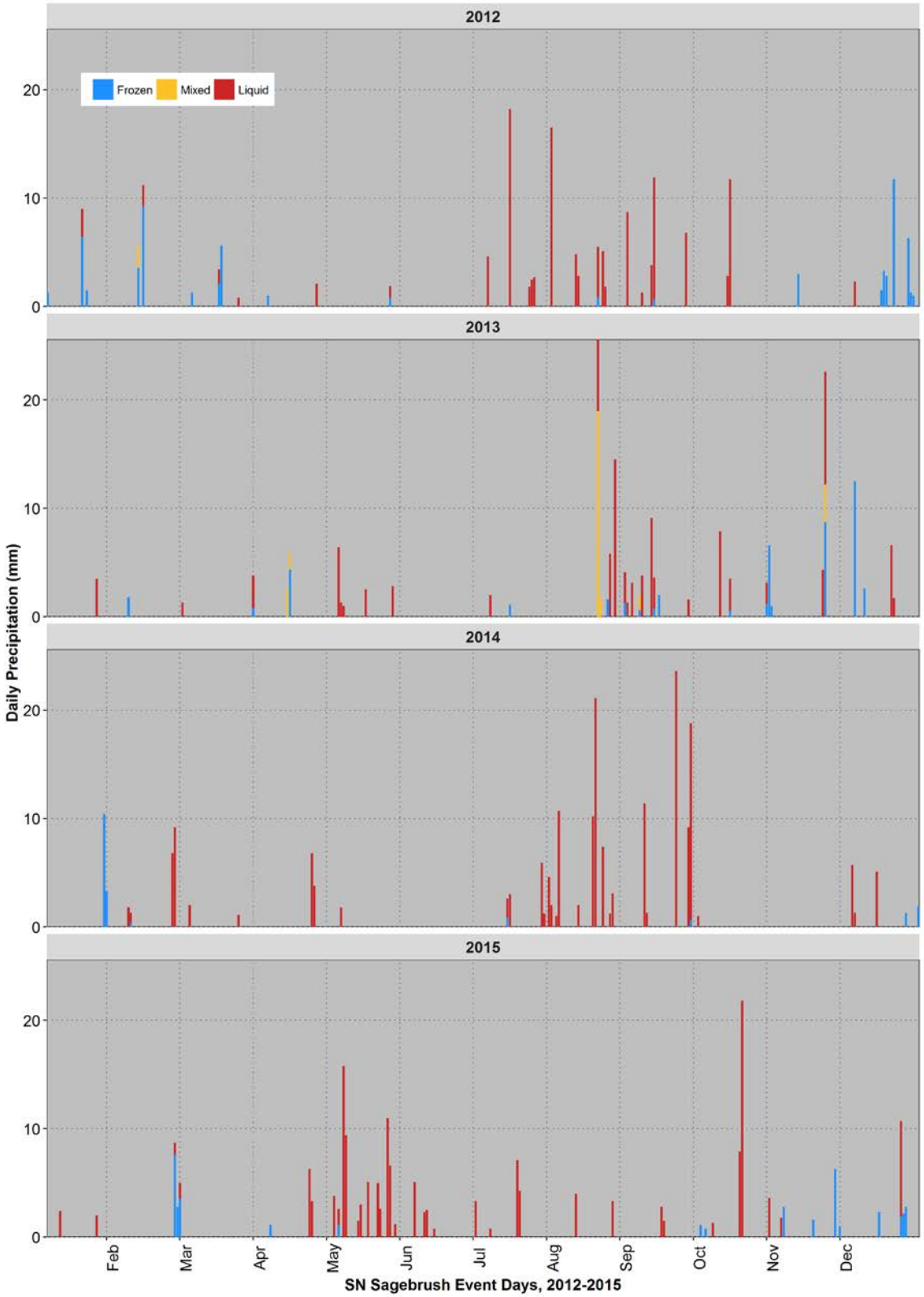

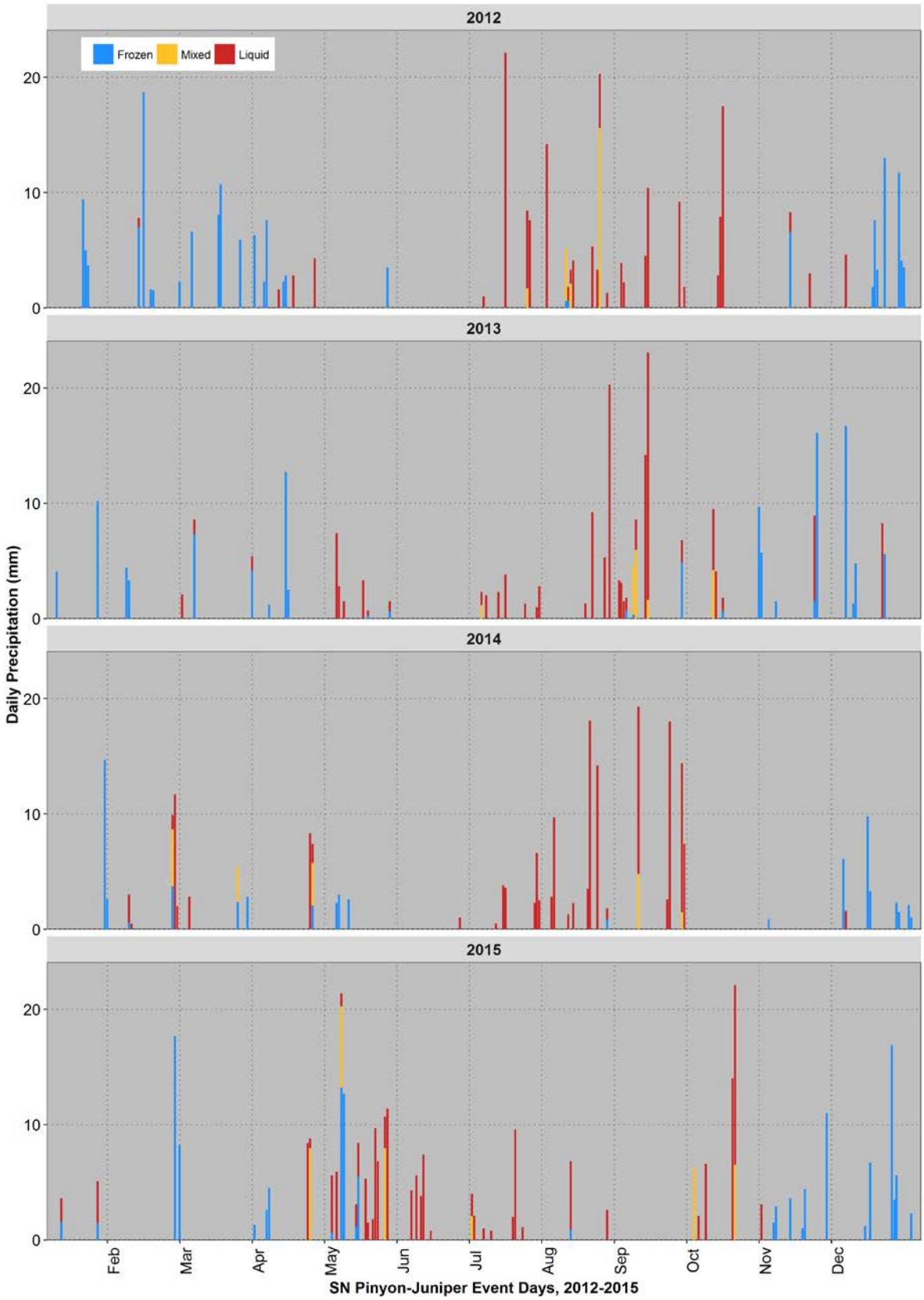
2012
2013
2014
2015
Frozen
Mixed
Liquid
Daily Precipitation (mm)
0
10
20
Feb
Mar
Apr
May
Jun
Jul
Aug
Sep
Oct
Nov
Dec
SN Pinyon-Juniper Event Days, 2012-2015

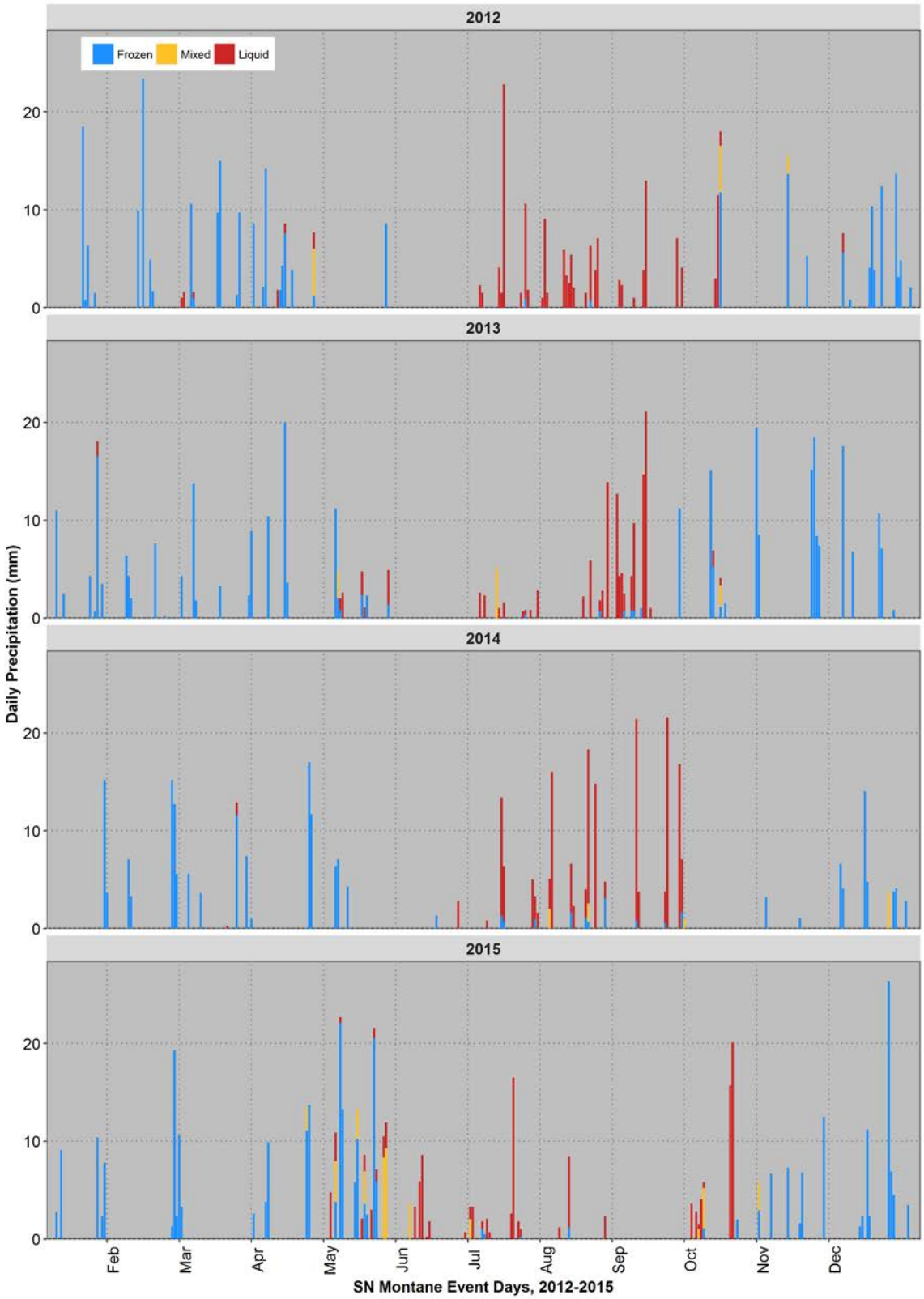
2012
2013
2014
2015
Frozen
Mixed
Liquid
Daily Precipitation (mm)
0
10
20
Feb
Mar
Apr
May
Jun
Jul
Aug
Sep
Oct
Nov
Dec
SN Montane Event Days, 2012-2015

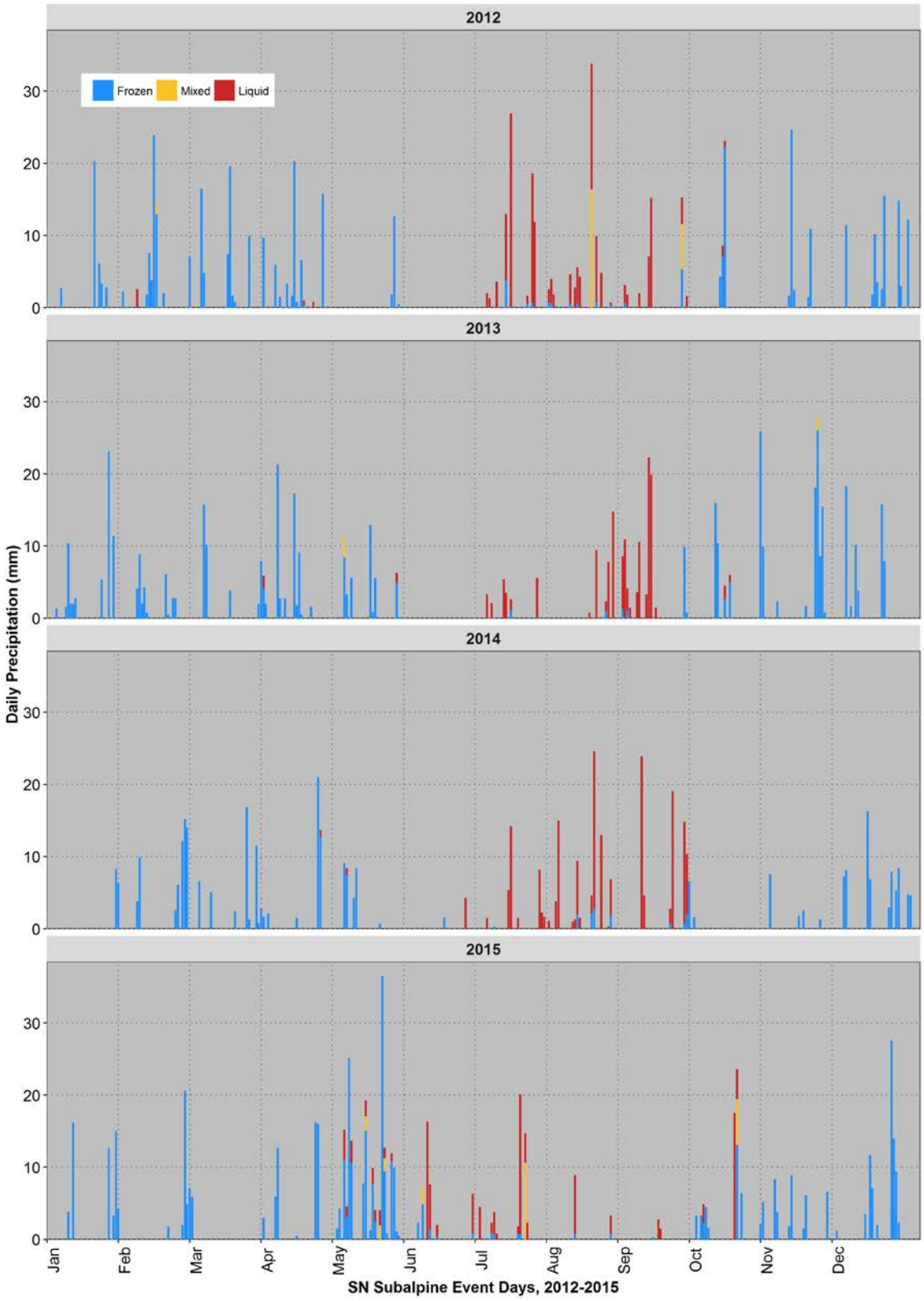
2012
2013
2014
2015
Frozen
Mixed
Liquid
Daily Precipitation (mm)
0
10
20
30
Jan
Feb
Mar
Apr
May
Jun
Jul
Aug
Sep
Oct
Nov
Dec
SN Subalpine Event Days, 2012-2015

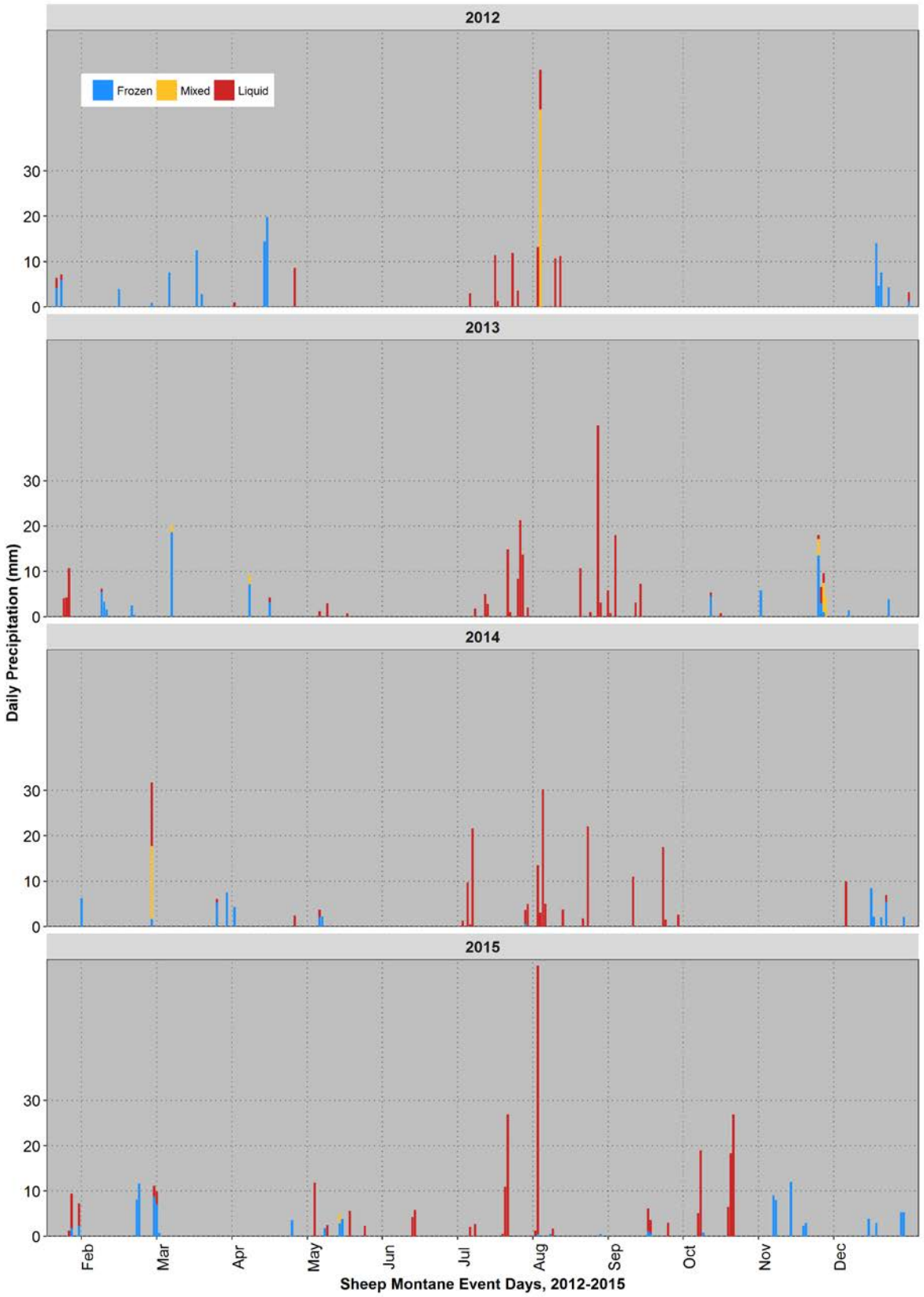
2012
2013
2014
2015
Frozen
Mixed
Liquid
Daily Precipitation (mm)
0
10
20
30
Feb
Mar
Apr
May
Jun
Jul
Aug
Sep
Oct
Nov
Dec
Sheep Montane Event Days, 2012-2015

3.9 Hail events.

Hail events at the SR Sagebrush site (top), SR Subalpine site (rows 2 and 3), and Sheep Range Montane site (bottom 2 rows). Other hail events at the SR Pinyon-Juniper and SR Montane sites were flagged by the GDM as substantial “mixed” summertime events, but either occurred at night when the camera was not recording or else melted in the 1-hour interval between images. In some cases, the hail melted quickly due to mixing with heavy liquid precipitation. However, at the upper elevation sites the hail remained intact and slowly melted in a manner which made the precipitation much more “effective” in recharging soil VWC.


Access - 8/1/2015 10:02:03 AM PST


TB Precip - 8/1/2015 11:02:35 AM PST


TB Precip - 8/1/2012 2:04:22 PM PST


TB Precip - 8/1/2012 3:04:31 PM PST

3.10 April 1 Snow Water Equivalent

Natural Resources Conservation Service (NRCS) Snow Telemetry (SNOTEL) and snow course data for 1 April in (top to bottom) 2012, 2013, 2014, and 2015. All years show the extent of the regional drought in the intermountain west.

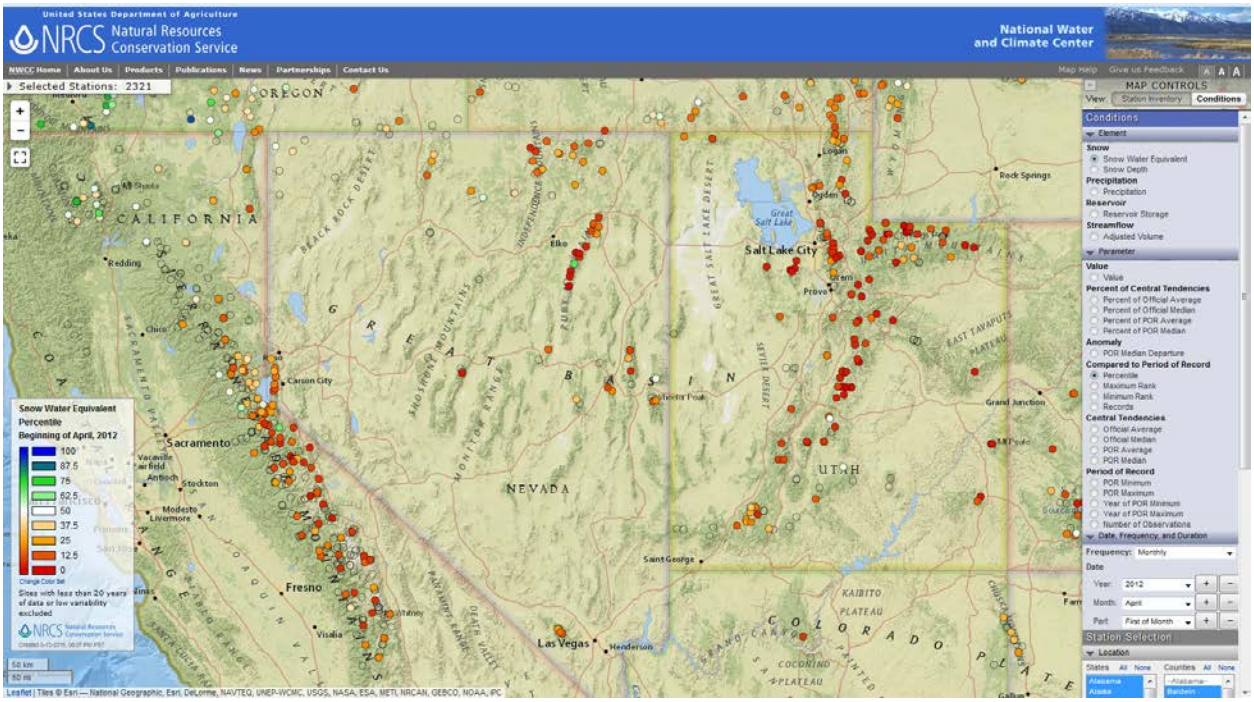

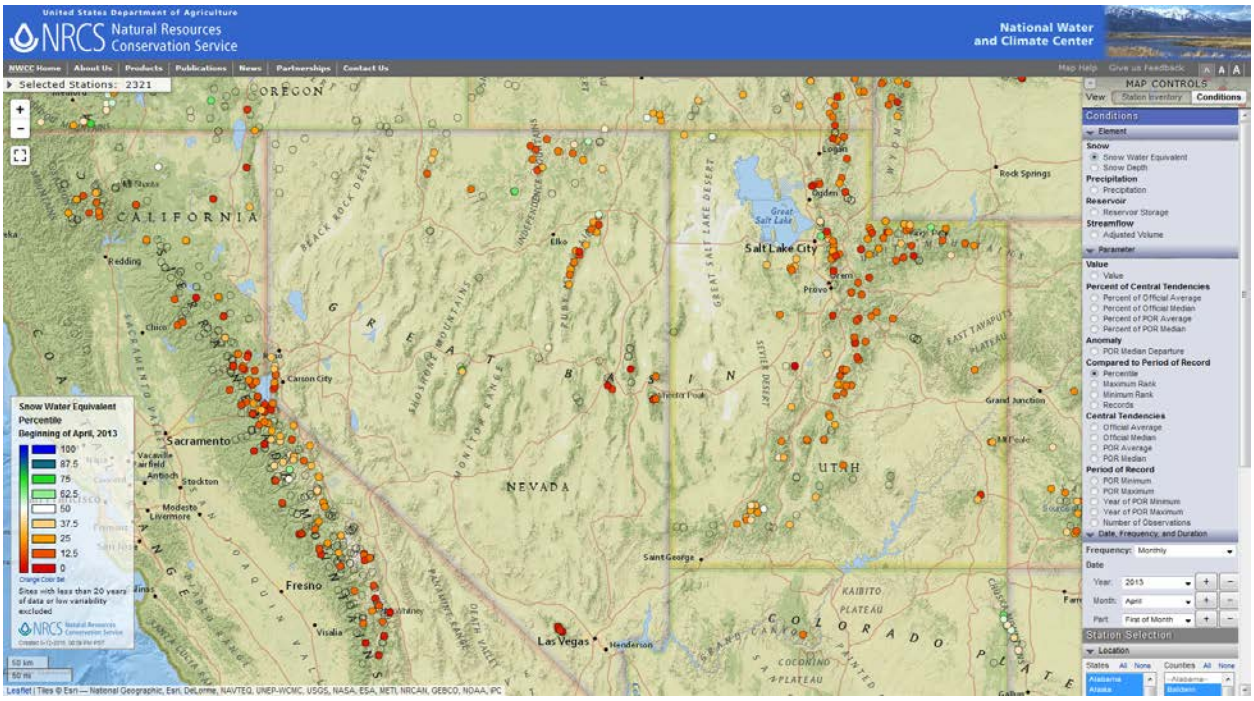

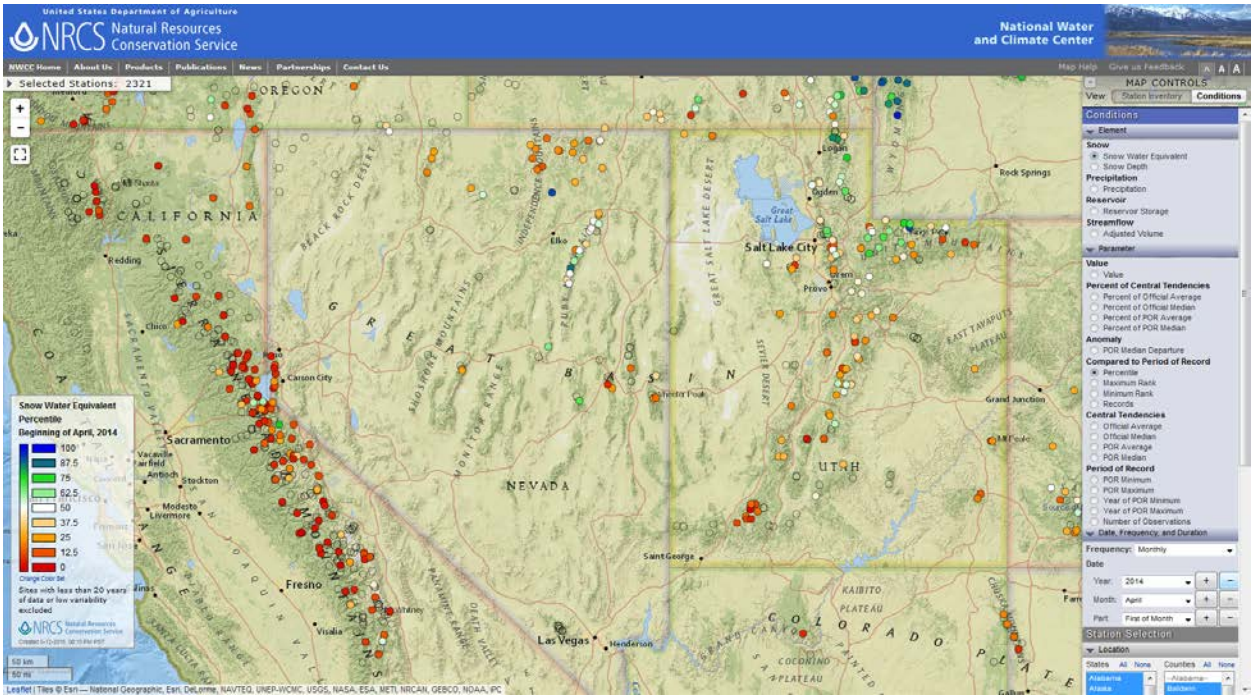
United States Department of Agriculture
NRCS Natural Resources Conservation Service
National Water and Climate Center
Selected Stations: 2321
MAP CONTROLS
Snow Water Equivalent Percentile Beginning of April, 2014
Sites with less than 20 years of data or low variability excluded
OREGON
CALIFORNIA
NEVADA
UTAH
Sacramento
Fresno
Las Vegas
Salt Lake City
Reno
Carson City
Rock Springs
Grand Junction
Saint George

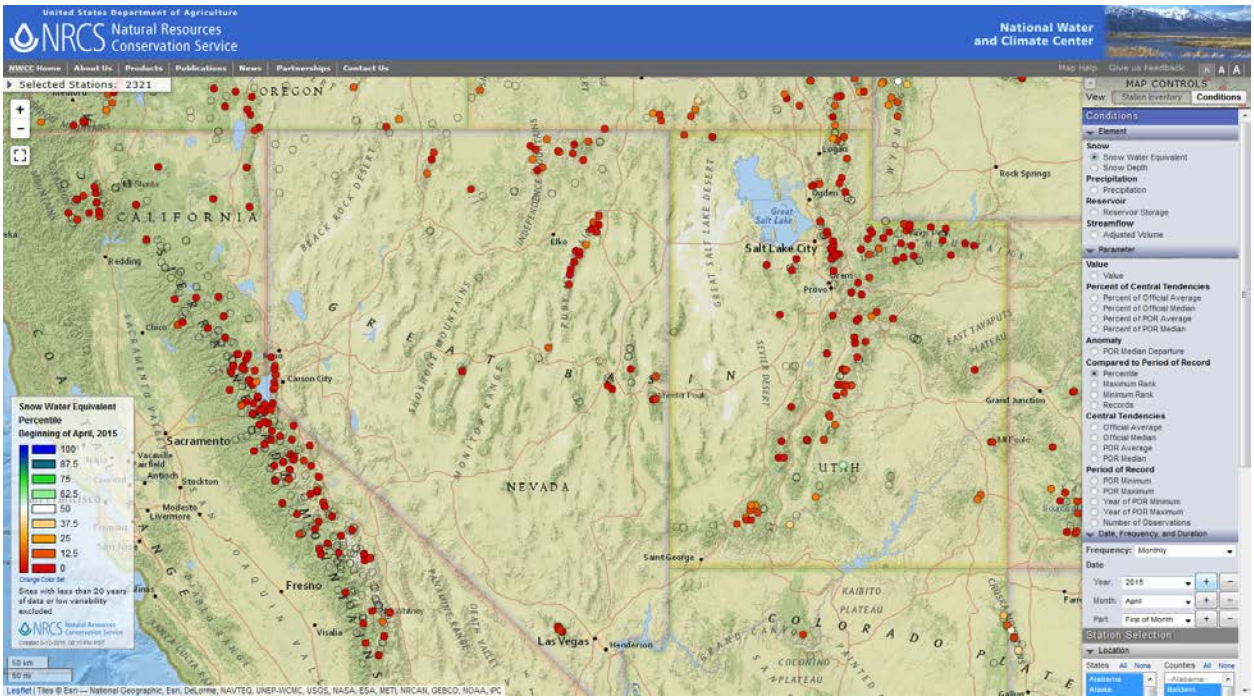
United States Department of Agriculture
NRCS Natural Resources Conservation Service
National Water and Climate Center
Selected Stations: 2321
MAP CONTROLS
Snow Water Equivalent Percentile Beginning of April, 2015
Sites with less than 20 years of data or low variability excluded
OREGON
CALIFORNIA
NEVADA
UTAH
Sacramento
Fresno
Las Vegas
Salt Lake City
Reno
Carson City
Rock Springs
Grand Junction
Saint George